PREDICTION OF DESIGN AND PERFORMANCE PARAMETERS IN AGRO-FORESTRY VEHICLES

BY

M. G. BENKER

PREDICTION OF DESIGN AND PERFORMANCE PARAMETERS IN AGRO-FORESTRY VEHICLES

METHODS, TESTS, AND NUMERICAL EXAMPLES

M.G. Bekker

DECEMBER 1983

TABLE OF CONTENTS

	Page
FOREWORD	vii
ABSTRACT	ix
RÉSUMÉ	x
PHASE I. MATHEMATICAL MODELS AND TIRE PERFORMANCE PREDICTION, METHODS AND PROCEDURES	1
OBJECTIVE	1
APPROACH	1
SCOPE	2
EVALUATION PROCESS	2
SUMMATION AND RECOMMENDATIONS	6
REFERENCES	8
APPENDIX A: MISSION DEFINITION	9
FUNCTIONAL REQUIREMENTS	9
OPERATIONAL REQUIREMENTS	9
MISSION PROFILES	10
REFERENCES	11
APPENDIX B: ENVIRONMENT DEFINITION	13
MECHANICAL GROUND PROPERTIES	13
DISTRIBUTION OF SOIL VALUES	19
GEOMETRICAL GROUND SURFACE PROPERTIES	19
REFERENCES	24
APPENDIX C: DATA BANK	25
REFERENCES	25
APPENDIX D: ROLLING RESISTANCE OF PNEUMATIC TIRES	27
PART I. UNYIELDING GROUND, OR HARD SURFACE ROAD	27
TIRE MODEL	28
MATHEMATICS OF TIRE EVALUATION	29
Tire Deflection	31
Rolling Resistance Coefficient	33
Coefficient of Energy Recovery	33
NUMERICAL EXAMPLES AND THEIR VERIFICATION	34
Bicycle Tire, 27 × 1.25, "Schwinn Puff"	35
Bicycle Tire, 26 × 1.375	37

TABLE OF CONTENTS (Cont'd)

Page

Earthmover Tire, 29.5 - 29 38
Automobile Tire, 7.00 - 15 39
Automobile Tire, 9.00 - 20 39
Truck Tire, 10.00 - 20 40
Truck Tire, 14.00 - 20 41
Construction Equipment Tire, 26.5 - 25 41
Cylindrical Tire, 16 × 15 6R, "Terratire" 42
Tire at Varying Load and Inflation Pressure 43
Conventional and Radial Tires 43
Wire Mesh Tires for Lunar Surface Locomotion 48
ACCURACY OF PREDICTIONS 49
PARAMETRIC ANALYSES AND CASE STUDIES 51
Worn and New Tires 51
Effect of Tread Radius on Rolling Resistance 53
Effect of Tire Diameter on Rolling Resistance 58
Effect of Tread Width on Rolling Resistance 59
Effect of Flat Tread Width on Rolling Resistance 62
Frame of Reference for Calculation of Rolling Resistance 64
Tire Geometry and Performance Maps 64
Spacing Sizes in Performance Marketing 68
Two Tires Against One 69
The Price of Inflation Pressure 71
Single Tire vs. Dual 73
Tread Design and Rolling Resistance 76
Rolling Resistance on a Flat and Curved Surface 78
Competitive Bids and Tire Drag 78
Fuel Consumption and Motion Resistance 80
CONCLUSION, COMMENTS and SUGGESTIONS 82
PART II. HOMOGENEOUS SOILS WITH SOFT, YIELDING SURFACES 83
TIRE MODELS 85
MATHEMATICS OF TIRE EVALUATIONS 85
Sinkage of the Rigid Wheel, or Tire 86
Critical Inflation Pressure at Rigid-Elastic Transition Point 86
Sinkage and Deflection of an Elastic Tire 86
Compaction Coefficient of Rolling Resistance of Rigid Tires 88
Compaction Coefficient of Rolling Resistance of Elastic Tires 88

TABLE OF CONTENTS (cont'd)

Page

Horizontal Ground Deformation Coefficient of Rolling Resistance 88
Tire Carcass Flexing Coefficient of Rolling Resistance . . 90
VALIDATION OF ROLLING RESISTANCE PREDICTIONS 90
7.00 - 16 Tire; Dry, Sandy Soil 91
14.00 - 20 Tire; Sandy Soil 96
11.00 - 20 Tire; Dry, Sandy Soil 98
Tires with Tread Buffed Smooth 99
1.75 - 26 Bicycle Tire; Sandy Soil 106
16 × 15 6PR Terratire; Sandy Soil 108
Dual Tires with Close Spacing 109
Field Tests 110
ACCURACY OF PREDICTIONS 111
EXAMPLES OF CASE STUDIES AND PARAMETRIC ANALYSES 114
Analysis of Catalogue Recommended Tire Options 115
Effect of Inflation Pressure in Soils of Varying Consistency 118
Effect of Tread Width 119
Effect of Tire Diameter 127
Effect of Tire Load 129
Probability of Success 134
PART III. NONHOMOGENEOUS, STRATIFIED GROUND, AND REPETITIVE GROUND CROSSING 137
INTERPRETATION AND CURVE FITTING OF BEVAMETER DATA 137
Nonhomogeneous Soils of Weak-Strong Type 138
Nonhomogeneous Ground of Strong-Weak Type 141
Repetitive Ground Crossing 141
TIRE MODELS 144
MATHEMATICS OF TIRE EVALUATION 144
Rigid Tire in a Mineral Ground 144
Elastic Tire in a Mineral Ground 147
Correction for Bernstein Integral 149
Correction for Rolling Resistance 150
Tire Rolling Resistance in Snow 150
Tire Rolling Resistance in "Organic" Ground 151
NUMERICAL EXAMPLES AND THEIR VERIFICATION 152
Elastic Tire in a Ploughed Field 152
Rigid Tire in a Ploughed Field 155
Accuracy of Predictions 156
Elastic Tire in Shallow Snow 159

TABLE OF CONTENTS (cont'd)

Page

Tires in Organic Soils 160
Rolling Resistance 162
MULTIPLE GROUND CROSSING 163
38 × 20 - 16 Terratires 164
12.5 - 20 EM Tire 165
Tires of Uneven Width 166
REFERENCES 169

APPENDIX E. VEHICLE THRUST-SLIP PERFORMANCE 173
GRANULAR SOILS 173
ORGANIC SOILS 173
REFERENCES 174

APPENDIX F. TERRAIN DAMAGE 175
SOIL COMPACTION 175
SURFACE SHEARING 176

APPENDIX G. TRADE-OFF CRITERIA AND OPTIONS 179

PHASE II. EVALUATION EXAMPLES OF AGRO-FORESTRY VEHICLES 181
SOIL AND VEHICLE PARAMETERS, INTERPRETATION, ETC. 181
ENVIRONMENT OF LOCOMOTION 181
Analysis of Field Data and Soil Parameters 181
Second Pass Bevameter Values 190
Soil Measuring Techniques 193
Summary of Prescott Environmental Input 193
EXPLORATORY STUDY OF TRACTION PARAMETRICS 194
Tractors and Their Equipment 194
Exploratory Example 194
Planter Rolling Resistance 195
Axle Load Distribution 197
Versatile 160 with 16.9 - 24 tires: Rolling Resistance . 197
Accuracy of Prediction 198
Relationship between Soil Value Spread and Rolling Resistance Spread 198
Rolling Resistance and Soil Moisture Content 201
Soil Surface Rut Damage vs. Moisture Content 203
Slope and Drawbar Pull 203
Soil Surface Shear Damage 205

TABLE OF CONTENTS (cont'd)

Page

Power and Fuel Consumption 206
Other Tires on Versatile Tractor 208
Conclusion 209

PARAMETRIC ANALYSES OF VEHICLES IN AGRO-FORESTRY, EXAMPLES AND CASE STUDIES 211
GENERAL 211
PLANTER IN PRESCOTT SOIL 211
Furrow Opening Reaction 211
Insertion Planter Load 212
Environment 212
Tires 212
Planter Rolling Resistance 212
Computations of the Maximum Number of Furrow Planter Modules 212
Computation of the Maximum Number of Insertion Planter Modules 214
Comparison between Furrow and Insertion Planters 216
Environmental Damage 216
TURF-TYPE SOIL DEFINITION 216
Turf Analog 218
Turf-Soil Characteristics 220
A PLANTER IN TURF-LIKE SOIL 221
Insertion Planter-Tractor Power 221
Furrow Planter-Tractor Power 221
TREE HARVESTER IN TURF-LIKE SOIL 223
Drawbar Pull and Slip 224
Rolling Resistance and Power 224
FORWARDING AND SKIDDING 226
Tires and Attachments 226
Computation of Pull-Slip, Thrust and Power 226
Conclusions 230
GENERAL CONCLUSIONS 231
REFERENCES 232

FOREWORD

The present study of optimization of terrain-vehicle systems in agroforestry is written in two Phases. Phase I is concerned with the methods and procedures used in parametric analyses for the purpose of system optimization, Phase II with analytical tests and examples of systems optimization based on bevametric field data and candidate vehicle consideration. Whenever possible, the results were verified, or corroborated by experiment.

In a broad sense, the study is an outline of engineering mechanics of pneumatic tires and their application to tractors. It also describes a first attempt of large scale definition of environmental data in bevameter terms, and the variety of parametric analyses that may be needed in a solution of engineering problems of vehicle mobility. Similar studies, performed in the past, were referred to, whenever required.

This work was originated in Canada during World War II, when I was serving in the Canadian Army, and may be considered as a sequel to my first report on the subject published in 1948, under the auspices of the Army and National Research Council of Canada. I am deeply grateful for, and appreciative of such a liberal long standing support.

Ms. B.A. Summers, Project Manager, supervised pertinent activities encompassing the totality of the Program involved.

The work described here owes much to Mr. T.B. Golob who provided the general input and guidance within the framework of that Program.

Dr. J.Y. Wong of Carleton University introduced computerized soil data processing and performed soil measurements used here.

M.G. Bekker

ABSTRACT

In this work, the engineering mechanics of pneumatic tires was outlined with specific applications to terrain-tire interface optimization which would enable one to perform parametric analyses aiming at the optimization of Terrain-Vehicle Systems.

In Phase I, methodology of specific operations in terrain-vehicle system evaluation, as well as the flow charts for first-order deterministic optimization of such systems, was presented in detail. This was verified on a large number of tire-soil systems, with particular consideration of soft ground surface crossing. Also the ramification and interpretation of input-output data were discussed, and the nature of predictive errors was explained. A statistical approach towards achieving maximum operational success was stressed.

Phase II is concerned with the application of the methods and procedures to specific parametric analyses applicable to forest technology.

Numerical examples corroborated by experiment were presented, and test calculations were performed with particular emphasis on the optimization of tractors for agro-forestry operations.

RÉSUMÉ

Dans le présent travail, on décrit les aspects mécaniques de l'étude technique de pneus. On traite d'applications particulières à l'optimisation d'une interface terrain-pneu qui permettrait d'effectuer des analyses paramétriques en vue d'optimiser les systèmes terrain-véhicule.

La première phase de cette étude traite de la méthodologie utiliseé pour des opérations particulières dans une évaluation de systèmes terrain-véhicule, accompagnée des diagrammes d'optimisation déterministe de premier ordre de tels systèmes, a été présentée en détail. Elle a été vérifiée avec un grand nombre de systèmes pneu-sol, notamment pour des sols tendres. La ramification et l'interprétation des données d'entrée et de sortie ont aussi été abordées, et la nature des erreurs de prévision a été expliquée. L'accent a été mis sur une méthode statistique de maximisation de la probabilité de succès des opérations.

La seconde phase de ce rapport concerne l'application des méthodes à des analyses paramétriques spécifiques en technologie forestière.

Les exemples numériques et les études de cas décrits sont tirés d'un programme quinquennal de plantation de peupliers il s'agit d'exemples et de modèles pour optimiser les systèmes véhicule-terrain dans les opérations agro-forestières.

On a présenté des exemples numériques corroborés par l'expérience et on a effectué des calculs d'essai portant particulièrement sur l'optimisation de tracteurs servant à des opérations agro-forestières.

PHASE I

PHASE I

MATHEMATICAL MODELS AND TIRE PERFORMANCE PREDICTION

METHODS AND PROCEDURES

OBJECTIVE

The objective of this study is the outlining of engineering methods for terrain-vehicle system optimization, and providing of guidelines for procedures in the implementation of the method, with emphasis on locomotion problems in agro-forestry.

Specifically, the method and procedures attempt to help the selection of the "best" out of available competing candidates, and/or to devise a new solution, better than those supplied by the market.

Basic ideas presented to that effect, though of long standing, have been re-examined, expanded, and refined in order to

- strengthen their verification for a larger number of cases encountered in agro-forestry
- illuminate their interpretation within the context of predictive power
- illustrate the broad scope and character of possible parametric analyses of the system under investigation

A comprehensive summary of these endeavours is presented in the Appendices, particularly in Appendix D, which contains new documentation and developments in respect to wheeled vehicles equipped with pneumatic tires.

APPROACH

The approach to the problem, compatible with applied mechanics, is based on unified physico-geometrical models and on a single soil-value system applicable to hard road, soft soil, snow, turf, peat moss, and muskeg, of any possible structure of the medium, either homogeneous or not, or stratified.

As stressed in Appendix D, the rigor of solutions achieved lies only in the statistical approach. Also the validity of assumptions made within the rules of engineering mechanics solely depends on their experimental verification, as demonstrated in Appendix D. In this context, further exploratory work was occasionally suggested.

SCOPE

The scope of this study includes:

- quantitative definition of the medium of locomotion, and a brief description of instrumentation needed for the definition's implementation

- quantitative definition of the mission

- brief description of the data bank

- algorithms and evaluation procedures, including

    - tire rolling resistance
    - tire pull-slip characteristics
    - slope and obstacle performance
    - power and fuel consumption (rudimentary)
    - terrain damage due to rut-making and slip

EVALUATION PROCESS

The evaluation process is shown in a flow chart, Fig. 1. It encompasses three basic elements: mission, environment of locomotion, and hardware performance.

The flow chart suggests a sequence and the types of evaluation steps, which may be narrowed or expanded to suit specific needs, as discussed later.

Locomotion value criteria which guide vehicle candidate selection have been discussed and exemplified for a simple case, since they depend on numerous specific requirements, demand, supply, etc., presently unspecified. The milestones of the process are

1. Mission definition (Appendix A), which provides quantitative data re:

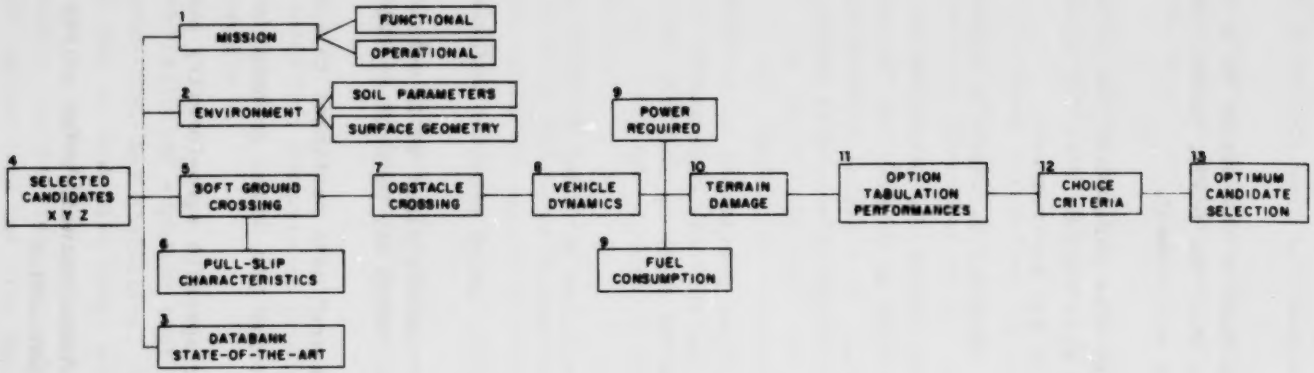

Figure 1. Flow chart for selection of optimum vehicle from a number of candidates. Simple deterministic approach in the first approximation

- functional requirements
- operational requirements

The first describes the size-form of the masses to be moved and the profiles of typical functions, so that the loads, geometries, and pertinent dimensions fit the constraints of environment.

The second describes in space-time parameters the postulated character of vehicle operations. This may also include cost and effectiveness of the operation within the given mission and environment.

2. Environment definition (Appendix B) which is expressed in

- mechanical soil properties, called the bevameter values, and additional terrain properties such as density and Terzaghian passive earth pressure coefficients. Statistical distribution of some of these parameters in spacio-temporal domain is needed for maximum reliability.

- geometrical terrain properties pertaining to terrain surface roughness, which affect ride comfort, directional stability, and speed (the problem subject to textbook solution is not considered here)

- characteristic obstacle profiles outlined by their envelopes, which affect vehicle mobility

3. The data bank (Appendix C), which provides information regarding

- power-weight-size-cost of vehicle class under consideration, and those of their components, which may be used in trade-off estimates

- engineering "state-of-the-art" data pertinent to automotive design

4. Vehicle candidate selection (1), which is based on

- hardware availability for specific agro-forestry purposes

and/or

- historical study of experience gained, which points to new avenues of approach to off-road locomotion

5. Soft and hard ground motion resistance of tires, which is determined in accordance with methods outlined in Appendix D, Parts I, II, and III.

6. Pull-slip characteristics of the vehicle, which define negociable slopes and draw-bar pull as well as traction efficiency (Appendix E).

7. Obstacle crossing performance, which is defined in the usual manner (1), as required to define vehicle's ability to cross fallen trees, irrigation ditches, etc.

8. Vehicle vibrations analysis, which is a textbook operation. For guidelines and references, see pertinent literature (1).

9. Power requirement definition for locomotion purposes which is evaluated according to standard techniques of automotive engineering (1, 2). For rudimentary treatment of the problems, see Appendix D, Part II. Fuel consumption determination is subject to the same standard techniques (1, 2). For a rudimentary approach, see Appendix D, Part II.

10. Terrain damage indices due to rut-making and slip, the least specified problem from an ecology viewpoint, which is treated from a purely mechanical angle of soil compaction and soil surface shear by vehicular traffic (Appendix F).

11. Options tabulation in numbers expressing vehicle performances, points 5 through 10, which are indexed as background information for decision (Appendix G).

12. Choice criteria and value judgments selection, which are flexible enough to encompass preferred values and "weight factors". Details available in literature (1, 3, 4).

13. Choice of the optimum candidate, which is tentatively illustrated by simple deterministic performance evaluation, both absolute and relative (Appendix G).

The process described attempts to provide the minimum of information for rational vehicle choice, which may be handled with a desk calculator as illustrated in Appendix D.

For a more sophisticated approach that includes cost-effectiveness, large number of scenarios, and statistical treatment of the problem, computerized programs may be (and have been) evolved from the method presented here. Such programs include additional performance and operational operational parameters, utility indices, reliability, maintenance, etc. (1), which were not included in the flow chart Fig. 1.

A general idea of a broad treatment of systems optimization is shown in Fig. 2. In this scheme the following information is included:

- XIII mission profiles composed of a number of terrain mixes which represent statistically significant scenarios (3)

- XIV integrated performance and utility indices (1) assumed for each case

- XV cost, maintenance, and reliability for selected mission and environment profiles (data bank)

- XVI operational analysis of cost-effectiveness and sensitivity analysis of parameters involved (1)

- XVII final choice based on the probability of success in mission accomplishment, in accordance with the postulated goals (1)

The evaluation process, Fig. 2, is in a sense an extension or supplement of the process described in Fig. 1.

The sequencing of operations in the evaluation process and the definition of their scope are subject to specific need and convenience. For example, Box 8, Fig. 1, Vehicle Dynamics, may include a study of vehicle vibration as a speed limiting factor and/or as a disturbance of vehicle stability, and steerability. It may also be evaluated before or instead of the assessment of soft ground crossing performance, if the latter is fixed for vehicle candidates - but the suspension characteristics cannot.

Details have been outlined in reference 1 and exemplified in references 3 and 4 which contain system optimization of specific vehicles, similar to that used in evaluation of lunar surface locomotion (1), and other terrestrial vehicles.

Appendices A through F provide a basic methodological element of such an evaluation.

SUMMATION AND RECOMMENDATIONS

The present Report, Phase One, provides the method and describes the evaluation process for selection of an optimum vehicle for industrial applications such as those in agro-forestry.

The method originally used on a number of occasions in the realm of lunar and terrestrial locomotion has been here re-evaluated, refined, expanded, and verified, within a wide scope of parametric analysis of vehicles equipped with pneumatic tires.

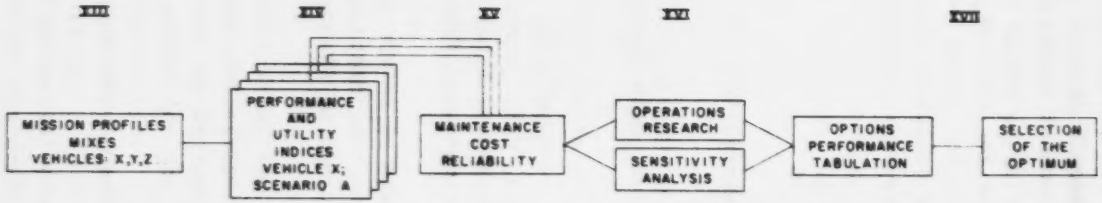

Figure 2. Flow chart for vehicle optimization from a number of candidates operating in a number of mission profile mixes. Using basic approach of flow chart, Figure 1, and including additional performance and utility indices, cost maintenance, etc., a statistical selection of the optimum is evolved to attain the best probability of overall success

It offers a good-to-fair confidence level for predictions of the order of merit of vehicles in off-the-road locomotion, for agro-forestry; it also may be considered as a basis for a broad operations research effort toward optimization of cost-effectiveness in off-road locomotion.

The present study has stressed the importance of accurate and/or statistically meaningful terrain measurements as well as the need for quantitative definition of mission and environment requirements.

It is essential that these points be the subject of careful consideration when providing numerical input data for Phase Two of the present study, whereby specific vehicles will be evaluated for planting and harvesting hybrid poplar cuttings on five-year rotation plantations.

REFERENCES

1. M.G. Bekker. Introduction to Terrain-Vehicle Systems. The University of Michigan Press, 1969.

2. J.Y. Wong. Theory of Ground Vehicles. John Wiley and Sons, 1978.

3. M.G. Bekker. Engineering optimization of terrain-vehicle systems - A case study of a concept analysis... . Report No. 10421 (LL 133) prepared for Land Locomotion Division, U.S. Army Tank Automotive Command, by AC - Electronics Defense Research Laboratories, General Motors Corp., U.S. Government Clearinghouse, 1969.

4. M.G. Bekker. Engineering optimization of remote control cross country vehicle concept. Report prepared for the Institute of Computer Sciences and Technology, National Bureau of Standards, U.S. Department of Commerce, April 30, 1973.

5. J.Y. Wong. Data processing methodology in the characterization of the mechanical properties of terrain. Journal of Terramechanics, 17(1): 13 - 41; 1980.

6. M.G. Bekker. Theory of Land Locomotion. The University of Michigan Press, 1st Ed. 1956, 2nd Ed. 1960.

APPENDIX A: MISSION DEFINITION

Mission definition encompasses a variety of requirements which must satisfy the user through terrain-vehicle system optimization.

FUNCTIONAL REQUIREMENTS

Functional requirements pertain to the specifics of the cargo or equipment (tools) to be carried, or trailed, which include

- form and dimensions of the envelope of cargo, equipment, etc.
- weight and CG location of the above-mentioned items
- other pertinent requirements such as towing forces, hitch geometry, driver's field of vision, etc.

OPERATIONAL REQUIREMENTS

Operational requirements may be formulated in a broad or narrow scope, depending on equipment under scrutiny. Usually, they pertain to the desirable, or acceptable

- cargo delivery rate, and/or
- equipment production rate
- constraints for alternate environmental and functional requirements
- schedules, travel plans, and timetables: stops, refuelings, distances, timing
- personnel number to be accommodated
- additional requirements: automation, night work, servicing of equipment, etc.

On the environmental side, the desirable or acceptable locomotion requirements are specified at least in terms of

- bevameter parameters for the "softest" and "weakest" soil
- maximum negotiable slopes
- maximum prohibitive envelopes of obstacles, fallen trees, irrigation ditches, etc., if any
- minimum speeds allowable by terrain roughness, furrows, etc.
- range of travel and operating distances
- refueling locations, etc.

MISSION PROFILES

Assumption of a single, general travel-work mission allows the optimization of the terrain-vehicle system only within a narrow spectrum of working conditions and constraints. To better approximate the desired optimum of locomotion, a number of specific mission profiles, or "sorties", is needed. These encompass

- representative sample of geological-environmental structures of the ground, in the areas of interest

If, for instance, the area to be traversed is covered with (1) peat moss, (2) sandy loam, (3) clayey loam, and (4) snow, then, theoretically, one may consider a number of combinations of travel through these areas during the vehicle's life cycle:

$$\binom{4}{2} \frac{4!}{2!(4-2)!} = 6$$

$$\binom{4}{3} \frac{4!}{3!(4-3)!} = 4$$

$$\binom{4}{4} \frac{4!}{4!(4-4)!} = 1$$

Totally, there are 11 combinations, or 15 if the single type of terrain is included. Usually, the probability of occurrence of some of these combinations is small. They may be thus eliminated, reducing the number of terrain mixes, for practical purposes.

In general, the formulation of terrain mixes in mission profiles is guided by

- terrain survey providing percentage of areas covered by various types of soil and their "coexistence" in terrains of interest

- climatological considerations which eliminate, or emphasize, temporal states of the ground

- selection of at least two profiles: one for the most difficult and the other for the easiest terrain. Then, the "in-between" profiles may be introduced as necessary.

In the final analysis, each mission profile is specified for selected length of travel, exemplified as shown in Table A1, where A_1 A_2 A_3, B_1 B_2

B_3, C_1 C_2 C_3 are the lengths of travel in percentages of the total distance $\sum A = \sum B = \sum C$.

Other considerations of mission profiles are available in reference A1.

Table A1

	Mission profile		
	A	B	C, etc.
Sandy loam	A_1	B_1	C_1
Clayey loam	A_2	B_2	C_2
Snow	A_3	B_3	C_3
Total length of travel	$\sum A$	$\sum B$	$\sum C$, etc.

REFERENCES

A1. M.G. Bekker. Engineering optimization of terrain-vehicle systems - A case study of a concept analysis... . Report No. 10421 (LL 133) prepared for Land Locomotion Division, U.S. Army Tank Automotive Command, by AC - Electronics Defense Research Laboratories, General Motors Corp., U.S. Government Clearinghouse, 1969.

APPENDIX B: ENVIRONMENT DEFINITION

When discussing vehicle Mission, it was shown that the medium of locomotion, called the Environment, cannot be separated from quantitative operational requirements. The "quantitized" Environment has thus become an essential, though often misrepresented, point of terrain-vehicle system optimization.

As in any engineering optimization, all the parameters involved, including terrain values, are expressed in dimensionally defined units compatible with applied mechanics. Terrain values applicable to off-road locomotion are of mechanical and geometrical character.

MECHANICAL GROUND PROPERTIES

Mechanical terrain value measurements, like most properties of materials, are based on analog testing. They are defined through simulation of vehicle action upon the ground by the action of instrument's plates.

The instruments, called the bevameters, have been exhaustively described in the international literature. For details and references see references B1 and B2.

A brief summation of principles involved and the recent developments in the discussed area are given below.

As it is often impossible and almost always impractical to simulate vehicle action upon soil by means of full-size replicas of loads and loading areas, smaller plates and loads are used as vehicle analogs, within the established rules for predictive accuracy (Appendix D) (B1, B2).

Since soils, snow, and to some extent turf, peat moss, and muskeg display two different types of mechanical properties, the minimum of two plate tests is required to predict vehicle performance.

The two different types of soil properties are cohesion and internal friction. The first involves the size of the loading area, the second - the load. These, in a sense conflicting factors, can be detected and resolved by two tests, each made with different plate size, as outlined in references B1 and B2. Then, the "cohesive" and "frictional" soil parameters may be separated and translated from the bevameter into vehicle action upon the ground, and the performance of the vehicle may be predicted using its scaled-down analog.

The two-plate test record consists of pressure p vs. sinkage z plot, which can be approximated for practical purposes by the exponential equation [B1] (B2):

$$[B1] \qquad p = [(k_c/b) + k_\phi]z^n$$

where k_c and k_ϕ are the "cohesive" and "frictional" moduli of soil deformation and n is the sinkage exponent.

Equation [B1], when plotted on log-log scale, represents for two plates having radii, or widths b_1 and b_2, two parallel lines (Fig. B1). Abscissae a_1 and a_2 yield two equations from which coefficients k_c and k_ϕ are determined; see Appendix D, Part III. The value of n is defined by the tangent of slope and of the lines.

The processing of p-z data measured in the field has been recently computerized by Canadian researchers (B3), so that the mean values and

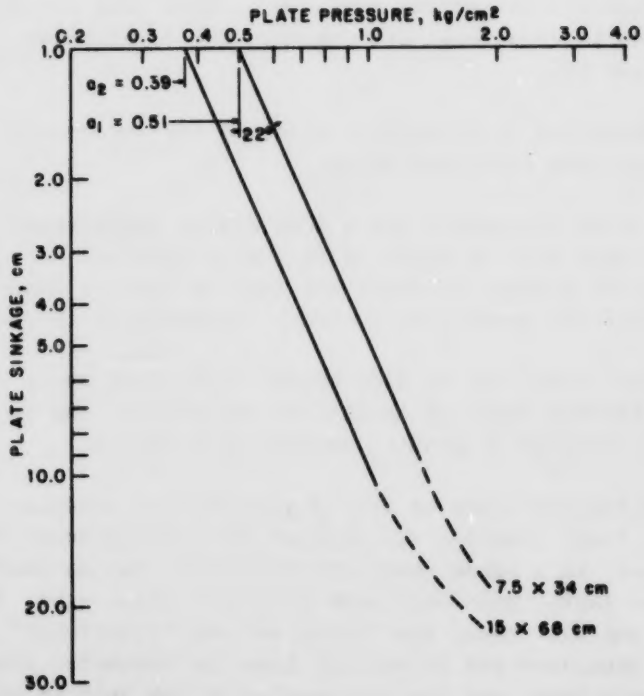

Figure B1. Standard bevameter plot measured in sandy loam by means of 7.5 cm × 34 cm and 15 cm × 68 cm plates (Tech. Univ. of Munich)

standard deviations of k_c, k_ϕ, and n values may be obtained with the minimum effort.

Equation [B1] involves soil parameters k_c, k_ϕ, and n related to vertical load-deformation characteristics p(z), which is responsible for motion resistance of the vehicle. Parameters related to the horizontal soil load-deformation $\tau(j)$, which produce the thrust propelling the vehicle and its appendages, are determined from the Coulomb-Mohr equation:

[B2] $\tau = c + p \tan \phi$

where c and ϕ are coefficients of soil cohension and friction, respectively, as determined in an unconfined shear test *in situ* under load p, with round and/or rectangular plates (B1, B2).

Computerized procedures for obtaining statistically meaningful c and ϕ data also have been developed in Canada (B3).

Additional soil parameters used in vehicle-terrain models, Appendix D, Parts II and III, and Appendix E, are soil density γ, slip coefficients K, or K_1, K_2, and Terzaghian coefficients of passive earth pressure K_c and K_γ (B1, B2). Soil density is irrelevant in "organic" ground.

To sum up, the empirical soil parameters which define mechanical ground properties for locomotion purposes are as follows:

Deformation	Parameters	Define
Vertical (penetration test)	k_c, k_ϕ, n, γ	Rolling resistance sinkage
Horizontal (shear test)	c, ϕ, γ, K*, K_c, K_γ	Thrust, drawbar pull, slope

*or K_1, K_2 (see Appendix E).

Field instruments for measuring parameters k_c, k_ϕ, n, c, ϕ, and γ are shown in Figs. B2 to B4. Figure B2 depicts an early German bevameter mounted on a tractor for agricultural purposes. Figure B3 shows a Canadian bevameter mounted on an all-purpose tracked vehicle. Figure B4 shows another Canadian bevameter, developed for forestry purposes. Note the power supply in the trailer.

All these instruments use plates for load-sinkage test and rotating rings for shear test. Some time ago, this writer devised a bevameter in which the plates were replaced with large diameter rigid cylindrical wheels. These were used instead of plates for sinkage-load measurements.

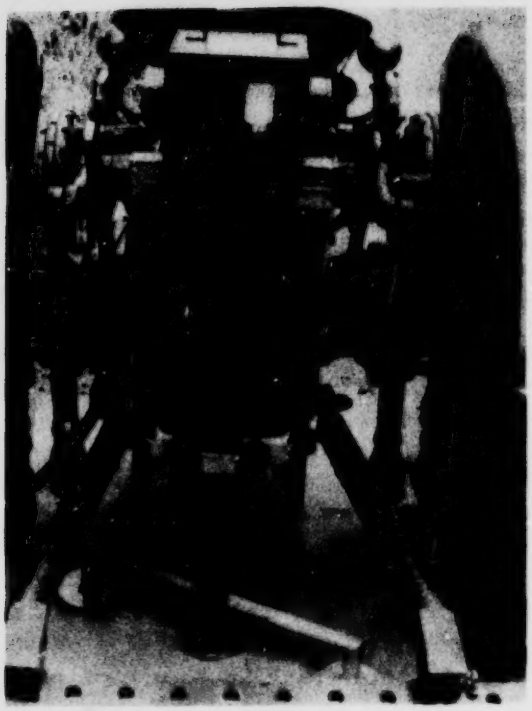

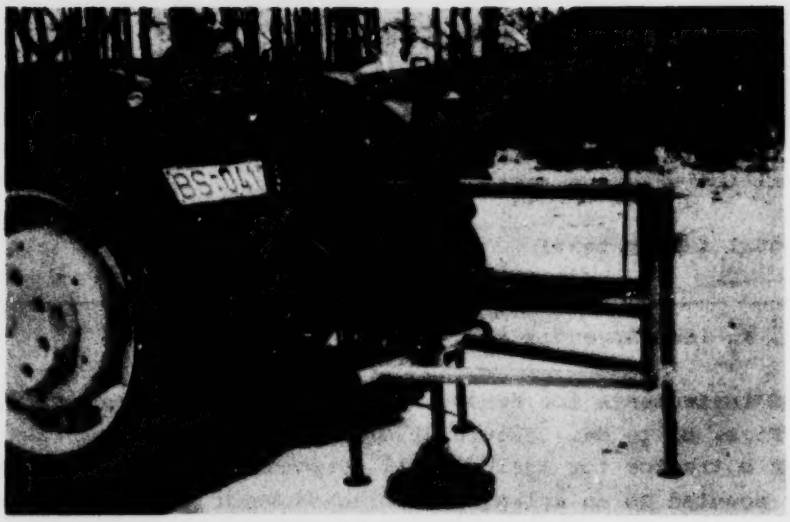

Figure B2. Bevameter instrumentation carried by an agricultural tractor (Braunschweig University)

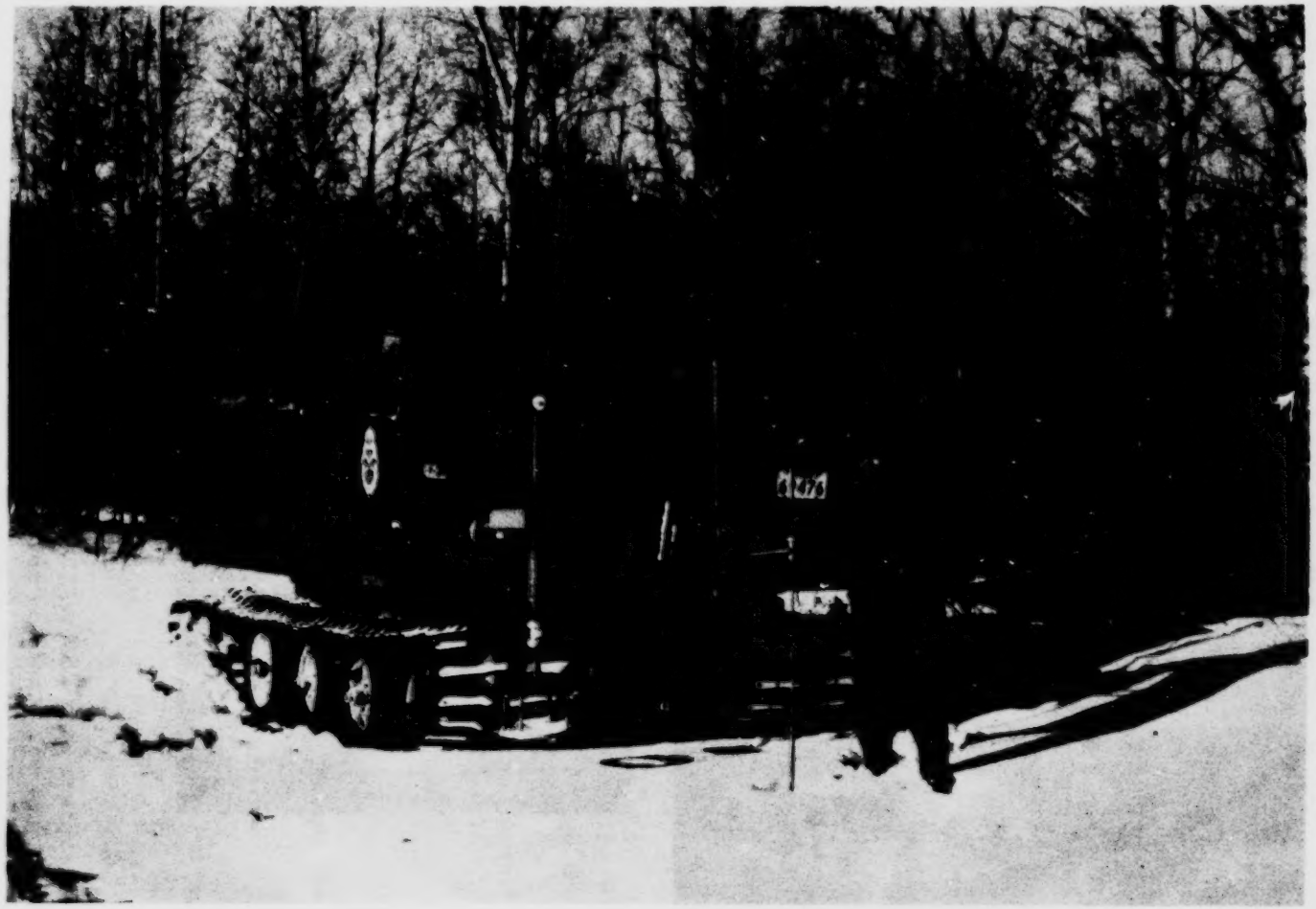

Figure B3. Canadian bevameter mounted on a tracked vehicle (Carleton University, Ottawa)

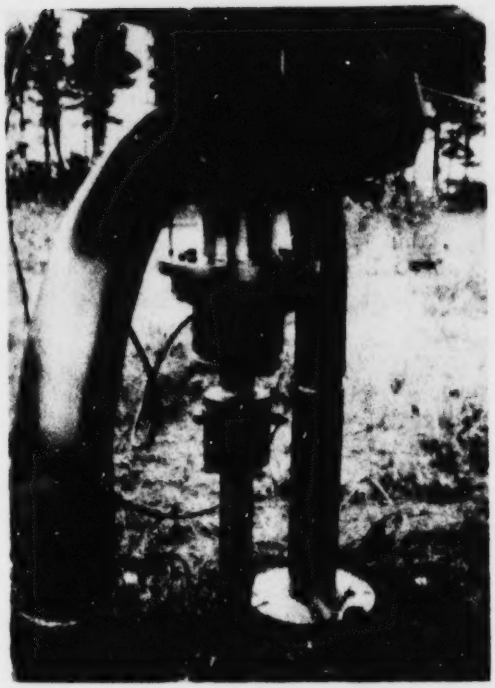

Shear Ring

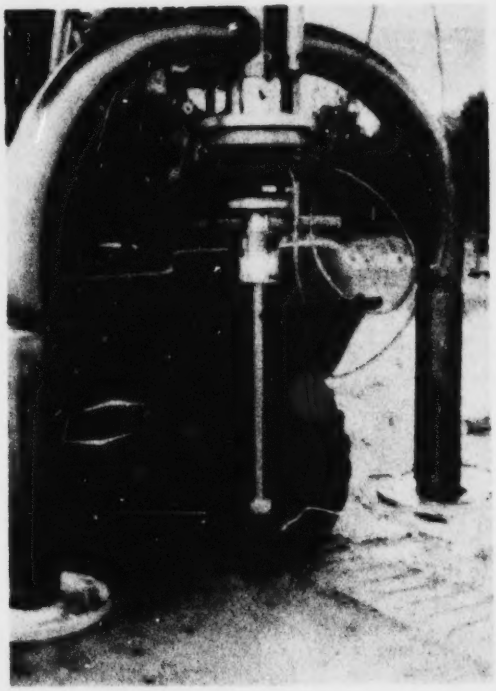

Penetration Plate

General view

Figure B4. Canadian bevameter PNFI, Petawawa National Forestry Institute (Canadian Forestry Service)

For soil shear test, another wheel with controlled slip was provided. Laboratory equipment of that type (Fig. B5) was described and successfully tested by the U.S. Army Land Locomotion Laboratory (B4). A prototype built later is shown in Fig. B6. The instrument was "overdesigned", however, and, though theoretically sound, was not much used. The British National Institute for Agricultural Engineering recently expressed an interest in pursuing this idea (B5).

Photographs and details of other bevameters of field and laboratory type are available in reference B1.

DISTRIBUTION OF SOIL VALUES

Distribution of soil values, both temporal and spatial, is needed for statistical evaluation of vehicle performance. Figures B7 and B8 illustrate the character of temporal distribution which is important for seasonal operations in agriculture and forestry. Figure B9 shows the spatial distribution of soil values, due to uneven moisture content caused by water level, or proximity of lakes, rivers, etc.

Peculiarities of terrain, such as

- depth of snow cover
- geometry and topology of swamp patches, or other surface obstacles

require specification, for safety and efficiency of vehicle operations (B1).

GEOMETRICAL GROUND SURFACE PROPERTIES

Geometrical ground surface properties include the size and the form distribution of

- fallen trees, or other obstacles to be negotiated
- furrows
- slopes
- ditches

In addition, whenever speed, steerability, and ride comfort enter the picture,

- the power spectral density (PSD) of the terrain is needed for typical, or at least critical, areas (B1).

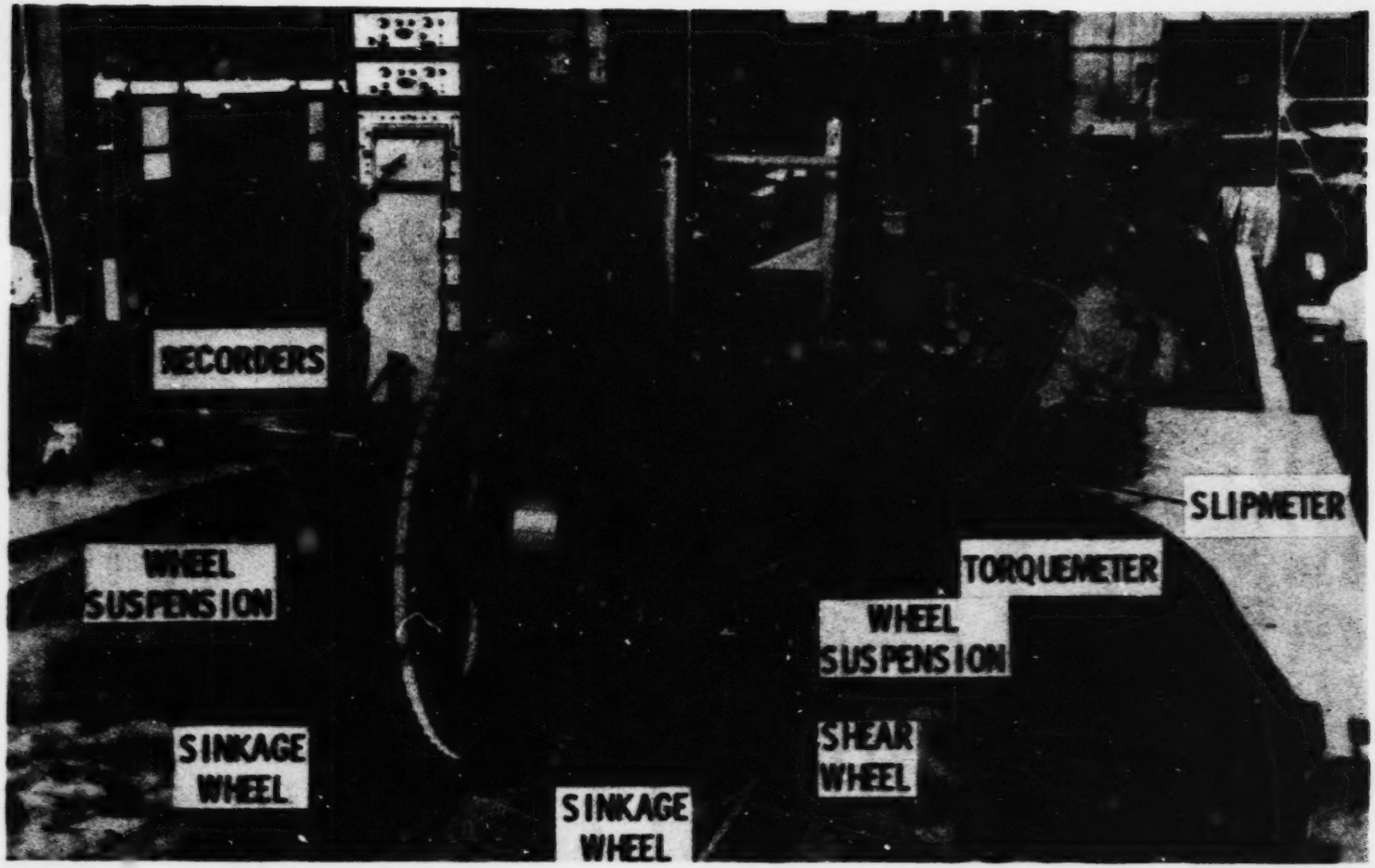

Figure B5. Land Locomotion Laboratory, wheeled-type bevameter for continuous recording of load sinkage p(z) relationship. Laboratory prototype (U.S. Army, Detroit Arsenal)

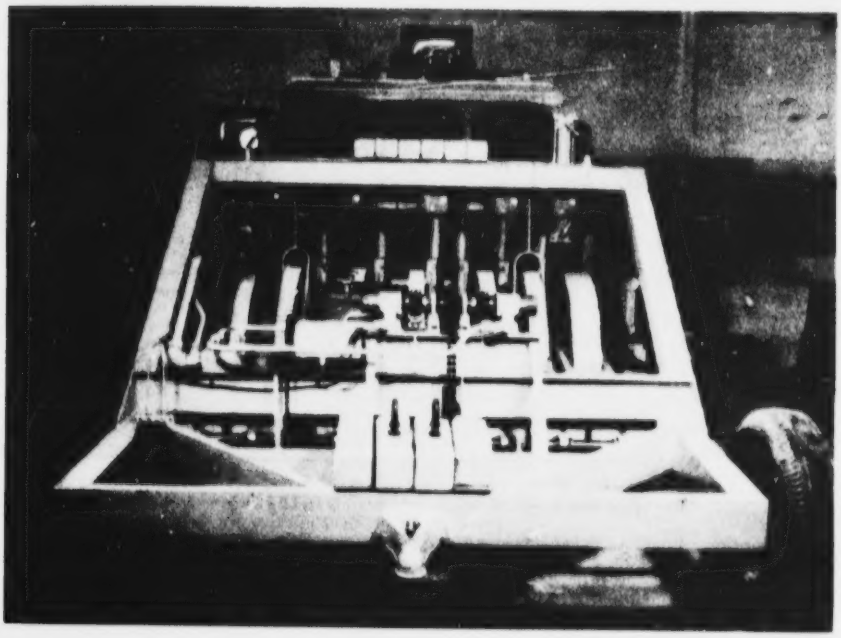

Figure B6. Rear view of the working prototype of the wheeled-type bevameter, Figure B5, developed for the Detroit Arsenal

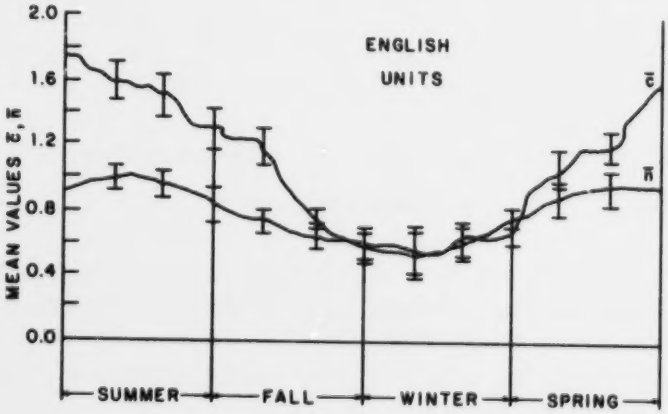

Figure B7. Statistical distribution of cohesion c and sinkage exponent n obtained during one-year period. Adapted from British measurements of an experimental field (Road Res. Laboratory)

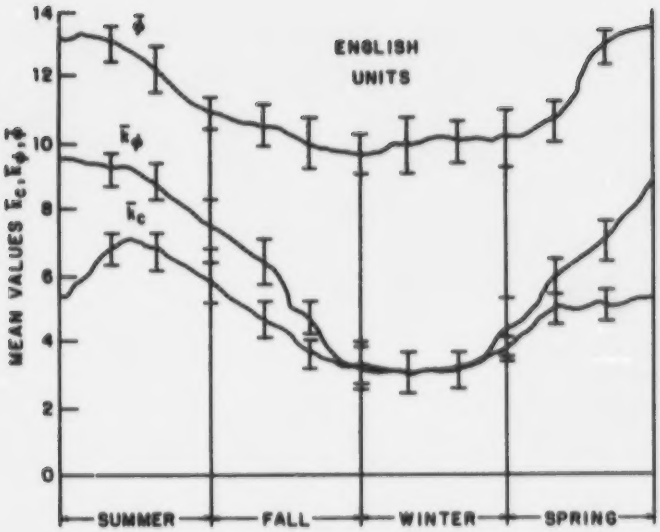

Figure B8. Statistical distribution of coefficients of sinkage k, and the angle of friction ϕ. Adapted from British measurements (Road Res. Laboratory)

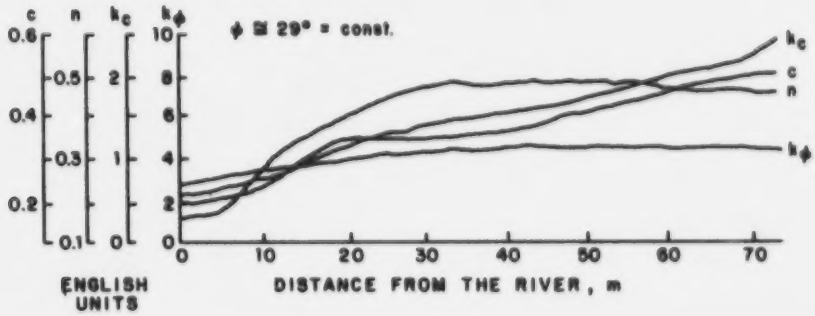

Figure B9. Statistical distribution of soil values k_c, k_ϕ, c, and n as a function of the distance from a river. Adapted from measurements by the Land Locomotion Laboratory, Detroit Arsenal

Figure B10 shows a sample of environmental input data concerning solid obstacles. Figure B11 illustrates ditch envelopes distribution which is relevant to locomotion failure. Vehicle performance on such obstacles is evaluated in accordance with standard procedures (B1).

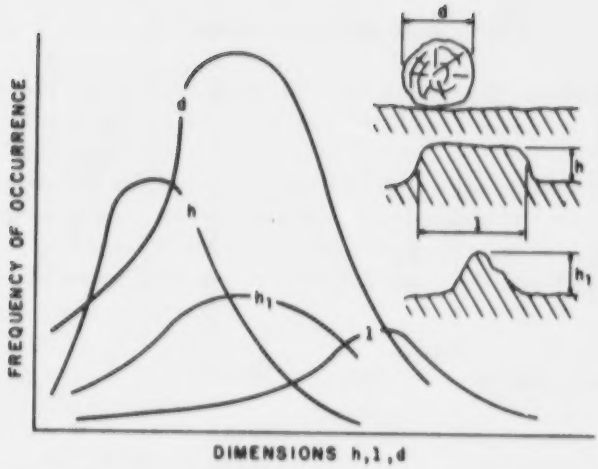

Figure B10. Sample of hypothetical distributions of obstacle dimensions

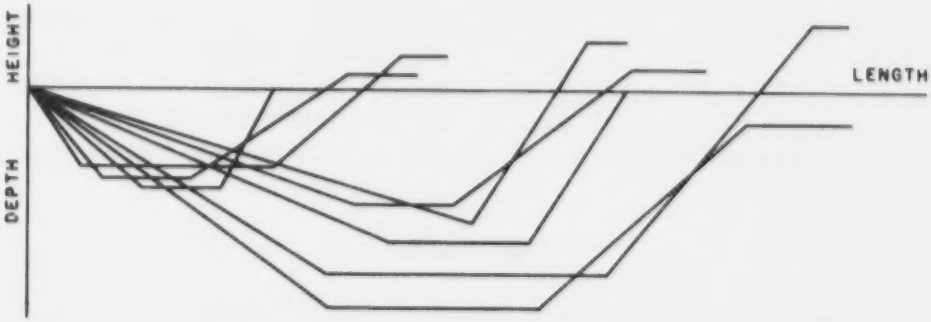

Figure B11. Sample of hypothetical distribution of critical ditch envelopes

Figure B12 shows statistics of slope distribution, and Fig. B13 the power spectral density (PSD) for an agricultural field, before and after ploughing. Note the dynamic response of the input at approximately 6.0 m^{-1} frequency, due to the corresponding to that frequency furrows spacing (B1).

Power spectral analysis of vehicle dynamics is a textbook operation which requires extensive computer programming. It is not considered in this report.

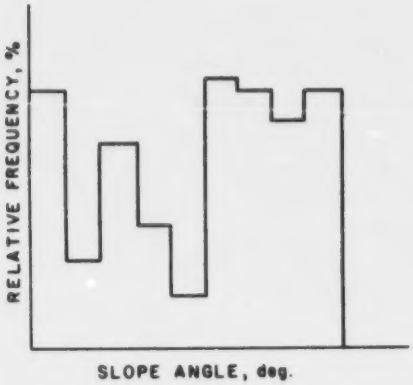

Figure B12. Sample of a hypothetical slope angle distribution

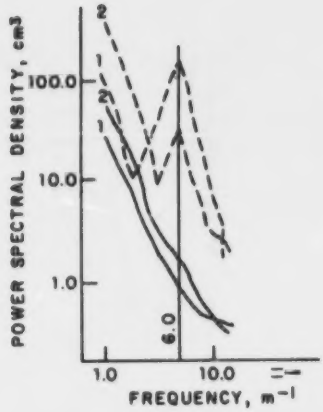

Figure B13. Two agricultural fields 1 and 2 (solid lines) show similar Power Spectral Density functions before ploughing. The functions also show similar response at frequency ~6 m^{-1}, after ploughing (dashed lines), which is due to similar spacing of the furrows (Braunschweig University)

REFERENCES

B1. M.G. Bekker. Introduction to Terrain-Vehicle Systems. The University of Michigan Press, 1969.

B2. J.Y. Wong. Theory of Ground Vehicles. John Wiley and Sons, 1978.

B3. J.Y. Wong. Data processing methodology in the characterization of the mechanical properties of terrain. Journal of Terramechanics, 17(1): 13 - 41; 1980.

B4. F. Pavlics. Bevameter 100 - A new type of field apparatus for measuring locomotive stress-strain relationships in soils. First Int. Conf. on Terrain-Vehicle Systems. Proceedings Minerva Tecnica, Torino, 1961.

B5. D. Gee-Clough, et al., Departmental Notes DN/T/899/01002 and DN/T/917/01002, 1978; 1979, Personal communication.

APPENDIX C: DATA BANK

Accumulation of catalogue data of equipment and vehicle components usually is not sufficient in systems evaluation.

For trade-offs and alternative solutions, some sort of generalization of such data is required. As an example, take maps of tire performance, Appendix D, Part II, Figs. D18, D19, D20, where a number of tire parameters such as inflation pressure, size, contact area, rolling resistance, etc., are plotted on the same graph.

Similar plots may be construed for complete vehicles. These readily produce in a comparative form

- weight-load-power relationship
- payload-curb weight-size characteristics
- form-size-power constraints, etc.

The variety of such generalized information is practically unlimited, and is abundantly illustrated in the literature (C1, C2).

The convenience of having prepared the data bank in such a form is obvious as it readily illustrates the "state-of-the-art". Information of that type re engines and power trains is of particular importance.

REFERENCES

C1. M.G. Bekker. Introduction to Terrain-Vehicle Systems. The University of Michigan Press, 1969.

C2. M.G. Bekker. Engineering Optimization of Terrain-Vehicle Systems - A Case Study of a Concept Analysis... . Report No. 10421 (LL 133) prepared for Land Locomotion Division, U.S. Army Tank Automotive Command, by AC - Electronics Defense Research Laboratories, General Motors Corp., U.S. Government Clearinghouse, 1969.

APPENDIX D. ROLLING RESISTANCE OF PNEUMATIC TIRES

PART I. UNYIELDING GROUND, OR HARD SURFACE ROAD

A practical engineering method for evaluation of rolling resistance of elastic tires was proposed some time ago by this writer and others (D1-D7). It was conceived as a tool for parametric evaluations and optimization of vehicle performance through a semi-empirical approach, as no practical rigorous solutions have ever been made available.

The initial success of the approach led to further refinement and studies of the method, from the viewpoint of its sensitivity and resolution, which led to small changes and improvements.

Numerous computations and comparisons with experiments, extending over a wide range of tire loads, inflations, and sizes sampled here, in numerical examples, hopefully illustrate the nature of the available solutions and also suggest areas for further development of the method.

It is pertinent to note that the method was primarily conceived for evaluation of Off-road Locomotion, where high speeds are the exception rather than the rule. In this context, tire deformation resistance f_t, with which this paper also is concerned, is one of the three components of terrain-induced resistance, the remaining two being resistances f_c due to ground compression and f_b due to horizontal ground deformation (Fig. D1).

Since tire rolling resistance f_t does not change for practical purposes within the speed range up to approximately 40 mph (64 km/h), the method does not consider the speed effect. Also, changes in "cold-warm" conditions do not necessarily apply though might be included if so desired.

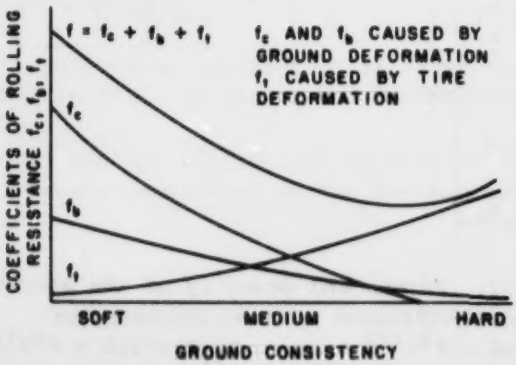

Figure D1. Components of tire motion resistance f, on the ground of varying consistency

The calculated rolling resistance is based on empirical tire input data produced on a static test rig. Thus some attention may be needed when comparing the calculated values with measurements performed on the rolling test stand, or road.

TIRE MODEL

Forces, pressures, tire geometry, and deflection are shown in Fig. D2, with trigonometric assumptions defining dimensions and parameters of the ground contact area.

The tire is assumed to be made of idealized, thin-walled pliable material which does not necessarily correspond to reality. The practicality of this assumption naturally depends on the acceptability of results produced as discussed in this paper.

Input data include: W = tire load; p_i - inflation pressure; A - ground contact area; p_g - average ground pressure; b_0 - width of the ground

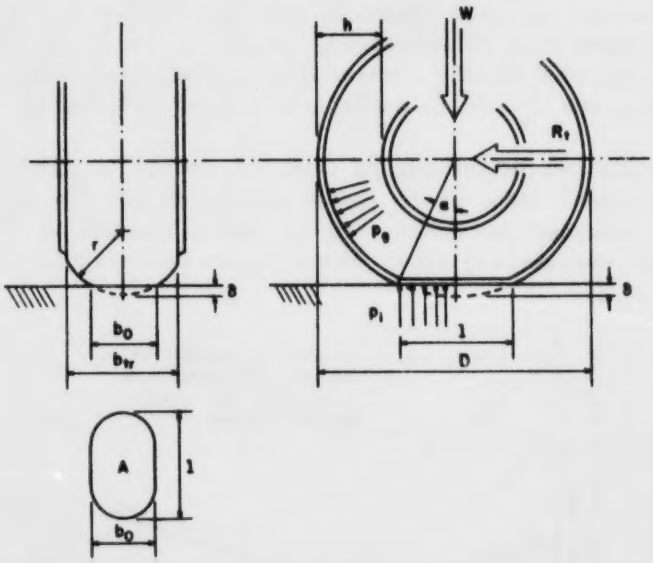

Figure D2. Forces and geometry of the assumed tire model:

$l = 2(D\delta - \delta^2)^{1/2}$ $\qquad$ $b_{tr} > 2(2r\delta - \delta^2)^{1/2}$

$b_0 = 2(2r\delta - \delta^2)^{1/2}$ $\qquad$ $p_g = W/A$

$\lambda = A/lb_0$ $\qquad$ $f_t = R/W$

contact area; l - length of the ground contact area; λ - "ellipticity" coefficient of the ground contact area; D - tire diameter; b - tread width; h - section height; r - tread radius.

Output data calculated are: f_t - rolling resistance coefficient; σ - deflection.

Data bank includes Deflection Charts as shown in Fig. D3, adapted from charts by Goodyear Tire and Rubber Co.

Information, Fig. D3, leads to plots of $p_i(p_g)$ as shown in Fig. D4 for early measurements of a 12.00 - 18 tire (D8).

Some irregularity of the pattern, and the unavailability of description of the method by means of which the input data were collected, suggest a less sophisticated approach than the automatized plots of Goodyear charts.

In general, it is important to note that the $p_i(p_g)$ lines are, for practical purposes, straight and parallel or nearly parallel, as further shown by this writer in Figs. D4 and D5, for a variety of tires.

Figures D4 and D5 were traced with the aid of catalogues and partially with the help of Goodyear Deflection Charts. In the latter case, there was no problem. In the first case, often only two points were available, which may be considered insufficient for interpolation. However, the parallelism of the lines was always strongly accentuated, which minimized the error.

A few lines shown in Fig. D4, which slightly deviate from the discussed pattern, pertain to catalogue data of the same tire size but different tread design and ply number. This indicates the need for discrimination of the detail of tire structure.

In any case, if Deflection Charts such as shown in Fig. D3 are available, then data shown in Figs. D4 and D5 are unnecessary.

Note that the old concept of "carcass stiffness" and the related functions of $p_i(p_g)$ became immaterial as the Deflection Charts provide a complete data bank.

MATHEMATICS OF TIRE EVALUATION

Mathematical relationships between the described tire parameters were elaborated in references D1 through D7. The working summary of equations used was abstracted below.

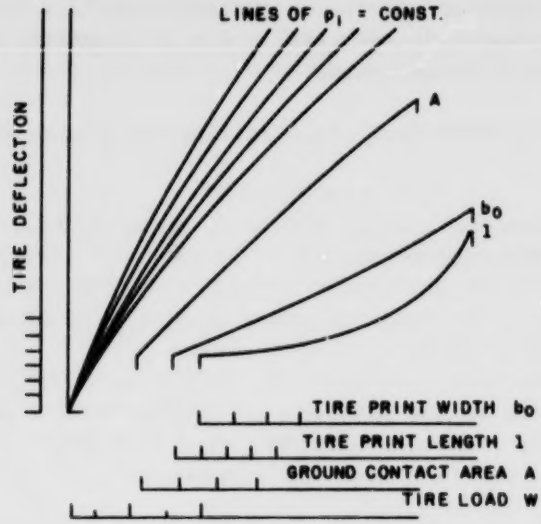

Figure D3. Generalized Deflection Chart for a pneumatic tire, plotted on a test stand

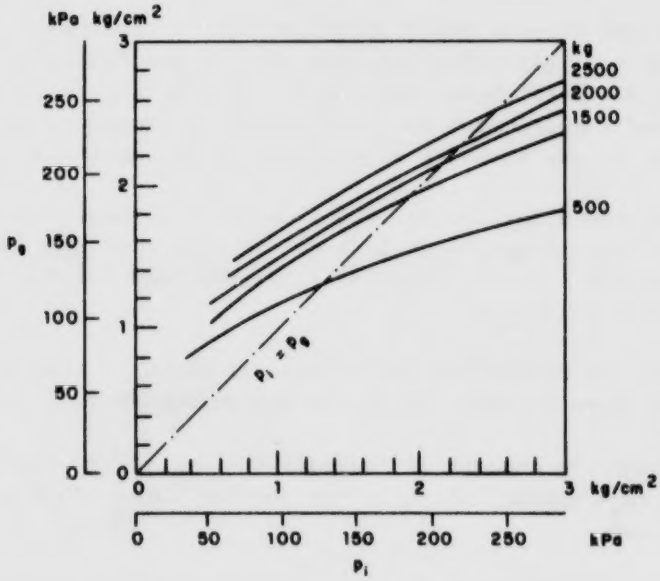

Figure D4. Early example of the measured inflation pressure P_i vs. average ground pressure p_g, for a 12.00 - 18 tire

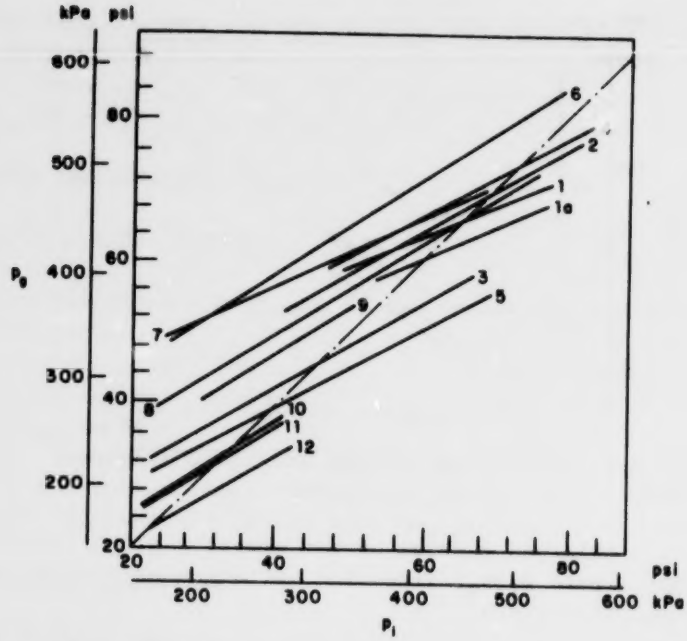

Figure D5. Lines of $p_i(p_g)$ for various tires (see Fig. D6 for enlarged portion of this graph):

1, 1a, 14.00 - 25 @ 8000 and 1000 lb (4.4 kN)
2, 18.00 - 25 @ 20000
3, 20.5 - 25 @ 12000
4, 24.00 - 35 @ 35000
5, 36.00 - 51 @ 40000
6, 33.5 - 39 @ 50000
7, 37.5 - 51 @ 60000
8, 26.5 - 29 @ 10000
9, 29.5 - 29 @ 20000
10, 8.50 - 16 @ 800
11, 8.50 - 16 @ 500
12, 67 × 34 - 25 @ 7000

Tire Deflection

Tire deflection calculations start with the solution of the following equation, by iteration:

[D1] $$(2r\sigma - \sigma^2)(D\sigma - \sigma^2) = (W/4\lambda p_g)^2$$

where $p_g = W/A$ and $\lambda = A/b_0 l$. Determination of λ requires the measurement of A, l, and b_0. A is the "elliptical" footprint of the tire, and l and b_0 are the axes of the ellipse (Fig. D2).

The footprint, however, usually consists of a series of disjointed lug and tread prints. The circumscribing of such a patterm may lead to sizeable error in the determination of pertinent parameters. To minimize that error, a few prints may be measured upon rotating the tire 5 to 10°.

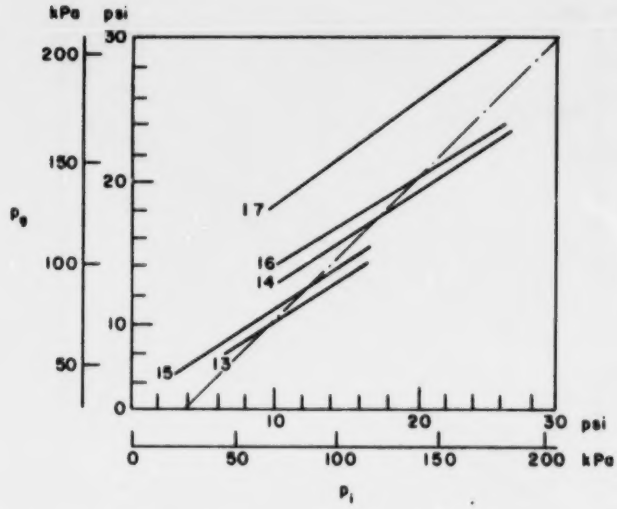

Figure D6. Enlarged portion of the graph, Fig. D5, which shows approximate $p_i(p_g)$ lines for inflation pressures lower than 20 psi (137.9 kPa):

13, 67 × 34 - 25 @ 4000 lb (17.8 kN)
14, 67 × 34 - 25 @ 7000
15, 7.00 - 16 @ 500
16, 11.2 - 28 @ 2000
17, 9.00 - 20 @ 1000

For an ideal ellipse, $\lambda = 0.78$. Modern tires for automobiles and cylindrical tires of "terratire" type have $\lambda \approx 1$. In general, values of $\lambda = 0.78$ to 1.0 may be encountered.

The solution of Equation [D1] is sensitive to λ and p_g as these values enter in the second power. It is suggested that the statistical approach would improve the accuracy of predictions by defining their limits.

Equation [D1] is valid if the calculated deflection σ produces

[D2] $$b_0 = 2(2r\delta - \delta^2)^{1/2} < b_{tr}$$

If the inequity [D2] is not satisfied, σ is calculated from the formula

[D3] $$\delta = \{D^2 - [D^2 - (4/2\lambda b_{tr} p_g)^2]^{1/2}\}/2$$

Note that Equations [D1] and [D3] may be conveniently transformed, assuming

$$p_g = W/A$$

whenever complete Deflection Charts are available.

Equation [D3] is used for determining the value of δ for cylindrical tires. In that case $\lambda = 1$, and

$$2b_{tr}(D\delta - \delta^2)^{1/2} = (W/p_g)^2 = A^2$$

which produces the solution:

[D4] $$\delta = \{D - [D^2 - 4(W/2b_{tr}p_g)^2]^{1/2}\}/2$$

Angle α, which describes the length of the ground contact area (Fig. D2), is measured in degrees:

[D5] $$\alpha = \cos^{-1}[(D - 2\delta)/D]$$

Equations [D1] through [D5] define all the parameters involved in the definition of the rolling resistance of pneumatic tires, except for one empirical value denoted by ε which will be discussed and determined later.

Rolling Resistance Coefficient

The rolling resistance coefficient may be thus expressed as follows:

[D6] $$f_t = [3.581b_0D^2p_g\varepsilon(0.0349\alpha - \sin 2\alpha)]/W\alpha(D - 2\delta)$$

Equation [D6] is based on the assumption that f_t is primarily generated by the compressing of the tire on its leading contact edge with the ground. The compression energy, however, may be partially recovered at the rebounding, trailing edge of the tire.

Practical rigorous solution of this process is lacking because of the complexity and diversity of tire structures and of their varying mechanical properties due to the changes of loads and inflation pressures, applicable within safety limits and design requirements.

Since in parametric analyses all these variations must be included, there was no choice but to resort to an empirical solution.

Coefficient of Energy Recovery

The coefficient of energy recovery ε shown in Equation [D6] reflects such a solution:

[D7] $$\varepsilon = 1 - \exp(-k\delta/h)$$

ε varies with tire deflection δ in reverse manner. For large deflec-

tions (high loads, low inflation), it tends to approach 1. For small deflections (low loads, high inflation), it approaches very small values, which is in agreement with intuition and experience: the softer the tire the smaller the energy recovery factor ε, and vice versa.

Numerical values of parameter k in Equation [D1] have been tentativel established for a large number of a variety of tires, whenever pertinent data were available.

Ideally, each tire type, or tires "families" may have a specific k-value. This ought to be checked for greater predictive accuracy. Thus far, several computations performed show that ε does not change much, even within such a great tire span as the bicycle-to-earthmover tire spectrum. It does change, however, as could be expected, for radial tires, when compared with biased and belted ones. Experience presently available yields the following values:

conventional tires, $k = 15$
radial tires, $k = 7$

Examples verifying these values are shown in the next sections.

Before proceeding further, however, it should be noted that deflections δ calculated by means of Equations [D3] and [D4] correspond to the idealized tire as shown in Fig. D2. In the case of pliable, thin-walled tires, the ideal converges with the real: the calculated values may be close to real ones. But in practice this is seldom the case.

Generally speaking, deflection δ in Equations [D3] and [D4] is a tran sient calculatory value introduced for the purpose of determining rolling resistance f_t.

NUMERICAL EXAMPLES AND THEIR VERIFICATION

Numerical examples referred to below were selected from a variety of tire evaluations computed by means of a desk calculator, HP-35.

In most cases English units were used because of the input data predominantly available in these units. For the convenience of the reader, the results were converted into SI units.

Computerized programs also were tried with success but have not been described in this paper because of proprietary character.

All the computations were compared with experimental data. Often, however, the latter were not properly documented so that it was difficult to ascertain if the discrepancies between predicted and measured value were due to the inaccuracy of the method, or deficiency of the experiment.

Bicycle Tire, 27 × 1.25, "Schwinn Puff"

This example shows extrapolations needed for tire evaluation because of incomplete input data, in one respect, and redundant, in the other.

Ground contact areas were given for three different loads at a constant inflation pressure, p_i = 70 psi (482.6 kPa), as tabulated below:

W lb	(kN)	A in.^{2}	(cm^2)
355.8	(1.6)	1.25	(8.1)
711.4	(3.2)	1.90	(12.3)
1067.5	(4.7)	2.50	(16.1)

However, the rolling resistance f_t was measured only for W = 150 lb (670 N) at two inflation pressures:

p_i psi	(kPA)	f_t meas.
70	(482.6)	
		0.0065 - 0.0059
95	(655.0)	

The values of f_t were determined by a deceleration test with 15 min allowed for tire warmup, and with an undetermined allowance for inflation pressure rise. Thus the measured rolling resistance did not entirely reflect conditions assumed for calculation purposes.

In order to determine the missing input data for W = 150 lb, a graph (Fig. D7) was constructed. It yields A = 1.8 in.^{2} (11.6 cm^2). Hence at p_i = 70 psi (482.6 kPa) the ground pressure p_g = 150/1.8 = 83.33 psi, or 574.6 kPa.

The ground pressure p_g at 95 psi (655.0 kPa) for which the f_t-value also was measured was determined from a graph (Fig. D8), based on parallel

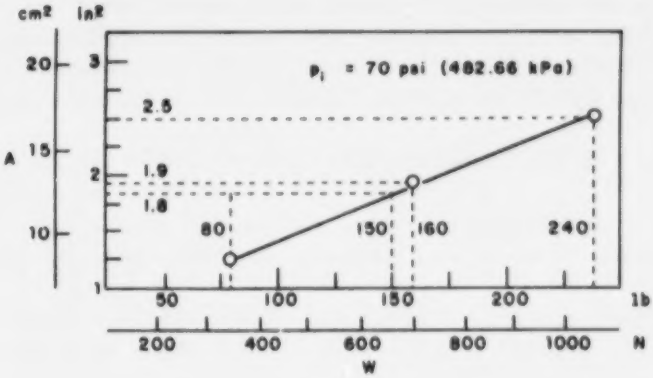

Figure D7. Load-ground contact area of a 27 × 1.25 "Schwinn Puff" bicycle tire

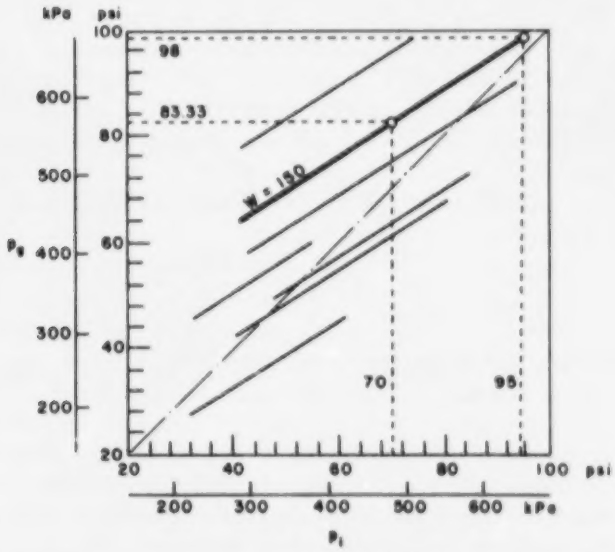

Figure D8. Extrapolation of the ground pressure value for a 27 × 1.25 bicycle tire at 95 psi (655.0 kPa) inflation pressure

lines of $p_i(p_g)$ plotted for other tires on Figs. D5 and D6. The bicycle tire follows the same trend shown in phantom lines and passes through the point with coordinates 70 and 83.33. The intersection of the ordinate 95 with line 150 yields p_g = 98 psi (675.7 kPa).

Thus the complete tire data input needed for calculation of rolling

resistance f_t for p_i = 70 psi and p_i = 95 psi at the load W = 150 lb is

p_i psi (kPa)	A in.^{2} (cm^2)	p_g psi (kPa)
70 (482.6)	1.8 (11.6)	83.33 (574.6)
95 (655.0)	1.53 (9.9)	98 (675.7)

From the catalogue: D = 27 in. (68.6 cm); b_{tr} = 1.1 in. (2.79 cm); h = 1.3 in. (3.3 cm); r = 1.2 in. (3.0 cm).

Since λ was not given, calculations were performed for the assumed min-max values of 0.78 - 0.9.

The results of step-by-step computations were reproduced below. The numbers of equations listed in the preceding section which were used at the given step are also given.

p_i psi (kPa)	W lb (N)	λ	δ [D1]	b_0 [D2]	α [D5]	ε [D7]	f_t [D6]
70 (482.6)	150 (670)	0.78	0.0729	0.8238 < 1.1	5.9570°	0.5688	0.0062
95 (655.0)	150 (670)	0.90	0.0631	0.7690 < 1.1	0.5418°	0.5172	0.0045

The results calculated and measured were summarized in Table D1. Considering the uncertainties due to incomplete input and measurement error, additional test data of f_t performed on 16 tires of the same size but different manufacturers (U.S. and Japanese) were also quoted (D10).

Table D1. Rolling resistance of 27 × 1.25 tire

		f_t		
W (lb)	p_i (psi)	Calc. (Schwinn)	Meas. (Schwinn)	Meas. (Av. of 16 tires)
150	70	0.0045 - 0.0062	0.0065	0.0055 - 0.0093
	95	0.0037 - 0.0051	0.0059	0.0049 - 0.0079

Bicycle Tire, 26 × 1.375

This example was calculated in order to further corroborate the result obtained with the 27 × 1.25 tire.

Input data were as follows: W = 150 lb (667 N); p_i = 50 psi (344.75 kPa); A = 2.23 in.^{2} (14.39 cm^2); p_g = 67 psi (462 kPa); D = 26 in.

(66 cm); b_{tr} = 1.4 in. (3.6 cm); h = 1.4 in. (3.6 cm); r = 1.3 in. 3.3 cm^2).

Measurements of rolling resistance were performed on a steel roller and yielded f_t = 0.0075. However, deceleration tests produced f_t = 0.0109 - 0.0079.

Since λ was not available, calculations were performed again, for two values:

λ	δ [D1]	b_0 [D2]	α [D5]	ε [D7]	f_t [D6]
0.78	0.0889	0.9449 < 1.4	6.7045°	0.6142	0.0076
0.90	0.0769	0.8810 < 1.4	6.2351°	0.5613	0.0055

The result was summarized in Table D2.

Table D2. Rolling resistance of 26 × 1.375 tire

f_t calc.	f_t meas.
0.0076 - 0.0055	0.0109 - 0.0079 (deceleration test)
	0.0075 (roller test)

Table D2 shows that the λ-value is close to 0.8, fitting the measured data.

Earthmover Tire, 29.5 - 29

This tire, being many times larger than the bicycle tire, presents a good case for testing the reliability of the discussed method.

Input data are: W = 16500 lb (7340 N); p_i = 20 psi (137.9 kPa); A = 510 $in.^2$ (3290.3 cm^2); p_g = 16500/510 = 32.35 psi (233.05 kPa); b_0 = 23.4 in. (59.4 cm); l = 22.8 in. (57.9 cm); λ = 510/23.4 × 22.8 = 0.95; D = 77.4 in. (196.6 cm); h = 24.2 in. (61.5 cm); r = 40 in. (101.6 cm); B_{tr} = 28 in. (71.1 cm).

Measurements of rolling resistance were performed on a steel roller and showed f_t = 0.0185 - 0.0230. Calculations yield

$$\delta = 1.7440 \qquad [D1]$$
$$b_0 = 23.3648 < 28 \qquad [D2]$$

$$\alpha = 17.2663^\circ \qquad [D5]$$
$$\varepsilon = 0.6607 \qquad [D7]$$
$$f_t = 0.0182 \qquad [D6]$$

The result was summarized in Table D3.

Table D3. Rolling resistance of 29.5 - 29 tire

f_t calc.	f_t meas.
0.0182	0.0185 - 0.0230

Automobile Tire, 7.00 - 15

This tire provided further verification of the method for intermediate sizes and lower inflation pressure.

Input data: W = 1100 lb (4892.8 N); p_i = 26 psi (179.27 kPa); A = 42 in.^{2} (271 cm^2); p_g = 26.19 psi (180.58 kPa); b_0 5.4 in. (13.7 cm); l = 8.7 in. (22.1 cm); λ = 0.89; D = 29.8 in. (75.7 cm); b_{tr} = 5.4 in. 13.7 cm); h = 7.4 in. (18.8 cm); r = 7.5 in. (19.0 cm).

Rolling resistance measurements showed f_t = 0.0121 - 0.0149. Calculations yield

$$\delta = 0.5747 \qquad [D1]$$
$$b_0 = 5.7585 < 5.4 \qquad [D2]$$
$$\therefore \delta = 0.5165 \qquad [D3]$$
$$\alpha = 15.1301^\circ \qquad [D5]$$
$$\varepsilon = 0.6490 \qquad [D7]$$
$$f_t = 0.0147 \qquad [D6]$$

This example (Table D4) illustrates the effect of the tread width b_{tr} upon the coefficient of rolling resistance.

Table D4. Rolling resistance of 7.00 - 15 tire

f_t calc.	f_t meas.
0.0147	0.0121 - 0.0148

Automobile Tire, 9.00 - 20

This tire provides another example.

Input data: $W = 3400$ lb (15.123 kN); $p_i = 65$ psi (448.17 kPa); $A = 63.3$ in.^{2} (408.4 cm^2); $p_g = 54.5$ psi (372.33 kPa); $b_0 = 6.9$ in. (17.5 cm); $l = 10.4$ in. (26.4 cm); $\lambda = 0.88$; $D = 40.59$ in. (103.1 cm); $b_{tr} = 7.8$ in. (19.8 cm); $h = 10.29$ in. (26.1 cm); $r = 15$ in. (38.1 cm). Measurements showed $f_t = 0.0111 - 0.0117$. Computations:

$$\delta = 0.5156 \qquad [D1]$$
$$b_0 = 7.7980 < 7.8 \qquad [D2]$$
$$\alpha = 12.9426^\circ \qquad [D5]$$
$$\varepsilon = 0.5284 \qquad [D7]$$
$$f_t = 0.0115 \qquad [D6]$$

Comparison between calculated and measured data is shown in Table D5.

Table 5. Rolling resistance of 9.00 - 20 tire

f_t calc.	f_t meas.
0.0115	0.0111 - 0.0117

Truck Tire, 10.00 - 20

This tire is not significantly different from the 9.00 - 20 tire evaluated in the previous example. Hence, the present example illustrates the sensitivity of the method.

Input data: $W = 4000$ lb (17.792 kN); $p_i = 70$ psi (482.65 kPa); $A = 68.5$ in.^{2} (441.9 cm^2); $p_g = 58.39$ psi (402.6 kPa); $b_0 = 7.7$ in. (19.6 cm); $l = 9.9$ in. (25.1 cm); $\lambda = 0.8986$; $D = 41.34$ in. (105 cm); $b_{tr} = 8.06$ in. (20.5 cm); $h = 10.67$ in. (27.1 cm); $r = 15.5$ in. 39.4 cm).

Test data showed rolling resistance $f_t = 0.0139 - 0.0122$. Calculations yield

$$\delta = 0.5406 \qquad [D1]$$
$$b_0 = 8.1157 < 8.06 \qquad [D2]$$
$$\therefore \delta = 0.5483 \qquad [D3]$$
$$\alpha = 13.2264^\circ \qquad [D5]$$
$$\varepsilon = 0.5373 \qquad [D7]$$
$$f_t = 0.0117 \qquad [D6]$$

The result was summarized in Table D6. This as compared with the 9.00 ti is obvious because the deflections δ of both tires are practically the same, 0.5156 in. and 0.5483 in.

Table D6. Rolling resistance of 10.00 - 20 tire

f_t calc.	f_t meas.
0.0117	0.0139 - 0.0122

Truck Tire, 14.00 - 20

This tire further illustrates the resolution of the method, at lower inflation pressures.

Input data: W = 6000 lb (26.668 kN); p_i = 45 psi (310.27 kPa); A = 127 in.^{2} (819.3 cm^2); p_g = 47.24 psi (325.72 kPa); b_0 = 10.3 in. (26.2 cm); l = 12.6 in. (32 cm); λ = 0.9786; D = 49 in. (124.5 cm); b_{tr} = 11.8 in. (30 cm); h = 14.5 in. (36.8 cm); r = 19 in. (48.3 cm).

Rolling resistance was measured in the amount f_t = 0.0259 - 0.0285. Calculations produced

$$\delta = 1.02 \qquad [D1]$$
$$b_0 = 10.0954 < 11.8 \qquad [D2]$$
$$\alpha = 16.5910^\circ \qquad [D5]$$
$$\varepsilon = 0.6519 \qquad [D7]$$
$$f_t = 0.0278 \qquad [D6]$$

Table D7 gives a summary.

Table D7. Rolling resistance of 14.00 - 20 tire

f_t calc.	f_t meas.
0.0278	0.0259 - 0.0285

Construction Equipment Tire, 26.5 - 25

This tire was evaluated in order to check the reliability of the method for lower pressures at high loads, similar to those of the previously calculated 29.5 - 29 tire. The sensitivity of the calculations was thus checked for larger tires.

Input data: W = 14240 lb (63.339 kN); p_i = 20 psi (137.9 kPa); A = 390 in.^{2} (2516.1 cm^2); p_g = 36.51 psi (251.74 kPa); b_0 = 21.7 in. (55.1 cm); l = 19 in. (48.3 cm); λ = 0.9459; D = 68.3 in. (173.5 cm); b_{tr} = 25 in. (63.5 cm); h = 21.65 in. (55 cm); r = 45 in. (114.3 cm).

The measured rolling resistance coefficient was f_t = 0.0154 - 0.0204 Calculations produced

$$\delta = 1.338 \qquad [D1]$$
$$b_0 = 21.7834 < 25 \qquad [D1]$$
$$\alpha = 16.0916^\circ \qquad [D5]$$
$$\varepsilon = 0.6043 \qquad [D7]$$
$$f_t = 0.0155 \qquad [D6]$$

The result was summarized in Table D8.

Table D8. Rolling resistance of 26.5 - 25 tire

f_t calc.	f_t meas.
0.0155	0.0154 - 0.0204

Cylindrical Tire, 16 × 15 6R, "Terratire"

This tire represents a radical departure from tire structures thus f considered. In this case $\lambda = 1$, and $b_{tr} = b_{tire}$ = 15 in. (38.1 cm). Accordingly, Equation [D4] was used, assuming that $p_i = p_g$ because of the pliability of the tire walls.

Input data: W = 700 lb (3113.6 N); p_i = 10 psi (68.95 kPa); p_g = 10 psi (68.95 kPa); D = 16 in. (40.6 cm); b_{tr} = 15 in. (38.1 cm); h = 4.5 in. (11.4 cm).

Goodyear catalogue for Terratires quotes a general figure, f_t = 0.01 for rolling resistance on a hard surface. Calculations yield

$$\delta = 0.3478 \qquad [D4]$$
$$\alpha = 16.9568^\circ \qquad [D5]$$
$$\varepsilon = 0.6863 \qquad [D7]$$
$$f_t = 0.0176 \qquad [D6]$$

Table D9 summarizes the results.

Table D9. Rolling resistance of 16 × 15 6R Terratire

f_t calc.	f_t meas.
0.0176	0.0169

Tire at Varying Load and Inflation Pressure

This was investigated a long time ago using the present method in its more primitive form (D2). The present example re-evaluates the data quoted in reference D2 in order to check the improvements introduced in this report.

The tire in question was of 7.00 - 16 size. It was measured under three loads and three inflation pressures as tabulated in Table D10.

Other input data are D = 30.43 in. (77.3 cm); b_{tr} = 5.72 in. (14.5 cm); h = 7.5 in. (19.0 cm); r = 5.12 in. (13.0 cm).

The average value of $\lambda = 0.85$ was assumed for the purpose of reducing the computations. Tire deflections often exceeded safe operational values for the sake of the argument. In all cases, the inequity $b_0 > b_{tr}$ was prevailing, and deflection δ was calculated from Equation [D3]. The results are shown in Table D10.

It may be concluded that the agreement between theory and experiment uniformly extends over the considered span of loads and inflation pressures, and that the method works even in cases of excessive loads and deflections.

Conventional and Radial Tires

These are intuitively expected to deform in a different manner, and thus produce different rolling resistances.

Following the theory, the differences are implicit in the measurable tire parameters such as W, b_0, l, A, p_i, p_g, and λ. In addition, the energy recovery factor ε must be different due to different elasto-plastic properties of the tires considered.

As mentioned in the second section, parameter k in Equation [D7] equals seven for radial tires.

$$\varepsilon = 1 - \exp(-7\delta/h)$$

This has been tentatively established by numerous computations, and is illustrated by the following numerical examples.

The first example is concerned with the evaluation of two 8.25 - 20 tires, one biased, the other radial, both under identical load and inflation conditions.

Table D10. Computation of rolling resistance of a 7.00 - 16 tire, and a comparison with the measured values

W		p_i		p_g							f_t	
lb	(kN)	psi	(kPa)	psi	(kPa)	δ [D1]	b_0 [D2]	δ [D3]	α [D5]	ε [D7]	Calc. [D6]	Meas.
300	(1.334)	1.0	(6.895)	3.5	(24.13)	1.5970	7.4304	2.8135	35.404	0.9964	0.0731	0.0800
		2.0	(13.79)	4.0	(27.58)	1.2370	6.6743	2.0998	30.459	0.9850	0.0589	0.0600
		4.0	(27.58)	5.5	(37.92)	0.9713	6.0001	1.0717	21.633	0.8827	0.0349	0.0360
500	(2.234)	1.0	(6.895)	5.0	(34.47)	1.9080	7.9743	4.0017	42.524	0.9997	0.0970	0.1100
		2.0	(13.79)	5.5	(37.92)	1.7080	7.6348	3.2111	37.912	0.9994	0.0810	0.0800
		4.0	(27.58)	7.2	(49.64)	1.2630	6.7344	1.7802	27.994	0.9716	0.0522	0.0550
700	(3.114)	4.0	(27.58)	6.0	(41.37)	1.5900	7.4171	2.7881	35.239	0.9962	0.0726	-
				6.7	(46.20)							
				8.2	(56.54)							

Table D11. Measured tire input data

Tire type	W	p_i	A	p_g	b_0	l	λ	D	b_{tr}	h	r
Conventional	3300	74	53.8	61.34	6.3	9.5	0.8989	38.7	6.3	9.35	11.5
8.25 - 20	(14.678)	(510.23)	(347.94)	(422.94)	(16.0)	(24.1)		(98.3)	(16.0)	(23.7)	(29.2)
Radial	3300	74	54.0	61.11	6.3	9.8	0.8746	38.7	6.3	9.2	14.0
8.25 - 20X	(14.678)	(510.23)	(348.4)	(421.35)	(16.0)	(24.9)		(98.3)	(16.0)	(23.4)	(35.6)

The measured tire input data are shown in Table D11. The first numbers denote pertinent values in English units, the second numbers, in parentheses below in SI units.

Rolling resistance measurements for these two tires did not specify test conditions, beyond the temperatures 273°F for conventional and 199°F for radial tires. Respective coefficients of motion resistance were found for speeds up to approximately 45 mph as follows: f_t conv. = 0.0125, and f_t rad. = 0.0100. Calculations yield

Tire type	δ	b_0	δ	α	ε	f_t
Conventional	0.51	6.7734 > 6.3	0.5920	14.2093°	0.6131	0.0144
Radial	0.475	7.2317 > 6.3	0.6308	14.67°	0.3812	0.0095

The result is summarized in Table D12.

Table D12. Rolling resistance of conventional and radial tires of 8.25 - 20 size

Tire type	f_t calc.	f_t meas.
Conventional	0.0144	0.0125
Radial	0.0095	0.0100

Considering the uncertainties involved, the result appears acceptable. Note that in this case k = 7 for radials. This indicates that for all conditions equal, the energy recovery factor ε plays a decisive role.

The problem is explored further in the following example, where test data encompass a wider spectrum of tires.

Two tires, conventional and radial of 7.50 - 15 size, were selected because of the availability of the necessary operative input data. However, the experimental data for rolling resistance f_t were not specifically available for these tires. Only average figures obtained from tests with 18 conventional and 12 radial tires (D11) were found, for regular T&RA loads and 35 - 55 psi (241.32 - 379.2 kPa) of inflation pressure; f_t conv. = 0.0146; f_t rad. = 0.0112. Tire input data are shown below:

Tire type	W	p_i	A	p_g	b_0
Conventional	2800	75	48.0	58.33	5.5
7.50 - 15	(12.454)	(517.12)	(309.7)	(402.18)	(14.
Radial	2800	75	49.0	57.14	6.1
750 R15	(12.454)	(517.12)	(316.1)	(393.98)	(15.

Tire type	l	λ	D	b_{tr}	h	r
Conventional	9.9	0.8815	31.0	6.2	8.0	8.0
7.50 - 15	(25.1)		(78.7)	(15.7)	(20.3)	(10.
Radial	9.8	0.8197	32.0	6.3	8.5	9.7
750 R15	(24.9)		(81.3)	(16.0)	(21.6)	(24.

Calculations show an interesting relation to the inequity $b_0 \neq b_{tr}$, shown in Equation [D2].

Tire type	δ [D1]	b_0 [D2]	δ [D3]	α [D5]	ε [D7]	f_t
Conventional	0.63	6.2235 = 6.2	0.6400	16.3917°	0.6931	0.01
Radial	0.616	6.9032 > 6.3	0.7196	17.2460°	0.4471	0.01

Results are summarized in Table D13.

Table D13. Rolling resistance of conventional and radial tires, 7.50 - 15

Tire type	f_t calc.	f_t meas.
Conventional	0.0194	0.0146
Radial	0.0143*	0.0112**

*7.50 - 15 and 7.50 R15 tires.
**averages of 18 conventional and 12 radial tires of varying loads, inflation pressures and dimensions.

It would be unwarranted to expect a better agreement, in absolute values, since the calculations and the measurements were performed in no homologous conditions. It should be noted, however, that the percentage of improvement in f_t for radial tires are almost the same as for the cal lated 7.50 - 15 tires and for the tested thirty tires:

$$100(0.0194 - 0.0143)/0.0194 = 26.3\%$$
$$100(0.0146 - 0.0112)/0.0146 = 23.3\%$$

The tested tires were of 78 - 13, 78 - 14, and 78 - 15 size with prefixes A, B, D, F, G, DR, and FR (D11).

It thus appears that both the order of magnitude and the trend in evaluation of radial and conventional tires is in agreement with the experiment.

To further illustrate that point, take the radial tire, Michelin 10.00 - 20X. Test stand measurements show rolling resistance coefficient $f_t = 0.0070$ at speed 40 mph (64 km/h), at the rated conditions.

This tire, according to catalogue data, provides the following input for the calculation of rolling resistance: $W = 4750$ lb (21.128 kN); $p_i = 75$ psi (517.12 kPa); $A = 77$ in.^{2} (496 cm^2); $p_g = 61.69$ psi (425.35 kPa); $b_0 = 7.8$ in. (19.8 cm); $l = 12.2$ in. (31.0 cm); $\lambda = 0.81$; $D = 41.4$ in. (105.0 cm); $b_{tr} = 8.6$ in. (21.8 cm); $h = 10.7$ in. (27.2 cm); $r = 15.5$ in. (39.4 cm). Calculations yield

$$\delta = 0.676 \qquad [D1]$$
$$b_0 = 9.055 > 8.6 \qquad [D2]$$
$$\delta = 0.7514 \qquad [D3]$$
$$\alpha = 15.4850^\circ \qquad [D5]$$
$$\varepsilon = 0.3883 \qquad [D7]$$
$$f_t = 0.0111 \qquad [D6]$$

Results shown in Table D14 indicate that the method of evaluation of radial tires produces consistent values compatible with the experiment performed on similar tires, in spite of some inevitable variation of their characteristics.

Table D14. Rolling resistance of a radial 10.00 - 20X tire

f_t calc.	f_t meas.
0.0111	0.0112*
	0.0070**

*Average of measurements made with 12 radial tires similar to 10.00 - 20X tire.
**Radial tire 10.00 - 20X, tested under rated conditions.

Wire Mesh Tires for Lunar Surface Locomotion

Tire geometry and the mathematical model used here, for prediction rolling resistance, do not specify material and tire structure. All the specifics in that respect are implicit in input parameters W, p_i, A, b_0, D, b_{tr}, h, and r which are available in the catalogues and Deflection Charts.

Accordingly, it appears logical to expect that any tire may be eval ated, using the discussed equations, if the proper input is available. order to check this assumption, two wire mesh tires developed by the General Motors-Boeing-NASA team for lunar surface locomotion were evalu- ated: the MOLAB (Mobile Lunar Laboratory) and the LRV (Lunar Roving Vehicle) tires. Their input data are shown below.

Tire	W (N)	p_g (Pa)	λ	D (m)	b_{tr} (m)	h (m)	r (m
MOLAB	889.6	5620	0.85	1.524	0.381	0.356	0.22
LRV	266.9	46014	0.84	0.818	0.22	0.22	0.11

Coefficients of rolling resistance for MOLAB and LRV wheel were measured a hard surface, with the following result: f_t MOLAB = 0.02, f_t LRV = 0. Calculations of f_t yield

k	Tire	δ [D1]	b_0 [D2]	α [D5]	ε [D7]	f_t [D6
7	MOLAB	0.061	0.3112	23.0811°	0.6986	0.0297
	LRV	0.0453	0.1843	27.2286°	0.7634	0.0398
5	MOLAB				0.5754	0.0245
	LRV				0.0428	0.0335

In this example, it was assumed that k = 7, in conformity with radi tires. This produced too high a value for f_t. Since it would be unjust fied to expect that wire mesh tires have the same coefficient of energy recovery as radial tires, k = 5 was postulated, with better results. Se Table D15 or a summary.

It seems certain that a better agreement between measured and calcu lated values could be obtained through proper adjustment of k-value. To this end, more experimental work would be needed.

Table D15. Rolling resistance of wire mesh tires, MOLAB and LVR

	f_t calc.	f_t meas.*
MOLAB	0.0245	0.02
LVR	0.0335	0.03

*Measurements were dependent on the uniformity of the mesh which was hand woven.

ACCURACY OF PREDICTIONS

Tables D1 - D15 (except Table D11) compare predicted and measured coefficients of rolling resistance f_t for a number of various size tires, on hard surface. An approximate visual summation of these tables is presented in Fig. D9: the filled circles denote calculated values, the open circles, those measured.

The spread of deviations between the two sets of these values appears random. It is reflecting the inaccuracies of tire input data and the often unspecified conditions of measuring tire rolling resistance.

For the numerical evaluation of the predictions, assume that Fig. D9 reflects a normal distribution of deviations d, between measured and computed data:

$$d = (f_t \text{ meas} - f_t \text{ calc})/f_t \text{ meas}$$

Then, the values of d implicit in Tables D1 - D15 may be grouped in two blocks, each containing 10 numbers:

0.3077	0.4061	0.3027	-0.0133	0.0162
0.2087	-0.0360	0.0171	0.1583	0.0410
0.0089	0.0733	0.0246	-0.0065	0.2402
0.0500	-0.1000	-0.1520	-0.3288	-0.2768

Following the regular procedures for estimating standard deviation σ of the block populations (D12), the ranges between the smallest and the largest number, in each block, were found as shown below.

$$0.3077 - (-0.0360) = 0.3437$$
$$0.2402 - (-0.3288) = 0.5690$$

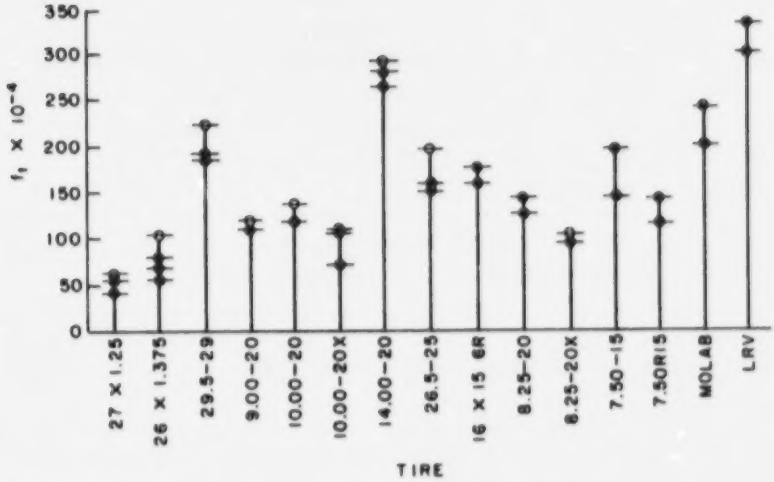

Figure D9. Comparison between calculated (filled circles) and measured (open circles) values of rolling resistance f_t, for various tires, in accordance with data, Tables D1 to D10 and D12 - D15

The estimated standard deviation σ is then

$$\sigma = (10 \times 0.325 \times 0.3437 + 10 \times 0.325 \times 0.5690)/20$$
$$= 0.1483$$

where 0.325 is the coefficient corresponding to the block size of 10 numbers (D12). The mean value of the distribution is: $\bar{d} = 0.4349/20 = 0.0217$. Thus upon rounding up the percentages, it may be expected that 68.3% of calculated values will deviate from those measured within the range of -13% to +17%.

Considering that the examples quoted here did not always represent a good input and well-specified test conditions, it is almost certain that the deviations d, between theoretical and experimental data, may be reduced further if both the tire measurements and the rolling resistance test are carefully designed.

Such a careful experiment was performed with related computations a long time ago (D12). It was re-examined in this paper, and the result was shown in Table D10.

Following the same procedure as before (D12), the distribution of deviations d was found in the form

0.0862	0.0183	0.0305
0.1182	0.0125	0.0509

The estimate of standard deviation was

$$\sigma = 0.395 \times 0.1067 = 0.0421$$

The mean value of $\bar{d} = 0.3166/6 = 0.0528$ was determined.

Taking two standard deviations as a measure of 95.4% probability that the measured and calculated values will not deviate more than -3% to +13%, one finds the accuracy quite remarkable.

In conclusion, the predictive power of Equations [D1] through [D1] appears to be quite adequate.

Sensitivity of these equations to various input data suggests that the method may be used in parametric evaluations and case studies of tire-vehicle optimization and tire design.

PARAMETRIC ANALYSES AND CASE STUDIES

Equations [D1] through [D7] comprise a large number of tire parameters. This makes it feasible to perform all kinds of trade-offs between these parameters and tire performance. Also, broader explanations of various phenomena related to tire behaviour are made possible.

Note that on hard surface, the tire optimization considered here is quite limited because hard ground imposes limited constraints upon rolling resistance caused by tire flexing, if the wear and speed problems are neglected.

However, on soft ground, where tire deflections also exist but in a much greater variety of ground constraints (see Fig. D1), the method described yields unique opportunities in tire optimization, unattainable by other methods. This will be discussed in the second part of this paper.

A few examples referred to below illustrate the point with reference to hard ground surface operations.

Worn and New Tires

These have been known to have different rolling resistances, reduced with tire wear. A general consensus of opinion seems to explain the phenomenon by the reduced rigidity of the worn tire, which may be correct.

However, our method for calculations of tire rolling resistance also indicates that the tread radius r may play an additional role. The following example purports to validate this assumption.

The input data for a 9.00 - 16 tire are listed as follows: $W = 2800$ lb (12.454 kN); $p_i = 65$ psi (448.17 kPa); $A = 37$ in.^{2} (238.7 cm^2); $p_g = 75.67$ psi (521.74 kPa); $\lambda = 0.84$; $D = 35.06$ in. (89.1 cm); $b_{tr} = 7.63$ in. (19.4 cm); $h = 9.53$ in. (24.2 cm); $r = 7.25$ in. (18.4 cm).

Calculations of rolling resistance for the new tread show

$$\delta = 0.5014 \qquad [D1]$$
$$b_0 = 5.2986 < 7.63 \qquad [D2]$$
$$\alpha = 0.7366^\circ \qquad [D5]$$
$$\varepsilon = 0.5458 \qquad [D7]$$
$$f_t = 0.0133 \qquad [D6]$$

The worn tread is assumed to have lost the outer portion rounded up by radius $r = 7.25$ in., reaching the flat shape on A-B level as shown in Fig. D10. From Fig. D10, the changed tire dimensions are $b_{tr} = 7.63$ in. (19.4 cm); $D = 32.8902$ in. (83.5 cm); $\lambda = 1$.

The removal of 1.0849 in. (2.75 cm) of tread does not change significantly the load-deflection curve of the tire, which mainly depends on internally pre-stressed tire walls, at a fairly high inflation pressure, 65 psi (448.17 kPa).

Accordingly, it is plausible to assume that tire ground contact length l does not change, but the width will be larger than the value previously

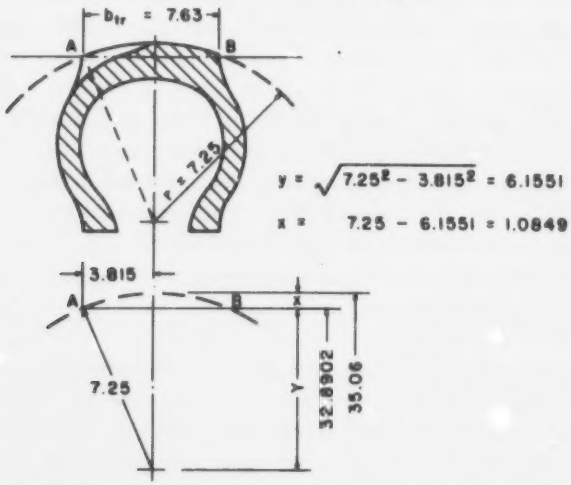

Figure D10. Geometry of a 9.00 - 16 tire with tread worn to A-B level fixed by tread width 7.63 in. (19.4 cm), and carcass thickness

calculated, by the ratio $b_{tr}/b_0 = 7.63/5.2986 = 1.44$. Thus the ground contact area A and the ground pressure p_g are

$$A = 37 \times 1.44 = 53.28 \text{ in.}^2 \ (343.74 \text{ cm}^2)$$
$$p_g = 2800/53.28 = 52.55 \text{ psi } (362.33 \text{ kPa})$$

With this modified input of the worn tire, calculations show:

$$\delta = 0.3749 \qquad [D4]$$
$$\alpha = 12.2576^\circ \qquad [D5]$$
$$\varepsilon = 0.4862 \qquad [D7]$$
$$f_t = 0.0088 \qquad [D6]$$

Reduction of rolling resistance because of tire wear is then

$$(0.0133 - 0.0088)/0.0133 = 0.3383$$

or, approximately 34%. This is in agreement with available data. Tests reported under the auspices of DOT quote the reduction of rolling resistance for unspecified biased and radial tires from approximately 0.0127 to approximately 0.0075, or 41% (D13).

The lack of Deflection Charts for worn tires makes it impossible to find more accurate results. Nevertheless, our conjecture appears practical, and discloses that the radius of tire tread r and the width of the tread b_{tr} may play important roles even when the rigidity of the tire is reduced due to the wear.

However, the role of tire stiffness change due to wear may be entirely immaterial. More tests incorporating the concept of tire parameters encompassed by Equations [D1] through [D7] would be needed to further elucidate the problem.

Effect of Tread Radius on Rolling Resistance

The variety of tread radii for the same or similar tire size appears somewhat arbitrary though calculations show a strong relationship between tread radius and rolling resistance (Equations [D1] and [D2]).

To illustrate the problem, a 23.5 - 25 tire was selected. Its characteristic input data are listed in Table D16. Four tread radii, r = 40, 50, 60 in., and a flat tread ($r = \infty$) were assumed. Note that the coefficient of "ellipticity" λ changes with deflection δ_m. Obviously, it also depends on tread radius r. Unfortunately, the latter relationship is not known by direct measurements since pertinent tests do not appear to have ever been made.

Table D16. Deflection Chart input data for a 23.5 - 25 tire*

A (in.^{2})	b_0 (in.)	l (in.)	λ	r (in.)	δ_m (%)	W × 10^3 (lb)	p_i (psi)
410	20.8	20.7	0.9522	50	20	20.8	25
						24.7	35
						28.7	45
						36.0	65
358	20.5	18.4	0.9491	50	16	16.0	25
						20.0	35
						23.0	45
						28.7	65
286	20.0	15.6	0.9167	50	12	11.8	25
						14.2	35
						16.0	45
						29.0	65

*Dimensions: D = 66.2 in. (168.1 cm); b_{tr} = 22 in. (55.9 cm); h = 20.67 in. (52.5 cm). Deflections: δ_m = 20%, 16%, 12%, measured.

However, the necessary information may be extracted from the Deflection Charts of tires having different radii r, at the same, or nearly the same diameters D as the 23.5 - 25 tire.

Figure D11 shows the graph thus construed, using three other tires satisfying this condition. It yields λ-values for radii up to 60 in. 150 cm) which corresponds to a practically flat tread (λ = 1), for diameters D from 63.2 to 77.4 in. (160.5 to 196.6 cm). From Fig. D11, λ-coefficients were chosen for the postulated tread radii as shown in Table D17.

Deflections δ, Table D17, were calculated for the 23.5 - 50 tire with tread radius r = 50 in. (127 cm), at measured deflections δ_m = 20, 16 and 12%:

δ_m (%)	δ [D1]	b_0 [D2]	δ [D3]
20	1.3457	23.0442 > 22	1.4797
16	1.1764	21.5644 < 22	-
12	0.9704	19.6059 < 22	-

For the sake of comparison, the same deflections were assumed as invariant when changing tread radii.

Table D17. Coefficient λ as a function of tread radius r, for a number of tire deflections δ_m and δ. Tire size: 23.5 - 25

r	δ_m (%)	δ	λ
40	20	1.4797	0.9420
	16	1.1765	0.9200
	12	0.9705	0.8850
50	20	1.4797	0.9522
	16	1.1765	0.9491
	12	0.9705	0.9167
60	20	1.4797	0.9900
	16	1.1765	0.9850
	12	0.9705	0.9700
∞	20	1.4797	1.0
	16	1.1765	1.0
	12	0.9705	1.0

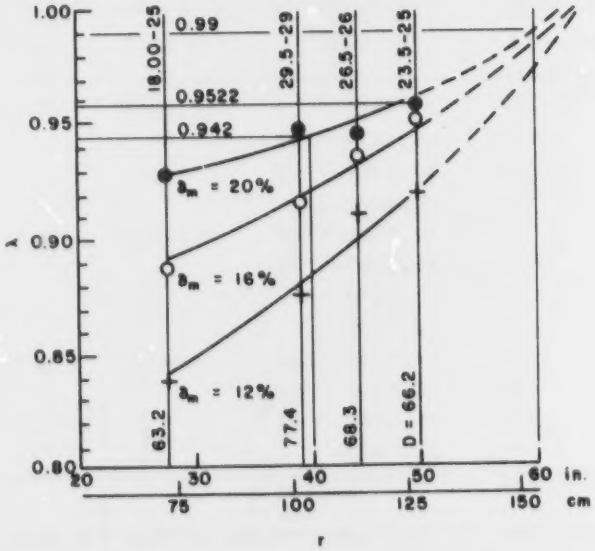

Figure D11. Relationship between the coefficient of "ellipticity" λ and tread radius r, for a number of measured deflections δ_m, and tire diameters D varying between 63.2 to 77.5 in. (160.5 to 196.6 cm)

This involved changes in ground contact areas A, which were calculated using Equation [D1] in the following form:

[D8] $$(2r\delta - \delta^2)(D\delta - \delta^2) = (A/4\lambda)^2$$

which was obtained assuming $W/p_g = A$. Equation [D8] yields

[D9] $$A = 4\lambda[(2r\delta - \delta^2)(D\delta - \delta^2)]^{1/2}$$

Equation [D9] is valid for δ's satisfying condition expressed by Equation [D2]. For $b_0 > b_{tr}$, the width of the ground contact area is constant, and the area is

[D10] $$A = 2\lambda b_{tr}(D\delta - \delta^2)^{1/2}$$

Solution of Equations [D9] and/or [D10], based on input, Table D17, is presented in Table D18.

In order to calculate the rolling resistance f_t, Equation [D6], formulae [D5] and [D7] were computed as shown below.

δ_m (%)	r	b_0 [D2]	α [D5]	ε [D7]
20	40	21.5580 < 22	17.1966°	0.6583
	50	24.1479 > 22		
	60	26.4858 > 22		
	∞	22.0000		
16	40	19.2599 < 22	15.3220°	0.5742
	50	21.5653 < 22		
	60	23.6470 > 22		
	∞	22.0000		
12	40	17.5155 < 22	13.9085°	0.5055
	50	19.6069 < 22		
	60	21.4959 < 22		
	∞	22.0000		

This completed list of input parameters needed for substitution in Equation [D6], which yields the rolling resistance f_t listed in Table D19. Table D19 confirms the expectations and shows the advantages of the flat tread, from rolling resistance viewpoint. It also indicates that the advantages practically disappear at low tire deflections.

Figure D12 summarizes the result in a graphic form. Although it presents a general picture, it refers to a particular tire. Fluctuations of f_t for other tires may be different, and each case should be analyzed on its own merit.

Table D18. Ground contact areas A, of a 23.5 - 25 tire with tread radii r = 40, 50, 60 in. and ∞, at measured deflections δ_m = 20, 16, and 12%

r	A		
	$\delta_m = 20$	$\delta_m = 16$	$\delta_m = 12$
40	397.4622	309.9579	246.6695
50	410.0039	358.0379	286.0139
60	426.2800	379.0704	331.8001
∞	430.5859	384.8430	342.0619

Table D19. Rolling resistance of a 23.5 - 50 tire with various tread radii at constant deflections (D = 66.2)

r	f_t		
	$\delta_m = 20$	$\delta_m = 16$	$\delta_m = 12$
40	0.0182	0.0143	0.0118
50	0.0180	0.0139	0.0113
60	0.0173	0.0133	0.0108
∞	0.0169	0.0131	0.0107

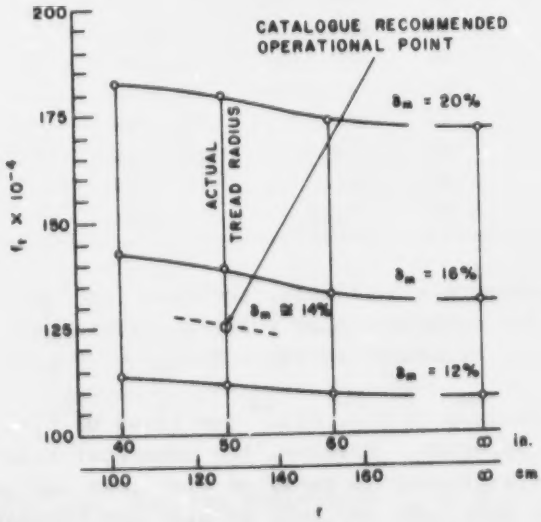

Figure D12. Rolling resistance f_t of a 23.5 - 25 tire as a function of variable tread radius r, for a number of constant measured tire deflections δ_m

Effect of Tire Diameter on Rolling Resistance

The effect of tire diameter upon rolling resistance has been well understood, although even simple parametric relationships of loads and dimensions involved appear to be unclear.

This numerical example illustrates how the discussed method may throw some light upon a quantitative evaluation of the problem.

For the sake of comparison, again the 23.5 - 25 tire was assumed with the same spectrum of deflections and input data as shown in Tables D16 and D17. With tire cross-section thus fixed, tire diameters D = 55, 65, 75 in. (139.7, 165.1, 190.5 cm) were assumed, together with the flat tread, for the sake of simplicity. This postulated constant tread width, $b_0 = b_{tr}$ = 22 in. (55.9 cm), and $\lambda = 1$.

The above constraints slightly modified the ground contact areas, which could not have been neglected. To determine the A's for various δ's, Equation [D10] was used. Upon substituting the deflection values δ for δ_m = 20, 16, 12%, and for various diameters D, contact areas were found as shown below. Values of α and ε were computed as in the previous cases.

δ_m (%)	D	A [D10]	α [D5]	ε [D7]
20	55	391.5604	18.8810	0.6583
	65	426.5754	17.3558	
	75	458.9265	16.1491	
16	55	350.1197	16.8193	0.5742
	65	381.2526	15.4629	
	75	410.0415	14.3893	
12	55	318.5987	15.2662	0.5055
	65	346.8314	14.0364	
	75	372.0733	13.0628	

With all the parameters available, Equation [D6] (with substitution $W/p_g = A$) was used for computation of rolling resistance. The results are shown for various tire diameters in Table D20.

Table D20 was plotted in Fig. D13. The trend of f_t-increase with the decrease of D is as expected. However, the numerical relationship between these two parameters expressed in terms of tire load and geometry suggests that computations of this type may help to plan and standardize tire dimensions in a more convenient way that would consider the economy of locomotion.

Table D20. Rolling resistance of a 23.5 - 25 tire for various tire diameters, a constant deflections with flat tread

	f_t [D6]		
D	δ_m = 20%	δ_m = 16%	δ_m =12%
55	0.0190	0.0146	0.0116
65	0.0173	0.0133	0.0106
75	0.0160	0.0123	0.0098

As a matter of interest, the recommended operational point of a regular tire with tread radius 50 in. was plotted on Fig. D13. The same point was marked on Fig. D12 for the sake of comparison.

Effect of Tread Width on Rolling Resistance

It may be deduced from Equation [D2], and tire geometry, Fig. D2, that

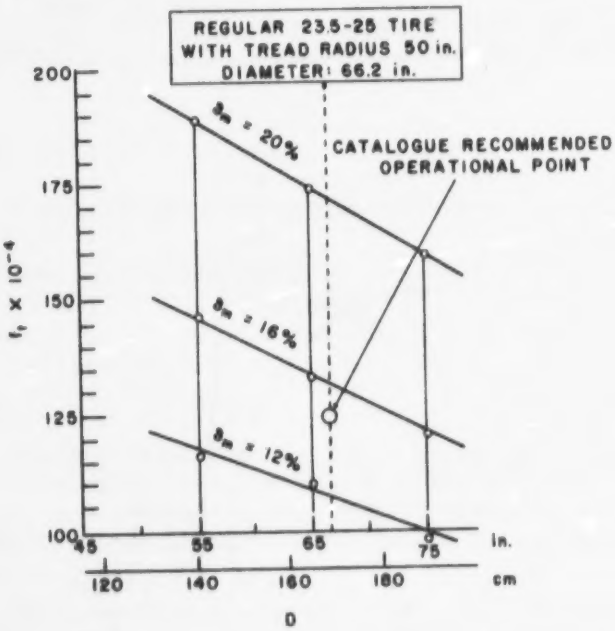

Figure D13. Rolling resistance f_t of a 23.5 - 25 tire with flat tread (λ = 1), for various tire diameters D, at constant deflection δ_m

tread width b_{tr} is irrelevant for values $b_0 < b_{tr}$. The following example illustrates the point.

Take again for the sake of comparison a 23.5 - 25 tire with tread radius r = 50 in. (127 cm) and b_{tr} = 22 in. (55.9 cm). Tire characteristics were given in Table D16, and the calculated tire deflection δ, for measured deflections δ_m, in Table D17. For the convenience of the reader pertinent parameters are listed in Table D21.

Six hypothetical tread widths were selected: b_{tr} = 19, 20, 21, 22, 23, and 27 in. (48.3, 50.8, 53.5, 55.9, 58.4, and 68.6 cm). Figure D14 implies that the above widths do not involve much change in tire cross-

Table D21. Deflection characteristics of a 23.5 - 25 tire with regular parameters: r = 50 in. and b_{tr} = 22 in.

δ_m (%)	δ	λ	A
20	1.4797	0.9522	410
16	1.1765	0.9491	358
12	0.9705	0.9167	286

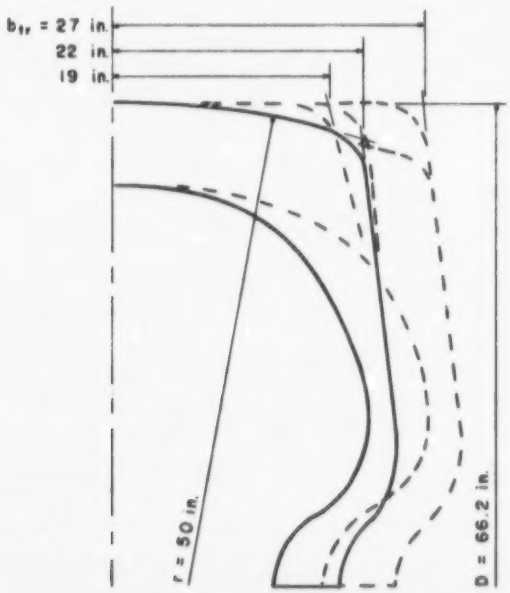

Figure D14. Half cross-section of a regular 23.5 - 25 tire (solid lines) with contemplated widening of the tread width (interrupted lines)

section. Accordingly, the deflection characteristics may practically remain unchanged for all the tread widths.

This assumption certainly does not change the trend of tread width effect upon rolling resistance, analyzed below.

To save space, the step-by-step calculations reported below pertain only to b_{tr} = 19 in. (48.3 cm), and to A = 410 in.^{2} (2645.16 cm^2):

$\delta = 1.4797$ [D1] $\quad b_0 = 24.1479 > 19$ [D2]
$\delta = 1.9999$ [D3] $\quad \alpha = 20.0188$ [D5]
$\varepsilon = 0.7657$ [D7] $\quad f_t = 0.0248$ [D6]

In a similar manner, other assumed tread widths were introduced and the rolling resistance calculated. The results were summarized in Table D22.

Identical calculations were performed for contact areas A = 358 and 286 in.^{2} (2309.67 and 1845.16 cm^2) as well as for all the tread widths considered. The result was plotted in Fig. D15.

Figure D15 also gives the ratio of ground contact length l to width b_0, i.e., the aspect ratio of the area. The value of l was obtained from the equation

$$l = 2(D\delta - \delta^2)^{1/2}$$

which was shown in Fig. D2 and is implicit in Equation [D1].

Figure D15 shows the interdependence between the aspect ratio of the ground contact area and rolling resistance. It also demonstrates dramatically the fluctuation of the tread width effect upon rolling resistance, depending on the relative size of the tread width b_{tr} and the ground contact width b_0.

Table D22. Calculatory steps results for determining rolling resistance of a 23.5 - 25 tire with tread radius r = 50 in. and with various tread widths b_{tr}, at a constant ground contact area, A = 410 in.^{2}

b_{tr} (in.)	δ	b_0 (in.)	α	ε	l	l/b_0	f_t
9	1.9999	19	20.0188	0.7651	22.6622	1.19	0.0248
20	1.7993	20	18.9785	0.7290	21.5291	1.08	0.0222
21	1.6277	21	18.0429	0.6931	20.5041	0.98	0.0200
22	1.4797	22	17.1966	0.6583	19.5701	0.89	0.0180
23	1.3457	23.0442	16.3938	0.6234	18.6841	0.81	0.0164
↓	↓	↓	↓	↓	↓	↓	↓
27	1.3457	23.0442	16.3938	0.6234	18.6841	0.81	0.0164

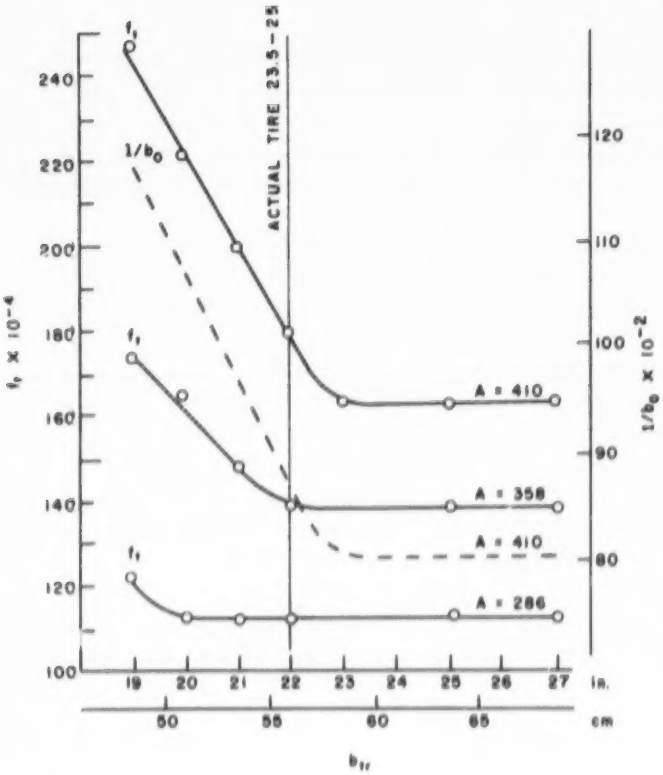

Figure D15. Rolling resistance f_t of a regular 23.5 - 25 tire with r = 50 in., as a function of tread width b_{tr} at constant ground contact areas A. Also the ground contact area aspect ratio $1/b_0$ as a function of b_{tr}

The relationship between δ, A, B_{tr}, $1/b_0$, and f_t displayed by Fig. D15, for the given tire and load, may be helpful in the optimization of tire geometry.

As a matter of interest, the location of the regular 23.5 - 25 tire was shown on the discussed graph. Note that high deflection, low pressure tires are more sensitive to tread width effect than the high pressure tires.

Effect of Flat Tread Width on Rolling Resistance

In the preceding example a 23.5 - 25 tire with tread radius r = 50 in.

was considered. Flat tread tire, r = ∞, shows different performance. This may be seen by repeating the same calculation as before, for λ = 1.

The result was plotted in Fig. D16. On Fig. D16, which pertains only to A = 410 in.^{2}, the f_t curve for r = 50 in. was replotted for comparison purposes, together with $1/b_0$ aspect ratios.

It may be concluded that the flat tread tire is more economic, particularly for higher deflections, and that the smaller the ground contact aspect ratio the smaller the rolling resistance.

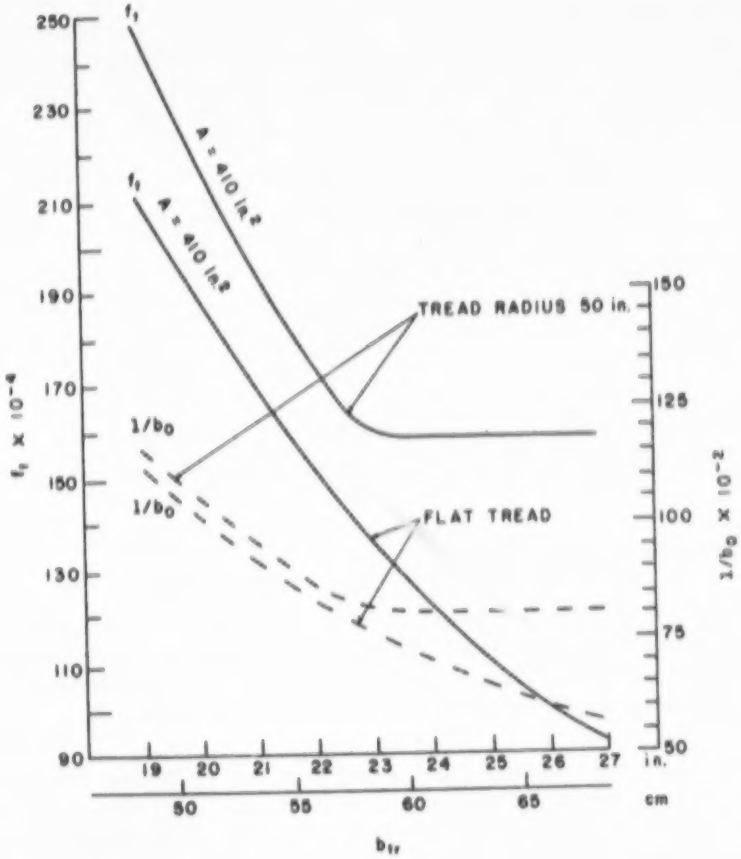

Figure D16. Rolling resistance f_t of a 23.5 - 25 tire with flat tread (λ = 1) as a function of tread width b_{tr} at constant ground contact area A. For comparison rolling resistance curve of the same tire with r = 50 in. is retraced from Fig. D15 (solid lines). Also given are ground contact area aspect ratios $1/b_0$ as a function of b_{tr} (interrupted lines)

Frame of Reference for Calculation of Rolling Resistance

In the two preceding examples, rolling resistance f_t was evaluated assuming the ground contact area A as a constant at varying tread radii.

However, in the example related to the effect of tire diameter upon rolling resistance, tire deflections δ_m and δ were assumed constant.

This precludes a direct comparison between the effects of tire tread width and tire diameter though it may serve other purposes in the optimization of rolling resistance.

In order to have comparable tire width and diameter effects on rolling resistance, the 23.5 - 25 tire, Table D20, was recalculated as shown in the two preceding examples. The result was shown in Fig. D17, which is based on A = 410 in.^{2}.

On Fig. D17 the rolling resistance for δ = 1.4797 (δ_m = 20%) was replotted from Fig. D13. The difference is obvious.

Note that deflection δ = 1.4797 refers to A = 410 in.^{2} of the regular tire, Table D21. Figure D17 thus shows the difference between similar values measured in different frames of reference: A = const. or δ = const.

This indicates a need for more specificity when comparing tire rolling resistances. The method discussed here hopefully outlines the needed approach.

Tire Geometry and Performance Maps

Parametric evaluations of tire rolling resistance as a function of tire structure, geometry, and size, have been helped by ready-made assemblies of pertinent parameters, i.e., by load-geometry-performance maps of tires.

Though the approach to this problem described here has been tackled only recently, simple geometry maps have been known for decades. For example, a map based either on the computations, or experiment, shown in Fig. D18, served well the preliminary selection of wheel envelopes and postulated ground contact areas.

Similar use may be found for an experimental tire map traced by an automatized Firestone method (D14), shown in Fig. D19. The tire is of

FR78 - 14 size, radial and steel belted. The graph perfectly fits the method described here of rolling resistance computation though it contains less information than the Deflection Chart. Maps on Fig. D18 and D19 are, in a sense, complementary.

A performance map for comparative tire evaluation was shown in Fig. D20. It was obtained by calculations reported below. Input Data: 29.5 - 29 tire; D = 77.4 in. (196 cm); b_{tr} = 28 in. (71.1 cm); h = 20.50 in. (52.1 cm); r = 40 in. (101.6 cm).

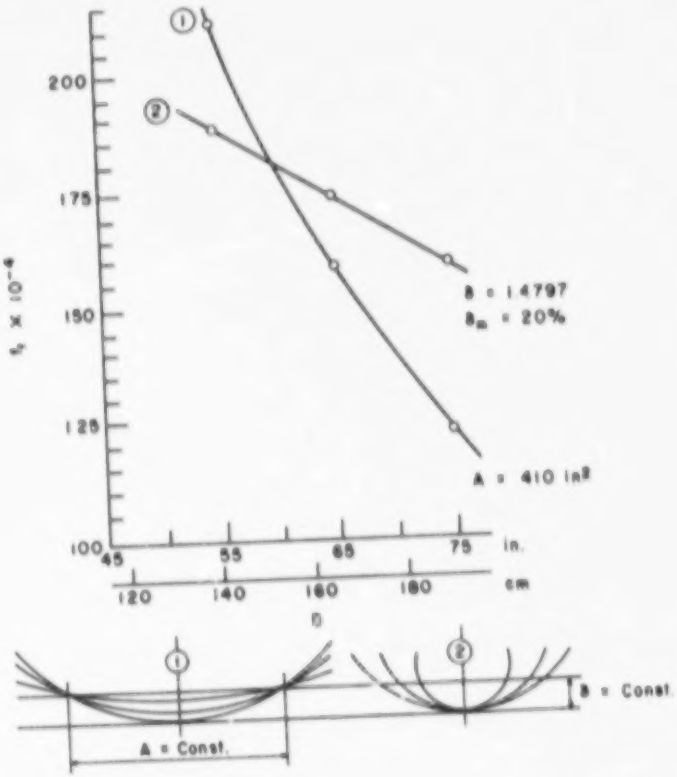

Figure D17. Rolling resistance f_t of a 23.5 - 25 tire with flat tread (λ = 1) as a function of tire diameter D, at constant ground contact area A. For comparison, f_t-curve is retraced from Fig. D13, at constant deflections δ, (δ_m), and flat tread

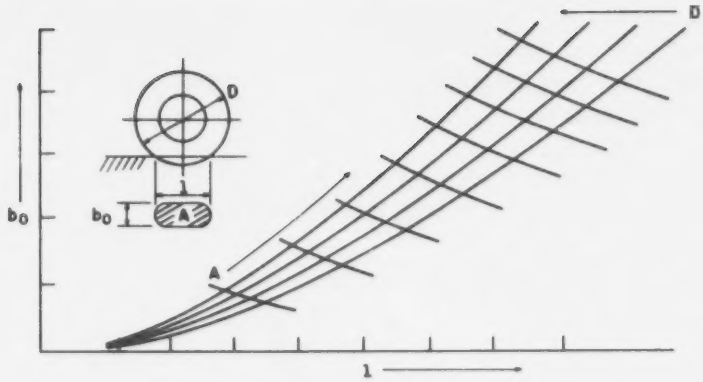

Figure D18. Tire geometry map adapted from Rotta and Fielding (D7)

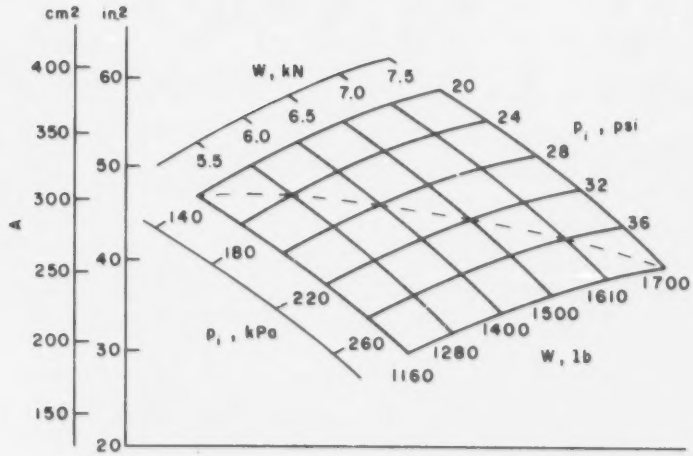

Figure D19. FR78 - 14 tire load-ground contact area map adapted from Prettyman (D14)

Goodyear Deflection Chart yields for the measured deflections δ_m:

δ_m (%)	b_0	l	A	λ	p_i (psi)	W × 10^3 (lb)
20	23.8	24.8	560	0.9484	25	21
					45	31
					60	36
16	23.1	21.8	460	0.9134	25	17
					45	24
					60	29
12	21.4	18.5	345	0.8714	25	13
					45	17
					60	21

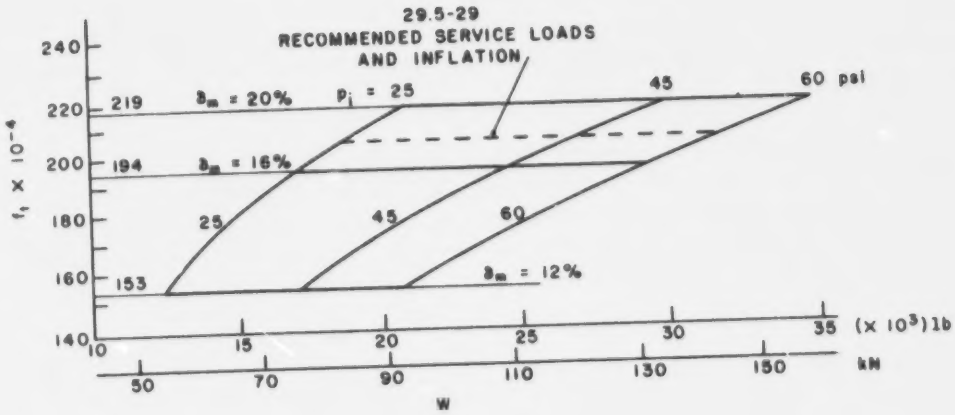

Figure D20. 29.5 - 29 tire performance map computed with the method outlined in the present paper

and the computations show:

δ_m (%)	δ [D1]	b_0 [D2]	α [D5]	ε [D7]	f_t [D6]
20	1.9223	24.5021	18.1345	0.7537	0.0219
16	1.6340	33.6928	16.7089	0.6980	0.0192
12	1.2785	20.0644	14.7685	0.6062	0.0153

Since for the specific $W(p_i)$ values derived from the Deflection Charts rolling resistance is constant, the combining of calculated f_t's with corresponding W's and p_i's produces the graph given in Fig. D20.

On Fig. D20 the catalogue recommended loads and inflation pressures also were plotted in a dashed line. This delineates the "safe" working conditions for loads and pressures located below the recommended line, up to the admissible minimum deflection δ_m.

This map is useful in optimization, or selection of low rolling resistance tires, for which regular catalogue data are inadequate.

In this mapping, also, tire internal structure may be appreciated as shown in Fig. D21, obtainable directly from the Deflection Charts.

The above type of mapping was described previously as a computation input for rolling resistance evaluation (Figs. D4, D5, and D6). In the present case, it may serve another purpose. Note that the 18.00 - 25, 23.5 - 25, and 29.5 - 25 tires cluster in two groups, at W = 15000 lb (66.72 kN), separated by a marked difference in ground pressure p_g. The

tires are of similar size, hence the rationale for the difference in carcass stiffness causing the differences in p_g is a legitimate question. The stiffer the tire the lower the rolling resistance (Equations [D1] - [D7]). Is the clustering of four similar tires under the same load conditions justified?

Figure D21 may help to detect inconsistencies in tire design. It indicates that the lower the location of $p_i(p_g)$ lines for W = const., the higher the rolling resistance as defined by the method discussed here. Automatic tire print-load signature processing such as that by Firestone (D14) yields the data required in pertinent studies.

Spacing Sizes in Performance Marketing

A need for supplying the market with tire sizes that may be required to uniformly cover all possible load ranges is obvious. An example is shown in Fig. D22.

The graph displays an almost even spacing of load W vs. inflation p_i

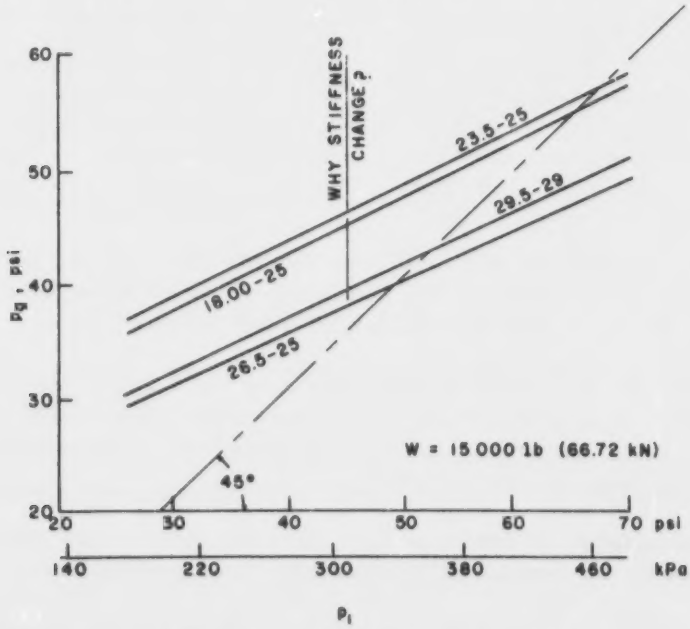

Figure D21. Tire map of four similar-in-size tires showing the relationship between inflation and ground contact pressures $p_i(p_g)$ at constant load W. Note the clustering of the tires, which raises the question of their stiffnesses in carcass design

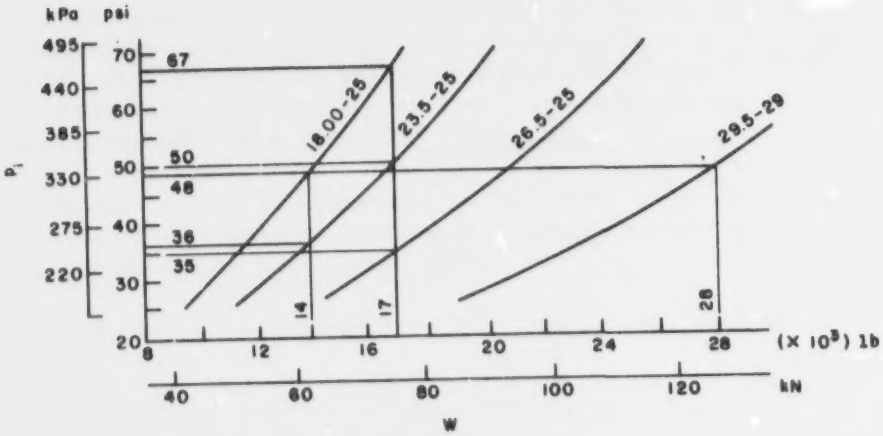

Figure D22. Catalogue load-inflation curves at recommended service conditions, for a number of specified tires. Rock lug tread, speeds up to 30 mph (48 km/h)

lines for four tires of similar size and similar tread design designated for work on rock ground. The loads and inflation are those recommended by the manufacturer for use at specified speeds (up to 30 mph, or 48 km/h).

This uniformity of load-size spacing reflected on Fig. D22 is lost, however, when the rolling resistance-inflation-load tire map is traced (Fig. D23). The f_t-p_i-W maps overlap in a rather haphazard way and do not seem to uniformly follow the size change as demonstrated by Fig. D22.

What is the significance of this apparent inconsistency in performance rating is not well understood. Has it been the result of consistency in load and geometry growth rating?

The fact that tires 23.5 - 25 and 26.5 - 25 cover the same loads at almost the same sizes but display significant differences in rolling resistance (0.0120 to 0.0180), at recommended work conditions, may suggest a need for structural changes or elimination of the less economic tire, unless there are other reasons for preserving the status quo.

Similar comment may be made with reference to the 18.00 - 25 tire. Does it belong to the 29.5 - 29, 26.5 - 25, and 23.5 - 25 tire family? Note that the same question was raised when discussing Fig. D21.

Two Tires Against One

A 29.5 - 29 tire with 28000 lb (124.54 kN) load at the recommended

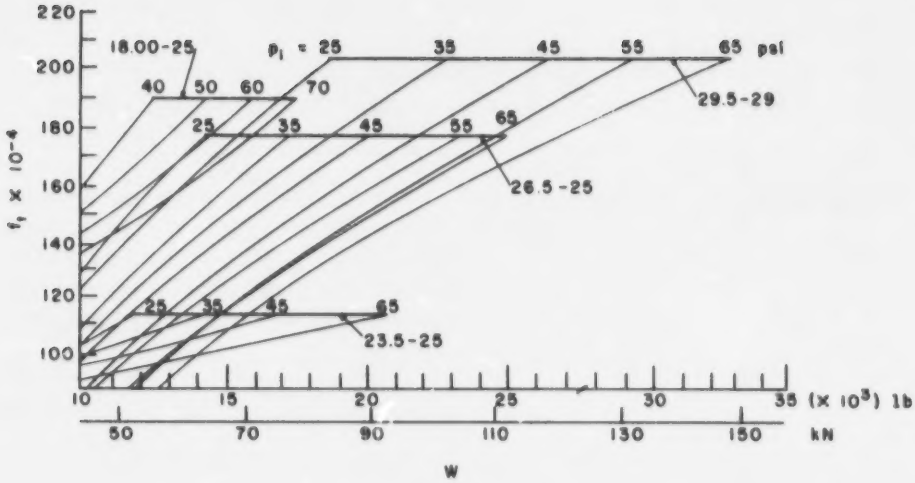

Figure D23. Rolling resistance-inflation pressure-load map for a number of specified tires. Horizontal lines define load conditions prescribed by curves, Fig. D22

48 psi (331 kPa) inflation pressure can be considered. According to the service load charts, either of the two tires, 23.5 - 25 and 18.00 - 25, each carrying 14000 lb (62.27 kN) at 37 psi (255.11 kPa) and 49 psi (337.85 kPa), respectively, can do the same job, in an assembly of two (Fig. D22).

Without considering engineering problems involved, find which tire is preferred in dual or tandem combination to replace a single 29.5 - 29 tire. Choice criteria: rolling resistance, tire weight, size, envelope, and cost as shown in Table D23.

Table D22 represents a value matrix from which the optimum tire may be chosen in accordance with the weight criteria.

Table D23. Trade-off parameters for 23.5 - 25 and 18.00 - 25 tires as a substitute in dual or tandem configuration for a single 29.5 - 29 tire

Tire	Load	Infl. pres.	Roll res.	Drag	Tire weight	Cost	Envl.
29.5 - 29	28000	48	0.0202	100	100	100	100
23.5 - 25	14000	36	0.0115	56	91	146	137*
18.00 - 25	14000	48	0.0190	94	86	122	109*

*two tires

It also shows the marked difference between 23.5 - 25 and 18.00 - 25 tires, which was mentioned before. Should the 18.00 - 25 tire be inflated to p_i = 70 psi (482.65 kPa), its rolling resistance would be still higher (0.0164) than that of the 23.5 - 25 tire. Perhaps size 20.5 - 25 should have been considered as a promising candidate.

The above example illustrates a small sample of parameters used in optimization of tire rolling resistance. There are many other parameters of different nature as exemplified below.

The Price of Inflation Pressure

It is no news that the higher the inflation pressure the smaller the rolling resistance. Thus, on a hard ground the inflation goes up. However, if the ground surface is rock-strewn or uneven, the price of inflation pressure is high: in the first case bruising and wear of the tire are accelerated by pressure elevation; in the second, dynamic loads W_{dyn} may dangerously exceed the static load W_{stat}. Hence, optimization of tire pressure is imperative.

The size effect of bruising body, or protuberance, upon tread vulnerability has been recently defined together with empirical methods for its evaluation (D15). It is now possible to trace lines of critical height H of the protruding body which produces bruises at the given speed and inflation pressure. An example of such a line is shown in the interrupted line, in Fig. D24.

The example was related to a hypothetical probability density curve of encountering the given size H of the protuberance. It was based on limited experience and illustrates the method rather than specific numerical constraints imposed upon inflation pressure.

In the same vein, the W_{dyn}/W_{stat} curves were traced on Fig. D24 for each particular tire. (Only one curve was provided for all the tires because of the same tread.) Theoretical and experimental determination of such curves is a textbook operation (D1, D7) for both the stochastic and deterministic conditions. The curves in Fig. D24 were assumed as an educated guess for the purpose of illustrating the method.

Consider a set of tires which are to carry load W = 17000 lb (75.62 kN). Figure D22 yields the following catalogue recommended service data for hard rock lug treads and speeds up to 30 mph (48 km/h):

Tire:	26.5 - 25	p_i = 35 psi	(241.3 kPa)
	23.5 - 25	p_i = 50 psi	(344.7 kPa)
	11.00 - 25	p_i = 67 psi	(452.0 kPa)

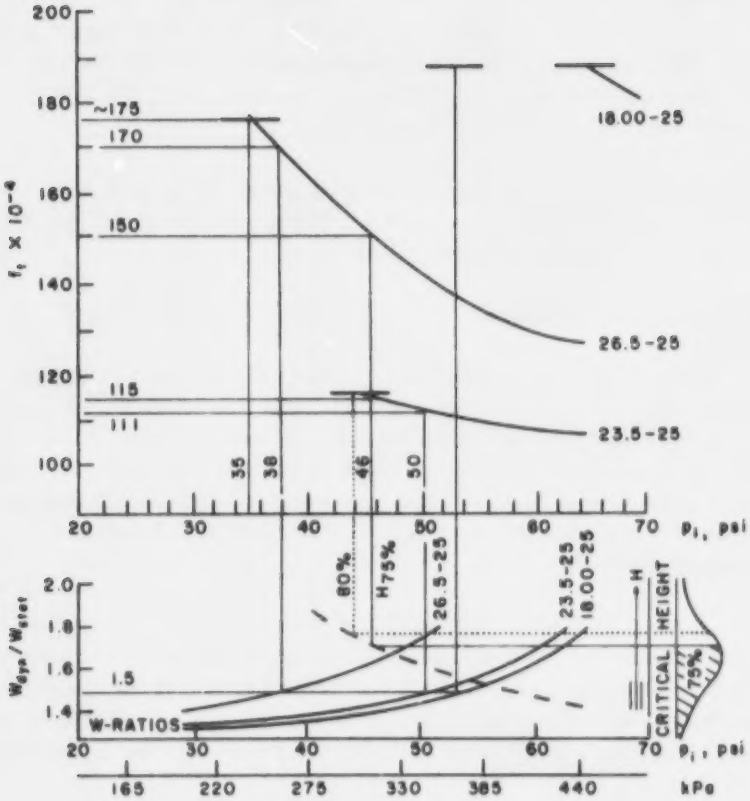

Figure D24. Rolling resistance f_t vs. inflation pressure p_i (upper graph), and the assumed bruising height H of protuberances vs. inflation, together with dynamic/static load ratios (lower graph). The upper diagram derived from Fig. D23; the lower, assumed with the probability density function of H, for the purpose of method demonstration

Question: which tire and which inflation pressure (if necessary below the service data) should be selected assuming the constraints of H and W_{dyn}/W_{stat} shown in Fig. D24? Specific values are: bruising height, H-safe over 75% of encountered protuberances, and $W_{dyn}/W_{stat} = 1.5$. The winner is the tire with the lowest rolling resistance f_t.

Using the graph in Fig. D23, values of possible f_t's were plotted as a function of p_i in the upper graph of Fig. D24. Introduction of lower graph constraints yields the following:

	Tire	p_i	f_t
Dynamic loads	26.5 - 25	<38	0.0170
	23.5 - 25	<50	0.0111
	18.00 - 25	-	-
Tread bruising	26.5 - 25	<46	0.0150
	23.5 - 25	<46	0.0115

Hence, the winner is the 23.5 - 25 tire with p_i = 46 psi and f = 0.0115.

Note that if the larger probability of avoiding bruising protuberances were assumed, say 80% (dotted line, Fig. D24), then the 23.5 - 25 tire would be eliminated as a candidate.

On a smooth flat ground strewn with sharp stones, again the 23.5 - 25 tire with 46 psi and f_t = 0.0115 would be the choice. On a clean, uneven surface, the same tire with p_i = 50 and f_t = 0.0111 should be selected.

These examples illustrate how the qualitative elements of tire life evaluation may be quantitized together with the optimum of rolling resistance.

Single Tire vs. Dual

The section entitled "Two Tires vs. One" dealt with a number of trade-offs, assuming the same tire load for each candidate, irrespective of dimensions and tire configuration. That did not necessarily cover the question of "singles vs. duals" as often discussed in professional circles.

Unfortunately, the "duality vs. singleness" is a configuration problem which cannot be separated from other tire parameters. Hence, any configuration comparison also reflects the combined effects of other parameters. An example illustrates the point quantitatively, assuming rolling resistance f_t as a common denominator.

To maximize the focusing of single vs. dual configuration *per se*, overlapping inflation pressures and loads were assumed together with tire envelopes dimensionally as close to each other as possible. The task was not easy as available catalogues contain information usually widely dis-

persed. The best selected tires fitting our requirements are 24 - 21 DT single and 11.2 - 28 dual, as shown roughly drawn to scale in Fig. D25. Their dimensions and deflection characteristics are shown in Table D24. Two loads were selected for comparison: 6000 lb (26.69 kN) and 4000 lb (17.79 kN).

Computations of rolling resistance f_t were performed in the usual manner as exemplified before. For the sake of brevity the intermediate computational results were not quoted. The final result was shown in Fig. D25.

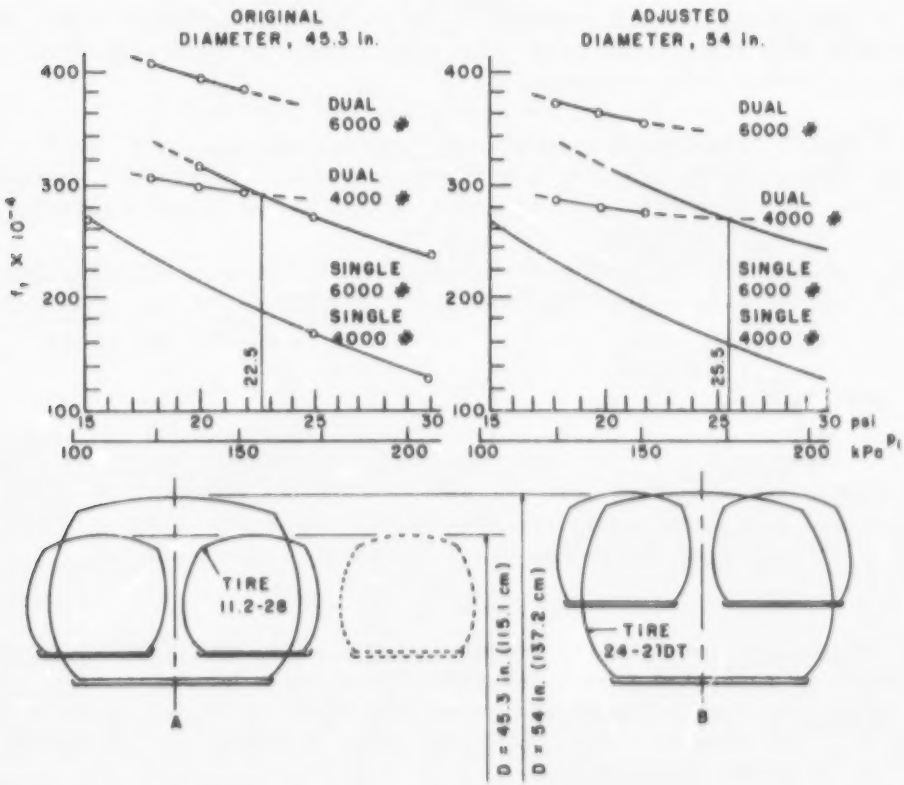

Figure D25. Rolling resistance of single and dual tires at a number of inflation pressures and two loads. Figure D25A pertains to tire dimensions published in the catalogues. Figure D25B pertains to the dual tire diameter adjusted to the same value as that of the single tire

Table D24. Input data for calculation of rolling resistance of the 24 - 21 DT single tire and of the 11.2 - 28 dual tire, for two loads and the corresponding range of inflation pressures

		p_i	A	b_0	l	λ
Single, 24 - 21 DT, Sand Rib, E7; D = 54 in. (137.2 cm); b_{tr} = 18.9 in. (48 cm); r = 19.5 in. (49.5 cm); h = 16.5 in. (41.9 cm).	6000#	20	250	18.6	16.7	0.8048
		25	220	17.1	15.9	0.8091
		30	190	15.8	14.9	0.8079
	4000#	15	204	16.5	15.7	0.7875
		25	148	14.0	12.9	0.8195
		30	130	12.9	11.6	0.8687
Dual, 11.2 - 28, All Traction; D = 45.3 in. (115.1 cm); b_{tr} = 8.9 in. (22.6 cm); r = 9 in. (22.9 cm); h = 7.8 in. (19.8 cm)	3000#	18	142	9.15	17.5	0.8868
		20	135	9.10	17.1	0.8675
		22	130	9.00	16.8	0.8597
	2000#	18	108	8.60	15.1	0.8317
		20	102	8.48	14.7	0.8182
		221	96.5	8.33	14.4	0.8045

Figure D25A shows the result for the original tire diameters quoted in the catalogues, i.e., 54 in. for the single, and 45.3 in. for the dual. The following conclusions may be deduced from the graph:

- the single tire, say, at 20 psi has 27% lower rolling resistance than the dual, for 6000 lb load
- 11.2 - 28 tire is overloaded at 6000 lb in dual configuration
- load of 4000 lb for the dual is more realistic. The single is approximately 40% better under that load, at 20 psi
- note that three single 11.2 - 28 tires produce the same rolling resistance as one 24 - 21DT tire, at approximately 22.5 psi, if the first are loaded with 2000 lb each, and the second with 6000 lb

The motion resistance comparison shown in Fig. D25A reflects a distortion due to unequal outside diameters of the tires considered. Hence the single looks much better than it should because it has larger OD.

To correct that distortion, it is plausible to assume that the deflection characteristics and the cross-section dimensions of the 11.2 - 28 tire

remain unchanged, for practical purposes, when its rim diameter is increased by approximately 9 in. (22.9 cm) so that the OD of the dual tire equals that of the single (see Fig. D25B).

Calculations of rolling resistance of such an "adjusted" tire diameter were performed for the same deflections δ as those calculated before for the original tire diameter D = 45.3 in. Hence, the ground contact area A had to be adjusted also using Equation [D9] or [D10], depending whether $b_0 > b_{tr}$, or not, as previously shown in the sections concerned with the "Effect of Tire Diameter...(and) Tread Radius." Angle α also was recalculated for the new, 54 in., OD. ε remained the same as for the original diameter.

The result was shown in Fig. D25B. As expected, the 11.2 - 28 tire is now more reasonably loaded, and the rolling resistance gain of the single was reasonably reduced to 18% and 35% for 6000 and 4000 lb loads, respectively.

Figure D25B gives a more rational comparison between duals and singles because both have the same outside diameter. Also note that the three "adjusted" 11.2 - 28 tires produce the same rolling resistance as the single 24 - 21 DT tire, at an inflation pressure ~25.5, for 6000 lb load.

All this underscores the interdependence of various tire parameters, which cannot be totally eliminated when considering the "duality vs. singleness" of a given set of tires. To fully appreciate the problem more information than presently available would be necessary, along the lines discussed in the above numerical example.

As usual, any generalization is impossible and each case should be considered on its own merit.

Of a particular interest might be the analysis of duals vs. singles, when assuming unequal inflation pressures for both cases.

Tread Design and Rolling Resistance

Tread design mainly affects tire stiffness, which is reflected in ground contact area and tire deflection characteristics. Hence, tread design may be evaluated in terms of rolling resistance, using the method discussed here.

A 23.5 - 25 tire with three different treads is shown in Fig. D26. Tire input is: D = variable, see below; b_{tr} = 22 in. (55.9 cm); r = 50 in. (127 cm); h = 20.67 in. (52.5 cm); and

p_i = 35 lb W = 17810 in.
p_i = 45 lb W = 20640 in.
p_i = 55 lb W = 23210 in.

Tread	D (in.)	A (in.^{2})
1	64.1	372
2	66.1	336
3	66.5	331

Upon following the usual procedure of f_t evaluation, the result was plotted in Fig. D26.

The differences between the three treads are somewhat biased with the assumption of λ = 0.85, which was averaged from the Deflection Chart for tread 2. In addition, tire diameters are not the same. An adjustment of these deviations could have been made as shown before (Fig. D25). However, the differences would lie within the limits of the error of the method.

The example indicates that it should be possible to classify tread signatures in definite groups as a function of rolling resistance, and to explore the optima of design within a variety of tire dimensions.

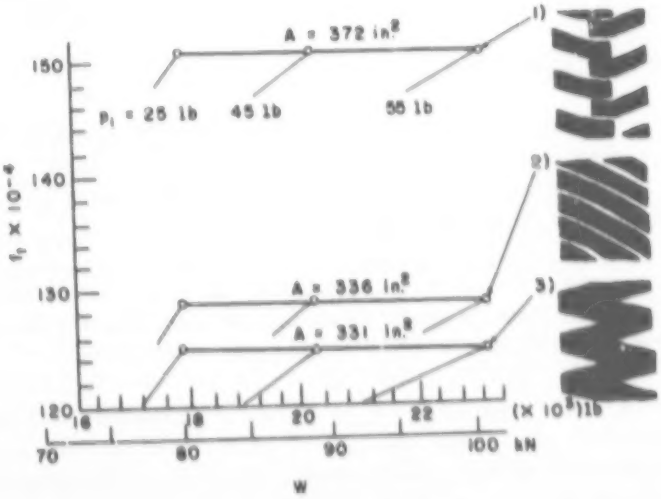

Figure D26. Effect of tread design upon tire rolling resistance f_t at various loads and inflation pressures for constant ground contact areas A. Tire size: 23.5 - 25

For instance, an increased rolling resistance of a certain useful tread design could be compensated by an increase of tire diameter which would reduce the resistance. Other cases of similar problems may be profitably solved without great investment in experimentation and time.

Rolling Resistance on a Flat and Curved Surface

This problem is important when comparing test results of tire rolling resistance, performed on a flat road and on a laboratory dynamometer with different drum diameters.

A solution based on the method presented in this paper and published some time ago (D16) yields the following equation for rolling reistance $f_t d$ of a tire tested on the drum with D_d diameter:

$$[D11] \qquad f_t d = (1/W)(180/16\pi b_0 p_g)\{D^2\varepsilon\{[(\pi/90)\alpha - \sin 2\alpha]/\alpha(D - 2\delta)\} + D_d{}^2\varepsilon\{[(\pi/90)\alpha_d - \sin 2\alpha_d]/\alpha_d(D_d - 2\delta_d)\}\}$$

The meaning of symbols was shown in Figs. D27 and D2.

Experimental corroboration of the result calculated for a 7.00 - 16 tire at 9.2 psi (63.4 kPa), for 500 lb (2224 N), was shown in Fig. D28 as a function of number drum/tire diameter ratios, D_d/D. Note that there is a critical value of that ratio beyond which test results are not acceptable.

More work seems to be needed to further develop Equation D11.

Competitive Bids and Tire Drag

When a large number of tires is acquired through competitive bids, many factors are considered before the final choice is made. Among them, however, the rolling resistance does not seem to have much priority though over-all energy savings involved may be enormous.

Tires of the same nominal size, produced by various manufacturers, never have exactly the same geometry and deflection characteristics, and, hence, may differ significantly from an economy viewpoint.

As an example, take two 10.00 - 20 tires produced at different times by two manufacturers. The tread design of each is of a common highway truck type (the 10.00 - 20 tire evaluated before is a different type). Other characteristic data of the considered tires were listed in Table D25.

Using that input, it was calculated that the rolling resistance of the two tires is: Tire X, $f_t = 0.0164$; Tire Y, $f_t = 0.0222$.

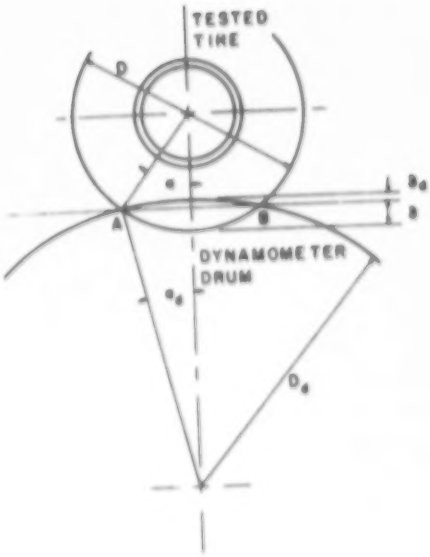

Figure D27. Geometry of tire deflection on tire-dynamometer drum interface AB. Rolling resistance is assumed to result from tire deflection caused by the curvature of the drum

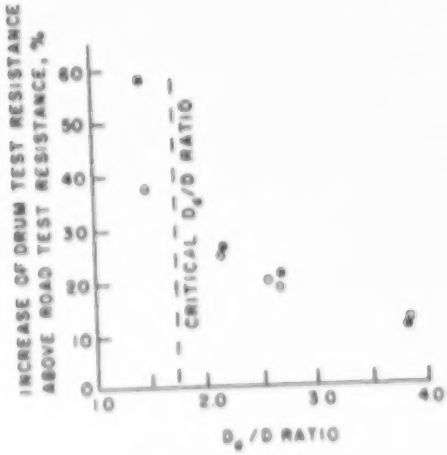

Figure D28. Increase of rolling resistance of a 7.00 - 16 tire on a dynamometer drum with a number of diameters as compared with rolling resistance on a flat road. Data calculated from Equation [D11] are marked with dots, those measured, with circles

Table D25. Catalogue and deflection chart input for two 10.00 - 20 tires produced at different times by two manufacturers*

	D	A	h	r	b_{tr}	λ	W	P_i	W_{tire}
Tire X	41.12	61.2	10.56	9.62	6.8	0.85♦	4000	70	103
	104.4	394.8	26.8	24.4	17.3		17.8	275.8	458
Tire Y	41.5	73	10.75	15.5	7.0♦	0.85	4000	70	105
	105.4	471.0	27.3	39.3	17.8		17.8	275.8	467

*Upper rows in lb-in. units, lower, in SI units.
♦Assumed.

The difference, 0.0058, is significant though tire weights are practically the same, 467 N and 450 N. If a large number of tires is contemplated the parasite drag, 17.8 × 0.0058 = 103.2 N (23.2 lb), per tire grows rapidly. Considering a 10000 km road stretch, the energy saving due to the selection of tire X amounts to 28.7 kW h.

The example is probably slightly biased with some input data which were not readily available. Nevertheless, the orders of magnitude of losses involved appear correct.

Fuel Consumption and Motion Resistance

A change of 0.0010 in the rolling resistance resulted in an average fuel consumption effect of 2.2 cm^3/km on the EPA urban cycle and 1.5 cm^3/km on the highway cycle. In general, a 10% change in the rolling resistance coefficient resulted in a 2% change in vehicle fuel consumption, as reported by EPA researchers upon completion of extensive tests (D16, D17).

The tests underscore the usefulness of the calculatory method of rolling resistance evaluation, discussed here. To compare the calculated results with those measured by EPA, take the X and Y tires considered in the previous section.

In order to simplify the calculations though at some cost of the "comparability" of results concerned, assume the constant speed 80 km/h at 4000 lb load (17.8 kN). The aerodynamic drag may be assumed to equal 1.5 times tire drag according to data used in EPA tests (D17), which were performed with 3800 lb (16.8 kN) vehicle weight.

To complete the list of input data assume further that fuel consumption of the engine is 0.22 kg/HPh, the coefficient of transmission efficiency is 0.85, and specific weight of gasoline is 0.75 kg/L.

Denote the rolling resistance power by HP_x and HP_y, and the power required for overcoming the aerodynamic drag by HP_{xa} and HP_{ya}. Then,

$$HP_x = 4 \times 0.0164 \times 80 \times 10^6/(2.2 \times 75 \times 3600) = 8.8350$$
$$HP_{xa} = 8.8350 \times 1.5 = 13.2525$$
Total power: $HP_x + HP_{xa} = 13.2525$
$$HP_y = 8.8350 \times 0.0222/0.0164 = 11.9595$$
$$HP_{ya} = 13.2525$$
Total power: $HP_y + HP_{ya} = 25.2120$

Accordingly, the fuel consumption is

Tire X: $22.0875 \times 0.22 \times 10^3/(80 \times 0.73 \times 0.85) = 97.8898\ cm^3/km$
$= 24.1663$ mi/gal

Tire Y: $97.8898 \times 25.0875 = 111.7373\ cm^3/km = 21.1714$ mi/gal

The calculated rolling resistances and fuel consumptions of tires X and Y were plotted on the graph, Fig. D29. On the same graph identical experimental plots by EPA were drawn as recorded in reference (D18).

Comparison between calculated and measured values is nearly perfect. The lower rolling resistance of the hypothetical vehicle with X and Y tires of 10.00 - 20 size is mainly due to the pure highway cycle, at constant speed.

Figure D29 indicates that it is possible to predict fuel consumption when calculating rolling resistance by means of the method described in this report.

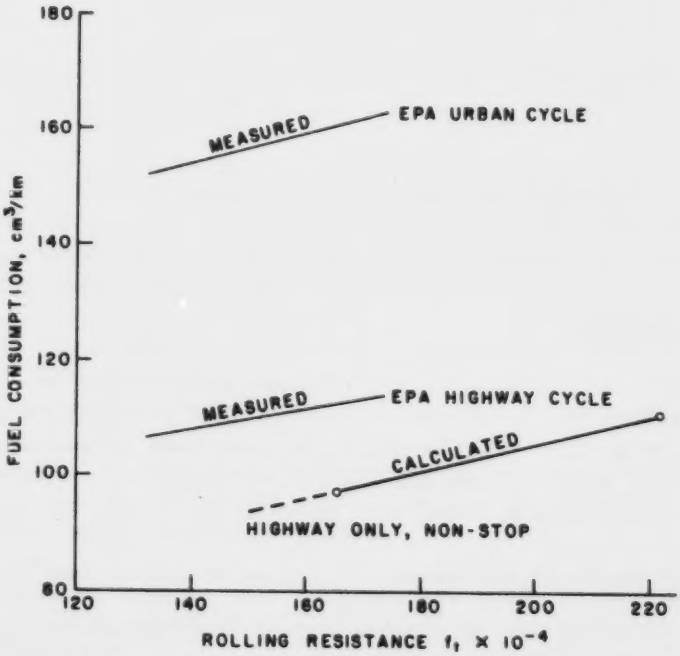

Figure D29. Calculated fuel consumption of a hypothetical car with 10.00 - 20 tires compared with that measured for a passenger car with standard tires, at a similar gross weight

This might save much time and expense when optimizing vehicle and economy.

CONCLUSION, COMMENTS AND SUGGESTIONS

The simple engineering method for evaluation of rolling resistance of elastic tires on unyielding ground appears to work, for practical purposes.

It opens a broad perspective of parametric tire optimization, whereby tire geometry, loads, and an empirical coefficient represent a mechanically complete tire characteristic, at speeds when hysteresis and heat generation are of little significance. This approach is of importance, particularly in off-road locomotion.

Introduction of tire geometry and loads into the calculation of rolling resistance enables the engineer to trade off various tire parameters, at the design stage, as well as in actual operational cycles.

Fuel consumption, economy, tire life may be approached in a quantitative way with a computer, besides the costly experimentations.

Standardization of tire sizes, loads, tread designs, etc., may be helped in a novel scrutiny of parameters involved.

Studies of tire carcass internal structure and materials may be related quantitatively and directly to tire load and geometry, in a semi-empirical manner rather than the fully empirical one.

It appears that a comprehensive research program may be inexpensively conducted along the topic ideas discussed in this paper. The nature of such an activity and its program hopefully have been illustrated, at least in part, with the numerical examples which were treated at length to provide a "feel", besides the "know-how" as to where to go.

Naturally, further improvement of the method discussed here would be necessary.

APPENDIX D. ROLLING RESISTANCE OF PNEUMATIC TIRES

PART II. HOMOGENEOUS SOILS WITH SOFT, YIELDING SURFACES

Part I of this Appendix presented a method for solution of rolling resistance of elastic tires, on hard surface. Part II continues the presentation in relation to soft, yielding surface of a homogeneous ground.*

The reader is referred to Fig. D1, which depicts three components of tire rolling resistance. The carcass flexing resistance f_t was considered to be the only component generated by unyielding surfaces. Now, in soft ground, two more components are added: the unit resistance f_c, due to vertical soil deformation (compaction, rut making), and the unit resistance f_b, caused by horizontal soil deformation and called, somewhat inaccurately, the bulldozing resistance.

The carcass flexing resistance may exist in soft ground if the tire is deflected, or may not, if the ground is soft relative to tire load and inflation pressure, so that the tire behaves like a rigid wheel.

The method presented here is based on two separate mathematical and geometrical models of the road-wheel system. The first defines the rigid condition of the tire; the second, the elastic one (Fig. D30).

There is no practical continuity between the two models. The transition from rigid-to-elastic, or vice versa, lies on the path of changes overshadowed in this limiting case, by the intangibles of the system, which can be approximated only by a heuristic reasoning.

This does not prevent acceptable practical predictions of rolling resistance for the tires, even at the point of discontinuity, by means of a simple technique rather than by a still nonexistent rigorous solution.

The technique is based on a semi-empirical approach in which mechanical and geometrical parameters of the system are processed in accordance with the principles of applied mechanics.

Soil parameters serving that purpose have been defined in literature; they are called Bevameter Soil Values and are listed below (D2, D6, D7, D9).

---

*Non-homogeneous soils will be discussed in Part III of this Appendix.

k_c	"cohesive" coefficient of sinkage
k_ϕ	"frictional" coefficient of sinkage
n	exponent of sinkage
K_γ, K_c	Terzaghi's parameters of passive earth pressure
ϕ	soil friction angle (unconfined test)
c	soil cohesion (unconfined test)
γ	soil density

Statistical character of these values, even in the most strictly controlled laboratory conditions, must be recognized whenever comparison between theory and experiment is made. The same applies to the measurements of wheel performance, which inevitably display data scatter that may not be acceptable in point-to-point correlation.

This topic will be illustrated in the following calculations though statistics was not used for the sake of time and space economy.

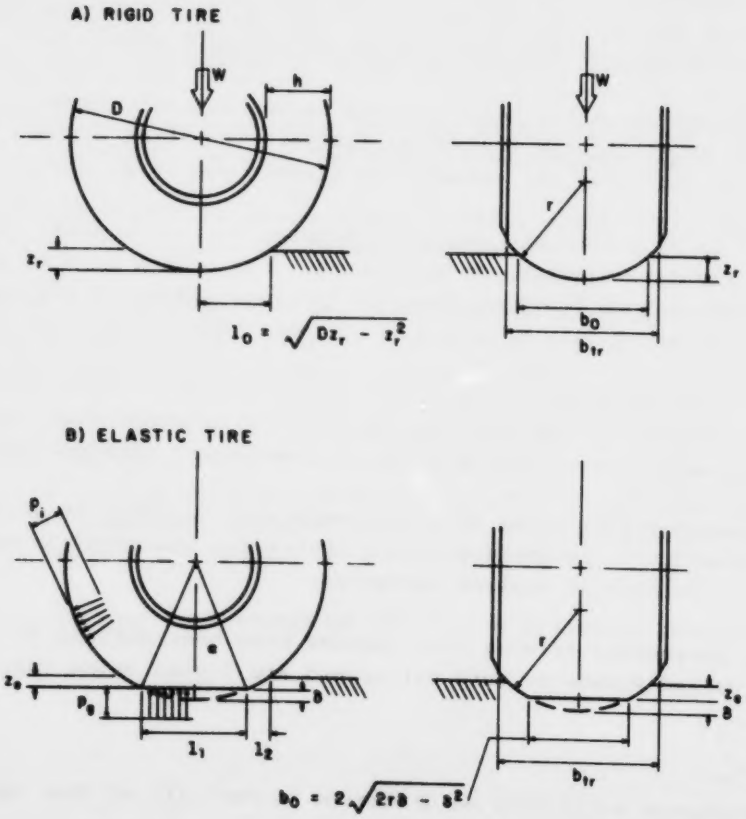

Figure D30. Forces and geometry of the assumed tire model

TIRE MODELS

As mentioned before, two tire models were used. They represent an idealized structure of tire-soil forces, tire geometry and deformations involved in the system (Fig. D30). The validity of the models is determined only by their experimental verification, which is the main subject matter of this report.

Input data include tire load W; inflation pressure p_i; average ground contact pressure p_g, obtained from tire deflection tests; width of ground contact area, b_0, b_{tr}, or l_0, depending on circumstances specified later; tread width b_{tr}; tread radius r; section height h; overall tire diameter D.

The rigid tire model with tread curvature r is considered in soft ground as a flat tread model, whereby $b_0 = b_{tr}$, unless sinkage z is unusually low. However, in that case a flat surface may often give a better approximation of the system.

In the case of the elastic tire model, it is assumed that the main load portion is supported by the deflected tire carcass b_0. This may be easily checked when calculating b_0. However, close to the transition point, when the tire becomes rigid, this assumption involves an error, as mentioned before. Error estimates may be made heuristically, which is described when discussing numerical examples.

The data bank includes Deflection Charts such as shown on Fig. 3, or tire maps, which define tire carcass supporting power ($p_g - p_i$) for the given load and inflation presure p_i.

Soil parameters k_c, k_ϕ, n, c, ϕ, K_γ, K_c are determined in accordance with established techniques (D2, D6, D7, D9, D19), preferably in the form of mean values with the estimates of standard deviations.

Experimental data of tire performance used for verification, or monitoring of calculations, also should be given within the bank width of the empirical error.

MATHEMATICS OF TIRE EVALUATIONS

Mathematical relationships between the described system's parameters have been discussed in references D2, D6, D7, and D9. A working summary of equations used for prediction of rolling resistance is presented below.

Sinkage of the Rigid Wheel, or Tire

Sinkage of the rigid wheel, or tire is expressed by the formula

[D12] $z_r = \left(3W/\left\{b_{tr}(3 - n)D^{1/2}[(k_c/b_{tr}) + k_\phi]\right\}\right)^{2/(2n + 1)}$

However, if $b_{tr} > l_0$, where

[D13] $l_0 = (Dz_r - z_r^2)^{1/2}$

Equation [D12] is modified, as follows

[D14] $z_r = \left(3W/\left\{b_{tr}(3 - n)D^{1/2}[k_c/(Dz_r - z_r^2)^{1/2} + k_\phi]\right\}\right)^{2/(2n+1)}$

Solution for z_r is obtained by iteration. The case is common for wide tires. It may also occur at low sinkages. For a great majority of cases Equation [D12] may be simplified in the form:

[D15] $z_r = \left\{3W/[(3 - n)D^{1/2}(k_c + k_\phi b_{tr})]\right\}^{2/(2n+1)}$

which has been used widely in the solution of numerical examples.

Critical Inflation Pressure at Rigid-Elastic Transition Point

Critical inflation pressure at rigid-elastic transition point is defined by equation

[D16] $p_{cr} = [W(n + 1)/b_{tr}(Dz_r - z_r^2)^{1/2}] - (p_g - p_i)$

which is based on the assumption of flat tread. Considering at this stage tread curvature, r would require surface integration of ground pressure, when deducing Equation [D12], and would lead to complex solution defying a non-programmable desk calculator. This may be avoided considering a more simple approach as discussed in this paper.

In general, the tire is considered rigid, or elastic for the given load and inflation pressure, in accordance with the following inequities:

[D17] $p_i < p_{cr} \rightarrow$ ELASTIC; $\qquad p_i > p_{cr} \rightarrow$ RIGID

Sinkage and Deflection of an Elastic Tire

Sinkage and deflection of an elastic tire, like sinkage of a rigid tire (deflection zero), is determined from an equation analogous to Equation [D12], or [D14]. However, k_c denominator is here again determined by

the smaller value, be it b_0 or l_1 (Fig. D30) depending on deflection δ unknown in advance. Accordingly, a system of equations has to be solved to determine elastic tire sinkage z_e, deflection δ, and other transient parameters denoted by F, K, A, B, G, and C which help to define ground contact lengths l_1 and l_2 (Fig. D30).

The following equations and procedure have been evolved to solve the problem as described in references D3, D6, D7, and D9.

Calculate (note: for a flat tread tire, $b_0 = b_{tr}$)

[D18]
$$F = 1/(n + 1)$$
$$K = F/(n + 2)$$
$$B = WF/2$$

For $b_0 < b_{tr}$	For $b_0 > l_1$
Upon assuming b_0 determine:	Upon assuming l_1 calculate:
[D19] $A = b_0 p_g[(F^2/2) - K]$	$A = b_{tr} p_g[(F^2/2) - K]$
[D20] $z_e = \{p_g/[(k_c/b_0) + k_\phi]\}^{1/n}$	$z_e = \{p_g/[(k_c/l_1) + k_\phi]\}^{1/n}$
[D21] $G = b_0 p_g z_e/(n + 1)$	$G = b_{tr} p_g z_e/(n + 1)$

[D22]
$$C = G[(D/2) - (z_e/3)]$$

[D23]
$$l_2 = [B - (B^2 - 4AC)^{1/2}]/2A$$

[D24] $l_1 = (W/b_0 p_g) - l_2 F$	$l_1' = (W/b_{tr} p_g) - l_2 F$
	Repeat calculations until l_1' and l_1 converge.

[D25]
$$\delta = (D/2) - [(D/2)^2 - (l_1/2)^2]^{1/2}$$

[D26]
$$b_0' = 2(2r\delta - \delta^2)^{1/2}$$

Repeat calculations until b_0' and b_0 converge.

Considering the above two cases, note that the denominator of k_c is always the smaller dimension of the ground contact area.

Equations shown here yield z_r, z_e, δ, b_0 and l_1 values needed for

calculation of rolling resistance. At the point of transition from elastic to rigid, it should be expected that $z_e = z_r$. This does not usually happen. As mentioned before, inequities (D17) are based on $l_1 = 0$, for a rigid tire, and involve certain error.

Hence, it is always useful to monitor z_r vs. z_e, considering their convergence as a transition from elastic to rigid, or vice versa.

Compaction Coefficient of Rolling Resistance of Rigid Tires

Compaction coefficient of rolling resistance of rigid tires is determined from equation (1), reference D20.

[D27] $$f_c = b_{tr}[(k_c/l_0, \text{ or } b_{tr}) + k_\phi]z_r^{n+1}/W(n + 1)$$

which neglects tread curvature.

Compaction Coefficient of Rolling Resistance of Elastic Tires

This is defined by the same basic equation taking the following forms:

For $b_0 < b_{tr}$

$$f_c = \frac{(b_0 k_\phi + k_c)z_e^{n+1}}{W(n + 1)}$$

For $b_0 > l_1$

$$f_c = \frac{b_0[(k_c/l_1) + b_\phi]z_e^{n+1}}{W(n + 1)}$$

If b_{tr} is the smallest dimension of the ground contact area,

[D29] $$f_c = (b_{tr}k_\phi + k_c)z_e^{n+1}W/(n + 1)$$

Horizontal Ground Deformation Coefficient of Rolling Resistance

This is an almost entirely empirical value though based on the analog of passive earth pressure of a retaining wall as propounded by Terzaghi (D6, D21).

The formula originally proposed in terramechanics (D2) underwent much testing and some modifications leading to the following form:

[D30]
$$f_b = b_{tr}(zcK_c + 0.5z^2\gamma K_\gamma)/W \qquad \text{"general" shear}$$
$$f_b = b_{tr}(0.6667zcK_c + 0.5z^2\gamma K_\gamma)/W \qquad \text{"local" shear}$$

Equations [D30] represent passive pressure acting upon a retaining

wall of height z_r, or z_e (Fig. D31). The problem lies in the selection of coefficients K_c and K_γ from Terzaghi's tables (D21).

In most cases there is no indication if soil failure takes place through the "general" or "local" shear. For loose frictional soils ($\phi \sim 30°$), close to maximum density, experimental evidence shows that $K_\gamma = 30$. For lesser densities, it may reach value $K_\gamma = 10$. It is within these limits that K_γ may be assumed although for well-controlled laboratory experiments, one may narrow the test results to $K_\gamma = 10$ to 20, or less.

Cohesive soils have been less experimented with because of inherent difficulties in reproducing original soil characteristics. Equations [D30], however, are acceptable if friction ϕ and cohesion c are measured by means of a bevameter, i.e., by the "unconfined" soil test. Civil engineering soil tests produce to high values, as discussed in the literature (D6, D9).

Working with cohesive soils defies point-to-point correlation of the theory and experiment. Statistical approach is a must. Unfortunately, this has not yet been recognized by the profession, and even the most expensive models of soil-vehicle relationship are deterministic. No wonder that they often fail to predict black and white, where everything is grey, with all the possible shades.

The introduction of low and high limits for f_b results in the predictive band width which depends on sinkage z_r, or z_e, entering Equations [D30] in the second power. This is why at high wheel sinkages the result is enclosed by a wider band of error than at low sinkages.

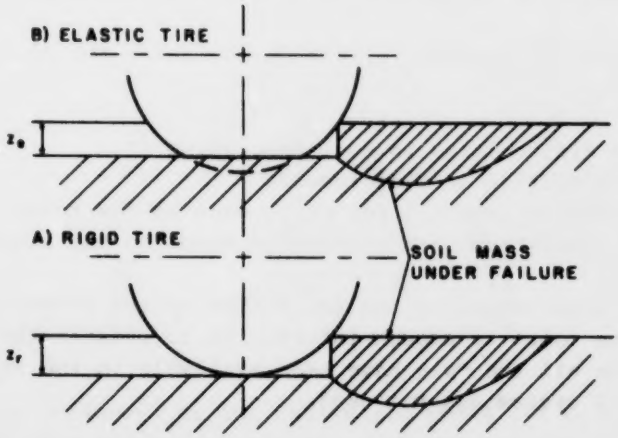

Figure D31. Horizontal soil deformation assumed for a rigid and elastic tire

The outcome is compatible with rules of soil mechanics, and the error of prediction is unavoidable, particularly when excessive loads impart excessive soil deformation (D7).

To minimize the error, further work is needed, particularly with cohesive soils and their statistical variability.

Tire Carcass Flexing Coefficient of Rolling Resistance

This was defined in Part I by Equation [D6], which is reproduced below for the convenience of the reader. It applies only to elastic tires since rigid tires do not flex by definition, and display $f_t = 0$.

[D6] $$f_t = [3.581bD^2p_g\varepsilon(0.0349\alpha - \sin 2\alpha)]/W\alpha(D - 2\delta)$$

The value of b is defined by b_0 if the latter is smaller than b_{tr}, and by b_{tr} if it is not.

Coefficient ε and angle α are

[D7] $$\varepsilon = 1 - \exp(-k\delta/h)$$

[D5] $$\alpha = \cos^{-1}[(D - 2\delta)/D]$$

Values of k are assumed 15 or 7 for the regular and radial tires, respectively.

VALIDATION OF ROLLING RESISTANCE PREDICTIONS

Controlled tests of rolling resistance encounter the following four problems:

(1) enormous difficulties in soil processing
(2) resulting scatter of measurements
(3) difficulties in controlling slip, when no-tow tests are applied
(4) lack of statistical procedures for handling the problems.*

All this has often obscured the validation of the theory by experiment. Nevertheless there is enough information to present the case as shown below. Since all the data have been available in the English system of measures, the SI system was not used.

---

*Computerized method of bevameter data processing developed by Wong (D19), eliminates the problem to a large extent.

7.00 - 16 Tire; Dry, Sandy Soil

Input data are as follows: $D = 30.5$, $r = 7.0$, $k_c = 0.3$, $n = 0.92$, $b_{tr} = 5.5$, $h = 6.64$, $k_\phi = 3.7$, $k_\gamma = 10 - 30$, $c = 0$.

	p_g	
p_i	W = 750	W = 1650
10	15.5	25.0
20	20.0	30.0
30	25.0	34.0
40	30.0	48.0

The values of $p_i(p_g)$ were obtained for two different loads W from the deflection chart partially reproduced in Fig. D32.

Since the chart was available only for higher inflation pressures, 50, 60, and 70 psi, while our interest pertains to the low pressures, 10, 20, 30, 40 psi, the needed p_g's were extrapolated by drawing a line through the high pressure points, Fig. D33.

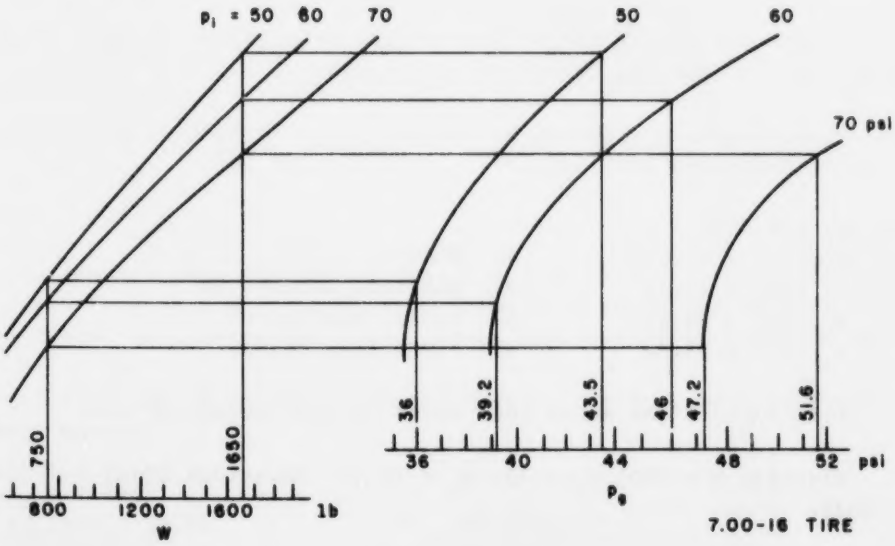

Figure D32. Fragment of the Deflection Chart for a 7.00 - 16 tire, reproduced from the Goodyear chart with the purpose of determining p_g for tire loads 750 and 1650 lb, at 50, 60 and 70 psi. Note that the original chart did not provide p_g for lower inflation pressures which are of interest in this case

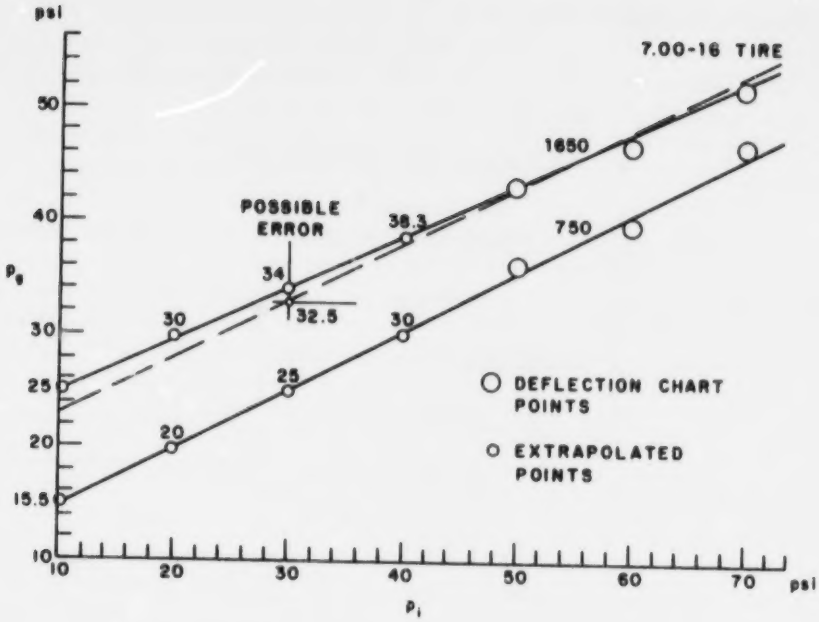

Figure D33. Extrapolation of p_g for lower inflation pressures, from those given for higher p_i values, Fig. D32

The reader may recall the structural characteristics of this graph by comparing Figs. D5 and D6, Part I of this Appendix.

Calculations start with the definition of RIGID-ELASTIC CRITERION (REC), using Equations [D15] to [D17]. For W = 750 lb:

$z_r = 4.8757$	
$p_{cr}(10) = 17.92$	1. ELASTIC
$p_{cr}(20) = 23.42$	2. ELASTIC, BORDERLINE
$p_{cr}(30) = 28.42$	3. RIGID, BORDERLINE
$p_{cr}(40) = 33.42$	4. RIGID (see below)

Solutions of the above four cases of tire behaviour are

1. Elastic; W = 750; $p_i = 10$; $p_g = 15.5$. Equations [D18] - [D30], [D5] - [D7].

$F = 0.5206$	$z_e = 4.6478$	$l_1 = 6.3174 > 4.24$	$f_c = 0.2121$
$B = 195.3$	$G = 159.0903$	$\delta = 0.3307$	$f_b = 0.0475$
$b_0 = 4.24 < 5.5$	$C = 2175.6538$	$\alpha = 11.9538$	0.1426
$A = -2.8128$	$l_2 = 9.7824$	$\varepsilon = 0.5262$	$f_t = 0.0051$

$f = f_c + f_b + f_t = 0.2647$
$\qquad\qquad\qquad\quad 0.3598$

(The b_0-value quoted here was obtained after a number of iterations.)

2. Elastic, borderline; $p_i = 750$; $p_i = 20$; $p_g = 20$. Assuming tire elasticity the following were calculated:

$F = 0.5208$	$z_e = 6.0975$	$l_1 = 4.9297$	$f_c = 0.2820$
$B = 195.3$	$G = 232.6577$	$\delta = 0.2005$	$f_b = 0.0818$
$b_0 = 3.33$	$C = 3075.1536$	$\alpha = 9.3011$	$\quad 0.2454$
$A = 2.8505$	$l_2 = 12.1573$	$\varepsilon = 0.3642$	$f_t = 0.0021$

$f = 0.3659$
$\quad\;\; 0.5295$

(The b_0-value quoted here was obtained after a number of iterations.)

The calculated rolling resistance appears abnormally high. Note that the calculated value of $z_e = 6.0975$ is larger than $z_r = 4.8757$. All this indicates that the tire is RIGID. Pertinent calculations are referred to below:

3. Rigid; $W = 750$; $p_i = 30$; $p_g = 25$. Now, inflation pressure is irrelevant.

$z_r = 4.8757$	$f_c = 0.3003$	$f_b = 0.0523$	$f = 0.3526$
		$\quad 0.1569$	$\quad 0.4572$

4. Rigid; inflation pressure irrelevant. For $W = 750$, as in case 3,
$f = 0.3526$
$\quad\;\; 0.4572$

The results were plotted on Fig. D34. Heuristic fitting of tire rolling resistance at the rigid-elastic transition point was marked with the double T-bar, in interrupted lines. Note the scatter of measured values.

Calculations of rolling resistance at $W = 1650$ lb were performed in the same manner.

$z_r = 8.4952$

$p_{cr}(10) = 27.13$	1. ELASTIC
$p_{cr}(20) = 32.13$	2. ELASTIC
$p_{cr}(30) = 38.13$	3. ELASTIC
$p_{cr}(40) = 43.85$	4. ELASTIC, BORDERLINE

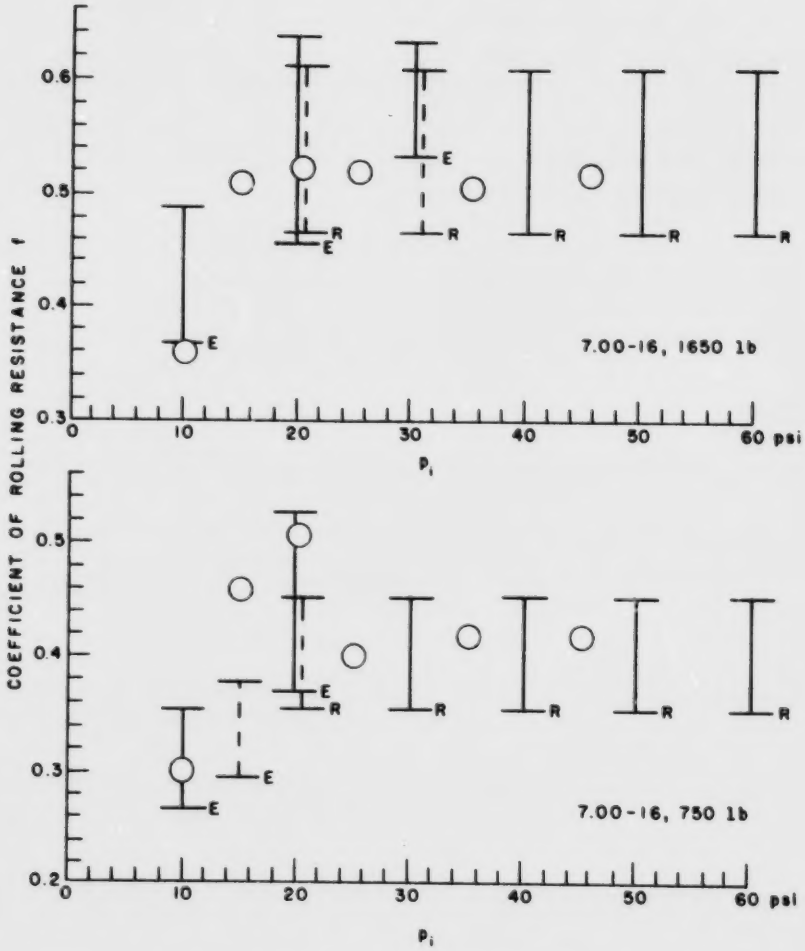

Figure D34. Calculated and measured values of rolling resistance of a 7.00 - 16 tire at 750 and 1650 lb loads, in a sandy soil specified in the text, in terms of bevameter data. Letters R and E denote rigid and elastic state of the tire, respectively. Double T-bars traced in interrupted lines refer to additional check points of tire performance at various inflation pressures p_i

The main parameters of the calculations and the sought for solutions for the above four cases are

1. Elastic; W = 1650; p_i = 10; p_g = 25. Equations as before.

b_0 = 4.8	α = 13.7051	f_b = 0.0613	f = 0.3647
z_e = 7.8331	ϵ = 0.6250	0.1839	0.4873
δ = 0.4342	f_c = 0.2967	f_t = 0.0067	

2. Elastic; $W = 1650$; $p_i = 20$; $p_g = 30$. As per case 1.

$b_0 = 4.05$	$\alpha = 11.4840$	$f_b = 0.0906$	$f = 0.4592$
$z_e = 9.5180$	$\varepsilon = 0.4983$	0.2718	0.6404
$\delta = 0.3530$	$f_c = 0.3650$	$f_t = 0.0036$	

This appears to be a rather high value (Fig. D34). Note that $z_e > z_r$ as before. Again, the signs are that the tire is RIGID rather than ELASTIC. The double T-bar, interrupted lines, fit the general trend better. This is checked below:

3. Elastic; $W = 1650$; $p_i = 30$; $p_g = 34$. As before:

$b_0 = 3.59$	$\alpha = 10.0801$	$f_b = 0.1182$	$f = 0.5359$
$z_e = 10.8753$	$\varepsilon = 0.4124$	0.3546	0.7750
$\delta = 0.2354$	$f_c = 0.4190$	$f_t = 0.0024$	

It is obvious that the rolling resistance as calculated for the elastic tire is too high. Again $z_e > z_r$. The tire is RIGID (interrupted line double T-bar, Fig. D34). Calculations for the rigid tire are shown below.

$z_r = 8.4952$	$f_c = 0.3954$	$f_b = 0.0722$	$f = 0.4676$
		0.2166	0.6120

4. Rigid; $W = 1650$; inflation pressure irrelevant. Calculations as in the preceding point.

$f = 0.04676$
$\quad 0.6120$

The results were plotted in Fig. D34. Note again some scatter of measured data in the vicinity of $p_i = 15$ psi. The outcome may be considered satisfactory.

One may ask, however, why the REC determination was rather misleading in cases 2 and 3, by a substantial margin.

Besides the previous explanations related to the geometrical and mathematical models, one may note that the $p_i(p_g)$ values used in computations were extrapolated (Fig. D33). If the extrapolation error was such as shown in interrupted lines in Fig. D33, the p_g-values would be slightly altered. At $p_i = 30$ psi, $p_g = 32.5$ instead of 34. This would account for tire elasticity as deduced from p_{cr}, and the rolling resistance would be lower, converging with that of the rigid tire.

The lesson is that any extrapolation such as used here introduces

additional error, which would be avoided if proper Deflection Charts were available.

14.00 - 20 Tire; Sandy Soil

Input data: $D = 49$, $r = 19$, $k_c = 0.95$, $n = 1.11$, $b_{tr} = 11.8$, $h = 14.5$, $k_\phi = 3.58$, $K_\gamma = 10 - 30$.

Extrapolation of Deflection Charts, Fig. D35, yields $p_i(p_g)$ values at low inflation pressures (Fig. D36):

	p_g	
p_i	W = 2500	W = 4000
10	19.2	23
20	24.2	28
30	29.2	32.5
40	34	38

Table D26. Rigid-elastic criteria (REC) for a 14.00 - 20 tire, and its rolling reistance at 2500 and 4000 lb loads

W	p_i	p_{cr}	z_r	z_e	REC	f_c	f_b	f_t	f
2500	10	21	4.9481	4.4168	E	0.1366	0.0199	0.0043	0.1608
							0.0597		0.2006
	20	26	4.9481	5.4078	E*	0.1760	0.0414	0.0021	0.2195
							0.1241		0.3022
	30	31	4.9481	0	R	0.2390	0.0347	0	0.2737
							0.1040		0.3430
	40	36	4.9481	0	R	0.2390	0.0347	0	0.2737
							0.1040		0.3430
4000	10	30	6.6255	5.2184	E	0.1422	0.0241	0.0068	0.1731
							0.0723		0.2213
	20	35	6.6255	6.2595	E	0.1794	0.0346	0.0039	0.2179
							0.1038		0.2871
	30	32	6.6255	7.0706	E*	0.2042	0.0442	0.0025	0.2509
							0.1326		0.3393
	40	44	6.6255	(8.1017)	R	0.2766	0.0388	0	0.3154
							0.1164		0.3930

*Borderline

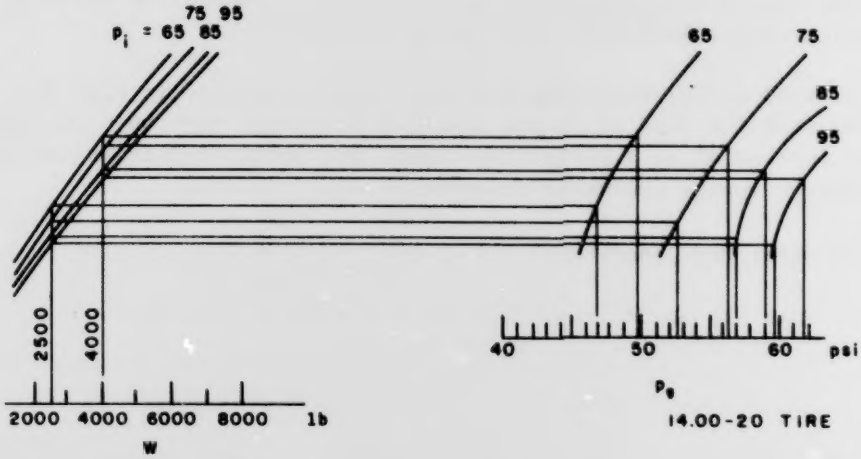

Figure D35. Fragment of the Deflection Chart for a 14.00 - 20 tire, reproduced from the Goodyear chart for 2500 and 4000 lb loads at 65, 75, 85, 95 psi, with the purpose of determining p_g

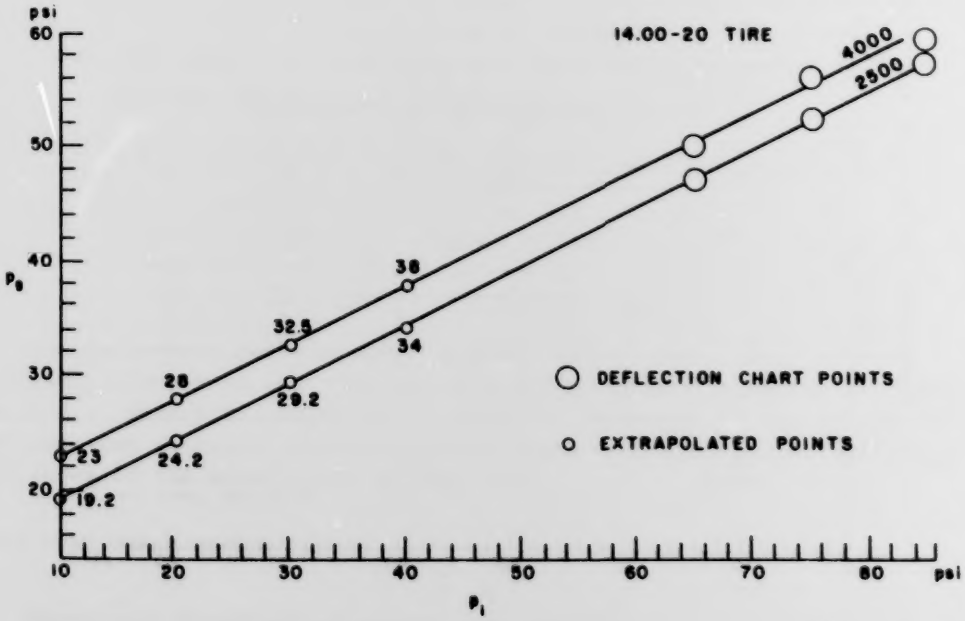

Figure D36. Extrapolation of p_g for low inflation pressures, using data for high inflation 14.00 - 20 tire, Fig. D35

Calculations were performed in the same manner as in the preceding cases. The results are summarized in Table D26. Compare the criteria of tire rigidity and elasticity: p_{cr} and z_e vs. z_r.

Calculated values were compared with those measured, in Fig. D37. The plot shows that the tire at 30 psi and 4000 lb should have been considered as rigid, instead of as a borderline case. The measured data at low inflation pressures appear scattered downward.

11.00 - 20 Tire; Dry, Sandy Soil

Input data are as follows: D = 42.7; r = 16, k_c = 1.5; n = 0.8, b_{tr} = 8.3, h = 10.07, k_ϕ = 5.0, K_γ = 10 - 30.

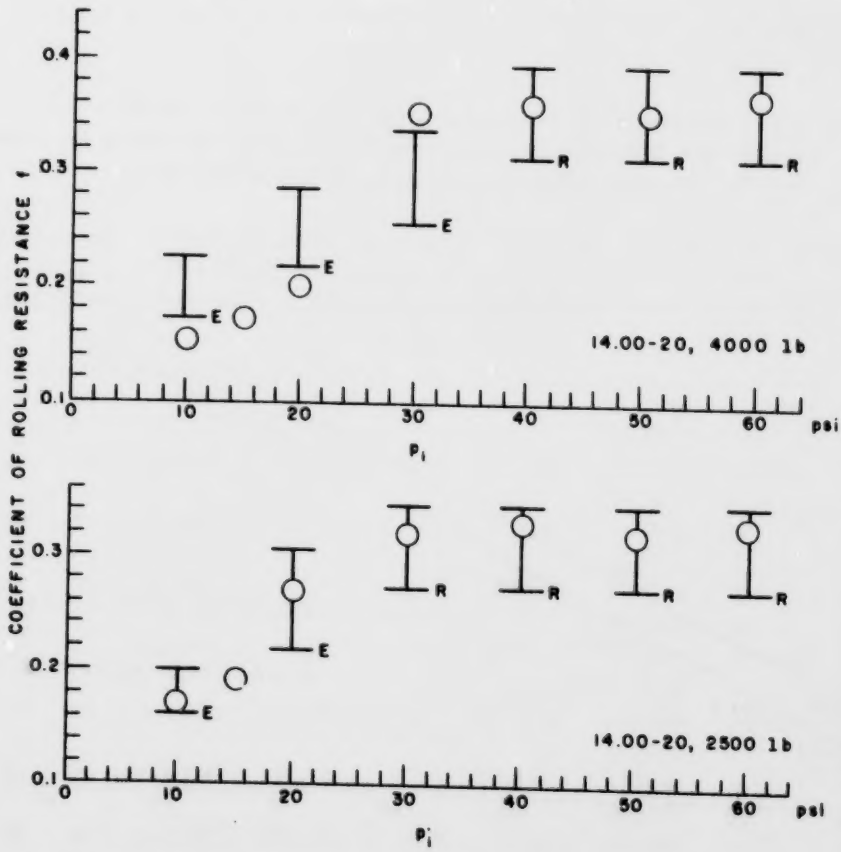

Figure D37. Calculated and measured values of rolling resistance of a 14.00 - 20 tire in sandy soils specified in the text in terms of bevameter data. Compare with Fig. D34

Extrapolation of Deflection Charts for two tire loads yields:

	p_g	
p_i	W = 2200	W = 3100
10	20	25
20	23	28
30	26.5	32
40	30	35
60	37	47

Calculations performed as before are summarized in Table D27. The results are compared with measurements in Fig. D38.

It is difficult to explain the discrepancy at 3100 lb load, for rigid tires. There is no such trend in previous examples.

Note that all the tests with 7.00 - 16, 14 - 20, and 14.00 - 20 tires were performed in a laboratory soil bin, in the same soil. However, soil data for each tire are slightly different because of difficulties in soil racking and compacting for the purpose of keeping soil consistency unchanged. The amount of soil variation is shown in bevameter values:

Tire	k_c	k_ϕ	n
7.00 - 16	0.3	3.7	0.92
14.00 - 20	0.95	3.58	1.11
12.00 - 20	1.5	5.0	0.8

The tests were performed in the late 1950's, under this writer's direction. They were instrumented in a rather primitive manner by today's standards. Better equipment and statistical treatment of the problem would have resulted in better agreement between the theory and experiment than that shown in the upper graph of Fig. D38.

Tires with Tread Buffed Smooth

Tires with tread buffed smooth were the subject of unprecedented experimentation though the reason for the tread amputation was not clear (D22).

Table D27. Rigid-elastic criteria (REC) for a 11.00 - 20 tire and its rolling resistance at 2200 and 3100 lb loads

W	p_i	p_{cr}	z_r	z_e	REC	f_c	f_b	f_t	f
2200	10	29	6.1812	5.3773	E	0.1970	0.0327	0.0043	0.2340
							0.0982		0.2995
	20	29	6.1812	6.3578	E	0.2333	0.0457	0.0025	0.2815
							0.1371		0.3729
	30	35	6.1812	7.5224	E*	0.2753	0.0640	0.0014	0.3407
							0.1921		0.4688
	40	42	6.1812	0	R*	0.2882	0.0432	0	0.3314
							0.1296		0.4178
	60	55	6.1812	0	R	0.2882	0.0432	0	0.3314
							0.1296		0.4178
3100	10	25	8.0471	7.0946	E	0.2225	0.0404	0.0029	0.2658
							0.1212		0.3466
	20	32	8.0471	8.1205	E	0.2526	0.0530	0.0021	0.3077
							0.1590		0.4137
	30	38	8.0471	9.5119	E*	0.2935	0.0727	0.0011	0.3673
							0.2181		0.5126
	40	45	8.0471	0	R*	0.3288	0.0520	0	0.3808
							0.1560		0.4848
	60	58	8.0471	0	R	0.3288	0.0520	0	0.3808
							0.1560		0.4848

*Borderline

To demonstrate the versatility of the method discussed here, samples of test results were compared with calculations based on bevameter techniques.

As noted before, the treadless torus-like tires would require, in rigid state, the integration of tire-soil losses along the curved ground contact area, instead of along a flat surface, to account for resistance R.

$$R = \iint (p_g)\, dx\, dy + y\int (p_g)\, dx$$

This, however, would lead to involved computations, without much gain in accuracy. Accordingly, a simplified solution was used here. It is based on tire contact width defined by the chord, instead of by the arc, assuming that the chord b, Fig. D39, satisfies the equation:

[D31] $b = 2r \sin \mu$

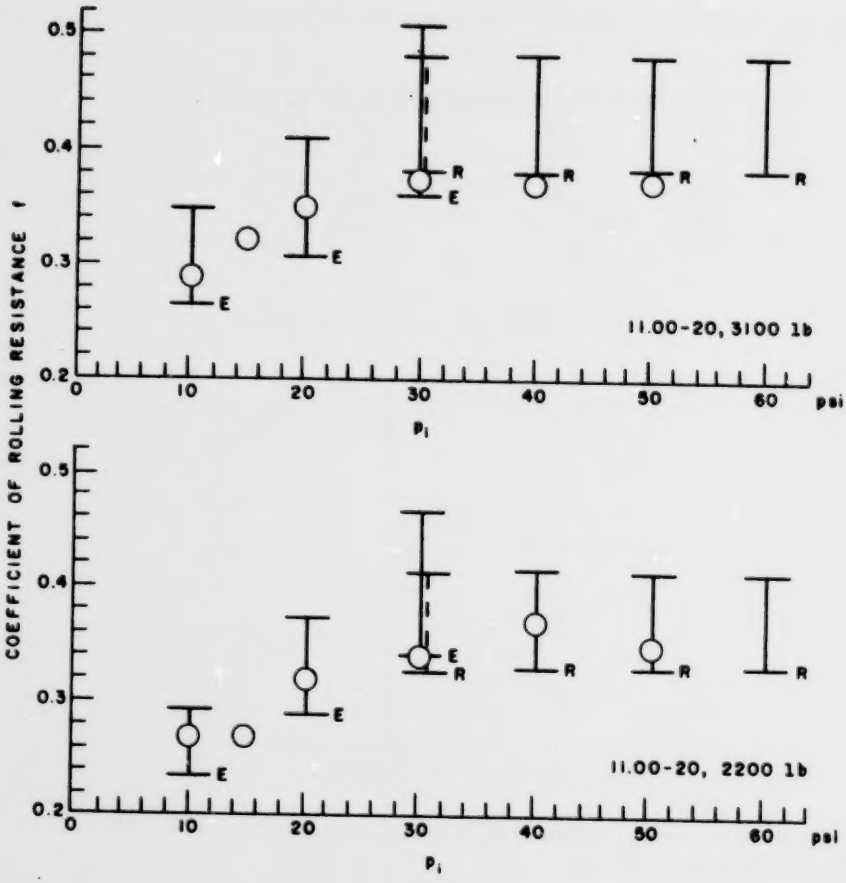

Figure D38. Calculated and measured values of rolling resistance of a 11.00 - 20 tire in sandy soils. Compare Figs. D34 and D37

where μ is the angle of friction between the tire and the soil, usually equal to the angle of soil internal friction ϕ.

Since soil density was varying during the tests, reportedly producing friction angle within the band width of 35-38°, the b-values were assumed as follows:

$$b = 2 \times 3.45 \quad \sin 35^\circ = 3.96$$
$$\sin 38^\circ = 4.25$$

1. Tire 4.50 - 18 4PR, at a constant deflection on hard surface $\delta = 15\%$. Input data: $D = 27.1$, $r = 3.45$, $p_i = 31.4$, $k_c = 3.1$, $h = 3.8$, $W = 448$, $p_g = 37.65$, $k_\phi = 10.4$, $n = 0.64$.

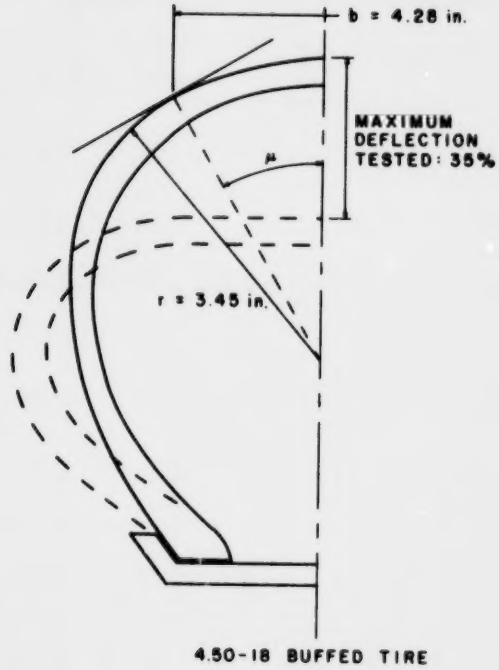

Figure D39. Experimental 4.50 - 18 tire with the buffed-off tread

Calculations show the following:

$z_r = 2.0865$ $\quad$ $p_{cr} = 17.6 < 31.4$ $\quad$ RIGID

$f_c = 0.2151$ $\quad$ $f_b = 0.0124$

0.0374

$f_{calc} = 0.2275$ $\quad$ $f_{meas} = 0.3$

$z_{calc} = 0.209$ $\quad$ $z_{meas} = 2.04$

The result of the calculations is satisfactory. Note that sinkage measurement (in sand) with two decimal accuracy is unrealistic.

Six more cases were calculated for rigid surface tire deflection $\delta = 15\%$. The input data are shown below. Assuming p_g values for the constant ground contact area $A = 11.9$ in.^{2} as measured on hard surface, at $p_i = 11.9$ psi,

W	p_g	k_c	k	n	b_0
470	39.5	*	10.6	0.74	3.96
467	39.2	*	11.9	0.69	3.96
467	39.2	2.6	13.0	0.64	4.25
470	39.5	3.3	14.4	0.65	4.25
469	39.4	6.4	15.2	0.66	4.25
468	39.3	7.0	15.7	0.69	4.25

*Incorrect measurements, neglected.

Note the spread of tire loads and soil properties. The result of calculations of rolling resistance and sinkage were plotted on Fig. D40.

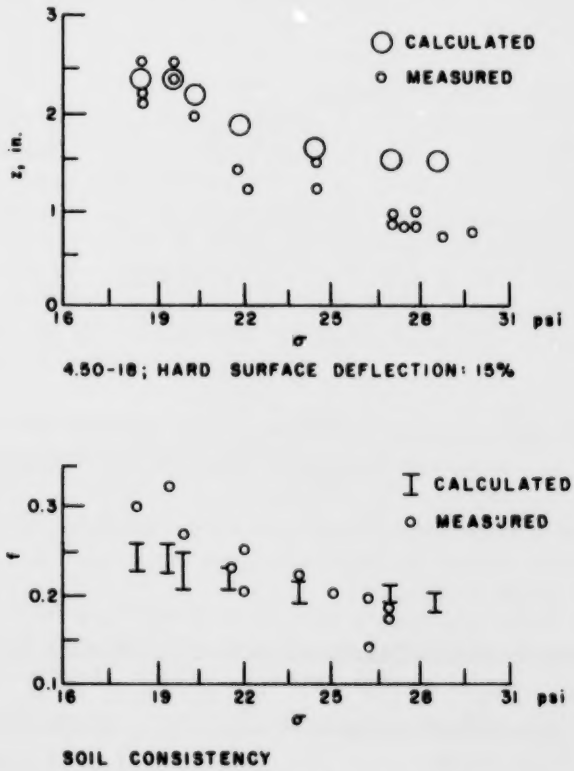

Figure D40. Calculated and measured values of rolling resistance and sinkage of a 4.50 - 18 buffed tire, at load and inflation yielding 15% deflection on a hard surface. Sandy soil of varying consistency δ

Sinkage measurements below 1 in. are definitely inaccurate. Rolling resistance at very loose soil, $\sigma = 19$, was measured with considerable slip, thus yielding unreliable comparison with calculated values.

The value of σ defines a "consolidated" soil strength expressed by pressure acting upon a 2-inch-wide strip load, at the depth of 2 in.

[D32] $\sigma = [(k_c/2) + k_\phi]2^n$

Evidently, other strip load width, and sinkage depth, could have been selected. The 2-in. value is close to the dimensions involved in the tests.

2. Tire: 4.50 - 18 4PR, at constant deflection on hard ground: $\delta = 25\%$. Input data: $W = 291$, $p_g = 12.99$, $k = 9.7$, $p_i = 8$, k_c = incorrect, neglected, $n = 0.72$.

Computations yield the following:

$z_r = 1.6073$ $\quad p_{cr} = 13.4 > 8$ $\quad$ ELASTIC

Following regular procedures for an elastic tire, calculations show

$F = 0.5814$	$b_0 = 2.5$	$\varepsilon = 0.7820$	$f_b = 0.0092$
$A = -1.4516$	$\delta = 0.3432$	$f_c = 0.0973$	0.0276
$B = 84.5930$	$\alpha = 12.9230$		$f_t = 0.0101$

$f_{calc} = 0.1166$ $\quad f_{meas} = 0.15$

0.1350

$z_{calc} = 1.5$ $\quad z_{meas} = 0.92$

Three more cases were calculated for rigid surface tire deflection $\delta = 25\%$ at a constant ground contact area $A = 22.4$ in.^{2} and $p_i = 8$ psi. The input data are shown below.

W	p_g	k_c	k_ϕ	n	b_0
291	12.99	*	9.7	0.72	2.75
288	12.86	3.5	11.9	0.64	2.90
290	12.95	5.2	14.7	0.64	3.00
279	12.40	7.0	15.7	0.60	2.95

Calculated sinkages and motion resistance were plotted in Fig. D41.

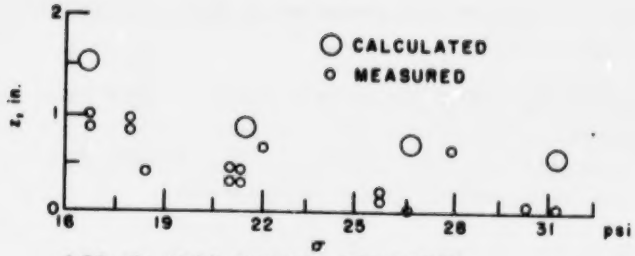

4.50-18; HARD SURFACE DEFLECTION

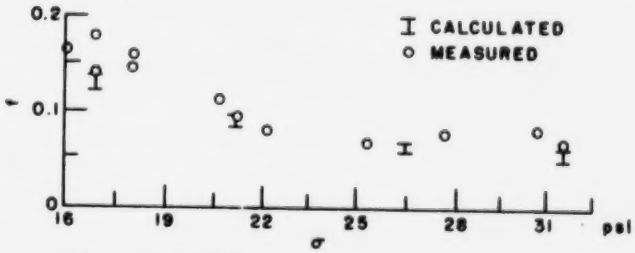

SOIL CONSISTENCY

Figure D41. Calculated and measured values of rolling resistance and sinkage of a 4.50 - 18 buffed tire, at loads and inflation pressures yielding 25% deflection on a hard surface. Sandy soils of varying consistency δ

Note the unacceptable sinkage measurements. Undoubtedly, calculations in this case are more accurate than the experimental data.

3. Tire: 4.50 - 18 4PR, at constant deflection on hard surface: $\delta = 35\%$.

Calculations were performed as in the preceding case, assuming constant ground contact area $A = 35.1$ in.^{2}, at inflation pressure $p_i = 8$ psi. The tire was, as expected, ELASTIC. Input data:

W	p_g	k_c	k_ϕ	n	b_0
448	12.76	1.3	11.6	0.68	3.3
459	12.96	0.9	9.9	0.69	3.3
460	13.1	4.4	14.4	0.67	3.5
471	13.42	1.4	16.1	0.87	3.5

Calculated sinkages and motion resistance were plotted in Fig. D42 together with measured values.

Note again the scatter of experimental data. There is a strong bias in sinkage measurements. Statistical evaluation appears inevitable for a closer scrutiny of the method. Nevertheless, the latter displays good trend and correlation with rather crude experiments.

1.75 - 26 Bicycle Tire; Sandy Soil

Input data:

$D = 28.17,$
$b_0 = 2 \sin 38^\circ = 1.23,$
$h = 1.4,$
$r = 1.0.$

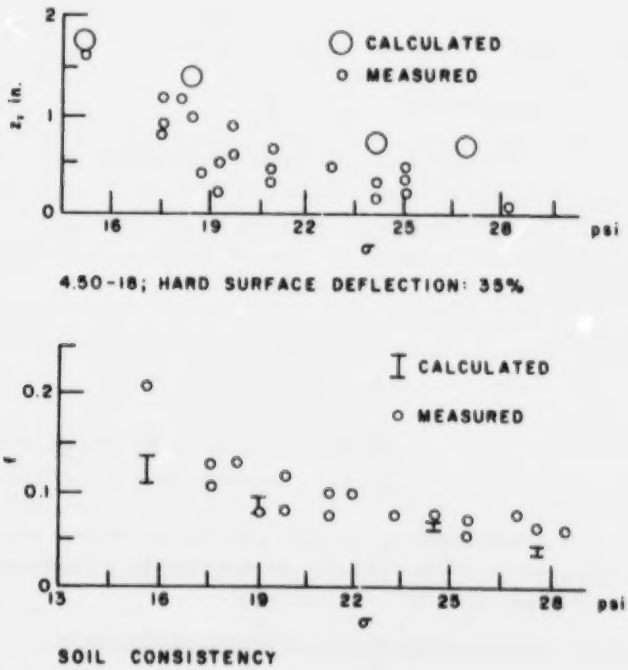

Figure D42. Calculated and measured values of rolling resistance and sinkage of a 4.50 - 18 buffed tire, at loads and inflation pressures yielding 35% deflection on a hard surface. Sandy soils of varying consistency δ

W	p_i	p_g	k_c	k_ϕ	n	Defl.
102	42	45.4	0.9	9.2	0.71	15%
212	34.8	38	0.5	9.3	0.71	35%

Calculations yield:

$z_{r15\%} = 1.8165$ $\quad p_{cr} = 17.49 < 42$ RIGID

$z_{r35\%} = 3.3862$ $\quad p_{cr} = 28.97 < 34.8$ RIGID

The calculated and measured coefficients of rolling resistance are

W	f_c	f_b	f_{calc}	f_{meas}
102	0.1944	0.0119	0.2063	0.23
		0.0358	0.2302	
212	0.2651	0.0199	0.2850	0.37
		0.0599	0.3250	

Note that the sinkages of the tire exceed the height of its cross-section. As a result, there was an additional drag measured, due to soil interference with tire mount. In consequence, measured data are higher than the calculated ones.

However, the sinkages show good agreement between computations and experiment.

W	z_{calc}	z_{meas}
102	1.82	1.89
212	3.39	3.52

It may be surprising to find that the tire at W = 212 lb and p_i = 34.8 psi, producing 35% deflection on an unyielding surface, performs like a rigid wheel in soft soil. This may be found only with the help of bevameter soil data, or similar soil values. Empirical indices and numerices are useless, and produce misleading results and wrong conclusions such as in reference D22.

Obviously, bicycle tires may work in loose sand as elastic tires.

This, however, would require unrealistic loads and inflation pressures. After all, who rides a bike in soft sand?

16 × 15 6PR Terratire; Sandy Soil

Input data: $D = 17$, $h = 5$, $b_{tr} = 15$.

Calculations start, as usual, with determination of the mode of tire performance, under the above specified conditions. In this case, however, since the tire is very wide, Equation [D14] is used. Upon a few iterations,

$z_{r220} = 0.47$
$z_{r460} = 0.68$
$p_{cr220} = 7.15 \approx 7$ RIGID-ELASTIC BORDERLINE
$p_{cr460} = 13.6 > 7.2$ ELASTIC

Tire performance under W = 220 lb load was calculated assuming rigid mode of operation:

$l_1 = 2.7873$ $f_c = 0.1312$ $f_b = 0.0045$
0.0135

$f_{calc} = 0.1357$ $f_{meas} = 0.11$
$z_{calc} = 0.47$ $z_{meas} = 0.43$

Tire performance under 460 lb load was calculated for the elastic mode of operation, starting with Equations [D18]-[D26], where l_1 value was determined from the converging assumed and calculated values:

$F = 0.6135$ $l_1 = 2.44$ assumed
$A = -5.8152$ $z_e = 0.4172$
$B = 141.105$ $l_2 = 1.8200$
$l_1 = 2.4493$ calculated

Accordingly, upon determining $\delta = 0.088$, $\alpha = 8.2517°$; $\varepsilon = 0.2320$:

$f_c = 0.0657$ $f_b = 0.0017$ $f_t = 0.0018$
0.0051

$f_{calc} = 0.0692$ $f_{meas} = 0.0674$
0.0726
$z_{calc} = 0.4172$ $z_{meas} = 0.37$

The results speak for themselves. Note the need for observing the right procedures in using the smaller dimension of the tire print.

Dual Tires with Close Spacing

A pair of 4.50 - 18 buffed tires was mounted in dual arrangement: (a) without spacing and (b) with 1-in. spacing.

Though the effect of such spacing can hardly be detected, tests in sand showed (D22) a slight difference in rolling resistance between the two configurations, at 914 lb load:

$$f_{\text{zero spacing}} = 88/914 = 0.0963$$

$$f_{\text{1-in. spacing}} = 96/914 = 0.1050$$

For the two tires widely spaced so that they acted as singles, the rolling resistance was:

$$f_{\text{single}} = 42/462 = 0.0909$$

This example shows that considering the dual tires as a single wide tire gives predictions of rolling resistance in agreement with experiment.

Tire and soil input data are (lb-in.): (b_t was calculated from tire dimensions shown in Fig. D39, assuming two contact widths plus spacing)

W	p_i	p_g	b_t	k_c	k_ϕ	n
914	9.7	13.3	11.14	2.4	11.6	0.74
914	9.7	13.3	12.14	2.4	11.6	0.74

Other tire dimensions: D = 27.1; h = 3.8; r = 3.45.

Following Equations [D18]-[D25] and [D5]-[D7], calculations yield for the single tire:

$$F = 0.5747 \qquad z_e = 1.1177$$
$$b_0 = 3.7 \qquad \delta = 0.5367$$
$$A = -2.1948 \qquad \varepsilon = 0.6886$$
$$B = 131.3189 \qquad \alpha = 16.1800$$

$$f_c = 0.0692 \qquad f_b = 0.0035$$
$$f_t = 0.0136 \qquad 0.0104$$
$$f = 0.0863$$
$$0.0932$$

which is in a fair agreement with the measured value f = 0.0909.

For the dual tires with and without spacing, computations show:

Zero Spacing	1 in. Spacing	Zero Spacing	1 in. Spacing
$F = 0.5747$	$F = 0.5747$	$\varepsilon = 0.3928$	$\varepsilon = 0.2873$
$A = -6.6021$	$A = -7.1947$	$\alpha = 7.8321$	$\alpha = 6.4550$
$B = 262.6379$	$B = 262.6379$	$f_t = 0.0027$	$f_t = 0.0015$
$l_1 = 3.69$	$l_1 = 3.00$	$f_b = 0.0046$	$f_b = 0.0048$
$z_e = 1.1175$	$z_e = 1.0993$	0.0137	0.0144
$G = 95.1548$	$G = 102.0087$	$f_c = 0.1041$	$f_c = 0.1116$
$C = 1253.9020$	$C = 1344.8385$		
$l_2 = 4.3078$	$l_2 = 4.5527$	$f = 0.1114$	$f = 0.1179$
$l_1 = 3.6932$	$l_1 = 3.0443$	$= 1.1205$	$= 0.1275$
$\delta = 0.1264$	$\delta = 0.0858$		

As reported previously, the measured values were: $f = 0.0963$ and $f = 0.1050$

Considering the inherent inaccuracies of the theory and experiment, the result appears satisfactory. It shows the basic soundness of the assumptions made, when calculating rolling resistance of dual tires with a small spacing.

Field Tests

All the previously described verifications of predicted tire rolling resistance were based on laboratory tests, in soil bins.

Difficulties in the homogenization of soil at the desired consistency level as well as the inaccuracies involved in instrumentation and data processing were shown to play a significant role in comparing the theory and experiment on a point-to-point basis. The need for statistical correlation was stressed.

These problems are magnified and compounded in field testing of actual vehicles and their tires. To illustrate the point, one may recall conflicting reports and contradictions plaguing the user as to the merits of predictive methods promoted.

However, the situation is no worse in the field than in the laboratory if the field tests are performed with maximum diligence and understanding of the problem.

As an example, take classic tests performed in Germany more than two decades ago (D23). The purpose of the tests was to determine rolling resistance of an agricultural tractor on a ploughed, consolidated stubble soil of clayey type.

Soil parameters were determined with a fine bevameter. Although their spacio-temporal coincidence with tractor measurements was not specified for statistical purposes, good raw data enabled this writer to perform computation on point-to-point basis.

For the sake of brevity only the front wheels of the tractor are discussed below. The input data are given in METRIC system (kg,cm) as follows: Tire, 5.50 - 16: $D = 69$, $r = 19$, $p_b = 1.84$, $b_{tr} = 11.5$, $W = 272$, $k_c = 5$, $h = 11$, $p_i = 1.5$, $k_\phi = 0.5$, $n = 0.84$.

Calculations yield:

z_r	$= 2.8842$	
p_{cr}	$= 2.6802 > 1.5$	ELASTIC
F	$= 0.5435$	for $b_0 = 9.0$
A	$= 0.7327$	$\alpha = 10.3346$
z_e	$= 1.9378$	$\varepsilon = 0.5338$
δ	$= 0.5597$	

And the motion resistances are:

$f_c = 0.0641$ $\quad f_b = 0.0010$ / 0.0031 $\quad f_t = 0.0061$

$f_{calc} = 0.0712$ / 0.0733 $\quad f_{meas} = 0.098$

Note that a few tenths' change in soil values and in inflation pressure may cause a change in rolling resistance coefficient f of the order of 20%.

Obviously, the measurements were not taken with such accuracy. Four bevameter plots used here, for the estimation of k_c, k_ϕ and n values, were not sufficient for a good statistical approximation. Considering the surface of a ploughed stubble, one cannot expect a better accord between the calculated and measured values.

Automatic, computerized mass data processing developed at Carleton University in Canada (D19) is the solution to the problem, in field explorations.

ACCURACY OF PREDICTIONS

Accuracy of predictions of tire rolling resistance on hard ground depends on the error of predictive methods, on tires, and tire-surface interface as shown in Part I of Appendix D.

In the case of soft, yielding ground, this error is augmented by inaccuracies intrinsic in soil measurements and soil data processing.

Numerical examples and their verification reported in this report illustrate the cumulative error. Accordingly, as mentioned before, Figs. D33, D34, D37, D38, and D40-D42 should be looked upon on the background of inaccuracies involved in the verifying experiments and soil reprocessing.

To emphasize the point, Fig. D43 illustrates the inevitable spread of rolling resistance measurements performed in a very elaborate series of experiments.

Soil data processing requires curve fitting. The latter is always biased by the logarithmic character of the penetration-load relationship, and by the local inhomogeneities of the otherwise homogeneous soil or snow (Figs. D44 and D45).

This problem has been recently attacked in Canada (D19); statistical, fully computerized data processing yields the mean values and their standard deviations, as exemplified below, with fair consistency, except for snow. The latter should have been considered a stratified medium instead of a homogeneous one, which the computer was not programmed to do. This led to negative k_c-values equated to zero because of their relatively small significance in reference to other values

	MC%	n ± s	k_c ± s	k_ϕ ± s
Sandy loam*	1	0.93 ± 0.13	118 ± 9.3	8510 ± 1476
	5.6	0.77 ± 0.02	19 ± 6.4	8426 ± 1844
	12	0.75 ± 0.09	2 ± 2.6	8295 ± 1624
	Test			
Snow	1	1.33 ± 0.11	0	744 ± 356
	2	1.58 ± 0.25	0	745 ± 995
	3	1.45 ± 0.10	0	519 ± 174

*estimate, insufficient sample.

All the data reported above are given in SI units. Note the rather wide spread of k_c values in sandy loam, which together with high k_ϕ values indicates a strong frictional character of that soil.

The figures reported here represent a typical field test sample, where homogeneity is practically zero.

Early laboratory statistical tests performed by Land Locomotion Laboratory in Detroit showed the results listed below.

Bevameter	n	k_c	k_ϕ	c	ϕ
Wheel type	1.18+0.05	0.4 +0.32	3.58+0.41	0.24+0.09	29.5+2.10
Conventional	1.11+0.05	0.11+0.26	3.92+0.50	0.15+0.09	28.0+1.85

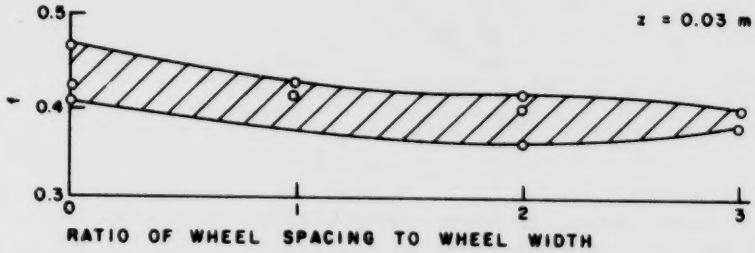

Figure D43. The band width of measurements of rolling resistance coefficient, as a function of the ratio of wheel spacing to wheel width. Experimental data obtained in sand with two wheels made of wood, at a constant sinkage

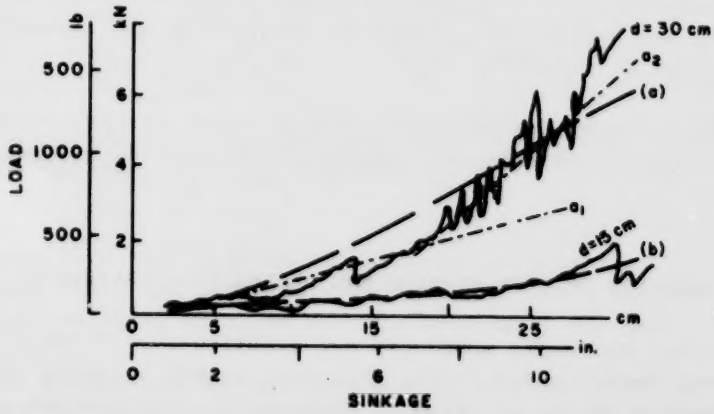

Figure D44. Canadian bevameter plot obtained with 30 and 15 cm plates, in snow. (a) and (b) are representing curves fitted by means of computerized Wong method (D19). In this case, however, it is fair to assume that snow is not homogeneous. Thus two lines a_1 and a_2 represent a better fit, which the computer was not programmed to do. (b)-line appears correct. For processing nonhomogeneous soil-snow data, see Part III of this Appendix

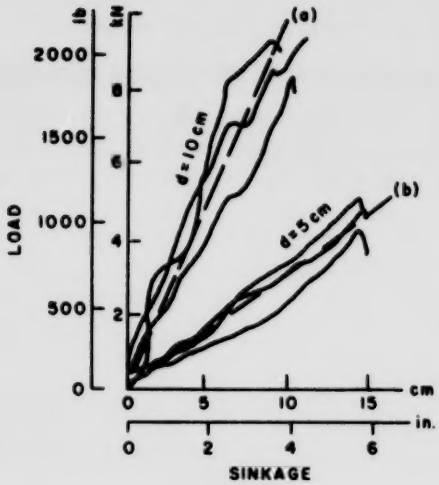

Figure D45. Canadian bevameter plot made with 10 and 5 cm penetration plates, in sandy loam field, near Ottawa. Computerized Wong method (D19) shows good fit of interpolation lines (a) and (b), and reliable k_c, k_ϕ, n-data thereby obtained (see text)

Soil tested was sand. All the values are given in lb-in. system. Data processing was performed by visual curve fitting and "manual" computations as described in reference D7.

These figures hopefully exemplify the nature of errors, or rather spreads of calculated and measured values. Graphs, Figs. D43-D45, illustrate the point.

EXAMPLES OF CASE STUDIES AND PARAMETRIC ANALYSES

Assuming that the basic soundness and practicality of the discussed method have been demonstrated in the preceding pages, examples of application of this method to the solution of engineering problems are presented in the foregoing sections.

In a number of cases, input data were selected for the purpose of emphasizing the point, and the calculations simplified for the sake of economy of space. In no case, however, was the methodological aspect of the example sacrificed, or were unrealistic assumptions made which would compromise the practicality of discussed solutions.

Analysis of Catalogue Recommended Tire Options

The manufacturer of a 4 × 4 agricultural tractor, of GVW = 22000 lb (9820 kg) offers a variety of eight combinations of four tires, in single and dual configurations. Option guidelines are qualitative and/or based on descriptive past experience.

In this example, more rational quantitative guideposts are presented which consider the environment (soil) and economy, in terms of soil properties and rolling resistance.

As an illustration of the approach to the problem, only two tires and their configurations are assumed.

23.5 - 25 SINGLE. $D = 64$; $b_{tr} = 22$; $r = 50$; $h = 20$; $p_i = 15$; $p_g = 20$. Tire load $W = 5500$.

18.00 - 25 DUAL. $D = 64$; $b_{tr} = 20$; tire spacing $\Delta = 3$; $r = 45$; $h = 20$; $p_i = 15$; $p_g = 20$. Extra tire weight $W_t = 600$; load $W = 6100$. All the dimensions in lb-in. system. The tractor is expected to operate in soils having the following characteristics:

	k_c	k_ϕ	n	c	ϕ	K_γ	K_c
Arid	50	10	0.7	0	32	10-30	
Dry	45	7.5	0.6	0	30	10-20	
Moist	28	5.0	0.5	0.1	25	5-10	12-25
Wet	20	9.5	0.45	0.2	22	5-10	10-20

Soil density, approximately 0.06 lb/in.^{3}

Bevameter data tabulated above represent an educated guess based on numerous field tests and laboratory experiments. They represent a sandy loam of an agricultural soil, at various seasons of the year.

In order to shorten the calculations without diminishing the tutorial content, only one wheel is considered, running on virgin soil. This applies to front tires of the tractor. The rear tires run on a compacted soil with slightly different properties, which is not considered. The reader interested in the problem is referred to pertinent literature (D9).

Following the previous examples, the regular sequence of calculations yields (b_0 and l_1 values obtained after a few iterations):

	SINGLE	DUAL
Arid	z_r = 2.42	z_r = 1.35
	l_0 = 12.20 < 22	l_0 = 9.2799
	p_{cr} = 29.8 > 15	p_{cr} = 20.32 > 15
	Elastic	Elastic
	F = 0.5882	F = 0.5882
	b_0 = 16.3	l_1 = 3.35
	z_e = 1.8368	z_e = 0.7301
	δ = 0.6747	δ = 0.4444 negligible
	α = 11.7865	
	ε = 0.3971	
	f_c = 0.0640	f_c = 0.0624
	f_t = 0.0053	
	f_b = 0.0040	f_b = 0.0010
	0.0121	0.0031
Arid	f = 0.0733	f = 0.0634
	0.0813	0.0655
Dry	f = 0.1162	f = 0.1205
	0.1371	0.1320
	Elastic	Rigid
Moist	f = 0.2695	f = 0.2094
	0.4060	0.2672
	Rigid	Rigid
Wet	f = 0.3983	f = 0.2514
	0.5897	0.3538
	Rigid	Rigid

The mid-values of f were plotted in Fig. D46 as a function of soil consistency σ, calculated from equation:

[D33] $\delta = [(k_c/15) + k_\phi]5^n$

which defines the ground pressure acting on a 15-in. wide footing, at the depth of 5 in.

Soil	σ
Arid	41.13
Dry	27.58
Moist	15.35
Wet	12.03

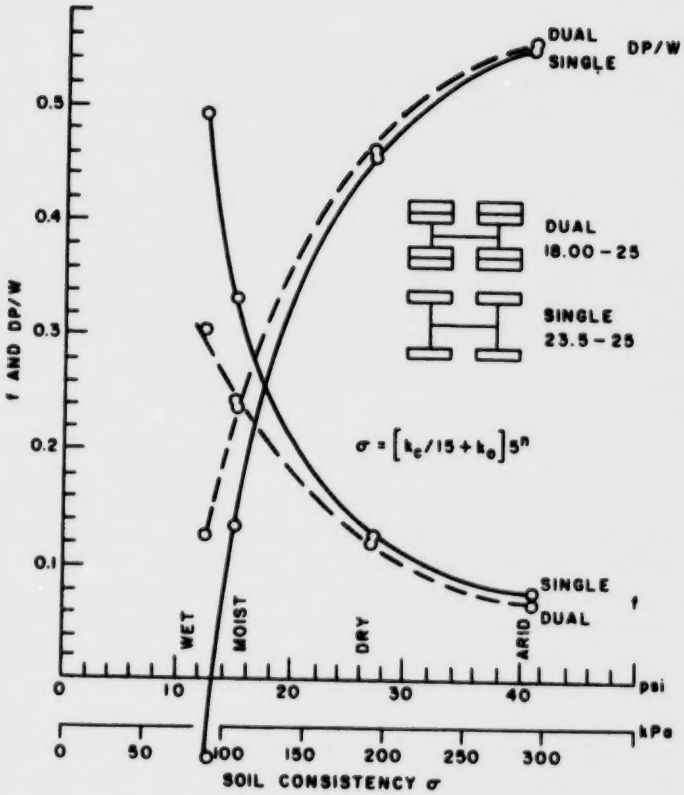

Figure D46. Rolling resistance coefficient f and drawbar/tire load ratio DP/W, for two tires and two configurations as specified above. Note the small difference in tires' performance over a wide range of soil consistency δ

Figure D46 shows that the 23.5 - 25 single tire cannot operate in wet soil. More insight may be obtained when analyzing the maximum attainable drawbar pull DP/W, which according to the well-established formula equals (D1, D2, D7, D9)

[D34] $DP/W = \tan \phi + (A/W)c - f$

where A is the size of the ground contact area: $A = l_0 b_0$, or $(l_1 + l_2)b_0$, with $b_0 < b_{tr}$ (Fig. D30).

Upon calculation of l and b values as shown before, soil values c and ϕ, the ground contact area A, and tire load W are substituted in Equation [D34], which yields

Soil	DP/W Single	DP/W Dual
Arid	0.5476	0.5605
Dry	0.4017	0.4511
Moist	0.1359	0.2367
Wet	-0.0736	0.1210

The above DW/W values were calculated for the previously determined mid-values of rolling resistance coefficient f, and plotted as a function of soil consistency σ, on Fig. D46.

The draw-bar pull which is an exponent of travel efficiency shows clearly that the 23.5 - 25 tire cannot operate in wet soil.

The tabulated values of f and DP/W as well as Fig. D46 present a quantitative input for system analysis which enables one a more rational choice of recommended tires. Such a choice would be further aided if statistical distribution of occurrence of particular soil states, depending on climate and geography, is available as shown elsewhere (D7).

Effect of Inflation Pressure in Soils of Varying Consistency

Rolling resistance coefficient f, for a 14.00 - 20 tire, was shown in Fig. D37 as a function of inflation pressure, at the load W = 2500 lb (1136 kg), acting upon dry sand (k_ϕ = 3.58; n = 1.11; ϕ = 32°).

In this section, the same tire was similarly evaluated, when acting on a sandy loam, at the same load. Loam properties were assumed changing with moisture content (MC%) as exemplified in the previous section by soil consistencies: Arid, Dry, Moist.

Tire input data: D = 49; b_{tr} = 11.8; r = 19; f = 14.5. Also, as previously (all dimensions in lb-in. units),

p_i	p_g
10	19.2
20	24.2
30	29.2

Calculations were performed in the usual manner, starting with the determination of z_r (Equation [D14]), followed by the definition of l_0

(Equation [D13]). Whenever $l_0 > b_{tr}$ sinkage z_r was determined from Equation [D15]. The next step defined p_{cr} (Equation [D16] and the mode of tire operation, RIGID or ELASTIC (Equation [D17]).

The motion resistance coefficient f was calculated from Equations [D27] and [D30], for rigid tires, and from Equations [D18]-[D26], [D28], or [D29], [D30], and [D6], for elastic ones. The "general shear" formula for f_b was assumed as being more "pessimistic", though the difference would not have been significant because of low soil cohesion c.

To simplify the presentation of the result, f-values were recorded in terms of mid-values of the band width. For the convenience of the reader, the lower and upper boundaries of the band were tabulated below.

p_i	Arid	Dry	Moist
10	0.0865 ± 0.0025	0.1342 ± 0.0060	0.3672 ± 0.0497
20	0.1323 ± 0.0044	0.2155 ± 0.0099	0.3672 ± 0.0497
30	0.1873 ± 0.0063	0.2192 ± 0.0127	0.3672 ± 0.0497

Graph, Fig. D47, illustrates the trend which becomes more pronounced, when considering the draw-bar pull/weight ratio, DP/W, also plotted on the graph, using Equation [D34].

The method provides quantitative values for the selection of an optimum inflation pressure, for the given soil and the required performance. The common practice may be now improved far beyond qualitative guesses.

Effect of Tread Width

Effect of tread width b_{tr} on rolling resistance f was indirectly considered in the preceding paragraphs, for tires with curved tread surface. In this section, tread width - rolling resistance relationship is considered, for flat tread. Complex interactions of f, b_{tr}, p_i, and soil parameters k_c, k_ϕ, n, c, ϕ, k_c, K_γ are discussed as primarily generated by the preponderance of k_c relative to k_ϕ, and vice versa.

The problem should have been the subject of parametric analyses, which would encompass all the important data. Such a task, however, would require a computerized approach. For the sake of brevity only an illustration of this approach is referred to below, in a simplified form, for two hypothetical, though not unrealistic, soils:

1. Dry sand: $k_\phi = 4$, $k_c = 0$, $n = 1$, $c = 0$, $k_{\gamma\ av} = 15$, $K_{c\ av} = 0$, $\gamma = 0.06$; $\phi = 30$

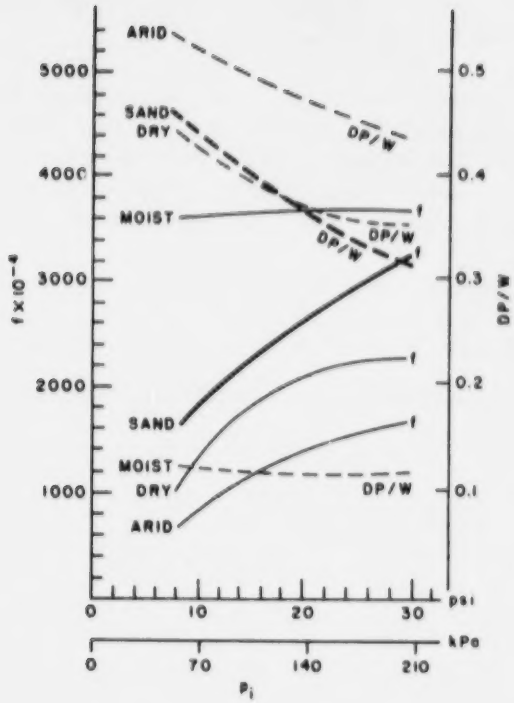

Figure D47. Drawbar pull/weight ratio DP/W, and the coefficient of rolling resistance f, of a 14.00 - 20 tire as a function of inflation pressure p_i, in sandy loam of varying moisture content, defined as: Arid, Dry and Moist. Heavy lines refer to the same tire acting upon dry sand. They were copied from Fig. D37. Tire load in all cases, W = 2500 lb (11.12 kN). Note different effect of inflation pressure change, in different soils.

2. Heavy clay: $k_\phi = 0$, $k_c = 50$, $n = 0.85$, $c = 0.1$, $K_{c\ av} = 6$, $K_\gamma = 0$, $\phi = 0$

All the units are given in lb-in.-psi system. The results were converted into SI system, kN-m-kPa, quoted in parentheses (Fig. D47). Calculations were performed in the English system.

Tire input data are size of 14.00 - 20 type; D = 49 in (1.25 m); basic tread width b_{tr} = 10 in. (0.25 m); inflation pressure p_i = 10 psi (68.95 kPa); load W = 2750 lb in sand and 2500 lb in clay (12.23 kN and 11.12 kN, respectively).

Dry Sand

Consider first the tire which performs like a rigid wheel because of high inflation pressure. From Equation [D14],

$$z_r = 6.01$$

Note that the smaller dimension of the ground contact area, be it b_{tr} or l_0, is here irrelevant because $k_c = 0$. Hence (from Equation [D27]),

$$f_c = 0.2627$$

and (from Equations [D30])

$$f_b = 0.0591$$

$$f_{av} = 0.3218$$

To investigate the effect of tread width, assume additional width b_{tr} = 12.5 in. (0.32 m); 15 in. (0.38 m); 20 in. (0.51 m); 30 in. (0.762 m). Following the same routine, rolling resistance f_{av} was calculated as listed below:

b_{tr}	f_{av}	TOM*
10	0.3218	R
12.5	0.2988	R
15	0.2811	R
20	0.2554	R

*TOM = Tire operation mode;
R = rigid, assumed

The result was plotted in Fig. D48.

Now, consider a lower inflation pressure p_i = 10 psi (68.95 kPa), which makes the tire perform like an elastic one. Since $k_c = 0$, any of Equations [D12] to [D15], may be used. Accordingly:

$z_r = 6.01$ $\quad$ $z_e = 4.8$
$l_0 = 16.0740$ $\quad$ $f_c = 0.1676$
$p_{cr} = 25.02$ 10 > ELASTIC $\quad$ $f_b = 0.0377$ $\quad$ $f_{av} = 0.2053$

In a similar way, f-values (av) were calculated for other b_{tr}-values as listed before. The result is tabulated below:

b_{tr}	z_r	p_{cr}	TOM*	z_e	f_{av}
10	6.01	25.0 > 10	E	4.8	0.2053
12.5	5.18	20.0 > 10	E	4.8	0.2565
15	4.59	16.7 > 10	E(R)	4.8	0.2811
20	3.7	11.8 ≈ 10	R	4.8‡	0.2554‡

*TOM = Tire operation mode, E = elastic, R = rigid.
‡Calculated as rigid and elastic, accepting the smaller value.

The result was plotted in Fig. D48. Note that the tire operation mode (TOM) is close to both rigid and elastic tire behaviour, the following criterion is useful, as discussed before:

$z_e < z_r$ the tire is elastic
$z_e > z_r$ which is impossible, defines a rigid tire

Heavy Clay

Heavy clay produces different tire performance, under conditions

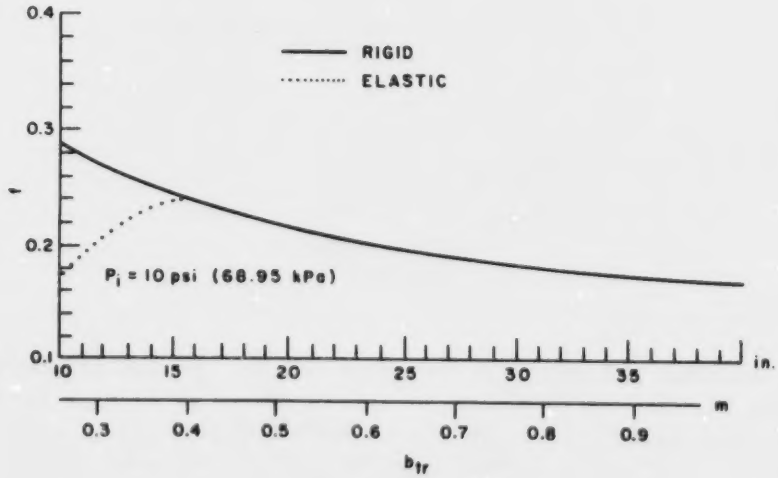

Figure D48. Effect of tread width b_{tr} on rolling resistance f. Basic dimensions of a 14.00 - 20 tire were used for computations, in loose sand defined by k_ϕ = 4, k_c = 0, n = 1. Tire performance in elastic mode of operation at p_i = 10 psi (68.95 kPa), and W = 2750 lb (12.23 kN), merges with performance of the rigid tire, at approximately 15 in. (0.38 m) tread width

similar to those considered for sand. First, for a rigid tire, proper k_c-denominator is all important. Calculations for flat tread b_{tr} = 10 in. (0.25 m), show (from Equation [D14])

$$z_r = 8.7$$

Hence, Equation [D15] was used with 10 in. (0.25 m) as k_c denominator to calculate

$$z_r = 5.4907$$

From Equation [D27]

$$f_c = 0.2524$$

and from Equation [D30]

$$f_b = 0.0132$$
$$f_{av} = 0.2656$$

Calculations for other b_{tr} values were performed in a similar way. The result shown below was plotted in Fig. D49, assuming rigid tire.

b_{tr}	z_r	TOM	f_{av}
10	8.7 5.49	R	0.2656
12.5	6.9 5.49	R	0.2688
15	5.7 5.49	R	0.2722
20	4.2 4.2	R	0.2444
30	2.6 2.6	R	0.1916

Now, consider again a low inflation tire, at pressure p_i = 10 psi (68.95 kPa), which produces elastic tire behaviour, up to a certain tread width. Calculations yield:

$z_r = 8.7$ $\qquad$ $l_0 = 15.4563$

$l_0 = 18.7740 > 10$ $\qquad$ $p_{cr} = 20.72 > 10$ $\qquad$ ELASTIC

$z_r = 5.4907$ for $k_c/10$

In this case l_1 becomes critical, being k_c denominator. It is defined by Equations [D18]-[D24].

$$F = 0.5405$$

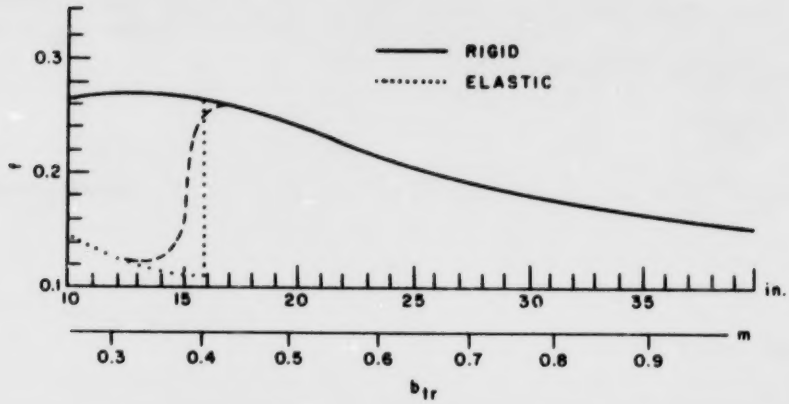

Figure D49. Effect of tread width b_{tr} on rolling resistance f. Basic dimensions of a 14.00 - 20 tire were used for computations, in heavy clay defined by $k_\phi = 0$, $k_c = 50$, $n = 0.85$. Tire performance in elastic mode of operation at 10 psi (68.95 kPa) and W = 2500 lb (11.12 kN), merges theoretically with performance of the rigid tire, at approximately 16 in. (0.41 m) tread width. Interrupted line represents estimated actual merger boundary

Upon a few trials

$$l_1 = 7.27$$

and

$$A = 8.3672 \qquad z_e = 3.3462 \qquad f_b = 0.0080$$
$$B = 675.625 \qquad f_c = 0.1389 \qquad f_{av} = 0.1469$$

Similar calculations for other tire widths yield

b_{tr}	TOM	f_{av}
10	E	0.1469
12.5	E	0.1286
15	RE	0.1156
20	R	0.2444
30	R	0.1916

The result was plotted in Fig. D49. Note the differences in Fig. D48.

In soils characterized by the preponderance of the "frictional" sink-

age parameter k_ϕ, the rolling resistance of an elastic tire initially increases with the increase of tread width, until the tire reaches the rigid mode of operation. In that mode, the tire shows steady decrease of rolling resistance with the increase of tread width, for the given p_i and W parameters. Length l_1 is irrelevant because $k_c = 0$ or is very small. Sinkage z_e remains constant.

In general, for a rigid tire, the rolling resistance drops with tread width increase, mainly because of rapidly decreasing sinkage z_r.

Soils characterized by the preponderance of the "cohesive" sinkage parameter k_c produce different tire performance because the length l_1 of the ground contact area enters the picture, becoming k_c-denominator.

In the elastic mode of operation, rolling resistance drops slowly with the tread width increase as l_1 also decreases. However, when the tire is rigidized by tread width growth, again a rapid decrease of rolling resistance occurs.

The transition from elastic-to-rigid mode of operation obviously does not occur instantaneously. There is no solution for that transition, however, and the algorithms for both modes are based on somewhat different premises as discussed before. The estimated transition line was shown by the interrupted line in Fig. D49.

Note that the tread width decrease cannot be unlimited. It stops at unrealistic values of z_r or z_e which necessitate unacceptable tire deflection needed to produce long enough l_1.

The result discussed here may appear to be novel. However, recent unpublished experiments performed in England show the same trends as presented below.

Take rigid wheel performance in k_ϕ-soil, Fig. D48. Note that within the range of b_{tr} = 10 - 12.5 in. (0.25 - 0.32 - 0.38 m, respectively), sinkage z_r = 5.4907 in. (0.14 m), and remains constant. Plot respective f-values as function of dimensionless product b_{tr}/D for z_r/D as shown below:

z_r/D	b_{tr}	f_{av}	b_{tr}/D
0.112	10	0.3198	0.2041
	12	0.3367	0.2551
	15	0.3536	0.3061

These figures were plotted in Fig. D50 together with the data obtained in British experiments made with wooden wheels of 0.23 m diameter and widths ranging from 0.025 to 0.125 m. The agreement is not incidental. Note that the sand, in both cases, was not the same, though close enough to produce comparable results.

Experimental data for k_c-soils are not available. This suggests a research program, with the particular point of interest: the transition from elastic to rigid mode of tire operation.

The k_ϕ- and k_c-soils considered in the preceding example are idealized ones. Natural soils are invariably a mixture of significant k_ϕ and k_c components. This is illustrated in Fig. D51 which considers a variety of soils, previously used in our computations of rolling resistance. The graph, Fig. D52, shows the latter as a function of tread width increase, at fixed loads and inflation.

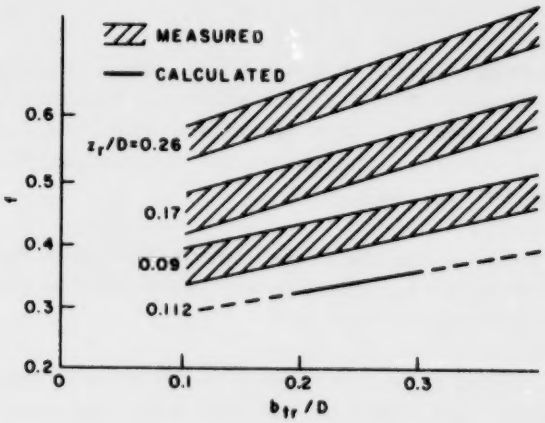

Figure D50. Dimensionless plot of relationship between rolling resistance f and tread width/-wheel diameter ratio b_{tr}/D, measured at constant sinkage/diameter ratio z_r/D, in sand defined by: $k_c = 0$, $n = 0.895$, $k_\phi = 940.8$ kN/m^{n+2}. The graph is based on tests made with wooden wheels of 0.23 m diameter, and width varying between 0.025 and 0.125 m. The above experimental data are compared with the calculated ones, for sand defined by $k_c = 0$, $k_\phi = 4$ $lb/in.^{n+2}$, (1085.7 kN/m^{n+2}) and $n = 1$. Basic dimensions of a 14.00 - 20 tire were used. Note the agreement between the theory and experiment despite differences in basic input data

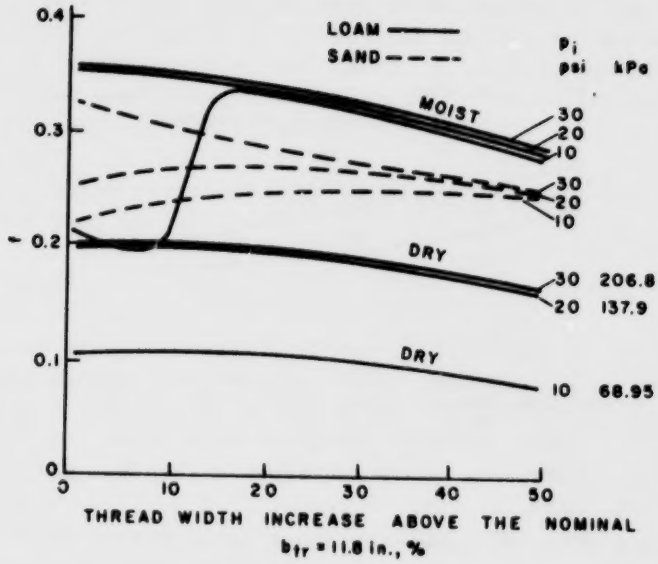

Figure D51. Rolling resistance f, of a 14.00 - 20 tire at various inflation pressures p_i, computed as a function of percentages of tread width increases above the nominal value of b_{tr} = 11.8 in. (0.3 m). Soils used in calculations are: dry loam, k_c = 45, k = 7.5, n = 0.6; moist loam, k_c = 28, k = 5, n = 0.5; loose sand, k_c = 0.95, k_ϕ = 3.58, n = 1.11. Tire load W = 2750 lb (12.23 kN)

The example proves that any generalization of tread interaction with rolling resistance is impossible. Each soil case has to be solved on its own merit, though certain trends are visible.

These trends are compatible with long-standing theoretical conclusions (D1, D2, D7) to the effect that long, narrow ground contact areas are preferred above the short, wide ones.

It seems thus that the present tire geometry may benefit if a more general approach considering soil properties is recognized.

Effect of Tire Diameter

Effect of tire diameter on rolling resistance, in "frictional" soils, again is different from that in "cohesive" soils. To illustrate the point, computations were performed in (1) dry sand and (2) heavy clay, having

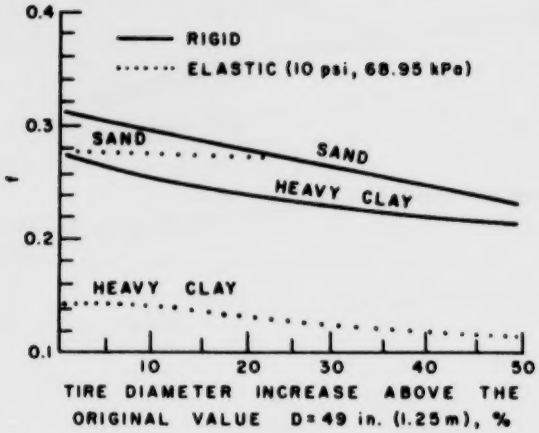

Figure D52. Rolling resistance of a 14.00 - 20 tire, in dry sand (k_ϕ = 4; n = 1; $K_{\gamma av}$ = 15; γ = 0.06), and in a heavy clay (k_c = 50; n = 0.85; K_c = 6; c = 0.1; γ = 0.06), as a function of percentage of tire diameter increase, above to baseline D = 49 in. (1.25 m). Tire load in sand: 2750 lb (12.23 kN), and 2500 lb (11.12 kN), in clay

properties specified in the preceding example. Tire data input included varying diameter, starting with D = 49 in. (1.25 m) baseline and b_{tr} = 10 in. (0.25 m). Loads and inflation pressure were the same as previously.

Dry Sand

Rolling resistance was computed with Equations [D27] and [D30], considering first a rigid tire, at very high inflation pressure. The result was plotted in Fig. D52, which shows the coefficient of rolling resistance f, as a function of percentages of tire diameter increase above the D = 1.25 m baseline.

The rolling resistance of the tire in elastic mode of operation was computed for p_i = 10 psi (68.95 kPa). Note that Equations [D28] and [D30] used here do not contain tire diameter D, hence rolling resistance in soils having k_c = 0 (or very small) is independent of D. It also is not affected by the length l_1, of the ground contact area (Fig. D30b).

However, the increasing diameter of the tire gradually reduces l_1,

which has the same effect as the "stiffening" of tire carcass. As a result, the tire becomes rigid at some point marked by the intersection of elastic and rigid f-lines (Fig. D52). The point also may be determined by computing p_{cr}, Equations [D16] and [D17], as well as by checking $z_e \neq z_r$ inequity. In the case considered, the said point coincides with approximately 20% increase of tire diameter.

Carcass flexing resistance f_t, Equation [D6], was not considered because it was very small.

Heavy Clay

Heavy clay affects the tire diameter - rolling resistance relationship in a different manner, because the latter depends on l_1, which often becomes the k_c-denominator, for $l_1 < b_{tr}$.

Computations start with Equations [D14] and [D13], which determine the denominator. If $l_0 > b_{tr}$, Equation [D12] is used. For $l_0 < b_{tr}$, Equation [D14] stands as the final z_r definition. The next step includes the determination of TOM, Equations [D16] and [D17]. For rigid tires, rolling resistance f is determined by Equation [D27], assuming b_{tr} or l_0 as k_c-denominator, whatever is smaller. For elastic tires, Equations [D18] through [D24] are processed, discriminating between b_{tr} and l_0 (flat tread tires). Rolling resistance is then defined by Equations [D25]-[D30] and [D6], always considering the proper k_c-denominator.

Computations of a 14.00 - 20 tire baseline specified in Fig. D52, and in the previous example, show decrease of rolling resistance with diameter increase, for rigid TOM. In the elastic tire operating mode, however, diameter increases do not affect rolling resistance, within a definite range of loads and inflation pressure, whenever a purely "frictional" k_ϕ-soil is encountered. This is not so in "cohesive" k_c-soil which is very sensitive to inflation pressure, where rigid and elastic modes of operation spell a great difference in rolling resistance.

Effect of Tire Load

Effect of tire load on rolling resistance depends much on soil types: k_ϕ-"frictional" or k_c-"cohesive". Computations performed for the two soils illustrate the point for a 14.00 - 20 tire.

Take soil parameters as specified in the preceding sections. Assume tire loads as follows:

1. Dry Sand: 3000; 4500; 6000; 7500 lb
   13.3; 20.0; 26.7; 33.4 kN

2. Heavy Clay: 2500; 4000; 5500 lb
11.1; 17.8; 24.5 kN

Dry Sand

Then, the computations performed in accordance with previous cases, yield in SAND:

W	z_r	f_c	f_b	f
3000	6.37	0.2705	0.0608	0.3313
4500	8.35	0.3099	0.0697	0.3796
6000	10.11	0.3407	0.0766	0.4173

for a rigid tire. If the inflation pressure is reduced to, say, 10 psi (68.95 kPa), then the tire becomes elastic and displays smaller rolling resistance as shown below:

W = 3000	z_r = 6.37	l_0 = 16.4788	P_{cr} = 27.2 > 10 E
	l_1 - irrelevant		
	z_e = 4.8 < 6.37		
	f_c = 0.1536	f_b = 0.0346	l_2 = 12.4234
	F = 0.5	A = -8.0	B = 750
	l = 9.4132	δ = 0.4563	α = 11.0758
	ϵ = 0.3763		
	f_t = 0.0037		

Thus

$$f_{av} = f_c + f_b + f_t = 0.1919$$

Other tire loads were substituted in the calculations performed in a similar manner, and the results were plotted, together with rigid tire performance, in Fig. D53.

The difference in rolling resistance for rigid and elastic TOM is striking. The minimum of rolling resistance $f_t \approx 0.147$, at the load $W \approx 5250$ lb (23.35 kN), may be a surprising result of the theory. Herein lies its usefulness.

The minimum is controlled by tire deflection δ (dashed line, Fig. D53), which should not be surpassed by an acceptable value. Note that the δ-values shown reflect theoretical calculations, and are generally smaller than the experimental values. Further work in this area is suggested.

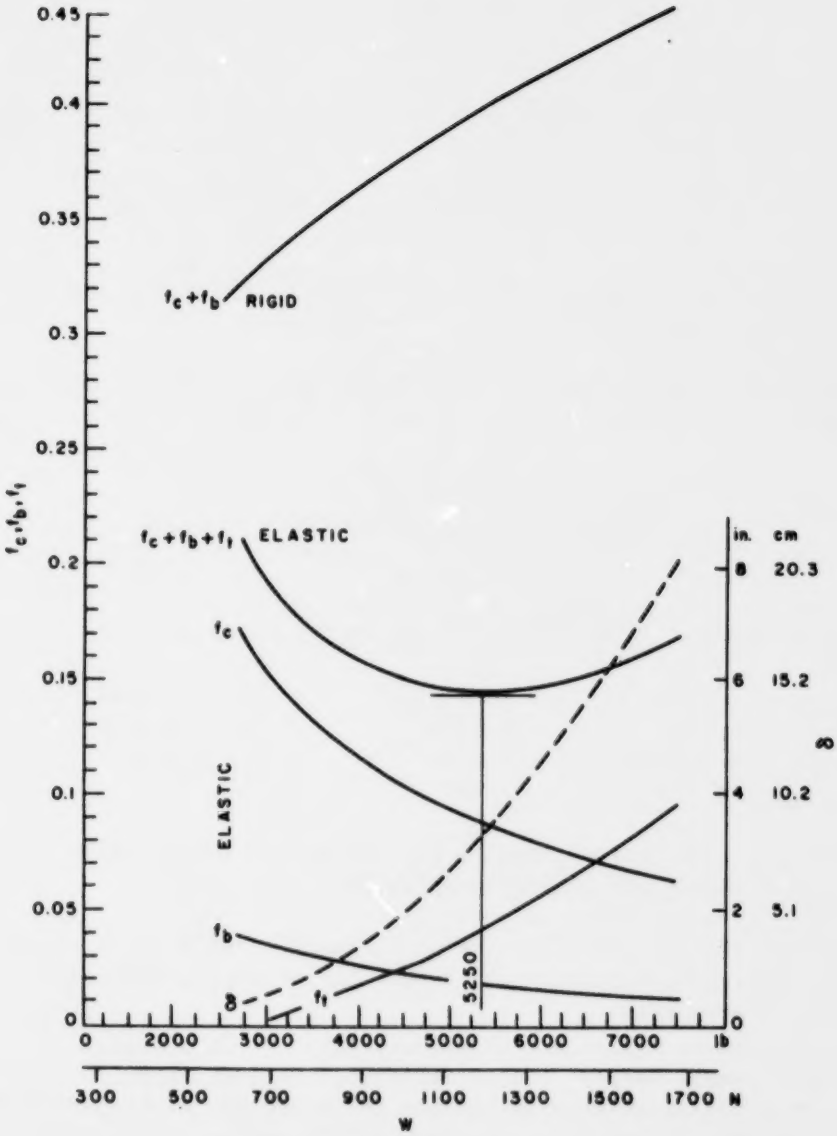

Figure D53. Rolling resistance components f, of elastic and rigid tires of 14.00 - 20 type with b_{tr} = 10 in. (0.25 m), plotted as a function of tire load W. Soil, sand: k_ϕ = 4, n = 1, γ = 0.06, K_γ = 15. Inflation pressure of the elastic tire p_i = 10 psi (68.95 kPa). Theoretical tire deflection δ illustrates the load limits.

Heavy Clay

Calculations performed for the heavy clay display a different result. Consider the rigid tire first, then, for

$W = 2500$ lb (11.1 kN),
$z_r = 8.7$ $\quad l_0 = 18.7246 > 10$

Hence

$z_r = 6.4907$ $\quad f_c = 0.2524$ $\quad f_b = 0.0132$
$f_{av} = 0.2625$

Rolling resistance was identically determined for other tire loads, and plotted in Fig. D54.

Elastic tire mode of operation involves computations in which l_1 enters as k_c-denominator. For $W = 2500$ lb (11.1 kN),

$z_r = 8.7$ $\quad l_0 = 18.7246 > 10$

Hence

$z_r = 5.4907$ $\quad l_0 = 15.4563$ $\quad P_{cr} = 20.7 > 10$ E
$F = 0.5405$ $\quad A = 9.8732$ $\quad B = 675.625$

After a few trials: $l_1 = 7.3$, which has been checked below,

$z_e = 3.3624$ $\quad l_2 = 10.4727$ $\quad l_1 = 7.3603$ OK
$\delta = 0.2780$ $\quad \alpha = 8.6391$ $\quad \varepsilon = 0.2499$
$f_c = 0.1396$ $\quad f_b = 0.0081$ $\quad f_t = 0.0018$
$f_{av} = f_c + f_b + f_t = 0.1495$

Identical computations lead to f_{av} evaluation for $W = 4000$ and 5500 lb. The result was plotted on Fig. D54.

Note the dissimilarity of tire performance under similar conditions, in two diametrically opposite soil types: "frictional", sandy and "cohesive", clayey soil.

In most cases, natural soils represent a mixture of both types of ground. Hence, tire performance cannot be determined without considering proper parameters of terrain, and computations such as shown here.

Only the performance of a rigid tire preserves the same basic shape, irrespective of soil type, though the numerical values of motion resistance depend on soil parameters k_c, k_ϕ, n, etc.

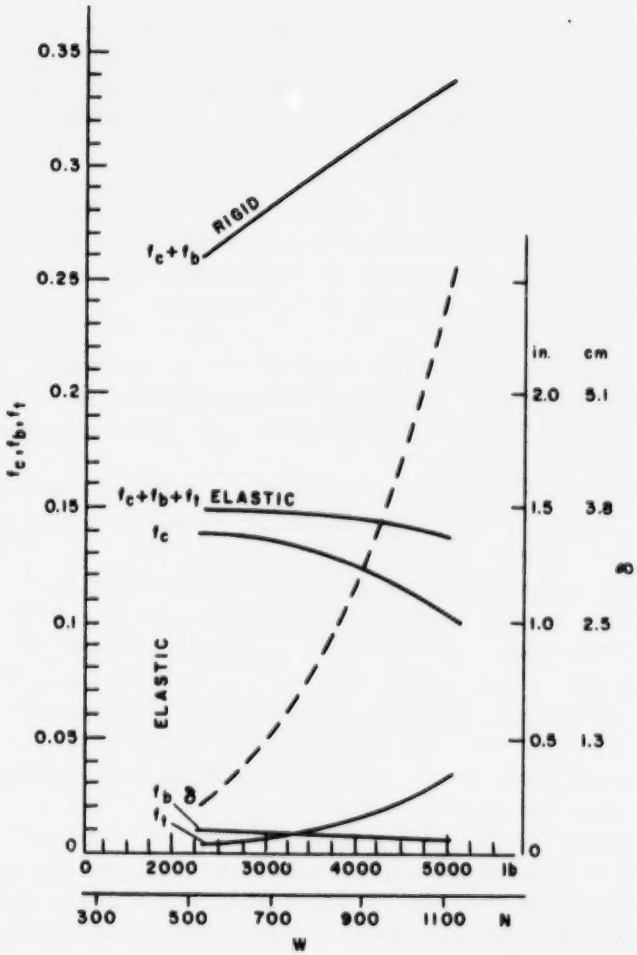

Figure D54. Rolling resistance components f, of elastic and rigid tires of 14.00 - 20 type with b_{tr} = 10 in. (0.25 m), plotted as a function of tire load W. Soil, heavy clay: k_c = 50, n = 0.85, c = 0.1, k_c = 6. Inflation pressure of the elastic tire p_i = 10 psi (68.95 kPa). Theoretical tire deflection δ illustrates the load limits.

Probability of Success

Probability of success in achieving the desired overall tire performance depends on random variations of soil properties, due to climactic (temporal) and geographic (spatial) changes, or both.

Solutions discussed before were based on singular deterministic soil input data, even though a certain band width was assumed for such data, when considering the "bulldozing" parameters of soil resistance K_c and K_γ.

To obtain a probabilistic solution, the distribution of sets k_c, k_ϕ, c, ϕ, and n values must be measured in terms of a single value which defines the given set. Such value is the moisture content, MC%. It defines unequivocally the variable soil parameters.

Once the probability density function of MC is known, respective soil parameters sets and, hence, the tire performance may be determined in terms of the probability of success in achieving the desired goals.

The problem was considered in detail in reference D7. For the reader's convenience, a brief illustration of the solution is given below.

Figure D55, upper graph, shows the relative frequency of occurrence of the given moisture content. A Gaussian distribution curve was assumed on the basis of measurements performed on a proving ground in England (D7). The lower graph shows sets of k_c, k_ϕ, c, and n values corresponding to the given MC. The graph was based on experimental, laboratory estimates. Since the moisture content may be correlated with, say, 10, 25, 50, 75, and 95% probability of occurrence, the corresponding tire performances also may be determined with the same probabilities.

Performances defined in terms of drawbar pull-weight ratio, or slope climbing ability, were calculated using Equation [D34]. Some simplifying assumptions were made for the sake of computational economy, without distorting the general picture (D7).

The results are shown in Fig. D56, for a rigid tire, having dimensions D = 40 in. (1.02 m) and b_{tr} = 11 in. (0.27 m). Graph (a) depicts the extent of tire load change needed to develop the desired DP/W, or climb the slope corresponding to that ratio, with 25 to 90% probabilities. Graph (b) shows similar relationships with reference to tire diameter change.

Obviously, similar computations may be performed for elastic tires as described before. To this end, computer programs are most useful.

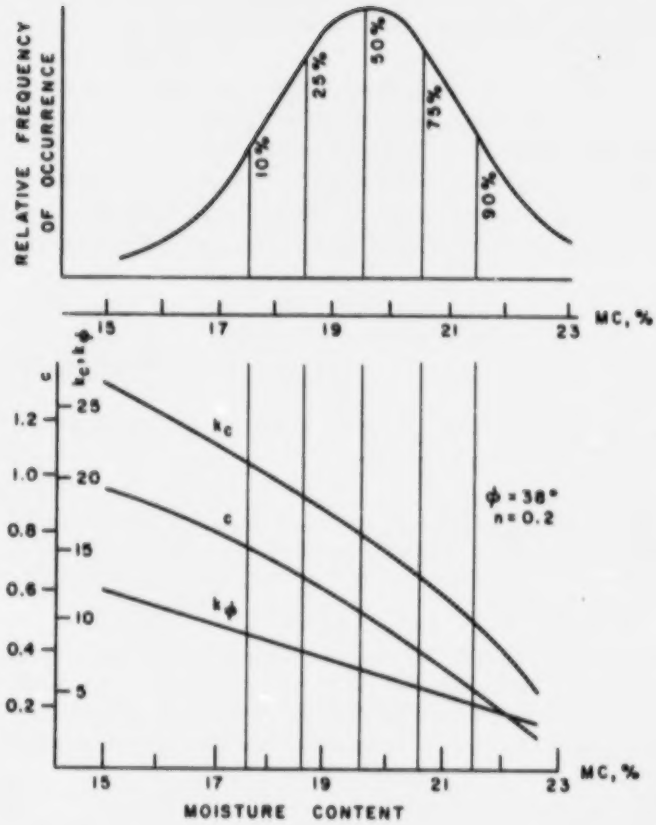

Figure D55. Soil parameters k_c, k_ϕ, n, c, and ϕ as a function of moisture content MC% (lower graph), and its relative frequency of occurrence in the given area (upper graph). Percentages denote the probability of occurrence, in Gaussian distribution

Figure D56 represents the "missing link" between manufacturers' assurances and customers' satisfaction. Both parties cannot rely on single deterministic claims of performance, as long as the same machine is supposed to operate in different climatic and geographical conditions.

Whoever recognizes that truism may offer the customer a quantitative probability of success, instead of a qualitative promise.

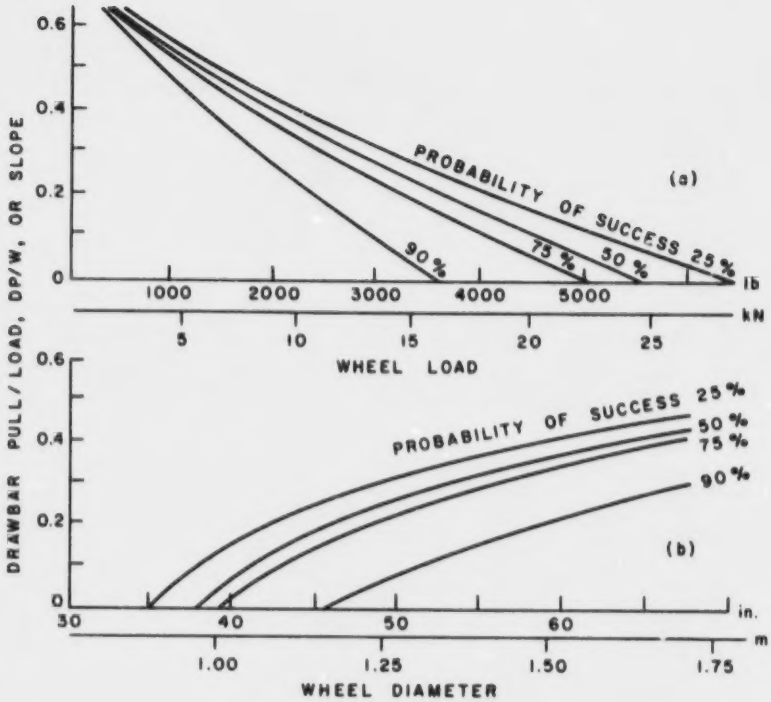

Figure D56. Probability of success in developing the postulated drawbar pull, or in negotiating the encountered slope, as a function of tire load (graph a). The same as function of wheel diameter (graph b)

APPENDIX D. ROLLING RESISTANCE OF PNEUMATIC TIRES

PART III. NONHOMOGENEOUS, STRATIFIED GROUND, AND REPETITIVE GROUND CROSSING

Part I of this Appendix presented a method for computation of tire rolling resistance on non-deformable ground such as pavement, frozen soil, rock, etc. Part II expanded the method to deformable ground which may be considered as homogeneous to the depth affected by tire load and geometry. These are usually laboratory soils, or natural soil masses deposited in a uniform natural process such as wind-blown sands, sedimental loams, etc.

The present chapter, Part III, extends further the same method to the yielding nonhomogeneous or stratified ground which predominantly exists in nature, in two basic configurations.

1. The W-S type, i.e., weak top soil overlying a stronger hard ground

which is represented by ploughed and/or tilled field, muddy soil with non-permeable hard bottom, snow on frozen ground, etc. The second configuration of soil mass is represented by

2. S-W type, i.e., by strong yielding top cover overlying a weak stratum

which may be found primarily in "organic" soils such as peat moss, turf, and muskeg.

Details of bevametric characteristics of nonhomogeneous "soils" may be found in references D6 and D7. Their general signatures of load-penetration performance are shown in Fig. D57, in log-log scale. For comparison, the straight lines p(z), defining homogeneous soil, also were plotted.

INTERPRETATION AND CURVE FITTING OF BEVAMETER DATA

The read-outs of bevameter load-penetration tests and the data processing are discussed in references D6, D7, D9, and D19.

In homogeneous soils, the problem is reduced to the interpolation of populations of p(z) points, using established methods for fitting a straight line for each population. The lines obtained by two plates of a different size are parallel, and define k_c, k_ϕ, and n parameters for the given population.

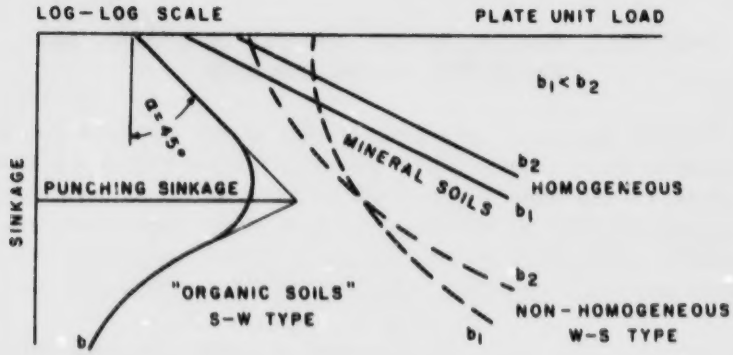

Figure D57. Load-sinkage curves of plates having widths or radii b_1 and b_2, in various types of soils, homogeneous or nonhomogeneous of W-S type (weak layer on strong substratum) or S-W type (strong layer overlaying a weak one). Note the difference between mineral and "organic" soils

Nonhomogeneous Soils of Weak-Strong Type

Nonhomogeneous ground of W-S type cannot be treated in a similar manner because the p(z) lines are not parallel and straight (Fig. D57).

Figure D58 reproduces bevameter measurements obtained in five tests on a ploughed field (D24). Averaging z over p, one may replace the two families of such measurements with mid-value single lines shown in Fig. D59. Obviously, other techniques to achieve that goal are available (D7).

However, the obtaining of a single set of k_c, k_ϕ, and n-values from lines, Fig. D59, is impossible since the regular technique based on the assumption of exponential function

$$p = kz^{n=const}$$

is not valid, because n ≠ constant.

A practical solution of such a problem may be obtained without the violation of the basic assumption, by subdividing the curved p(z) lines into a number of segments which can be fitted with straight lines, with acceptable accuracy. Then, the k_c, k_ϕ, and n parameters are obtained as usual (D7, D9) in a number of sets corresponding to the number of subdivisions which extend to the soil depth h, 2h, 3h, etc. (Fig. D60). The pertinent abscissae a and angles α yield,

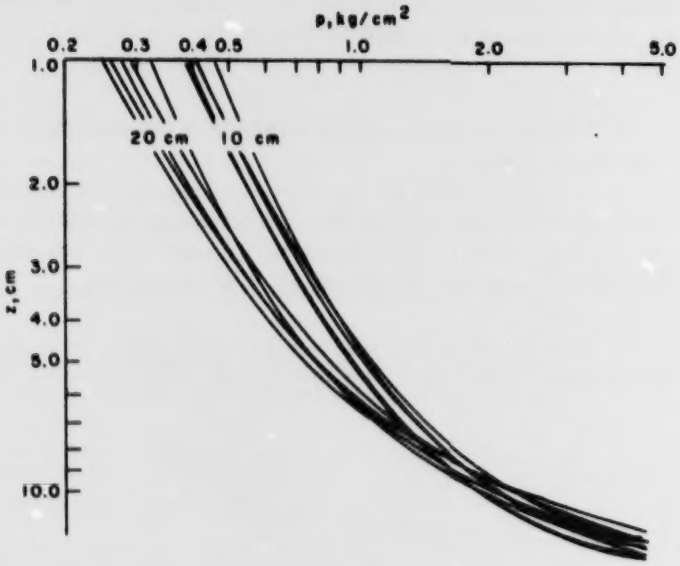

Figure D58. Bevameter curves p(z), measured in a ploughed field with 10 and 20 cm diameter plates. The depth of ploughing 20 cm. Note the curves convergence, characteristic of S-W type of nonhomogeneous ground

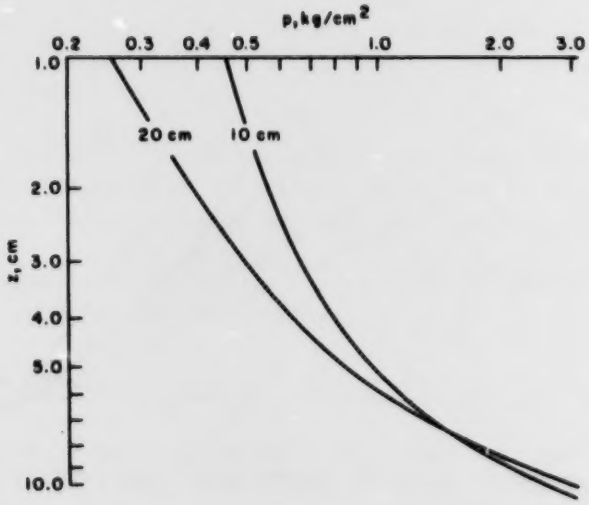

Figure D59. Families of curves, Fig. D58, replaced with two "average" curves using approximate "by eye" interpolation

$$k_\phi = (a_1 b_2 - a_1 b_1)/(b_2 - b_1)$$
[D35] $$k_c = (a_2 - a_1) b_1 b_2/(b_2 - b_1)$$
$$n = \tan \alpha$$

where b_1 and b_2 are bevameter plate half-diameters or widths. In Figs. D58 to D60, $b_2 > b$, as specified.

The Canadian computerized method for processing Equations [D35] is readily available (D19), though the segmentation of load-penetration curves p(z) has not been programmed at the date of this writing.

The larger the number of subdivisions h (Fig. D60), the better the accuracy of predictions. However, the amount of related work increases exponentially.

Numerous computations show that for work with a desk calculator, a three-layer subdivision is sufficient. In some cases, as shown for shallow snow layer, two layers are acceptable.

The thickness of each layer A, B, C, ..., Fig. D60, depends on sinkage z and load p, of the tire footprint. Only experience may be helpful in the

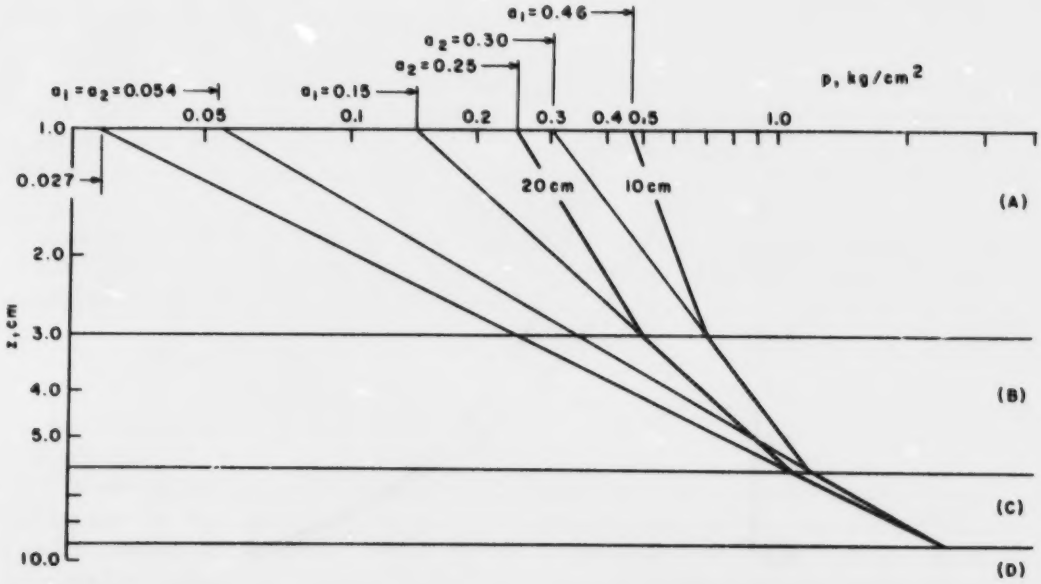

Figure D60. Curves, Fig. D59, replaced with straight lines at 3 cm intervals of depth z. Note the abscissae which lead to the determination of k_c, k_ϕ, and n-values for each segment, extending within layers A, B, C and D

proper estimate of h. A practical hint based on the assumption that wheel sinkage larger than 10-15% of wheel diameter D immobilizes the vehicle, and is therefore inconsequential, may be recommended.

[D36] $h = (0.1 \text{ to } 0.15)D/3$

The approximation refers to a very soft ground. In a hard soil, the value of h may be reduced considerably.

Nonhomogeneous Ground of Strong-Weak Type

Nonhomogeneous ground of S-W type presents other problems of curve-fitting into the measured p(z) population (Fig. D57).

Figure D61 shows a family of four load-penetration lines obtained in muskeg. They are traced on log-log scale after discarding the initial portion of p(z) lines which represent an insignificant load due to compression of surface vegetation (D6, D24).

For similar graphs obtained with two plates of different diameters, or widths, the k_c, k_ϕ, and n-values may be calculated from Equation [D35]. Note that since the mat resting on a semi-fluid bed is practically elastic,

$$n = \tan 45^\circ = 1$$

The straight lines, Fig. D61, yield a good prediction of sinkage and of the punching pressure (Fig. D57), beyond which the terrain-vehicle system collapses beyond recovery.

The k_c, k_ϕ, and n-values determined in the above described manner apply to mat deformation under the tire footprint, and to mat deflection under the complete loading area of the vehicle (D24).

Canadian computerized technique for statistical determination of k_c and k_ϕ values is readily available (D19).

Repetitive Ground Crossing

Repetitive ground crossing is an unavoidable reality: even when a two-axle vehicle travels only once along the given path, its rear wheels cross the ground already compacted by the front wheels.

The intricacies of the problem were discussed in reference D7. Experimental material based on bevameter measurements provided insight as to how to approach the problem from a practical viewpoint (D25).

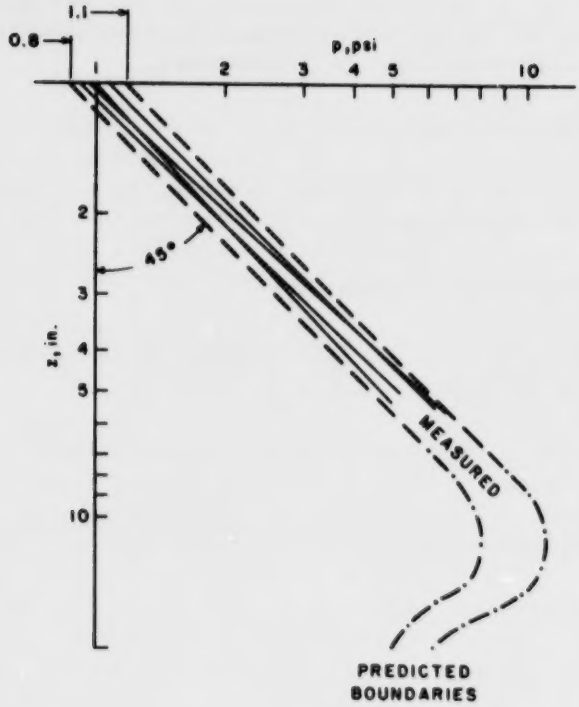

Figure D61. Bevameter plots p(z), calculated in muskeg for low and high boundaries on the basis of two sets of k_c, k_ϕ, and n-values, which were obtained from tests made with round plates. The field measurements obtained with a rectangular plate of 12 in. × 36 in. size, are enveloped by these boundaries as expected

The recent interpretation of multi-pass crossing by a group of researchers (D26), including this writer, led to the following equations which denote the changes in soil parameter $k = (k_c/b) + k_\phi$, after the I, II, III, etc. pass:

$$k_I = (k_c/b) + k_\phi$$

$$k_{II} = [(k_c/b) + k_\phi]z_I^{\,n} \qquad \text{[D37]}$$

$$k_{III} = [(k_c/b) + k_\phi](z_I z_{II})^n$$

etc.

Bevameter plot p(z) for multiple crossing the same rut in homogeneous soils is shown in Fig. D62.

For nonhomogeneous soils of W-S type, the plot is the same. However, since n ≠ constant, the $p = kz^n$ lines are sloped at a decreasing angle Ψ following the angles of the tangents (or secants, replacing the p(z) curve) to the p(z) curve segments which extend at intervals: $0 - k_I$; $k_I - k_{II}$; $k_{II} - k_{III}$, etc. In these soils, n-values for I, II, III, etc. pass are n_I, n_{II}, n_{III}, etc. and

$$k_I = (k_c/b) + k_\phi$$

$$k_{II} = k_I z_I^{n_{II}}$$

[D38]

$$k_{III} = k_I (z_I z_{II})^{n_{III}}$$

etc.

As shown later, assumptions underlying Equations [D37] and [D38] have been corroborated for 1-3 passes. There are no experimental data to go beyond that. Hence, more work in this area is required.

Multipass crossing in "organic" soils of S-W type cannot be evaluated with Equations [D37] and [D38]. For relatively light loads, the "soil"

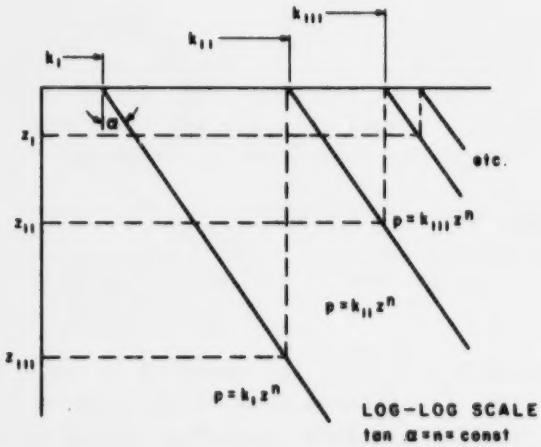

Figure D62. Bevameter plots for repetitive ground crossing. Note decreasing sinkage with second (II) and the third (III) pass

rebounds elastically and there is no need to re-evaluate its properties, for there is no change in k-parameters. For heavier loads, the mat deteriorates due to the tearing of the vegetation, which is beyond the approach considered here (see Appendix F). It seems that an experimental determination of safe and unsafe parameters, for each ecological structure of "organic" soil, is the practical answer.

Theoretical consideration of such problem and the equations which define tensional forces in the vegetation mat are available in work performed in Canada (D27).

TIRE MODELS

Tire models used in the formulation of algorithms for prediction of tire performance have the same geometry and physics as those shown in Part II and Part III of this study. Figures D63 and D64 reproduce the basic scheme for Tire Operation Mode (TOM), in rigid and elastic states. Tire input data are the same as before.

MATHEMATICS OF TIRE EVALUATION

Mathematical models assumed for prediction of tire rolling resistance are based, as usual, on the Bernsteinian integral;

[D39] $$W = b\int kz^n \, dx$$

which was described in detail in reference D28, assuming incomplete but simple closed solution which works well for low n-values. A more complete solution, indispensable for stratified soils, is given in the next section.

Rigid Tire in a Mineral Ground

Rigid tire rolling resistance in a mineral ground is computed as follows:

1. Calculate loads W_A, W_B, W_C, ... absorbed by soil layers A, B, C, ... assuming that the tire sinkage cuts through these layers. Then, the incomplete but valid for low n-values, Equation [D39], yields for a three-layer soil:

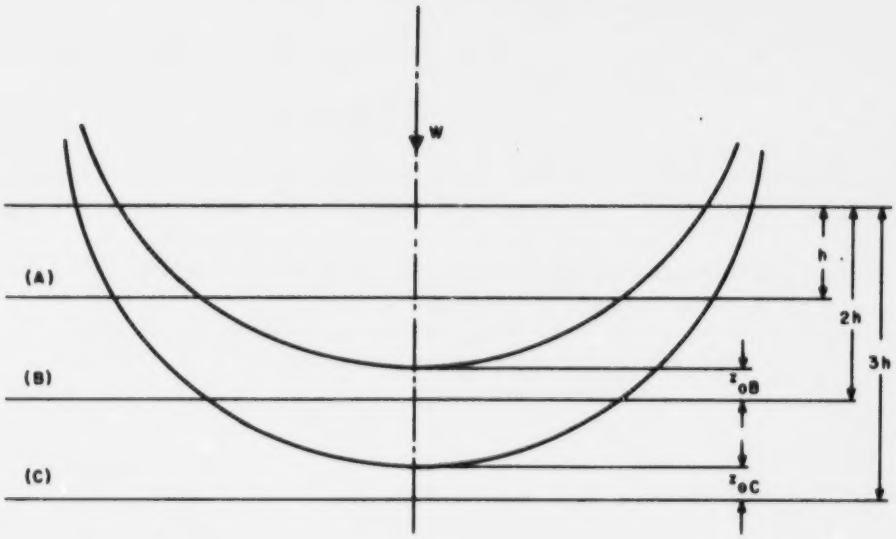

Figure D63. Sinkage denotations in B and C layers for a rigid wheel

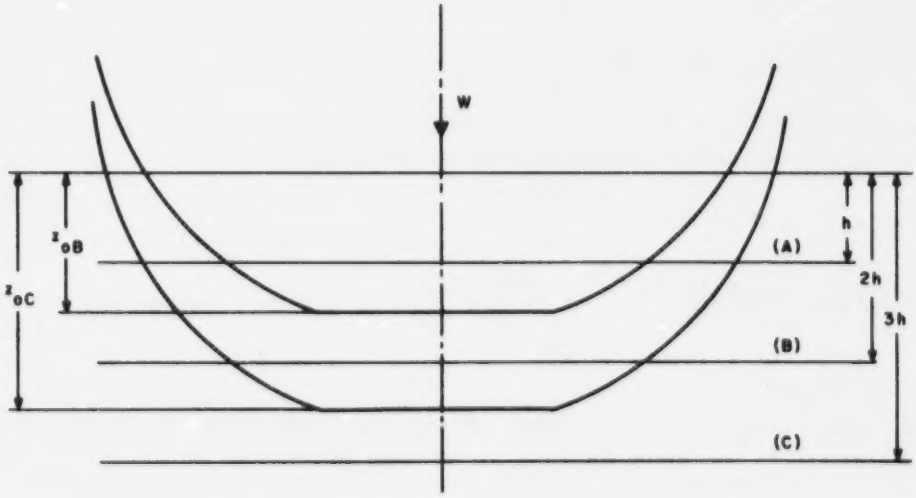

Figure D64. Sinkage denotations in B and C layer for an elastic wheel

$$W_A = 0.3333b_{tr}k_A(3 - n_A)D^{1/2}(h^{(2n_A+1)/2})$$

[D40]
$$W_B = 0.3333b_{tr}k_B(3 - n_B)D^{1/2}[(2h)^{(2n_B+1)/2} - (h)^{(2n_B+1)/2}]$$

$$W_C = 0.3333b_{tr}k_C(3 - n_C)D^{1/2}[(3h)^{(2n_C+1)/2} - (2h)^{(2n_C+1)/2}]$$

etc.

2. The tire stops sinking in layer B if $W_A + W_B > W$, or in layer C if $W_A + W_B + W_C > W$. The amount of sinkage is then,

[D41]
$$z_{oB} = [h^{(2n_B+1)/2} + (W - W_A)/0.3333b_{tr}k_BD^{1/2}(3 - n_B)]^{2/(n_B+1)} - h$$

$$z_{oC} = [(2h)^{(2n_C+1)/2} + (W - W_A - W_B)/0.3333b_{tr}k_C{}^{D1/2}(3 - n_C)]^{2/(2n_C+1)} - 2h$$

3. Rolling resistance due to soil compaction in the two top layers is calculated from equations

[D42]
$$R_{cA} = b_{tr}k_Ah^{n_A+1}/(n_A + 1)$$

$$R_{cB} = b_{tr}k_B[(h + z_{oB})^{n_B+1}]/(n_B + 1)$$

if the tire stops sinking in the B layer. If it rests in the C layer, then the analogical solution is obtained from equations

R_{cA} = as in Equation [D42]

[D43]
$$R_{cB} = b_{tr}k_B[(2h)^{n_B+1} - h^{n_B+1}]/(n_B + 1)$$

$$R_{cC} = b_{tr}k_C[(2h + z_{oC})^{n_C+1} - (2h)^{n_C+1}]/(n_C + 1)$$

4. The "averaged" coefficient of rolling resistance due to horizontal soil deformation, as shown in Part II of this Appendix, is

[D44]
$$R_{bav} = b_{tr}[(h + z_{oB})cK_c + 0.5(h + z_{oB})^2\gamma K_\gamma]$$

or

[D45]
$$R_{bav} = b_{tr}[(2h + z_{oC})cK_c + 0.5(2h + z_{oC})^2\gamma K_\gamma]$$

depending on whether the tire stops sinking in the B or C layer.

The total coefficient of rolling resistance f is then for a rigid tire,

[D46] $f = \sum R/W$

Elastic Tire in a Mineral Ground

Elastic tire rolling resistance in mineral ground is computed with ground pressure criteria. To this end,

1. Calculate loads W_A, W_B, W_C, ... using Equations [D40].

2. Calculate ground pressures p_g at the botton of each layer A, B, C, ..., assuming that they are attributed to k_c, k_ϕ, and n-values of each particular layer, Fig. D60. Use Equations [D35]:

[D47]
$$p_{gA} = k_A h^{n_A}$$
$$p_{gB} = k_B (2h)^{n_B}$$
$$p_{gC} = k_C (3h)^{n_C}$$

3. Compare p_g's, Equations [D47], with $(p_i + p_c)$. The tire stops sinking in B or C layer when $p_{gB} > (p_i + p_c)$ or $p_{gC} > (p_i + p_c)$, respectively. The amount of total sinkage z_e is independent of tire load W, for elastic TOM:

[D48]
$$z_{eB} = [(p_i + p_c)/k_B]^{1/n_B}$$
$$z_{eC} = [(p_i + p_c)/k_C]^{1/n_C}$$

4. Calculate load W_{eB} or W_{eC}, depending in which layer the tire stops sinking:

[D49]
$$W_{eB} = 0.3333 b_{tr} k_B D^{1/2} (3 - n_B)[(z_{eB})^{(2n_B+1)/2} - h^{(2n_B+1)/2}]$$
$$W_{eC} = 0.3333 b_{tr} k_C D^{1/2} (3 - n_C)[(z_{eC})^{(2n_C+1)} - (2h)^{(2n_C+1)/2}]$$

5. Calculate by iteration tire deflection δ for sinkage stop, either in layer B or C, whatever is the case. Use Equation [D1], Part I of this Appendix,

[D50]
$$(2r\delta_B - \delta_B^2)(D\delta_B - \delta_B^2) = [(W - W_A - W_{eB})4\lambda(p_i + p_c)]^2$$
$$(2r\delta_C - \delta_C^2)(D\delta_C - \delta_C^2) = [(W - W_A - W_B - W_{eC})/4\lambda(p_i + p_c)]^2$$

This yields other deflected tire parameters described in Part II of this Appendix

[D2] $b_0 = 2(2r\delta - \delta^2)^{1/2}$

[D5] $\alpha = \cos^{-1}[(D - 2\delta)/D]$

[D7] $\varepsilon = 1 - \exp(-k\delta/h)$

where k is 15, for regular, and 7 for radial tires; h is tire section height.

6. Rolling resistance R_c due to soil compaction is calculated, for particular layers, from equations:

[D51]
$$R_{cA} = b_{tr}k_A h^{n_A+1}/(n_A + 1)$$
$$R_{cB} = b_{tr}k_B[(z_{eB})^{n_B+1} - h^{n_B+1}]/(n_B + 1)$$

if the tire stops sinking in the B layer. If it stops in C,

R_{cA} = as in Equation [D51]

[D52] $R_{cB} = b_{tr}k_B[(2h)^{n_B+1} - h^{n_B+1}]/(n_B + 1)$

$R_{cC} = b_{tr}k_C[(z_{eC})^{n_C+1} - (2h)^{n_C+1}]/(n_C + 1)$

7. Rolling resistance R_b due to horizontal soil deformation is determined from equation

[D53] $R_{bav} = b_{tr}[z_e cK_c + 0.5(z_e)^2\gamma K_\gamma]$

where z_e is selected from Equations [D48] depending on in which layer the tire comes to rest in sinkage.

8. Rolling resistance R_t due to tire carcass flexing was defined in Part I and used in Part II; it serves the same purpose, now:

[D54] $R_t = [3.581b_0D^2\varepsilon(p_i + p_c)(0.0349\alpha - \sin 2\alpha)]/(D - 2\delta)\alpha$

9. The coefficient of rolling resistance f, for an elastic tire, is again: $f = \sum R/W$.

Correction for Bernstein Integral

This becomes necessary, in spite of the simplicity of Equations [D40], [D41], [D48], and [D49], whenever $n > 1$, or approaches that limit. Note that for $n = 3$, which is not abnormal in stratified ground, the above mentioned equations lead to absurdity.

This happens because Equation [D39] was developed into a series, and only the first two members of the series were considered for integration. As a result a more accurate solution with a few percent error was obtained by integration of Equation [D39] throughout the five members of the series. The corrected equations for loads W_A, W_B, W_C,... W_{eB}, W_{eC} are

$$W_A = b_{tr}k_A D^{1/2}\, h^{(2n_A+1)/2}[A_A - 2hB_A/D]$$

[D55]

$$W_B = b_{tr}k_B D^{1/2}\{(2h)^{(2n_B+1)/2}[A_B - 2(2h)B_B/D] - h^{(2n_B+1)/2}(A_B - 2hB_B/D)\}$$

$$W_C = b_{tr}k_C D^{1/2}\{(3h)^{(2n_C+1)/2}[A_C - 2(3h)B_B/D] - (2h)^{(2n_C+1)/2}[A_C - 2(2h)B_C/D]\}$$

Solutions for sinkages z_{oB}, z_{oC}, Fig. D63, are obtained by iteration from equations

$$W - W_A = b_{tr}k_B D^{1/2}\{(h + z_{oB})^{(2n_B+1)/2}[A_B - 2(h + z_{oB})B_B/D] - h^{(2n_B+1)/2}(A_B - 2hB_B/D)\}$$

[56]

$$W - W_A - W_B = b_{tr}k_C D^{1/2}\{(2h + z_{oC})^{(2n_C+1)/2}[A_C - 2(2h + z_{oC})B/D] - (2h)^{(2n_C+1)/2}[A_C - 2(2h)B_C/D]\}$$

Similarly, solutions for W_{eB} and W_{eC} are:

$$W_{eB} = b_{tr}k_B D^{1/2}[(z_{eB})^{(2n_B+1)/2}(A_B - 2z_{eB}B_B/D) - h^{(2n_B+1)/2}(A_b - 2hB_B/D)]$$

[D57]

$$W_{eC} = b_{tr}k_C D^{1/2}\{(z_{eC})^{(2n_C+1)/2}(A_C - 2Z_{eC}B_C/D) - (2h)^{(2n_C+1)/2}[A_C - 2(2h)B_C/D]\}$$

Coefficients A_A, A_B, A_C, B_A, B_B, and B_C, in Equations [D55]-[D57] are

$$A = 1 - 0.509n + 0.222n^2 - 0.052n^3 + 0.005n^4$$

[D58]

$$B = 0.25 - 0.26n + 0.137n^2 - 0.028n^3$$

where n is taken with subscripts A, B, and C as required for the given layer.

To sum up, whenever $n > 1$, or approaches that limit, Equation [D55] replace Equations [D40], Equations [D56] are used instead of Equations [D41], and Equations [D57] replace Equations [D49].

Correction for Rolling Resistance

Correction for rolling resistance due to horizontal soil deformation limits the R-value at abnormal wheel sinkage.

It was shown in Part II of this Appendix that R_b grows fast with sinkage z of the tire, because z enters Equations [D44], [D45], and [D53] in the second power. It was also pointed out that Terzaghian coefficients of passive earth pressure K_c and K_γ require some measurements, instead of the reliance on pre-computed tables.

Trial calculations and a closer analysis of the tire model shown in Fig. D31, indicate that the imaginary retaining wall z_e or z_r cm high is structurally unstable for heights larger than

[D59] $$z_{max} > (D/2)(1 - \cos \mu)$$

where μ is the coefficient of soil adhesion to the tread, usually and safely equal to the angle of soil's internal friction ϕ.

Accordingly, whenever the calculated tire sinkage is larger than z_{max}, no higher values than z_{max} should be used for $(h + z_{oB})$, $(2h + z_{oC})$ (Equations [D44] and [D45] or z_e (Equation [D53]).

Tire Rolling Resistance in Snow

Tire rolling resistance in snow is evaluated basically in the same manner as that in layered soils of W-S type considered before. Of particular interest may be a shallow layer of snow resting on a hard ground, which is discussed in the section concerned with numerical examples.

"Homogeneous" deep snow is of little importance since wheeled vehicles cannot operate under such conditions, unless the snow mass is laced with

ice sheets produced by consecutive thaw and freeze occurring between the snow falls. Then, the snow may be considered as a layered mass of W-S type, and regular bevameter techniques are applicable.

Tire Rolling Resistance in "Organic" Ground

Tire rolling resistance in turf, peat moss, and muskeg is evaluated with regular bevameter data input. Thus the rolling resistance due to the compression of the vegetation is

[D60] $R_c = b_{tr}[(k_c/b_{tr} \text{ or } l_0) + k_\phi]z^2/2$

where $l_0 = (Dz - z^2)^{1/2}$ (see Parts I and II). Note that sinkage z enters in the second power, because n = 1 for practically all organic "soils" which exhibit elastic properties. Thus sinkage z due to vegetation compression is:

[D61] $z = p/[(k_c/b_{tr} \text{ or } l_0) + k_\phi]$

The above p(z) equation is valid within the values pertaining to the upper portion of the load-penetration curve (Fig. D57, S-W). Below the punching pressure p_p and sinkage z_p the vehicle is immobilized unless it is an amphibian of an "ice-breaker" type.

Punching pressure p_p of tire ground contact width b_{tr} or length l_0 is evaluated from equation (1) in reference D7,

[D62] $p_p = p_0(b \text{ or } 0.5d)/(b_{tr} \text{ or } l_0)$

where b or d are bevameter plate width or diameter which punch the vegetation mat at pressure p_0. Selection of b_{tr} or l_0 depends, as usual, on which dimension is smaller.

Punching sinkage z_p is then (D7)

[D63] $z_p = p_p/[(k_c/b_{tr} \text{ or } l_0) + k_\phi]$

Canadian researchers developed a modified solution for muskeg or turf, also based on two plate test. Plate load W and sinkage z are there related in the following form (D27):

[D64] $W = klz(b + 2mz)$

where k and m are special parameters calculated in two load-penetration tests; b is the plate width.

Tests thus far performed yield results similar to those obtained with the k_c, k_ϕ, and n-value system. The advantage of the Canadian approach is the possibility of calculating the tensional stresses in the vegetation mat, and its deflection.

Using bevameter values, mat deflection z_m is approximated by the formula (D24)

[D65] $$z_m = W_{veh}T_B/T_BT_T(k_c + T_Bk_\phi)$$

where T_B and T_T are wheel base and wheel tread, respectively, and the "secondary" motion resistance of the whole vehicle, due to mat deflection, is (D27)

[D66] $$R_{sec} = T_T[(k_c/T_T) + k_\phi]z_m^2/2$$

Trial computations and their limited verification (D6, D24), show that the rolling resistance due to horizontal vegetation deformation, if any, is negligible. Canadian work (D27) indicates that tension in the mat, rather than any conceivable compression, is accountable as implied by Equation [D64].

Rolling resistance due to carcass flexing may be sizeable because of the need for low pressure tires. It is determined by Equations [D2], [D5], [D7], and [D54] as shown in Part II.

NUMERICAL EXAMPLES AND THEIR VERIFICATION

Equations quoted in the preceding section have been applied to predicting tire rolling resistance and checked with the available experimental data. Computations and comparisons are shown below.

Elastic Tire in a Ploughed Field

Elastic tire in a ploughed field which was consolidated for five weeks, in a somewhat rainy weather, was computed for rolling resistance, using the following input data (D23):

Soil: Stubble ploughed to the depth of 20 cm. Bevameter measurements were made with 10 and 20 cm diameter plates, at five neighboring points. Moisture content fluctuation, 14 - 17%. The reported measured p(z) curves are reproduced in Fig. D58; their "mid-values", in Fig. D59, and the straight line approximations of the latter, in a three-layer soil, in Fig. D60. Layer thickness 3 cm. All values were given in the METRIC SYSTEM, cm-kg.

Statistical analysis of the soil sample, Figs. D58-D60, was not available. Following denotations and abscissae shown in Fig. D60, Equations [D35] yield the following soil parameters:

Layer	k_ϕ	k_c	n
A	0.040	2.1	0.4877
B	0	1.5	0.9490
C	0.054	0	0.6977

Other measurements and estimated soil parameters are $\phi = 35°$; $c = 0$; $\gamma = 0.0011$; $K_{\gamma av} = 15$; $K_{cav} = 0$.

5.50 - 16 Tire

Input data in METRIC SYSTEM, cm-kg, are $D = 69$, $b_{tr} = 10$, $W = 272$, $p_i = 1.5$, $p_c = 0.33$,* $r = 12$,* $h_t = 10$,* $\lambda = 085$.*

Calculations are reported in full detail, to illustrate the application of the method outlined in the preceding section. Following the numbered steps referred to in that section:

$$W_A = 0.3333 \times 10[(2.1/10) + 0.04](3 - 0.4877)(69)^{1/2} \times 3^{0.9877}$$

$$= 51.47$$

$$W_B = 1.5(69)^{1/2}[6^{1.449}(0.6765 - 12 \times 0.1027/69) - 3^{1.449}(0.6765 - 6 \times 0.1027/69)] \simeq 69.21$$

$$P_{gA} = [(2.1/10) + 0.04]3^{0.4877} = 0.42 < 1.5 + 0.33$$

$$P_{gB} = (1.5/10)6^{0.949} = 0.82 < 1.83$$

$$P_{gC} = 0.054 \times 9^{1.6977} = 2.25 > 1.8 \quad \underline{\text{Stop}}$$

$$z_{eC} = (1.83/0.054)^{1/1.6977} = 7.9662$$

$$W_{eC} = 0.54(69)^{1/2}[7.9662^{2.1977}(0.5628 - 2 \times 7.9662 \times 0.0644/69) - 6^{2.1977}(0.5628 - 12 \times 0.0664/69)]$$

$$= 108.03$$

*estimated.

$$(24\delta - \delta^2)(69\delta - \delta^2) = [(272 - 51.47 - 69.21 - 108.03)/4 \times 1.83 \times 0.85]^2$$

$$\delta \approx 0.172$$

$$b_0 = 2(24 \times 0.172 - 0.172^2)^{1/2} = 4.0489$$

Since δ and b_0 are small, tire carcass flexing resistance R_t is negligible. The tire is almost rigid.

$$R_{cA} = 10[(2.1/10) + 0.04]3^{1.4877}/1.4877 = 8.61$$

$$R_{cB} = 1.5(6^{1.949} - 3^{1.949})/1.949 = 18.74$$

$$R_{cC} = 0.54(7.9662^{2.6977} - 6^{2.6977})/2.6977 = 28.87$$

$$R_{bav} = 10 \times 0.5 \times 7.9662^2 \times 0.0011 \times 15 = 5.23$$

$$f = 61.45/272 = 0.2259$$

10 - 28 AS Tire

(This tire is now obsolete.) Input data in METRIC SYSTEM, cm-kg, D = 122, b_{tr} = 22, W = 700, p_i = 0.8, p_c = 0.35,* r = 22,* h_t = 17,* λ = 0.85.* Soil parameters for A, B, C layers, Fig. D60, as before. Following the same procedure:

$W_A = 81.54$ $\qquad$ $P_{gA} = 0.23 < 0.8 + 0.35$

$W_B = 93.44$ $\qquad$ $P_{gB} = 0.37 < 1.15$

$P_{gC} = 2.25 > 1.15$ $\qquad$ <u>Stop</u>

$$z_{eC} = (1.15/0.054)^{1/1.6977} = 6.0592$$

This sinkage practically reaches the bottom of B and the top of C layer. Calculation as before shows (n > 1):

$$W_{eC} = 8.12$$

$$(44\delta - \delta^2)(122\delta - \delta^2) = [(700 - 81.54 - 93.44 - 8.12)/4 \times 1.15 \times 0.85)]^2$$

---

*estimated.

$\delta = 0.0185$ $\alpha = 14.1853$

$b_0 = 17.7065$ $\varepsilon = 0.8062$

$R_{cA} = 10.26$ $R_{bav} = 6.66$

$R_{cB} = 18.74$ $R_t = 10.37$

$R_{cC} = 1.84$

$f = 47.51/700 = 0.0679$

Rigid Tire in a Ploughed Field

Rigid tire in a ploughed field of the same structure and mechanical properties as shown before (Fig. D60) was evaluated for rolling resistance f, as follows:

5.5 - 16 Tire

Input data the same as in the preceding case. METRIC SYSTEM, cm-kg.

$W_A = 51.47$	Layer A	$\sum W = 51.47 < 272$	
$W_B = 69.21$	B	$120.68 < 272$	
$A_C = 0.5628$	C	$280.70 > 272$	Stop
$B_C = 0.2463$			
$W_C = 160.02$			

$$272 - 51.47 - 69.21 = 10 \times 0.054(69)^{1/2}\{(6 + z_{oC})^{2.1977}[05628 - 2(6 + z_{oC})0.2463/69] - 6^{2.1977}(0.5628 - 2 \times 6 \times 02463/69)\}$$

by iteration

$2h + z_{oC} = 6 + z_{oC} = 8.85$, and $z_{oC} = 2.85$

$R_{cA} = 8.61$

$R_{cB} = 18.74$

$R_{cC} = 0.54(8.85^{2.6977} - 6^{2.6977})/2.6977 = 46.62$

$R_{bav} = 6.46$

$f = 80.43/272 = 0.2957$

10 - 28 C Tire

Input data as before, all in METRIC SYSTEM, cm-kg:

$W_A = 81.54$	Layer A	$\sum W =$	$81.54 < 700$
$W_B = 93.44$	B		$174.98 < 700$
A_C, B_C as before	C		$676.39 < 700$
$W_C = 501.41$			

The selection of stratum thickness h = 3 cm made the load support in C layer short by 700 - 676.39 = 23.61 kg. One might forego such a difference and assume the tire stops sinking at the very bottom of C. For greater accuracy, however, consider the extension of wheel sinkage into the D-layer. Its properties are (Fig. D60), $k_c = 0$, $k_\phi = 0.027$, and $n = 2.0503$. Hence,

$$700 - 676.39 = 22 \times 0.027(122)^{1/2}\{(9 + z_{oD})^{2.5503}[0.5298 - 2(9 + z_{oD})0.0516/122] - 9^{2.5503}(0.5928 - 18 \times 0.0576/122)\}$$

by iteration

$z_{oC} = 0.3$ cm

and

$R_{cA} = 10.26$ $\qquad$ $R_{cC} = 109.89$

$R_{cB} = 18.74$ $\qquad$ $R_{cD} = 50.87$

$z_{max} = 8.17$ (for $\mu = 30$) and $R_{bav} = 12.11$

$f = 201.87/700 = 0.2884$

Accuracy of Predictions

Accuracy of predictions depends on the assumptions underlying the model of tire-soil relationship, and on the reliability of input data as

well as on the accuracy of field, or laboratory, measurements of tire performance. The latter is of particular importance because it is most often ill-defined.

Comparison between calculated and measured rolling resistances of 5.50 - 16 and 10 - 28 AS elastic tires are as follows:

Tire	f_{calc}	f_{meas}
5.50 - 16	0.2259	0.13
10 - 28 AS	0.0679	0.118

There are no measurements available for rigid tires, since they are not used in agricultural tractors, nor is the TOM in the considered soil rigid.

The above comparative listing of f-values, in elastic TOM, merits some qualifications:

The measured f = 0.13 and 0.118 was "corrected" for friction in the driveline. This was done in a towing test performed on a hard pavement. Such a test, however, involves tire rolling resistance R_t due to carcass flexing, which was not identified though it is different in soft ground and hard road.

Only five bevameter tests were made, each with 10 and 20 cm diameter plates. The closeness of the pertinent curves, Fig. D58, indicates the clustering of tests in a relatively small area rather than along the path, where towing tests for determination of 0.13 and 0.118 values were performed.

The reported variation in moisture content, 14 - 17%, is indicative of possible substantial variation of k_c, k_ϕ, and n-values.

It is not known if the place and the time of tractor towing tests and bevameter measurements coincided.

Considering the roughness of the surface and subsurface of a ploughed stubble field, it must be assumed that the reported (D23) load-penetration curves, Fig. D58, were smoothed out by an unspecified process.

Our replacing the five curve families with two "average" curves, Fig. D59, certainly did not contribute to the accuracy of input data.

All this raises the question of proper organization of bevameter test, and of the corroborative tire (vehicle) test. Under the reported condition, the correlation between f_{calc} and f_{meas} could not be better.

As shown in Part II of this Appendix, the standard deviation of n-values measured in a relatively smooth dry sandy field may reach ±14% of the mean. Variation of k_ϕ, in the same field, was of the order of 20%.

Such input variability must affect the point-to-point correlation between theory and experiment.

As an illustration, assume a conservative variation of n in C layer (Fig. D60): n = 1.6977 ± 5%, all other parameters equal. Calculations for the 10 - 28 AS tire yield

n	f_{calc}	f_{meas}
1.6128	0.0820	0.118 ± ?
1.6977	0.0674	
1.7826	0.0660	

Larger variation of n-band width, being completely realistic, undoubtedly would bring closer the calculated and measured values.

For further illustration of this point, assume that in the C layer, k_ϕ = 0.065 instead of k_ϕ = 0.054 (Fig. D60). This is not only plausible but, perhaps, unavoidable. Then, all other conditions equal, for the 5.50 - 16 tire:

k	f_{calc}	f_{meas}
0.054	0.2259	0.13 ± ?
0.065	0.1574	

The above examples illustrate how risky is the point-to-point correlation between the predictions and actual measurements. Nothing short of statistical approach, even in controlled laboratory work, can produce meaningful result.

The lack of such an approach was often the cause of lack of common language between the theorist and the experimentator, between the seller and the buyer.

As exemplified here and in Part II, Appendix D, the method presented here offers a common denominator for predictions and the estimates of their realization.

Elastic Tire in Shallow Snow

Elastic tire in shallow snow layer is evaluated for rolling resistance in the same manner as it is in a mineral ground of W-S type. The following example illustrates the point.

Ground characteristics expressed in bevameter p(z) plot is shown in Fig. D65. The snow-pavement "ground mass" was divided in two layers, A and B. Two straight lines sloped to normal at 74° and 40° replaced the load-penetration curve.

The bevameter plate, 20 cm in diameter, practically equalled the tire footprint, and was used in direct determination of k-values. At depth approximately 7.5 cm the p(z) curve levelled off, indicating formation of ice. A-layer was 2 cm thick; B-layer, approximately h = 5.5 cm. Snow values are $k_A = 0.0086$, $n_A = 0.8098$, $k_B = 0.0015$, $n_B = 3.4876$ (Fig. D65). Tire input data: $W = 576$; $D = 76.4$; $b_{tr} = 18.4$; $h_t = 8$;* $r = 8$;* $\lambda = 0.9$; $p_i = 2.25$; $p_c = 0.49$.* All in METRIC SYSTEM, cm-kg. Calculations yield

$$A_A = 0.7079 \qquad B_A = 0.1144 \qquad W_B = 365.73 < 576$$
$$W_A = 2.40 \qquad P_{gB} = 8.61$$

which indicates that the tire stops sinking in B layer, in elastic TOM, and the measured depth of ice crust formation, z = 7.5 cm.

$$(16\delta - \delta^2)(76.4\delta - \delta^2) = [(576 - 2.4 - 365.73)/4 \times 2.74 \times 0.9]^2$$

and

$$\delta = 0.617;\ b_0 = 6.1616;\ \alpha = 10.3118;\ \varepsilon = 0.6855$$

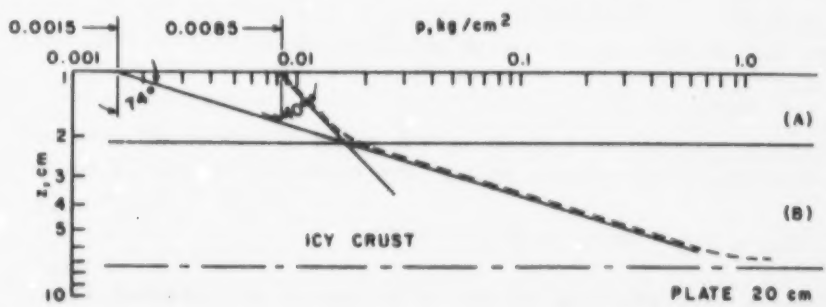

Figure D65. Bevameter p(z) plot for a round plate with 20 cm diameter, in shallow snow

*estimated.

$R_t = 2.39$ R_{bav} - negligible $R_{cA} = 0.31$; $R_{cB} = 51.81$

$f = 54.5/576 = 0.0946$

The above coefficient of motion resistance refers to crossing virgin snow, i.e., to front tires of the vehicle.

Actual towing tests measured rolling resistance of a 4 × 4 vehicle, which when reduced by 15% for losses in the uncoupled rotation of the drive line, amounted to $R_{meas} = 102$ to 121 kg.

To calculate the motion resistance of the complete vehicle it is fair to assume that the rear tires run on incompressible icy crust, and therefore produce only the carcass flexing resistance $R_t = 2.39$. Accordingly, the rolling resistance of the whole vehicle may be calculated as follows:

$$R_{calc} = 2 \times 51.81 + 2 \times 2.39 = 104.8 \text{ kg}$$

which is very close to the measured values, shown before.

Tires in Organic Soils

Tires in "organic soils", such as turf, peat moss, and muskeg, involve evaluation of punching loads and sinkage, which limit practical consideration of rolling resistance.

Punching loads are determined as discussed before. Take envelopes of bevameter measurements made with 10 and 20 cm plates, in a turf-covered meadow (D23), reproduced in Fig. D66, in the upper right corner. The "mid-values" of the enveloped areas are plotted in the lower graph. From the abscissae: $k_\phi = 0.01$; $k_{c_2} = 4.7$; $n = 1$. The punching pressure p_p, for the 10 cm plate, is 6.4 kg/cm^2. As expected, the punching pressure p_p for the 20 cm plate is approximately 3.2 psi. The problem is to draw the p(z) curve for the 40 cm diameter plate which may represent the footprint of a huge tire.

Following algorithms quoted in the section concerned with mathematics of tire evaluation in organic soils, the equation of p(z) line is

$$p_{40} = [(4.7/20) + 0.01]z \cong 0.24$$

It produces a straight line sloped to normal at 45° (dashed line, Fig. D66). The punching pressure and sinkage are

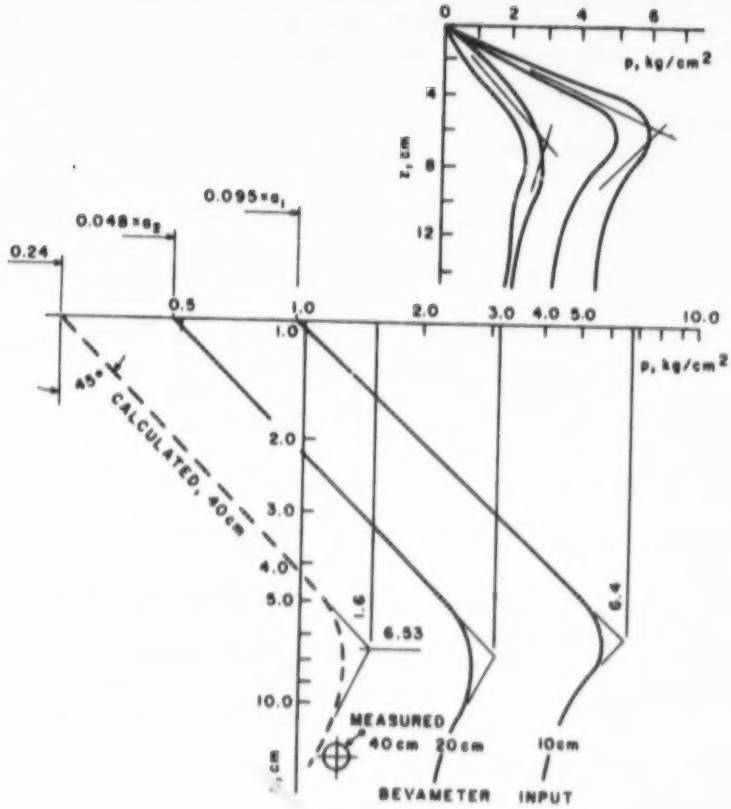

Figure D66. Bevameter envelopes plot p(z), measured in peat moss (upper right) and the "averaged" p(z) lines of the same plot obtained with 20 and 10 cm diameter plates (lower graph). The averaged plot was used to calculate the load-penetration line for a 40 cm diameter plate (dashed lines). The calculated line falls close to the measured point marked with a circle

$$p_{p40} = 6.4 \times 10/40 = 1.6$$

$$z_{p40} = 1.6/0.245 = 6.53$$

Following the general form of load-penetration curves for 10 and 20 cm

diameter plates, the curve for 40 cm plate passing through points 1.0 - 0.24 ; 1.6 - 6.53 was traced as shown in interrupted line, Fig. D66. The point measured on that line was shown by a circle ($z = 12$; $p = 1.25$), indicating fairly good agreement with experiment.

Equivalence of circular and rectangular plate measurements for determination of k_c, k_ϕ, and n-values has been well established in mineral soils (D7). This is also confirmed in "organic" soils, thus indicating further the soundness and generality of the bevameter method.

As an illustration, take measurements made in muskeg with 13.54 in. and 23.45 in. diameter plates. These produced the following muskeg parameters, for low and high envelope lines, of p(z) plots, at the punching pressure measured with 13.54 plate, $p_p = 13$ psi (D6, D24):

low: $k'_\phi = 0.08$ $n = 1$ high: $k''_\phi = 0$ $n = 1$

$k'_c = 8.65$ $k''_c = 13.46$

all dimensions in ENGLISH SYSTEM, lb-in.

If the round plate measured parameters k_c, k_ϕ, and n are general, then the calculated low-high lines of the envelope for a rectangular plate, say of 12 in. × 36 in. size, should enclose the measured lines of the rectangular plate in question.

Calculated envelope abscissae are:

low: $p = (8.65/12) + 0.08 = 0.8$
high: $p = (13.46/12) + 0 = 1.1$

at 1 in. sinkage (k-value). The calculated boundaries were traced in Fig. D61. The measured values also plotted in Fig. D61 fit the predicted band width well.

The example implies that statistics in measurements and calculations is a necessary tool, in "organic" soils.

Rolling Resistance

Rolling resistance in turf, peat moss, and muskeg is calculated in the same way as in mineral soils.

Example: Calculate rolling resistance of a Terratire with inflation pressure 8 psi and such load W as required to produce a footprint 12 in. long and 36 in. wide. Assume muskeg properties: $k'_\phi = 0.08$; $k'_c = 8.65$;

$k_\phi^* = 0$; $k_c^* = 13.46$. Punching pressure measured with 13.54 in. diameter plate is 13 psi. Check if the Terratire does not exceed the punching pressure,

$$p_{p\ terratire} = 13(13.54/2)/12 = 7.33 < 8\ psi$$

The punching pressure is exceeded for $p_i = 8$ psi.

This suggests that the lowering of inflation pressure to at least 7 psi, all conditions adjusted to keep the footprint unchanged, will produce marginal sinkage performance,

$$z_{low} = 7/[(8.65/12) + 0.08] = 8.75$$

$$z_{high} = 7/[(13.46/12) + 0] = 6.24$$

and the rolling resistance is

$$R_{low} = 36[(8.65/12) + 0.08]8.75^2/2 = 1104$$

$$R_{high} = 36[(13.46/12) + 0]6.24^2/2 = 786$$

Since the tire load, under assumed conditions, amounts to $W = 7 \times 36 \times 12 = 3024$ lb, the corresponding variation of the coefficient of rolling resistance f, in muskeg, is $f_{max} = 0.3651$ to $f_{min} = 0.2599$.

The example illustrates the nature of the problem, which does not allow the point-to-point correlation of predicted and measured vehicle performance in muskeg, because of the high nonhomogeneity of that medium (D24).

Considering the realistic input data k_c, k_ϕ, and p_p used in this example, the difficulties in operating even low inflation pressure tires in "organic" soil cannot be overlooked.

MULTIPLE GROUND CROSSING

Multiple ground crossing by tires of the same width are evaluated using the same procedures as those used for the first pass. The k-values, $k = (k_c/b \text{ or } 1_0) + k_\phi$, change, however, from pass to pass, as shown in Equations [D37] and [D38], or better, in direct bevameter measurements.

The problem has not yet been fully understood: do dry sands compact under wheel action in the same manner as moist sandy loams? How do

"organic" soils deteriorate and loosen, instead of compacting? How does the soil density and cohesion change after each pass?

A general solution appears to be available, however, at least for most common compactible soils such as encountered in agriculture and forestry, as shown by the following numerical examples.

38 × 20 - 16 Terratires

Sandy, wet loam in a laboratory soil bin: $k_c = 1.2$; $k_\phi = 0.31$; $n = 0.44$; $c = 0.015$; $\phi \approx 30$. Moisture content ~ 16%.

Estimated parameters: $K_{cav} = 20$; $K_{\gamma av} = 25$. Changes of cohesion c in each tire pass were not given although they must have been sizeable, considering the moisture content of the loam. Also, density changes due to soil compaction were not reported (D25). As a result, the following educated guesses based on available information (D7) led to the assumption of the following:

$$\gamma_I = 0.0016 \qquad C_I = 0.015$$
$$\gamma_{II} = 0.0018 \qquad C_{II} = 0.030$$
$$\gamma_{III} = 0.0019 \qquad C_{III} = 0.060$$

Tire data input is $D = 97.5$, $b_{tr} = 47$, $h_t = 28$, $p_i = 0.5$, $p_c = 0.2$, $W = 600$. All the soil and tire parameters are quoted in METRIC SYSTEM, cm-kg.

Calculations reported below in detail yield:

First Pass

$$z = \left((3 \times 600)/\{47[1.2(97.5z - z^2)^{1/2} + k_\phi](3 - n)(97.5)^{1/2}\}\right)^{1.0638} \approx 4.5$$

$$l_0 = 20.45 < 47$$

$$p_{cr} = 0.6986 > 0.5 \quad \text{ELASTIC}$$

$$F = 0.6944 \qquad A = -1.4313$$

$$K = 02846 \qquad B = 208.32$$

upon a few iterations $l_1 = 8.8$ (see Part II),

$$z_e = \{(0.5 + 0.2)/[(1.2/8.8) + 0.31]\}^{1/0.44} = 2.7804$$

$$R_c = 47[(1.2/8.8) + 0.31] \times 2.7804^{0.44}/1.44 = 63.52$$

$\delta \approx 0.2$ $\alpha = 5.1917$ $\varepsilon = 0.1016$ R_t negligible

$$R_b = 47(2.7804 \times 0.015 \times 20 \times 0.5 \times 2.7804^2 \times 0.0016 \times 25)$$
$$= 46.47$$
$$\sum R_{calc} = 110$$

Second Pass

$z = 2.6$; $l_0 = 15.7074 < 47$; $p_{cr} = 0.9703 > 0.5$ ELASTIC

upon a few iterations $l_1 \approx 13.63$; $z_e = 1.3092$; $R_c = 30$; $\delta = 0.5$;

$\alpha = 8.2131$; $\varepsilon = 0.2349$; $R_t = 0.86$; $R_b = 38.73$

$$\sum R_{calc} \approx 70.0$$

Third Pass

The tire obviously must remain ELASTIC as it runs over a "harder" soil.

$l_1 \approx 14.65$; $z_e = 1.0266$; $R_c = 23.45$; $\delta = 0.5534$; $\alpha = 8.6413$; $\varepsilon = 0.2565$

$R_b = 59.75$; $R_t = 1.55$

$$R_{calc} \approx 85.0$$

12.5 - 20 EM Tire

Input: $D = 104$, $b_{tr} = 32.5$, $h_t = 25$,* $r = 30$,* $p_i = 1.5$, $p_c = 0.3$, $W = 1200$. Soil characteristics identical with that for 38 × 20 - 16 Terratire. Note the lack of statistical approach. Calculations performed as before yield:

First Pass	$R_{calc} = 409$	TOM:	RIGID
Second Pass	135		ELASTIC
Third Pass	130		ELASTIC

*estimated.

The calculated R's and those measured (D25) are plotted in Fig. D67. Considering the uncertainties involved in bevameter input and motion resistance measurements, the result is not bad.

Also note that the calculations were performed for homogeneous soil, although the reported bevameter load-sinkage curves implied a slightly stratified ground due to limited depth of the soil bin.

Tires of Uneven Width

Tires of uneven width, repeatedly crossing the same path, are evaluated as shown in the following example of an agricultural tractor. Input data, all in METRIC SYSTEM, cm-kg:

Front axle: $W = 1500$, $D = 91$, $b_{tr} = 22$, $p_i = 1.5$, $p_c = 0.3$

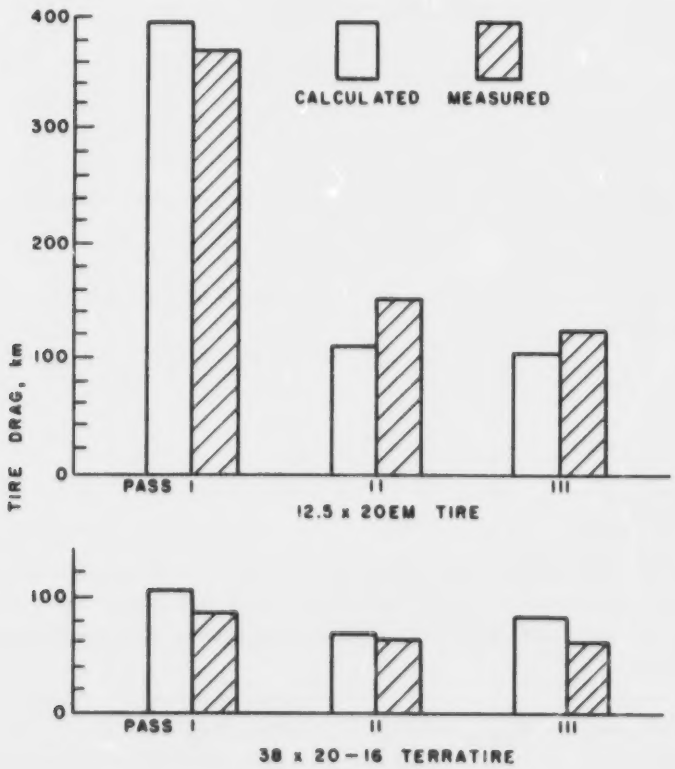

Figure D67. Measured and calculated drag of a 12.5 × 20 EM tire, and of the 38 × 20 - 16 Terratire, in a sandy loam

Rear axle: $W = 6000$, $D = 178$, $b_{tr} = 57$, $p_i = 1.0$, $p_c = 0.3$, $r = 60$, $h = 50$

Soil, ploughed dry sandy loam: $k_c = 1.8$, $k_\phi = 0.27$, $n = 0.404$, $K_{\gamma av} = 25$, $\gamma = 0.0012$, $\phi = 30$, $c = 0$. Calculations yield:

Front tire: $z = 17$; $l_0 = 35.4682 > 22$; hence, $z = 15.2479$

$p_{cr} = 1.11 < 1.5$ RIGID

$R_c = 252.70$; $z_{max} = 6.1$; $R_b = 12.28$

$\sum R = 265.0$

Rear tire is 57 cm wide and follows the rut made by the front tire 22 cm wide. In this process the rear tire must compact soil bar of cross-section ABCD, Fig. D68. The resulting motion resistance is denoted by R_c' and approximately equals the difference between compaction resistance R_c^0, which would occur in virgin soil to the depth of 15.2479 cm, and compaction resistance of the front tire R_c^F:

$$R_c' = R_c^0 - R_c^R$$

and

$$R_o' = 57\{[k_c/(178 \times 15.2479 - 15.2479^2)^{1/2}] + 0.27\}$$

$$\times\ 15.2479^{1.404}/1.404 = 569.7$$

$$l_o = 49.8159 < 57$$

$$R_c' = 569.7 - 252.7 = 317$$

The rear tire, upon levelling off the ABCD soil prism, will sink below the 15.2479 cm depth, under the load W' reduced as shown below:

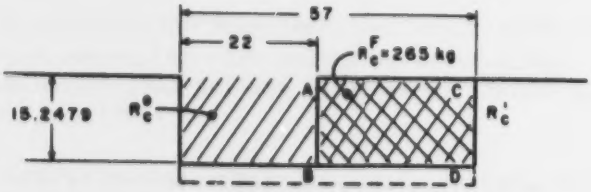

Figure D68. Dimensions of overlapping ruts of front and rear wheels of an agricultural tractor, and the forces generated by ground compaction

$$W' = 03333 \times 57(3 - 0.404)(178)^{1/2}[(1.8/49.8159) + 0.27]15.2479^{0.904} - 750 = 1601.27$$

The load compacting the soil under the total width of the rear tire is

$$W_c = 3000 - 1601.27 = 1398.73$$

The ensuing sinkage, consider second pass, is

$$z_c = \left(3 \times 1398.73/\left\{[1.8/(178z_c - z_c^2)^{1/2}] + 0.27\right\} \times 15.2479^{0.404}(3 - 0.404) \times 57(178)^{1/2}\right)1.1062 = 2.0661$$

$$l_0 = 19.0655 < 57 \qquad p_{cr} = 1.51 < 1.0 \qquad \text{ELASTIC}$$

$$F = 0.7122 \qquad K = 02963 \qquad B = 498.0862 \text{ for } W = 1398.73$$

upon a few iterations (see Part II ($b_0 < b_{tr}$))

$$b_0 = 27 \qquad A = -1.4983 \qquad z_e = 1.8583 \qquad \delta = 1.6501 \qquad \alpha = 11.0502$$

$$R_b = 0.5(57 - 22)6.1^2 \times 0.0012 \times 25 + 0.5 \times 27 \times 1.8583^2 \times 0.0012 \times 25 = 20.93$$

$$R_t = 7.59$$

$$\sum R_{calc} = 392$$

Accordingly, the rolling resistance of the complete tractor is

$$R_{calc} = 2(265 + 392) = 1314 \text{ kg}$$

$$f_{calc} = 1314/7500 = 0.1752$$

There is no direct field test available to corroborate these predictions. However, towing tests performed with the geometrically similar tractor of smaller weight in two very similar soils produced the following (D23):

$$f_{meas} = (544 \times 13 + 1400 \times 0.118)/1944 = 0.1213$$

$$f_{meas} = (544 \times 0.228 + 1400 \times 0.138)/1944 = 0.1632$$

which is practically the same as calculated above.

The method used here is thus sound in basic premises, if not in detailed outcome. It appears to deserve further elaboration of the techniques of data measuring and their processing.

REFERENCES

D1. M.G. Bekker. Theory of Land Locomotion. The University of Michigan Press, 1956, 2nd edition, 1960.

D2. M.G. Bekker. Off-the-Road Locomotion. The University of Michigan Press, 1960.

D3. M.G. Bekker. Tire selection for off-road vehicles. Des. News, September 17 and December 17, 1973.

D4. M.G. Bekker and E.V. Semonin. Motion resistance of pneumatic tyres. J. Automot. Eng. April 1975.

D5. M.G. Bekker. Practical aid to off road tire evaluation with bevameter techniques. Society of Automotive Engineers, 741133, 1974. Updated, SAE Trans. 1975.

D6. M.G. Bekker and J.Y. Wong. Terrain-vehicle systems analysis. Special Program, Universities of Madrid, Stockholm and Carleton University, Ottawa, Canada, 1974-1980.

D7. M.G. Bekker. Introduction to Terrain-Vehicle Systems. The University of Michigan Press, 1969.

D8. Y. S. Ageikin. Wheeled and Other Cross Country Vehicles (Prime Movers). Mashinostroenie (Kiev), 1972. (In Russian.)

D9. J.Y. Wong. Theory of Ground Vehicles. Wiley and Sons, 1979.

D10. F.R. Whitt and D.G. Wilson. Bicycle Science. The MIT Press, 1974.

D11. D. Schuring. The Rolling Loss of Pneumatic Tires. Rubber Chemistry and Technology, 1980.

D12. G.P. Box and N. Draper. Evolutionary Operation. John Wiley and Sons, 1969.

D13. Proceedings of Conference on Tire Rolling Resistance, DOT-TST-76-94, 1976.

D14. C.E. Prettyman. Computerized tire footprint measurements. Society of Automotive Engineers, 801511, 1981.

D15. B.L. Collier and J.T. Warchol. The effect of inflation pressure ... on tire performance. Society of Automotive Engineers, 800087, 1980.

D16. M.G. Bekker and E.V. Semonin. A note on tire rolling resistance due to test wheel curvature. Tire Science and Technology, May, 1977.

D17. B.C. Grugett et al. The effect of tire inflation pressure on passenger car fuel consumption. Society of Automotive Engineers, 810069, 1981.

D18. G.D. Thompson and M.E. Reineman. Tire rolling resistance and vehicle fuel consumption. Society of Automotive Engineers, 810168, 1981.

D19. J.Y. Wong. Data processing methodology in the characterization of the mechanical properties of terrain. Journal of Terramechanics, 17(1): 13 - 41; 1980.

D20. T.B. Golob. Development of terrain strength measuring system. Journal of Terramechanics. 18(2): 109 - 118; 1981.

D21. K. Terzaghi. Theoretical Soil Mechanics. Wiley and Sons, 1943.

D22. A.J. Green and N.R. Murphy. Stress under moving vehicles. Report 5, No. 3-545, Waterways Experiment Station, 1965.

D23. W. Sohne and F.J. Sonnen. Rolling resistance and drawbar pull of agricultural tractors, and an attempt of their correlation with mechanical soil values. First International Conference on Terrain-Vehicle Systems, Torino-St. Vincent. Edizioni Minerva Tecnica, Torino, 1961. (In German.)

D24. M.G. Bekker. Tracks in muskeg. SFM, Specialnotiser, Stockholm, 1975.

D25. I.C. Holm. Performance of Tires in Multi-pass Crossing.... Fortschrittberichte VDI, Nr 14, 1972. (In German.) Also doctorial thesis, Munich Technical University, 1970.

D26. Prof. W. Söhne, Dr. K. Steiner, Technical University Munich, and Prof. J.Y. Wong, Carleton University, Ottawa, Canada. Private communications.

D27. J.Y. Wong, et al. Characterization of the mechanical properties of muskeg with special reference to vehicle mobility. Journal of Terramechanics. 16(4): 163 - 180; 1979.

D28. M.G. Bekker. Theory of Locomotion. The University of Michigan Press. 1st Ed. 1956; 2nd Ed. 1960.

APPENDIX E. VEHICLE THRUST-SLIP PERFORMANCE

Thrust-slip performance definition as described in the literature (E1, E2) has been generally accepted in soil-vehicle evaluation. It is based on Coulomb-Mohr criterion of soil failure.

GRANULAR SOILS

Granular soils and snow display an asymptotic attenuation of slip-shear strength, and the basic Coulomb equation

[E1] $\tau = c + p \tan \phi$

used in Appendix D, Part II, takes the following form (E1, E2):

[E2] $T = (Ac + W \tan \phi)\{1 - (K/i_0 l)[1 - \exp(-i_0 l/K)]\}$

where T is the thrust generated by the ground at slip i_0. A is the ground contact area of the tire, or track, as shown in Appendix D; l is the length of A measured along the direction of motion; W is the load, and K, c, and ϕ are soil parameters specified before (E1, E3) (see Appendix B).

ORGANIC SOILS

For organic soils such as muskeg or turf, another form of Equation [E2] is more useful because the shear strength shows a hump with increasing slip i_0 and drops after reaching the maximal value (E3). Thus the integration of unit thrust along the ground contact area of length l and width b

[E3] $T = b \int_0^l \tau \, dx$

yields a more complex form for tire thrust, since, in this case,

[E4] $$\tau = [(c + p \tan \phi)/y_{max}]\{\exp[-K_2 + (K_2^2 - 1)^{1/2}]K_1 i_0 - \exp[-K_2 - (K_2^2 - 1)^{1/2}]K_1 i_0\}$$

Complete solution and the definition of y_{max} and slip coefficients K_1 and K_2, Equations [E3] and [E4], are available (E3).

Equations [E2] and [E3] refer to a single ground contact area $A = b \times l$. The thrust T_v of the total vehicle is obtained when multiplying

T by the number of A's, considering load distribution, static and/or dynamic, among the contact areas.

The net vehicle thrust, called the drawbar pull (DP), or slope (DP/W) is obtained by subtracting from T_v the rolling resistance of the tires $\sum R$ as presented in detail in Appendix D, Part II:

[E5] $$DP/W = (T_v - \sum R)/W$$

When calculating vehicle pull on slopes, or determining its slope climbing ability, the effect of suspension on the shifting of the CG of the vehicle is considered.

Equations of equilibrium for such cases have been developed for 8 × 8, 6 × 6 and 4 × 4 vehicles, and are available in the literature (E4). The equations readily serve the situations, when not all the axles are driven.

REFERENCES

E1. M.G. Bekker. Introduction to Terrain-Vehicle Systems. The University of Michigan Press, 1969.

E2. J.Y. Wong. Theory of Ground Vehicles. John Wiley and Sons, 1978.

E3. M.G. Bekker. Theory of Land Locomotion. The University of Michigan Press, 1st Ed. 1956, 2nd Ed. 1960.

E4. M.G. Bekker. Engineering optimization of terrain vehicle systems... Report No. 10421, U.S. Army Tank Automotive Command. U.S. Government Clearinghouse, 1969.

APPENDIX F. TERRAIN DAMAGE

In this study, terrain damage is measured in terms of soil compaction and surface shearing. These phenomena are known to directly affect the ecological balance, even though the mechanism of such an effect is not entirely clear.

SOIL COMPACTION

Soil compaction effect may be measured in terms of the depth of ruts made by the tires. However, a deep rut in soft soil may not have the same meaning as a shallow one in a hard ground. Therefore, the amount of energy spent on rut-making may be another measure of soil damage.

Evaluation of the depth of tire sinkage is reported in detail in Appendix D, Parts II and III. Thus, a direct comparison between the rut depths may be readily made, to determine the merit of the given tire, or vehicle configuration.

Note the ramifications of sinkage effect as described in Appendix D, Part III, for multiple crossing.

Soil Compaction Index is based on the assumption that tire motion resistance portion R_c (see Appendix D, Parts II and III), due to vertical soil compaction, expresses the vertical forces and/or energy absorbed by the ground. The compaction index I_c may be thus defined per unit of tire width b, in the following form:

[F1] $$I_c = R_c/b$$

The compaction energy related to I_c may be defined, per unit tire width, as,

[F2] $$E_c = R_c z/b$$

where z is the sinkage involved in the compaction process.

Value R_c in Equation [F1] has the following well-established structure (see Appendix D, Parts II and III):

$$R_c = bkz^{n+1}/n + 1$$

Hence, compaction index E_c is expressed by:

$$E_c = bkz^{n+1}/bz(n + 1)$$

or

[F3] $E_c + kz^n/(n + 1)$

where z is determined as shown in Appendix D, Part II.

SURFACE SHEARING

Soil Surface Shear Index is related to the slip of the tire ground contact area. Since there is no locomotion without slip, terrain damage due to the dislodgement of ground surface is unavoidable.

It has been well established that for slip i_0, the amount of horizontal soil deformation j grows linearly along the contact area, with the increase of the distance x measured from the leading edge of the ground contact area. The maximum horizontal soil deformation j_{max} occurs at the end of that area. For an elastic tire (Fig. F1a)

[F4] $j_{max} = i_0(l_1 + l_2)$

For rigid tires (Fig. F1b) a fair approximation is obtained, in the following form:

[F5] $j_{max} = i_0 l_0$

where values l_1, l_2, and l_0 may be readily calculated as shown in Appendix D, Parts II and III.

To control the amount of horizontal soil deformation j_{max}, it is logical to assume as a limit, $j_{max} < j_{crit}$, where j_{crit} is the ultimate destructive deformation of the ground, beyond which the shearing stress τ, and hence, the vehicle thrust, do not increase (see Equations [E1]-[E4], Appendix E).

The value of j_{crit} depends on the type of soil. Figure F2 shows j_{crit} for measured various types of ground:

Type of ground	j_{crit} (cm)
Stubble	2
Silt	2
Turf	6.2
Sand	2
Muskeg	19.5

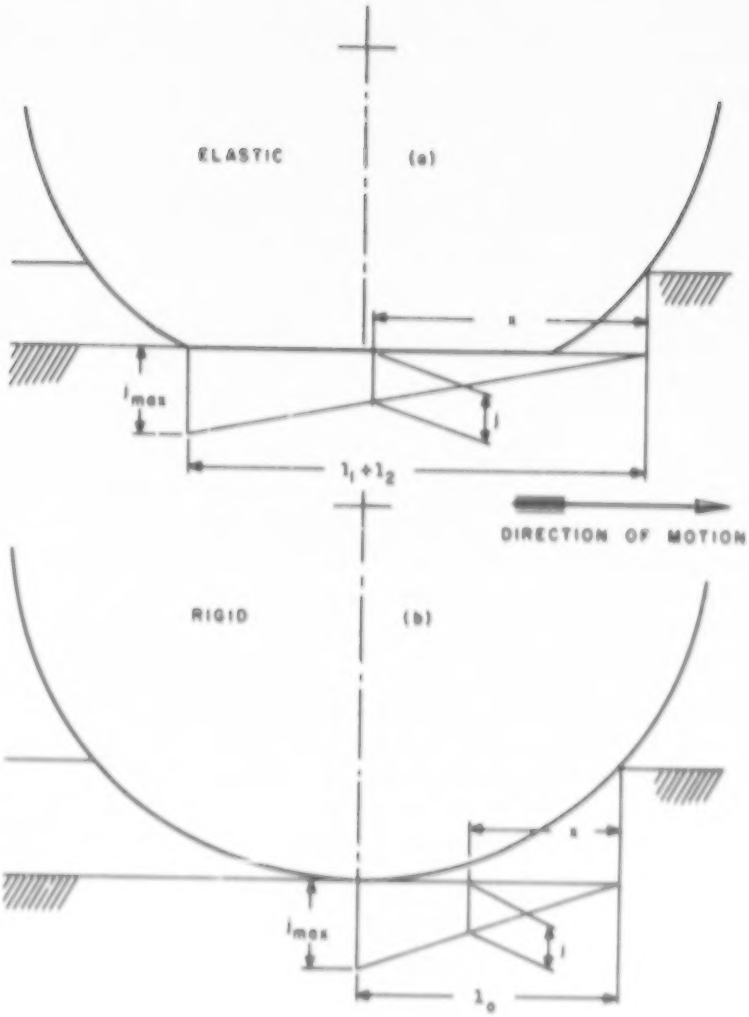

Figure F1. Linear increase of horizontal deformation j along the ground contact area of: (a) elastic and (b) rigid tire

It results from the foregoing that $i_0 l$ larger than j_{crit}, for the given material, results in churning the ground and tearing its surface with rapid deterioration of the locomotion.

Thus soil surface shear index I_s is expressed by the ratio of the actual shear length $i_0(l_1 + l_2)$, or $i_0 l_0$, to the critical shear length j_{crit}:

[F6]

Elastic tire $I_s = i_0(l_1 + l_2)/j_{crit}$

Rigid tire $I_s = i_0 l_0/j_{crit}$

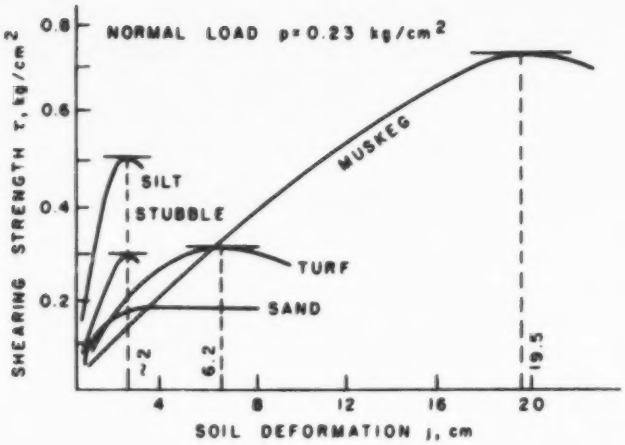

Figure F2. Shear-deformation $\tau(j)$ characteristics of various types of ground, under constant normal load of $p = 0.23$ kg/cm^2

For an "allowable" destructive shear distance $I_s = 1.0$. For less destructive slip, $I_s < 1$. For more soil surface destruction $I_s >> 1$.

APPENDIX G. TRADE-OFF CRITERIA AND OPTIONS

For restricted and, in a sense, preliminary selection of vehicle optimum, operations research techniques concerned with many variables, cost, and effectiveness, are not needed. A brief deterministic approach, such as illustrated in Fig. 1 is sufficient.

It is this approach which may be also considered for evaluation of equipment for planting and harvesting of the hybrid poplar cuttings, on five year rotation plantations.

The result of the process, shown in Fig. 1, is the tabulation of various performances of the considered candidate vehicles, within one set of mission and environment requirements. Such a table implies the kind and number of options available (see box 11, Fig. 1). Unfortunately, as exemplified in Table G1, various performances seldom have a common value denominator, which would enable one to make a simple choice of the optimum.

The various performances tabulated in Table G1 have specific numerical values. However, the order of preferences assigned to the given performance as such is not *a priori* determined. For example, if speed c_x of X-vehicle is larger than speed c_z of Z-vehicle, but the fuel consumption of $b_x < b_z$, then the trade-off may be based on the merit of fuel consumption vs. speed, and not on the numbers involved.

This value judgment depends on specific conditions, which usually are spelled out by the user, and lead to the commonly applied "weight factors" assigned to each performance. This complicates the issue.

Table G1. Mission-environment No. A.
Performance tabulations

Performance	Vehicle candidate			
	X	Y	Z	etc.
Motion resistance	a_x	a_y	a_z	
Fuel consumption	b_x	b_y	b_z	
Speed	c_x	c_y	c_z	
Slope climbing				
Drawbar pull				
Obstacle crossing				
Terrain damage, etc.	k_x	k_y	k_z	etc.

A useful and simple procedure, in a first-order optimization of vehicle performances, consists of using a general relative performance quality, rather than specific quantity.

In this procedure, each vehicle performance which is better than that of the other candidate is assigned sign (+). If it is worse, sign (-). If it is equal, sign (=). Summation of pluses, minuses, and equals yields an order of preference more easy to determine.

The procedure is illustrated in Table G2, for three vehicle candidates X, Y, and Z.

Each column of signs for each candidate refers to "better", "worse", or "equal", with respect to the two remaining candidates. For the larger number of candidates the number of columns increases. In a final analysis, the sum of pluses $\sum(+)$ defines the "best" choice. However, again the "weighing" of the value of particular performance cannot be avoided.

Table G2. Mission-environment No. A.
Relative quality of performance

Performance	Vehicle candidate		
	X	Y	Z
Soft ground crossing (DP/W)	(-) (+)	(+) (+)	(-) (-)
Obstacle crossing	(=) (-)	(=) (-)	(+) (+)
Fuel consumption	(+) (-)	(-) (-)	(+) (+)
etc.			
$\sum(+)$	2	2	3

PHASE II

[illegible]

[illegible]

[illegible]

PHASE II

EVALUATION EXAMPLES OF AGRO-FORESTRY VEHICLES

SOIL AND VEHICLE PARAMETERS, INTERPRETATION, ETC.

Canadian effort undertaken in connection with this program represents a pioneering activity in the realm of soil measurements by means of bevametric method.

Comparable measurements made in the United States and in Germany were more limited in scope and did not yield much statistical insight (1).

Thus, in a sense, the present report may be seen as a contribution to the large-scale terrain classification for locomotion purposes, and to the demonstration of technological merit of bevameter methods, in the assessment of numerous aspects of the terrain-vehicle relationship.

ENVIRONMENT OF LOCOMOTION

Soil properties and terrain surface geometry were given in reference 2. Considering that such a mass production of data was performed for the first time, the following comments appear appropriate.

Analysis of Field Data and Soil Parameters

Analysis of field data and soil parameters were performed on two sites, near Prescott, Ontario, as shown on the map, Fig. 1. The grain size distributions (2) indicated that both sites represent the same specimens of sandy loam.

Nevertheless the local homogeneity of the ground was poor although the measurements were made at the points located close to each other (Fig. 1).

Figure 2 shows the spread of load-sinkage measurements in 10 penetration tests performed with 15 cm diameter plate. Note that two of the measurements show abnormal, undoubtedly casual discrepancy, and ought to be discarded, or confirmed by additional measurements.

This invites the establishment of measuring procedures which would recognize the extrema *in situ*, when sampling soil properties.

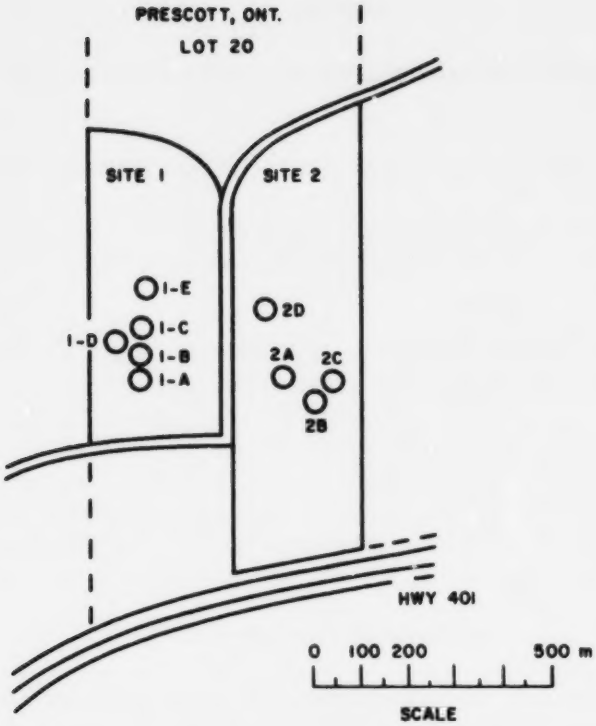

Figure 1. Map of the terrain measured, near Prescott, Ontario. Dots denote the spots where bevameter data were collected

For the purpose of this report not all the data (2) were used when attempting to determine a meaningful spread defined by standard deviation.

It is felt that in more strict sampling procedures for soil shear-penetration tests, monitoring the tests with graphic computer read-outs would be very useful.

Generally speaking, the test sites should be treated with the same technique, which was not the case, at this time. Figure 1 shows that in Site 1 the number of measurements was 11, whereas in Site 2, only 6 points were covered.

The variation of soil properties reported in both sites (2) was quite large, and the moisture content (MC) varied from 25 to 50%:

Site 1	MC = 27.3 to 51.6%
Site 2	MC = 24.1 to 52.0%

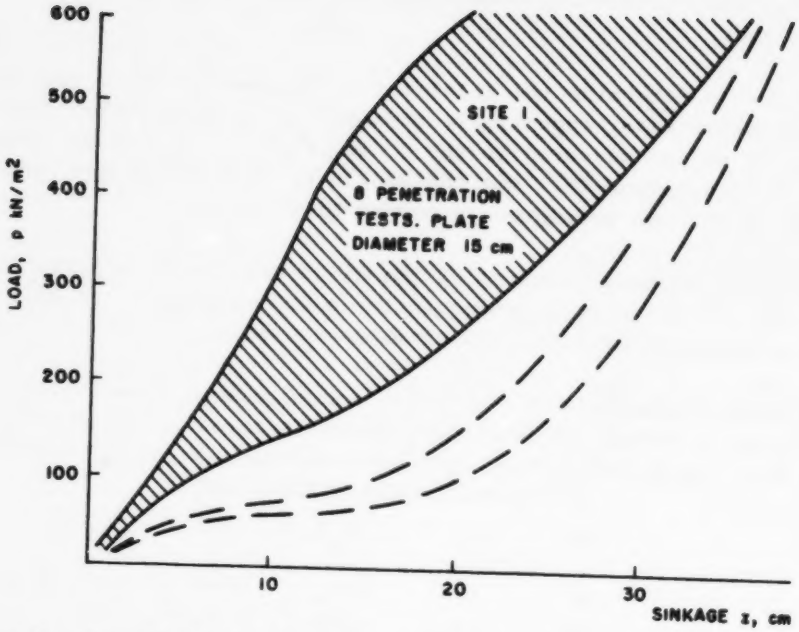

Figure 2. Spread of the load-penetration measurements, Site 1, Fig. 1. Note two "abnormal" curves marked with interrupted lines

This may be indicative of structural soil differences which make difficult any correlation of moisture contents with bevameter values, particularly when measured over a longer time span.

Spatial distribution of soil data should correspond to the temporal one, which would help to detect bias due to changes in soil structure.

To preserve some consistency, soil in Site 2 was not included in "averaging" terrain properties. The data of Site 2 were useful, however, in checking the practicality of various assumptions as described later.

In a final analysis, the mean bevameter values and their standard deviation were calculated for Lot 20 using data measured in Site 1 (Fig. 1):

$$k_c = 52 \pm 16$$
$$k_\phi = 2192 \pm 700$$
$$n = 0.87 \pm 0.14$$

This input was used in the preliminary calculations of rolling resistance for the purpose of data verification - by comparison with the avail-

able, though not necessarily commensurate, field tests of the tractors as discussed later.

In order to determine the relationship between moisture content, MC%, and the bevameter data, approximate straight lines were fitted into the population of points measured in the field, Figs. 3, 4, and 5. This was based on the assumption that the changes in k_ϕ, k_c, and n were solely due to changes in MC - an assumption somewhat biased.

A need for seasonal testing of the given area that includes the moisture content variation is a prerequisite in the assessment of soil parameters as a function of time, and climate.

Considering that Site 1 represents a homogeneous association area (3), the functions of bevameter values expressed in terms of moisture content, shown in Figs. 3, 4, and 5 were tabulated below.

MC%	k_c	k_ϕ	n
40	52*	2192	0.87
60	25*	1490	0.73
80	0	600	0.6

*Means of values reference 2.

Note that soil measurements did not encompass 60 and 80% moisture contents. Consequently, the practicality of our extrapolation was checked later.

As an aid in determining if the given soil sample is sufficiently homogeneous, the soil consistency parameters δ discussed in Phase I of this report could be tested on the spot, since separate k_c, k_ϕ, and n values may be misleading. Figure 6 shows the result for Site 1, assuming the consistency parameter, say:

$$\delta = [(k_c/0.3) + k_\phi]0.03^n$$

The graph shows the compounding of structural and moisture content variation of soil, which suggests caution when comparing calculated and measured data of actual vehicle performance, even in an area located nearby.

The low values of δ in plot 1-A apparently belong to a localized situation. A more characteristic and representative feature of this terrain is δ = 120-160 kPa, at MC = 30-40%.

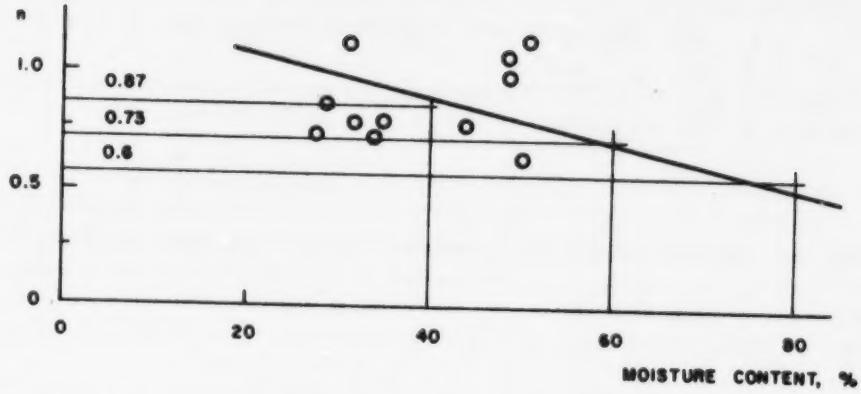

Figure 3. Extrapolation of n-values for 80% moisture content

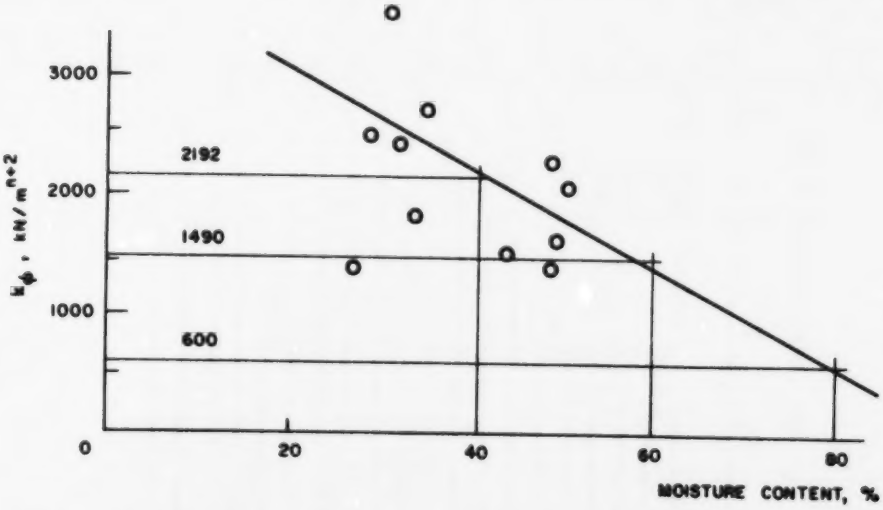

Figure 4. Extrapolation of k_ϕ-values for 80% moisture content

The δ-test may be a useful tool in sorting out the "local contaminations" of measurements, which is difficult when looking at k_c, k_ϕ, and n, separately.

Note that terrain sampling should not remain uncorrelated with the topography. The "isoclines" of ground surface might be as well superimposed on "isolines" of δ, or k_c, k_ϕ, n, and MC, at least in preliminary, exploratory tests. This should not be burdensome, when using computerized techniques and terrain maps.

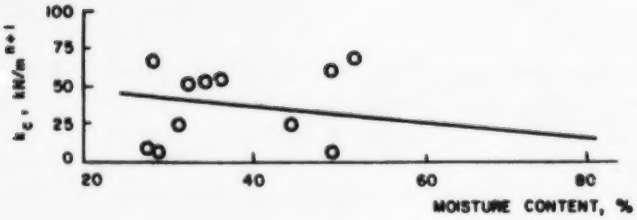

Figure 5. Extrapolation of k_c-values for 80% moisture content. Note that k_c is so small in reference to k_ϕ tht it may be assumed zero, considering the accuracy of the measurements

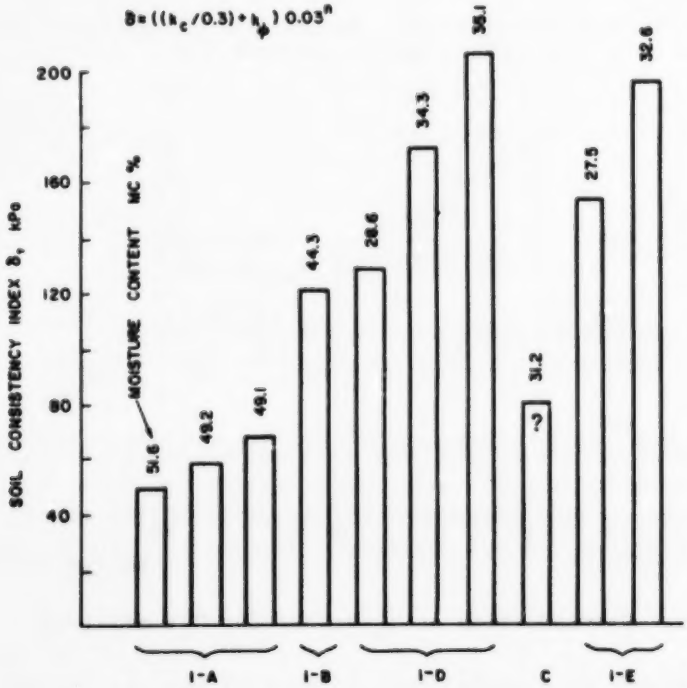

Figure 6. Test for soil "consistency" δ vs. moisture content. Points 1-A and C do not show consistency with the rest of the sample, and may denote inconsequential local disturbances

Measurement of the other soil data, c-ϕ-K, also requires more analysis because the referenced values were processed under "ad hoc" assumptions (2)

different from those specified in Phase I and references 1 and 3. This led to the introduction of a new equation with two additional parameters K, instead of one as postulated in Phase I and reference 3.

While the proposed change is not being questioned, its introduction at that time resulted in additional work, and has been put in abeyance.

It was determined that for practical purposes "loose" soils L, and "fragile" ones F, Fig. 7, may be approximated with K value defined in Phase I and reference 3, for slips to approximately 30-40%.

Since this procedure was quicker and well established, the new K_w and K_r parameters introduced in reference 2 had to be re-evaluated in terms of K.

The distribution of K-values was shown in Fig. 8. As an "average" K = 0.025 m was assumed in conformity with data Fig. 8, and other available sources (3).

This reminds us that the technique for K-determination should be nor-

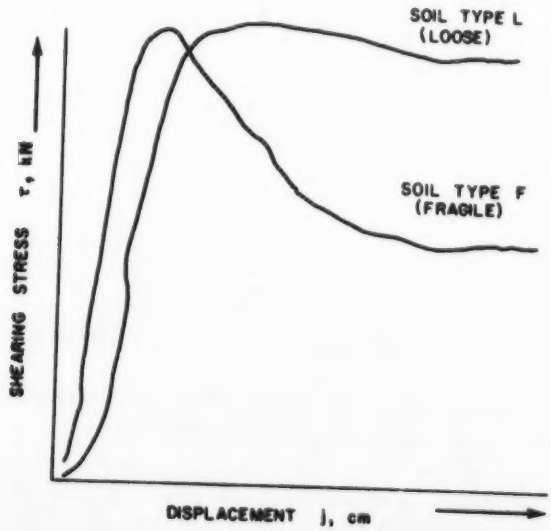

Figure 7. Two types of soil shear curves. For slip up to approximately 30%, the hump on F soil may be neglected, or minimized. Then both soils may be defined with one parameter K

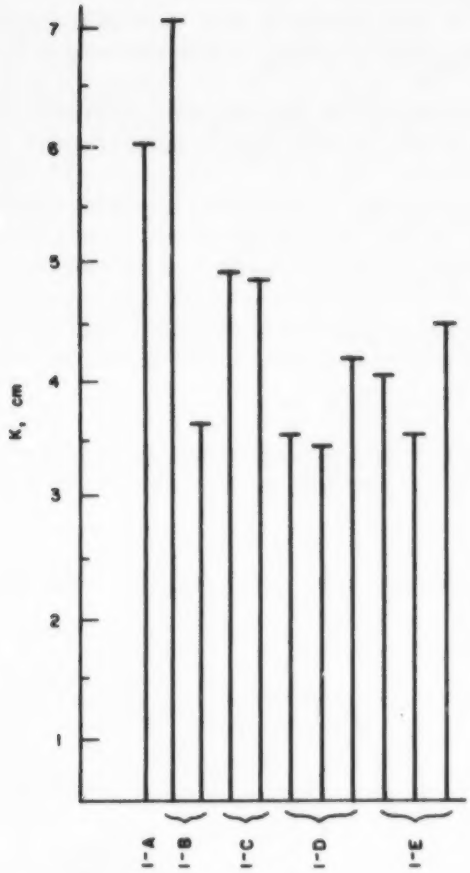

Figure 8. Distribution of shear parameters K measured at the peaks of shear curves. Experience indicates that they produce too-high values, and a "mean" K = 0.025 m was assumed

malized, considering that there is a difference between K-values measured at the peak of τ-curve, and with the peak eliminated.

This was analyzed some time ago (1, 3) and exposed too-high unrealistic K-values for sharp peaks, which biased the evaluation of vehicle performance.

A similar problem exists in the definition of c and ϕ. Peak τ-values always lead to unrealistic computation results, which was the case in reference 2.

Figures 9 and 10 show the distributions of friction angle ϕ and cohesion c, in Site 1. In accordance with the available experience, the following values were assumed for computations:

$c = 3$ kPa
$\phi = 28.4 \pm 3.38°$

Note that c was considered constant everywhere and all the time, which may be tolerable because in the case of pneumatic tires, where the ground contact area is small, the cohesive forces are insignificant in comparison with frictional forces.

As reported in Phase I and reference 3, three more soil parameters are needed for calculation of sinkage and rolling resistance due to horizontal soil deformation: K_c, K_γ, and γ.

These values are very sensitive in the estimation of the horizontal component of Rolling Resistance R_b (Phase I). The standard Terzaghian

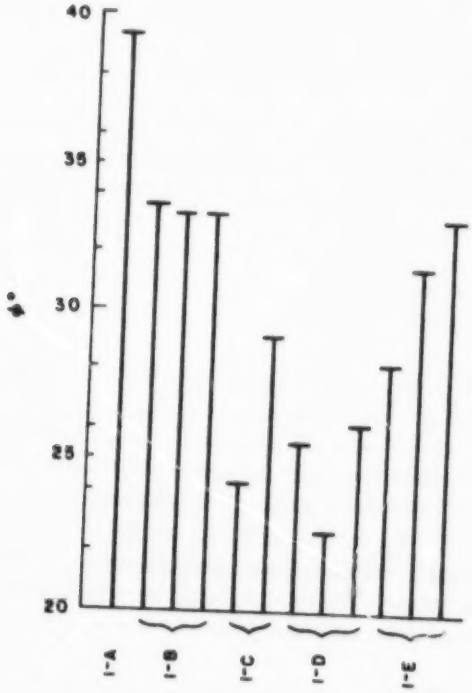

Figure 9. Distribution of internal friction angle ϕ. Measurements 1-C and 1-D show some "abnormality." Do they belong to the sample?

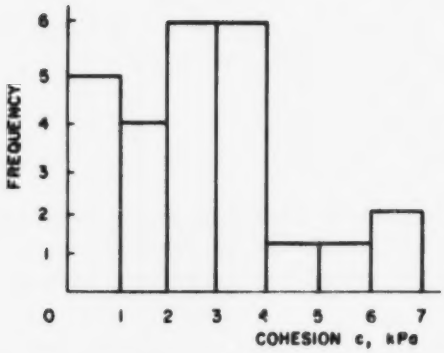

Figure 10. Distribution of cohesion values c. Again the measurements considered the peaks of shear curves, which produced too-high values. It was assumed that c = 3 kPa

tables may be too idealized though they appear accurate for homogeneous loose granular soils. Reference 2 did not refer to that problem. As a result an additional experiment was conducted simulating Terzaghi's retaining wall.

The experiment, though preliminary, if not primitive, yielded K_c and K_γ parameters compatible with experience: $K_c = 15$, $K_\gamma = 13$, $\gamma = 15$ kN/m^3. (Density was determined in the usual manner, though in virgin soil only.)

For computations of the rolling resistance due to horizontal soil deformation the formula related to "local shear failure" was used (see Phase I and reference 3.)

Soil parameters k_c, k_ϕ, and n were determined with means and standardized deviations, in the field. Parameters K_c, K_γ, ϕ, c, and γ were assumed constant solely because of lack of pertinent measurements. Fortunately, variations of K_c and K_γ are generally small, for a given area, although c and γ do change with the second pass - to what extent, one may speculate.

For a point-to-point correlation between soil measurements and prediction of vehicle performance, either strict measurements must be provided, or the correlation should be statistical.

Second Pass Bevameter Values

These were discussed previously and in the literature (3). It was suggested that because of uncertainties involved and insufficient experi-

mental evidence available, bevameter tests should be made and processed *in situ*, for repeated loadings.

Such tests were made but not processed numerically because of conditions beyond control (2). Consequently, for the purpose of this report, two curves of first and second load-deformation cycle were selected. The corresponding k_c, k_ϕ, and n-values were calculated "by hand". In this process, it was assumed that the second load-sinkage cycle starts again from "ground zero" (Phase I, reference 4).

Figure 11 shows the selected curves (tests designated "22/04/82") made with 10 and 15 cm plates (2). Their log-log plot is shown in Fig. 12. Pertinent soil values for this test and another (designated "16/04/82") were thus determined as follows:

	k_ϕ		k_c		n	
Site	Pass I	Pass II	Pass I	Pass II	Pass I	Pass II
1	650	2850	0	0	0.96	0.96
2	4200	7000	0	0	0.9	0.9

These figures were found to be close to those reported in reference 2; values 4200 and 7000 were measured even in the first pass in Sites 1 and 2. Thus, they are not unrealistic. The small k_c-values reported in reference 2 also are indicative of the plausibility that $k_c = 0$. Exponent n is almost constant, everywhere.

Accordingly, assuming the values above quoted, one may write:

SITE 1 $k_{\phi II} = 4.38k_{\phi I}$
SITE 2 $k_{\phi II} = 1.67k_{\phi I}$

Data available in the literature for sandy loam yield coefficients 2.34 to 1.55 instead of 4.38 to 1.67, which is reasonable considering the amount of organic debris present in both sites of the Prescott soil. This debris acts like straws in clay, in brick making.

Consequently, taking a rounded up average was assumed to be a safe approach:

$$k_{\phi II} = (4.8 + 1.67 + 2.34 + 1.55)/4 = 2.5k_{\phi I}$$

This crude approximation was later corroborated, when comparing the

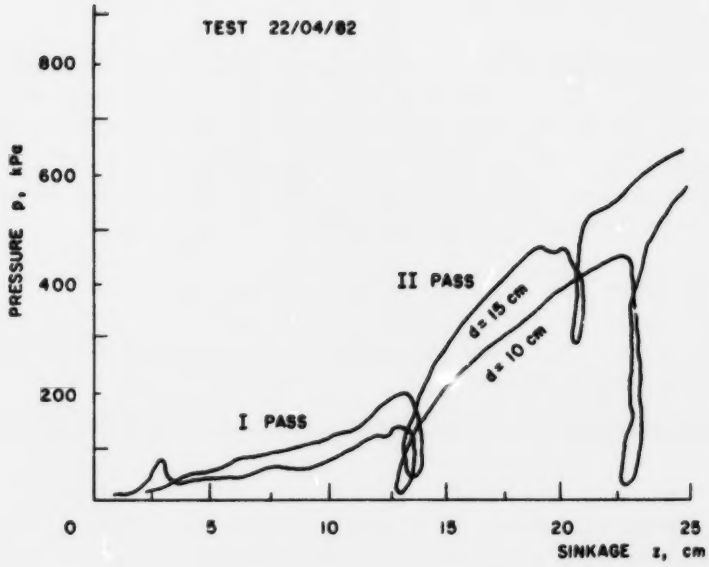

Figure 11. Load-penetration tests data for two consecutive passes

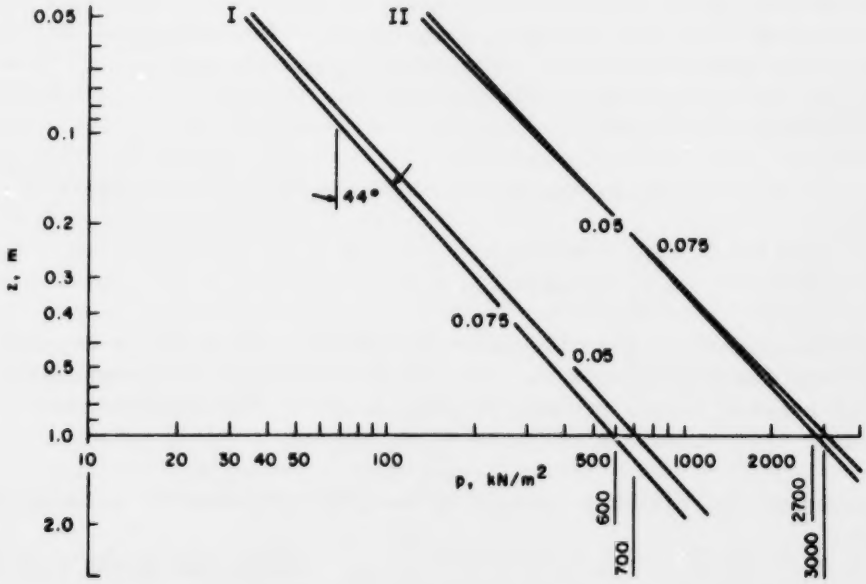

Figure 12. Test data, Fig. 11, replotted in log-log scale. Note that $k_c \cong 0$ as deduced from Fig. 5

calculated and measured rolling resistance of a tractor, even though the test was not directly correlated within this spatio-temporal frame.

Soil Measuring Techniques

Soil measuring techniques reviewed in the preceding sections may be recommended within the following rules:

- Spatio-temporal frame of measurements should be constricted as much as required for reliable soil sampling.
- Test procedures for c, ϕ, and K should be normalized, considering the effect of peak τ-values.
- Density γ and cohesion c should be determined for multipass compaction.
- Sample measurements of K_c and K_γ ought to be initiated.
- Use of δ-index should be introduced in the computer program in order to define *in situ* the uniformity of the given association area.
- Soil measurements may be best performed when using a rectangular grid map.
- Second and at least third pass bevameter data should be processed in the field, including all the soil values.

Summary of Prescott Environmental Input

A summary of Prescott environmental input provided in reference 2 and discussed in the preceding paragraphs is shown in Table 1.

Soils A and C represent one standard deviation band width of the mean represented by soil B. Table 1 was used to investigate the effect of soil value spread on tire rolling resistance.

Table 1. Soil data in Prescott area

	k_c		k_ϕ		n	
Soil	Pass I	Pass II	Pass I	Pass II	Pass I	Pass II
A	36	0	1492	3730	0.73	0.73
B	52	0	2192	5480	0.87	0.87
C	68	0	2892	7230	1.01	1.01

Table 2. Soil parameters and moisture content in Prescott area

	k_c		k_ϕ		n	
MC%	Pass I	Pass II	Pass I	Pass II	Pass I	Pass II
40	52	0	2192	5480	0.87	0.87
60	36	0	1492	3730	0.73	0.73
80	0	0	600	1500	0.6	0.6

Considering the moisture contents extrapolated from measurements reference 2, Figs. 3, 4, and 5, Table 1 may be rewritten in the form shown in Table 2.

Other soil parameters were assumed independent of soil moisture and soil compaction with the first pass because of lack of appropriate input. This deficiency may be tolerated, however, because of the apparent small sensitivity of performance to c and γ-values as mentioned before. The values of K's do not seem to change much, and were assumed also to remain constant as follows: $K = 0.025$ m, $K_\gamma = 13$, $\phi = 28.4°$, $K_c = 15$, $c = 3$ kPa, and $\gamma = 15$ kN/m^3.

EXPLORATORY STUDY OF TRACTION PARAMETRICS

Assume that a tractor tows a planter to the plantation site. This represents a simple case of tractor-trailer operation which is a matter of rather standard evaluation. It yields direct insight into phenomena involved, without the bias of additional operational requirements.

Tractors and Their Equipment

Tractors and their equipment considered in this study are shown in Table 3. Information about tire geometry and carcass stiffness is given in Table 4.

The tires mounted on the planter are of 36 × 20 - 12 size, and have the following dimensions: $D = 0.091$, $b_{tr} = 0.5$, $h = 0.3$, $p_i + p_c = p_g = 34.47$ kPa ($p_i = 4$ psi).

Exploratory Example

The Versatile 160 tractor (Fig. 13) with one or more planters was

Table 3. Tractors and the tires

Test tractor	Tires	Inflation pressure psi	Inflation pressure kPa
Versatile 160 (Fig. 13)	Goodyear 16.9 - 24	12	82.74
	Goodyear 13.6 - 24	14	96.53
	Rolligon 40 × 50 - 12*	4	27.58
Holder A 60 (Fig. 14)	Dunlop 14.5 - 75/20	20	137.9
	Rolligon 40 × 50 - 12*	4	27.58

*These are hypothetic tires selected for comparison only.

chosen for test computations since it could be investigated with three different tires (Table 3). The Holder was analyzed with two tires.

Terrain of operations was assumed as specified in Table 2 (compare Table 1), covering the 40-80% range of moisture content in Prescott soil.

Speed of locomotion limited by planter requirements: 2.4 km/h.

Planter Rolling Resistance

Planter rolling resistance, Fig. 13, was calculated for soils A, B, and C (Table 1) assuming axle load of 11.93 kN. For the mean value, soil B:

$F = 0.5347$	$p_i + p_c = 34.47$	$B = 1.5934$
$l_1 = 0.3350$	$z_e = 0.0078$	$b_2 = 0.0202$
$\delta = 0.0319$	$\alpha = 21.5823$	$\varepsilon = 0.7971$
$R_c = 0.0718$	$R_b = 0.1200$	$R_t = 0.1542$

Accordingly, the rolling resistance of the planter for the mean values of Prescott soil is as shown in Table 5.

Table 4. Tire geometry and carcass stiffness

Tire	D	b_{tr}	h	r	p_c
16.9 - 24	1.35	0.429	0.22	0.38	25.86
13.6 - 24	1.21	0.343	0.28	0.29	20.75
14.5 - 75/20	1.0	0.34	0.31	0.29	15.1
40 × 50 - 12	1.02	1.27	0.0	0.33	~0.0

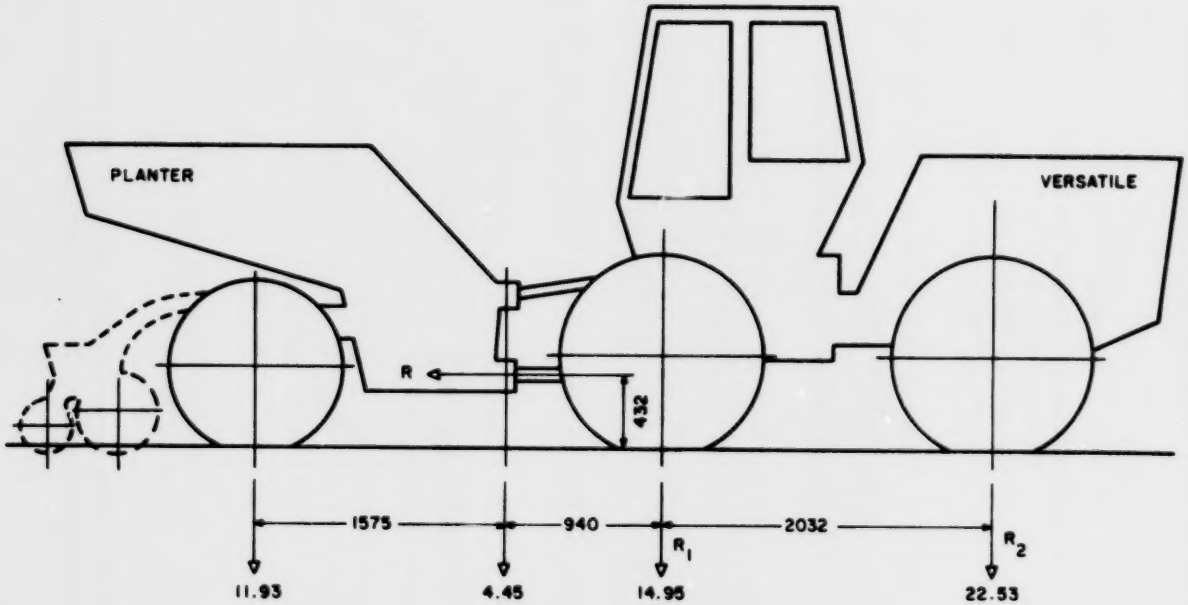

Figure 13. Geometry and load distribution of the Versatile 160 test tractor with one planter

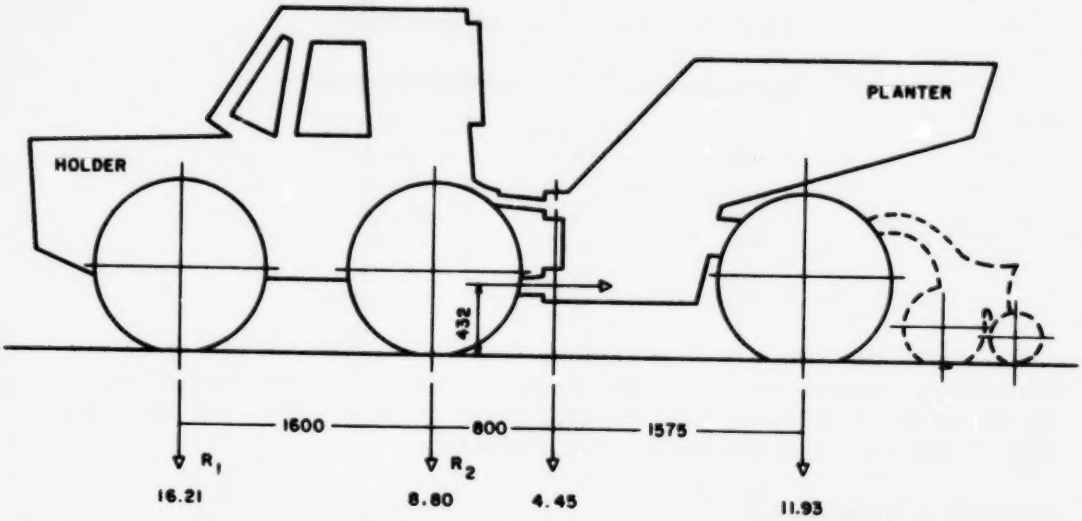

Figure 14. Geometry and load distribution of the Holder A 60 test tractor with one planter

Trial computations showed that the rolling resistance of the planter in soils A and C is, for practical purposes, the same because of low tire inflation pressure.

Axle Load Distribution

This depends on the number of trailers (planters). From equations of equilibrium we get the values shown in Table 6.

Versatile 160 Tractor with 16.9 - 24 tires: Rolling Resistance

The rolling resistance in soils A, B, and C was calculated as described in Phase I. The result was tabulated in Table 7 for soil B (mean values of Prescott ground), and plotted on the graph, Fig. 15, which also covers soils A and C.

Table 5. Planter rolling resistance, soil B

Planters	Rolling resistance (kN)
One	0.692
Two	1.384
Three	2.076

Table 6. Versatile 160 axle loads (Fig. 13)

Planter	R_1 (rear) (kN)	R_2 (front) (kN)
One	17.07	20.40
Two	19.19	18.28
Three	21.32	16.15

Table 7 provides a unique insight into the changes of tire geometry and rolling resistances, with the change of load. No other method enables one to follow so closely the interdependence of geometrical and physical tire parameters, from an engineering viewpoint.

Accuracy of Prediction

The accuracy of prediction of rolling resistance of the Versatile could not be verified directly because of lack of measurements performed in the same spatio-temporal frame as the time and location of Prescott measurements.

However, towing tests were performed in the same general area at a later date. A copy of the dynamometer tape was reproduced in Fig. 16.

Even this relatively smooth segment of the tape shows large variation of the pulling force. Other segments were more non-uniform. The read-out of the low values yielded R ≅ 750 lb (3.336 kN).

The Versatile was towed without the planter in the neutral gear. However, the differential and the drive line drag were not eliminated; hence, the measured values were higher than tire rolling resistance. Computations performed for the tractor without the planter ("zero trailer") yield R = 2.7 kN, which is close to the measured value R = 3.336 kN (Fig. 16). High peaks of the measured curve need explanation as to the setting of the draw bar vibration damping, uniformity of motion of the towing tractor, etc.

Although this test cannot be accepted as totally adequate, the general ball park of measured and calculated values appears satisfactory.

Relationship between Soil Value Spread and Rolling Resistance Spread

This may be established for the calculated cases on a percentage

Table 7. Computation output, soil B, 16.9 - 24 tire

No. of planters	R_c	R_b	R_t	R_{axle}	δ	z_e	b_0	l_1	l_2	W_{axle}
Front tire										
One	0.4039	0.3988	0.1418	1.8890	0.0208	0.0284	0.2450	0.3327	0.0949	20.40
Two	0.3756	0.3930	0.1115	1.7603	0.0184	0.0282	0.2300	0.3132	0.0985	18.28
Three	0.3502	0.3639	0.0823	1.5930	0.0159	0.0280	0.2160	0.2888	0.1032	16.15
Rear tire										
One	0.1493	0.1467	0.1117	0.8155	0.0182	0.0110	0.2325	0.3111	0.0433	17.07
Two	0.1593	0.1410	0.1439	0.8885	0.0207	0.0110	0.2500	0.3315	0.0410	19.19
Three	0.1684	0.1460	0.1833	0.9956	0.0235	0.0110	0.2650	0.3535	0.0316	21.32

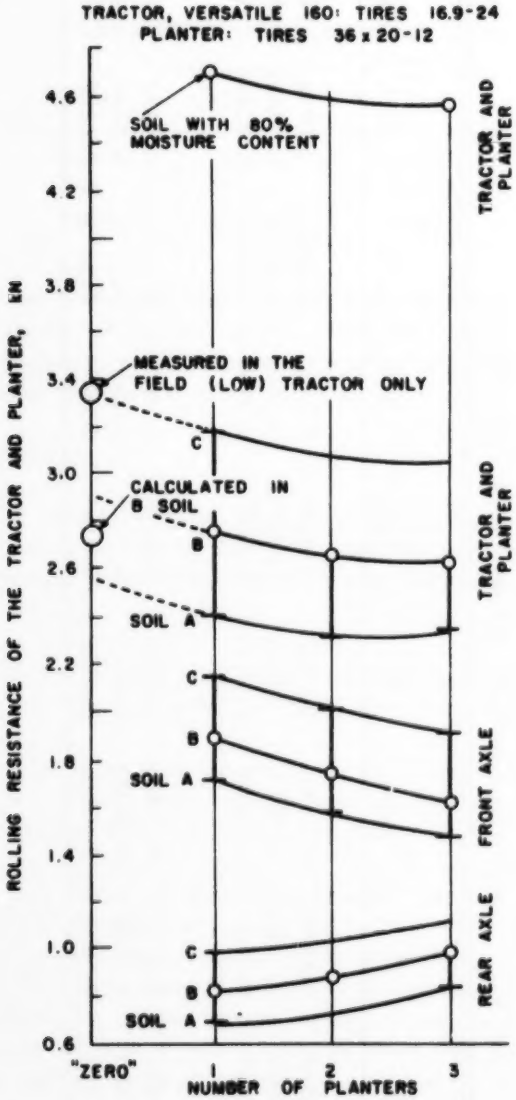

Figure 15. Rolling resistance to the Versatile 160 test tractor with planters in Prescott soils of 40, 60, and 80% moisture contents, covering the mean ± standard deviation. Measured points corroborate the calculations

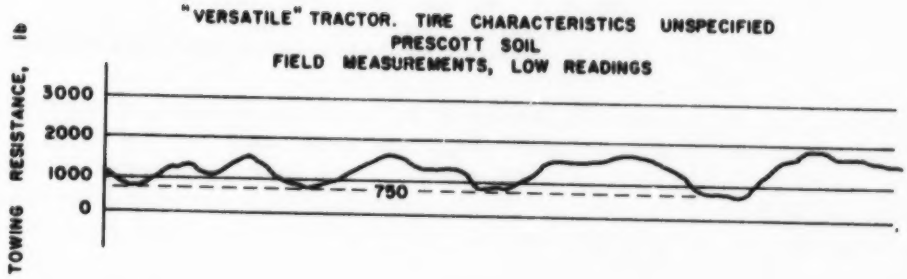

Figure 16. Copy of the dynamometer chart used in the corroboration of graph, Fig. 15

basis, considering the mean and standard deviation values of soil parameters (soils A, B, and C) and those of tractor (Versatile) rolling resistance, Fig. 15.

The graph shows the upper and lower limits of rolling resistance extending within approximately ±16% band width. The corresponding standard deviations of soil parameters are k_c, ±31%; k_ϕ, ±32%; n, ±16%.

It may be concluded that, in the case considered, a ±16% band width is a fair approximation for future calculations of the spread of rolling resistance of a vehicle if soil parameters display a ±30% spread. This may save extra work in approximate statistical comparisons as only mean values may suffice in the evaluation of vehicle performance.

Rolling Resistance and Soil Moisture Content

In Figs. 3, 4, and 5 based on actual measurement of Prescott soils, the extrapolation of soil values was reported as a function of MC%. The result for 40, 60, and 80% MC was listed in Table 2, for the first and second pass.

Using the same procedure as before, the rolling resistance of the Versatile test tractor was calculated and added to the rolling resistance of the planters (Table 5). The result was plotted in Fig. 17.

Note that MC ≅ 60% produces the most economic operation. Increase of MC to 80% "softens" the soil with approximately 150% increase of rolling resistance.

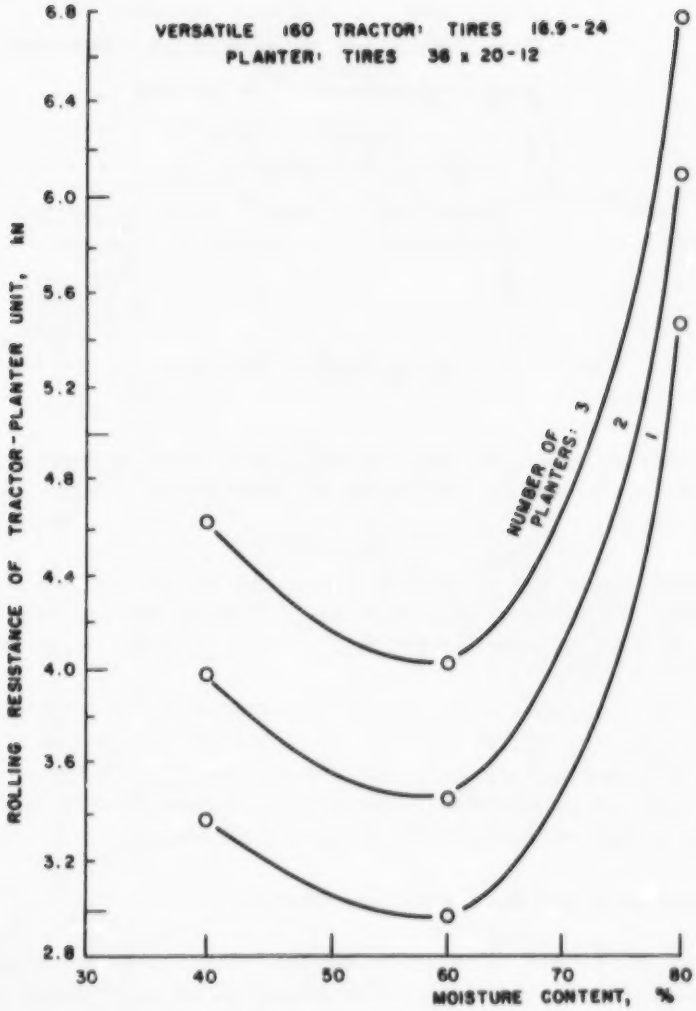

Figure 17. Rolling resistance vs. moisture content of tractor-planter units, in Prescott Soil, Site 1

Rolling resistance of the Versatile tractor alone approximates R = 5.5 - 0.692 = 4.81 kN, at 80% MC. If the high peaks are taken from the dynamometer chart, Fig. 16, then R = 1500 lb (6.67 kN). Reducing that value by 15% for differential and drive-line drag yields R = 5.67 kN, which is of the same magnitude as the calculated value R = 4.81 kN.

This may imply that Versatile tests, Fig. 16, were performed either in high moisture content soil, or in a "weaker" terrain, or both. In any case

there is no contradiction between measured and calculated values, considering the moisture content of Prescott area.

Soil Surface Rut Damage vs. Moisture Content

This was expressed in terms of Versatile tractor sinkage z_e, which was the sum of front and rear wheel sinkages, Fig. 18. Between 40 and 60% MC, the sinkage does not change much. Above 60%, it increases rapidly. This may help to define the critical soil state, in which the operations are detrimental to the environment, or to develop the tractor's running gear.

Since there is not much difference in rolling resistance and sinkage in soil states between 40-60% moisture content, Figs. 17 and 18, the future evaluation of soil - Versatile tractor relationship could be formed only in the 60-80% zone. Note that the soil with 40% MC is as "critical" as the soil with approximately 70% MC. The minimum soil damage under assumed conditions occurs at approximately 55% MC.

Slope and Drawbar Pull

These of the Versatile tractor were computed for one, two, and three towed planters, and 40, 60, and 80% MC, using procedures and input outlined

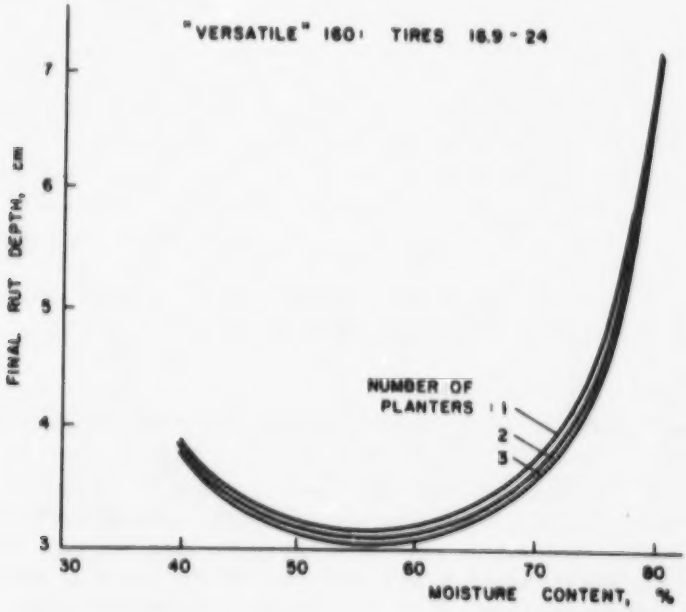

Figure 18. Theoretical rut depth of Tractor-planter units in Prescott Soil, Site 1

in Phase I and given in the section "Summary of Prescott Environmental Input". Each axle was evaluated separately, at slips varying between 0 to 30%. The result was plotted in Fig. 19.

The graph, Fig. 19, was cross-plotted in Fig. 20, which shows the drawbar pull, i.e., the reserve of pulling force (H - R), or the negotiable slope S.

As expected, the worst performance takes place at 80% MC. The best, at approximately 55% MC. Note that the performance difference for one and

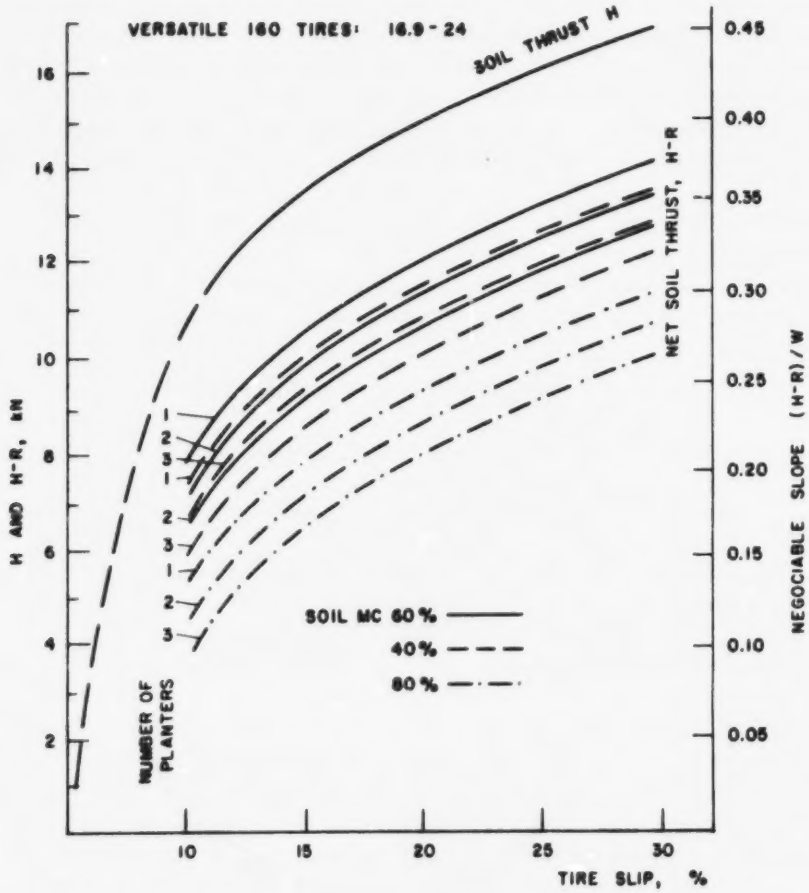

Figure 19. Soil thrust H and the drawbar pull H - R (where R is rolling resistance) vs. slip, for various Prescott soils and a number of planters. Also the negotiable slope as a function of slip

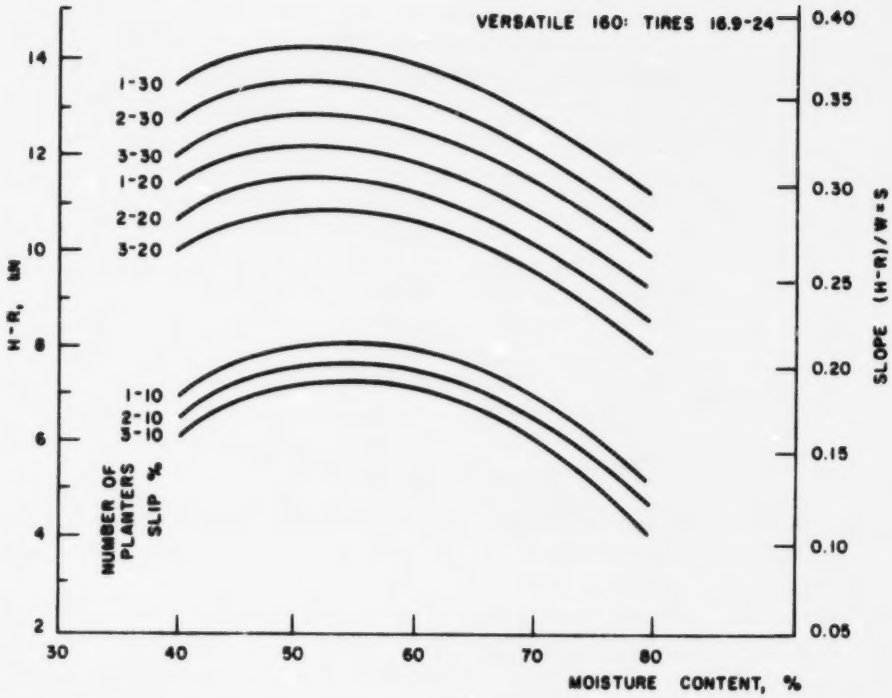

Figure 20. Drawbar pull H - R and the negotiable slopes vs. moisture content, at a number of slips and planter attachments

three planters is of the order of S = 0.04, and (H - R) = 1.5 kN. This indicates that towing of three or more planters is not a problem for the Versatile 160 tractor.

Soil Surface Shear Damage

This was estimated in accordance with data, Appendix F, Phase I, assuming K = 0.025 m. Computations yield the length of the ground contact areas, $l = l_1 + l_2$, given in Table 8.

The maximum assumed slip which is considered tolerable because of the economy and terrain damage is 30%. Accordingly the soil surface shear index I_s for MC = 40% and the front tire with one planter is $I_s = 0.4276 \times 0.3/0.025 = 5.13$. This means that the maximum soil displacement at the end of the ground contact area is exceeding 5.13 times the soil disruptive strain of 0.025 m.

Note that it remains to be determined if the tire will slip up to 30%, under the assumed conditions. Also the structure of soils with organic

Table 8. Length $l_1 + l_2$ of the ground contact area

No. of planters	MC (%)	Front tire	Rear tire
One	40%	0.4276	0.3544
	60%	0.4151	0.3474
	80%	0.4802	0.3583
Two	40%	0.4117	0.3725
	60%	0.3988	-
	80%	0.4675	-
Three	40%	0.3920	0.3851
	60%	0.3804	0.3866
	80%	0.4464	0.3927

debris and vegetation may withstand strains larger than 0.025 m. Calculations show that with three planters, at 80% MC the Versatile 160 tractor will slip only approximately 10%.

Slip calculations for front and rear tires with one, two, and three planters were plotted in Fig. 21. The front tires produce more surface shear than the rear ones, which is explained by the fact that the virgin ground is less compacted than the soil in the rut followed by the rear tire. Also note that the surface shear by front wheels is smallest when the tractor operates with three planters. This phenomenon is due to favorable load transfer.

In general, the Versatile 160 tractor may tow three planters with tolerable slip and reserve of power under the assumed conditions. If that presents an economic solution is the question of utilization of reserve power for purposes other than towing. More on the subject is discussed below.

Power and Fuel Consumption

These were calculated for the minimum and maximum rolling resistance, i.e., for 60 and 80% MC of soil. Only three planters were assumed. Tractor slip 30% also was assumed, although under the considered conditions this value was too high. For the coefficient of efficiency of the transmission $\eta = 0.85$ and locomotion speed 2.4 km/h, the following equation was used in power definition:

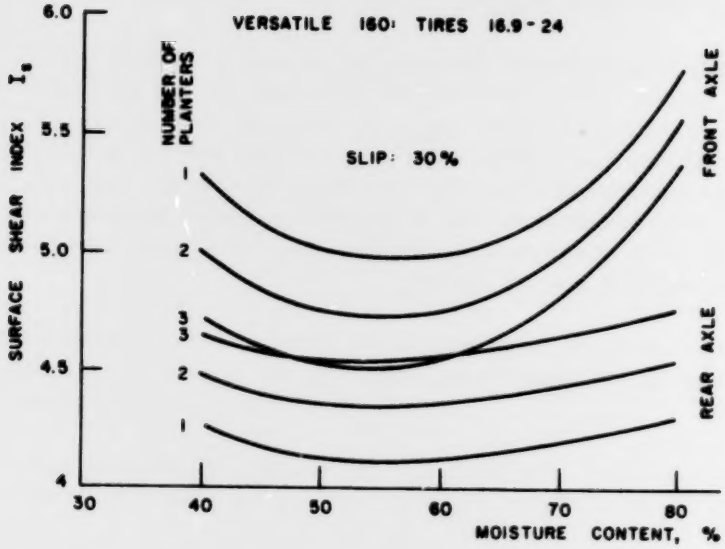

Figure 21. Surface shear index vs. moisture content for front and rear axles at 30% slip, and a number of planters

$$P(kW) = v(km/h) \times R(kN) \times 0.2359/0.85(1-0.3)$$

Fuel consumption F was calculated for tractor-planter rolling resistance, assuming engine fuel consumption 0.22 kg/kW h. Other input data are those given in Table 9. The specific weight of the fuel was 0.75 kg/L. These figures have only a comparative value because they neglect the detailed characteristics of the work cycle and transmission, which were not available in mission requirements (scenarios) and in the data bank.

The power consumed for planter towing, 3.87 to 6.47 kW, was a small fraction of Versatile's engine power, 62 kW.

Table 9. Versatile-planter rolling resistance

MC	Rolling resistance			P	F
(%)	Tractor	Three planters	Total	(kW)	(L/h)
60	2.3230	1.7446	4.0676	3.87	1.131
80	4.5611	2.2368	6.7979	6.47	1.89

Other Tires on Versatile Tractor

Tire 13.6 - 24; Drawbar Pull

This was calculated in MC 80% soil in order to compare its performance with the tractor equipped with 16.9 - 24 tires (see Table 4). Planter drag was eliminated. Calculations were performed for front and rear axles in order to illustrate the utilization of particular tire location, or rather the particular load distribution between the front and rear tires. The result was shown in Figs. 22 and 23.

Note that the front tire pulls the tractor with approximately half the force developed by the rear tire. This is not a right utilization of the tires.

Computations also show that the Versatile 160 tractor with 16.9 - 24 and 13.6 - 24 tires produces practically the same result (Fig. 24).

Hypothetical Tire 40 × 50 - 12, Rolligon; Drawbar Pull

This was also calculated to check the improvement of traction, when the Rolligon is used instead of the standard tires. The result was plotted on Figs. 22, 23 and 24. As expected, the Rolligon produces the best result, but at what cost?

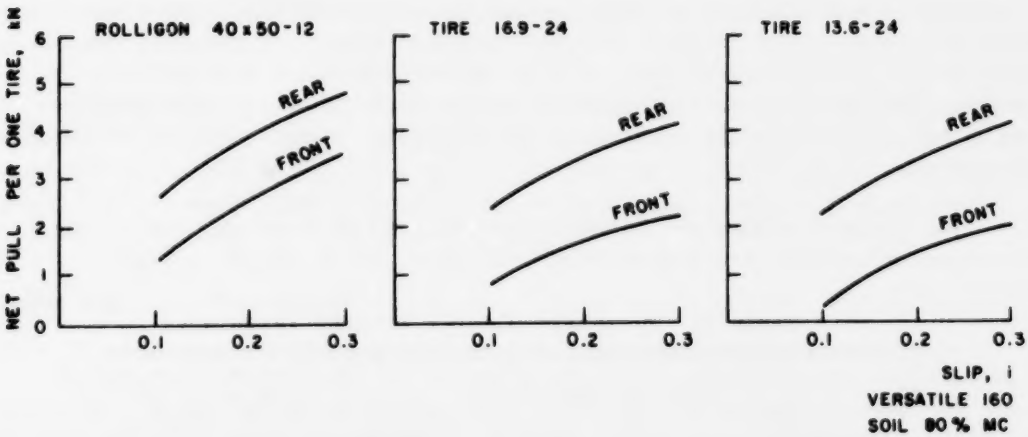

Figure 22. Changes in tire drawbar pull vs. slip, for the hypothetic 40 × 50 - 12 Rolligon, 16.9 - 24 and 13.6 - 24 tire. No planter towed

Conclusion

This chapter illustrated a great variety of topics which can be treated in a unified way by means of the bevametric method.

The generality of the method, and its simplicity, enable one to solve practically all the engineering problems, through parametric analyses which yield insight into the interdependence of all important factors, and lead to a rational optimization of soil-vehicle system.

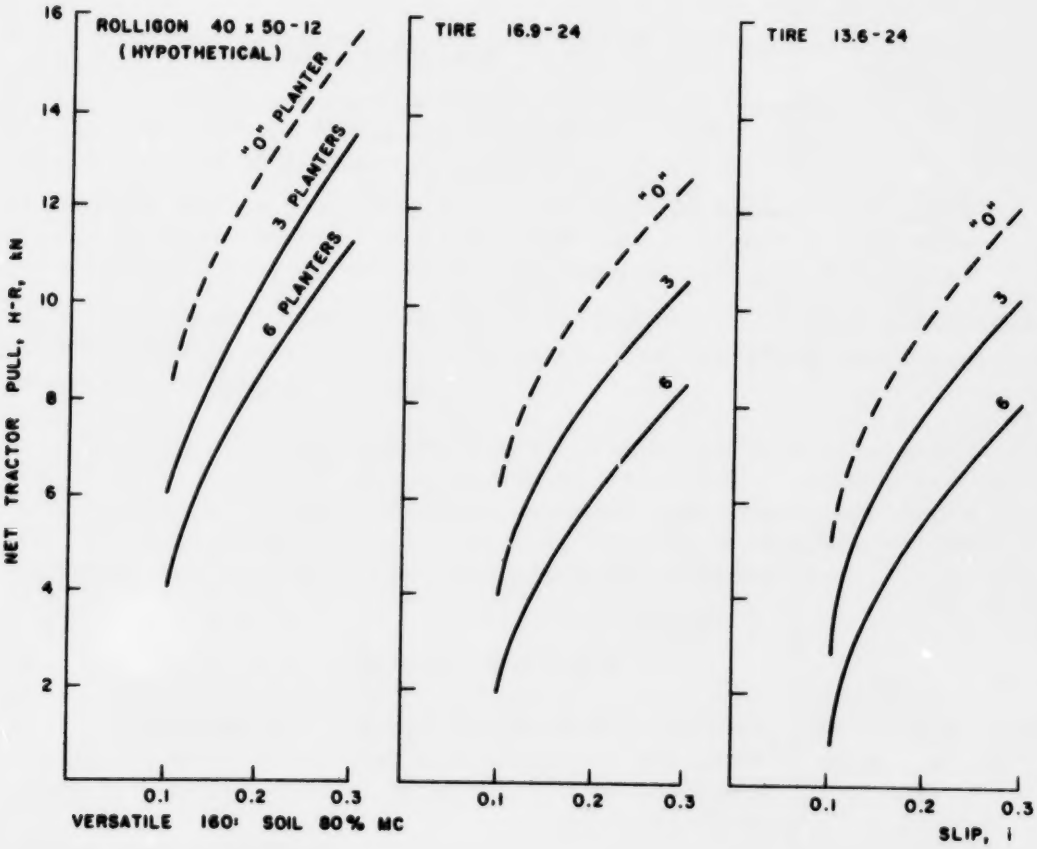

Figure 23. Changes in tractor drawbar pull, for three specified tires (Fig. 22) vs. slip, and for the number of planters towed: 0, 3 and 6

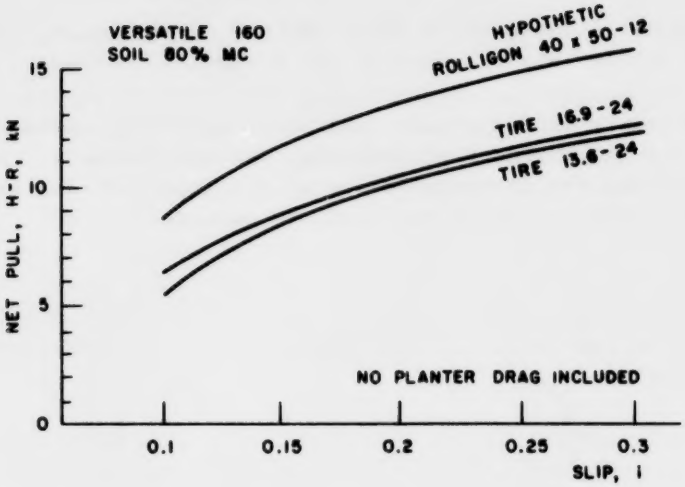

Figure 24. Drawbar pull vs. slip of Versatile 160 tractor equipped with three different tires. Note practical ineffectiveness of larger 16.9 - 24 tire as compared with the smaller, 13.6 - 24 tire

PARAMETRIC ANALYSES OF VEHICLES IN AGRO-FORESTRY, EXAMPLES AND CASE STUDIES

GENERAL

Conventional optimization of vehicular systems described in Phase I of this study may be aided by selective analysis of examples and case studies applicable to the planning of 5-year rotation poplar plantations.

To this end the vehicles described previously, Versatile 160 and Holder A60 test tractors, were used together with the variety of previously considered tires.

Parametric analyses reported here include such mission requirements as

- planting with furrow-type equipment
- planting with insertion-type equipment
- harvesting
- forwarding
- skidding

Following the NRC requirements, the Versatile 160 tractor was investigated with the planter and harvester attachments, and the Holder A60 tractor with skidder and forwarder attachments.

An additional type of ground, covered with turf-like soil, was introduced. Because of lack of direct bevameter data, its characteristics were assumed on the basis of scanty available measurements and experience. For comparison, planting operation in turf-like soil also was evaluated, though it will take place only in prepared Prescott-type soil.

PLANTER IN PRESCOTT SOIL

Two types of planting attachments were postulated: one which produces a slit, in which the cutting is planted, and the other in which the tree plant is inserted by means of an unspecified instrument (Fig. 13).

Furrow Opening Reaction

Furrow opening reaction acting on the tractor in a horizontal direction is 6.23 kN (1400 lb). It was assumed that all the forces and moments related to tractor-planter system are zero, except for the

horizontal drag 6.23 kN acting at point R (Fig. 13). The planter's processor consumes an additional 22 kW.

Insertion Planter Load

This was defined as directly chargeable to the tractor engine via hydraulic transmission. It was assumed not to exceed 22 kW of power.

Environment

The environment for the evaluation of the maximum number of planters of both types to be attached to the tractor, Prescott soil, was chosen at 40 and 80% MC, Table 2. Other soil parameters remained the same: $K = 0.025$ m; $K_c = 15$; $K_\gamma = 12$; $\gamma = 15$ kN/m^3; $c = 3$ kPa; $\phi = 28.4°$.

Tires

Tires were selected as previously: 16.9 - 24 (Goodyear) and hypothetic 40 × 50 - 12 (Rolligon). Their characteristics were described in Table 4.

Planter Rolling Resistance

This was calculated as shown in Table 5.

MC 40% - 0.692 kN
MC 80% - 0.7456 kN

Computations of the Maximum Number of Furrow Planter Modules

Computations of the maximum number of furrow planter modules which can be towed by the Versatile 160 tractor were based on the axle loads shown in Table 10.

To simplify the computations, the constant pulling resistance of the furrow planters was assumed to be the values given in Table 11.

Table 10. Axle loads for 40 and 80% MC

Number of planters	Rear axle (kN)	Front axle (kN)
One	18.45	19.03
Two	21.94	15.53
Three	25.49	12.03

The averages of drawbar pull for Prescott soil at 40 and 80% MC were calculated as shown in Table 12.

Note that the 16.9 - 24 tire is very sensitive to moisture content. The Rolligon, working with a great margin of safety, would perform almost without difference in 40% or in 80% MC soil. Table 12 was plotted in Fig. 25.

Figure 25 also shows the levels of towing resistances of one, two and three planters. It is obvious that a maximum of two furrow planters can be towed by the Versatile 160 tractor below 50% slip. The amount of slip with two planters depends on MC and on the tire as shown on the graph, and in Table 13. Rolling resistance is given in Table 14.

Assuming the coefficient of mechanical efficiency of the tractor's transmission $\eta = 0.85$, and the slips of tires shown in Fig. 25 (Table 13), the power required for propulsion including 44 kW for processor was calculated for 2.4 km/h:

Table 11. Planter and furrow opening

No. of planters	Total drag (kN)
One	6.9
Two	13.9
Three	20.8

Table 12. Drawbar pull vs. slip, 40 × 50 - 12, Rolligon

Slip (%)	Drawbar pull		
	40 × 50 - 12 Rolligon*	16.9 - 24 tire	
		MC = 50%	MC = 80%
10	8.44	8.00	6.48
20	13.27	12.26	10.72
30	15.95	14.26	12.65
40	17.67	15.36	13.69
50	18.75	16.03	14.36

*Hypothetical.

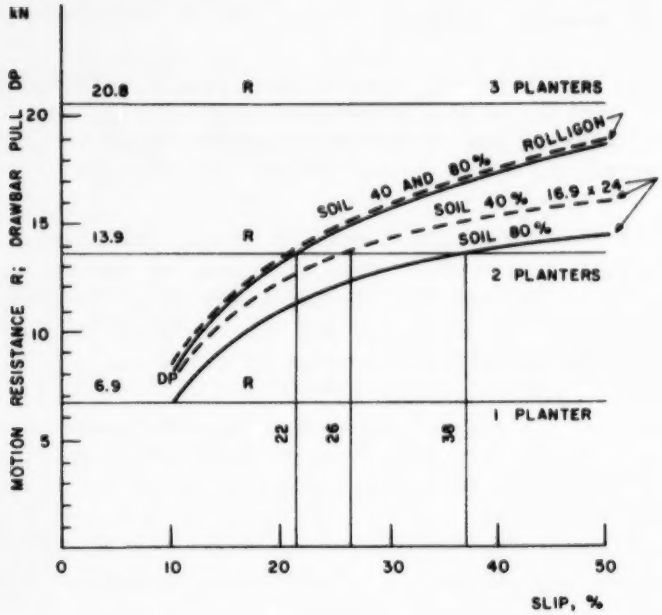

Figure 25. Motion resistance R of furrow planters and the drawbar pull DP (or H - R) of Versatile 160 tractor vs. slip, in Prescott soil with different moisture contents, for hypothetical 40 × 50 - 12 Rolligon, and agricultural 16.9 - 24 tire. Intersections of DP and R denote corresponding slip

$P_{40\%\ MC,\ 16.9 - 24} = 59.09$ kW
$P_{80\%\ MC,\ 16.9 - 24} = 64.04$ kW

Versatile with two furrow planters, Prescott soil

$P_{40\%\ MC,\ 40 \times 50 - 12} = 57.24$ kW
$P_{40\%\ MC,\ 40 \times 50 - 12} = 57.22$ kW

It follows that the Versatile 160 tractor is barely adequate for towing two furrow planters in Prescott soils as its engine power is 62 kW. Also, because of its structural characteristics it cannot pull more than two furrow planters as demonstrated in Fig. 25, unless Rolligon tires and slips larger than 50% are accepted. In 80% soil, the Versatile 160 with 16.9 - 24 agricultural tires is inoperative.

Computation of the Maximum Number of Insertion Planter Modules

Since in the case of an insertion-type planter, the power required for

planting is directly supplied by the tractor engine, the operational planter number was defined by the power available in the system.

Soil and tire input data were the same as in the preceding case, assuming that the engine of the tractor has to overcome the external resistances and supply 22 kW of power to each planter.

Axle load distributions were as shown in Table 6. Computations yielded the data given in Table 15. Also, for the convenience of the reader, planters' rolling resistances are reprinted in Table 15.

Table 13. Versatile tire slip when pulling two planters, Prescott Soil

Tire	Soil 80% MC	Soil 40% MC
40 × 50 - 12 Rolligon*	22%	22%
16.9 - 24 Tire	38%	26%

*Hypothetical.

Table 14. Rolling resistance of Versatile-planter unit, Prescott Soil

Tire	Soil MC	Tractor	Two furrow planters	Total resistance
40 × 50 - 12	40%	1.4116	13.9*	15.31
16.9 - 24	40%	2.6482	13.9	16.55
40 × 50 - 12	80%	1.3798	13.9	15.28
16.9 - 24	80%	4.5064	13.9	18.41

*Assumed constant.

Table 15. Rolling resistance, Prescott soil

	Tractor rolling resistance (kN)				Planter rolling resistance (kN)	
	40 × 50 - 12		16.9 - 24			
No. of planters	40% MC	80%MC	40% MC	80% MC	40% MC	80% MC
One	1.3838	1.3298	2.6988	4.6828	0.6920	0.7456
Two	1.3754	1.4844	2.6750	3.6046	1.3840	1.4912
Three	1.3996	1.3608	1.6354	4.5284	1.4912	2.2368

Adding the resistances shown in Table 15 gives the power required (η = 0.85; i ≅ 10%); see Table 16. The data from Table 16 were plotted in Fig. 26, and show again that only two planters may be towed.

Calculations of furrow and insertion type planters yield interesting comparative basis for evaluation of planter efficiency vs. power-torque characteristics of the tractor.

Table 16. Power consumption, various tires, insertion planter (2.4 km/h), Prescott soil

No. of planters	System power consumption (kW)				
	Insertion power	40 × 50 - 12 Rolligon*		16.9 - 24	
		40% MC	80% MC	40% MC	80% MC
One	22.0	~23.5		24.51	26.02
Two	44.0	~46.0		47.00	47.77
Three	66.0	~68.6		68.75	71.01

*Hypothetical.

Comparison between Furrow and Insertion Planters

Figures 25 and 26, though different in form, define the same maximum number of planters, of both types, which can operate with a Versatile 160 tractor. Figure 27 displays the complete power balance for all the eight cases considered and is self-explanatory.

It might be suggested that planter subsystem optimization should have been performed before the optimization of the tractor-planter system, for both the tactical and economy evaluation reasons.

Environmental Damage

Environmental damage, through sinkage, was recorded directly from computer tapes (see Table 17).

Actual sinkage may double. There is a clear difference between the Rolligon and the tire performance. Cost difference was not determined.

TURF-TYPE SOIL DEFINITION

Many bevameter data are available in organic soils such as muskeg.

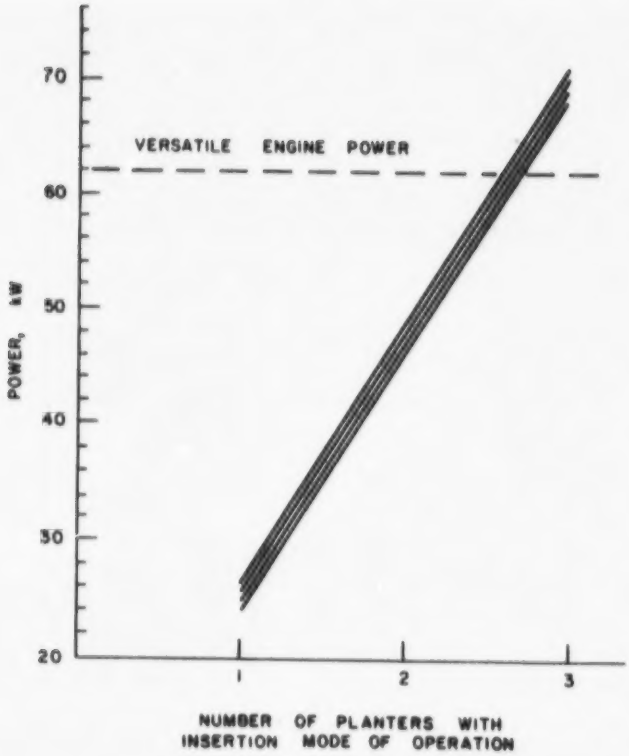

Figure 26. Power required to operate 1, 2 or 3 insertion-type planters in 40 and 80% soil moisture content, in Prescott soils, for Rolligon and 16.9 - 24 tires, at speed v = 2.4 km/h. The results overlap closely because of the overpowering requirement of 22 kW to drive the planting mechanism. Three planters cannot operate because of lack of engine power

Table 17. Sinkage, theoretical; insertion planter, Prescott soil

Tire	Sinkage (cm)	
	40% MC	80% MC
Rolligon 40 × 50 - 12	0.72	0.72 (insignificant)
Tire 16.9 - 24	3.92	7.05

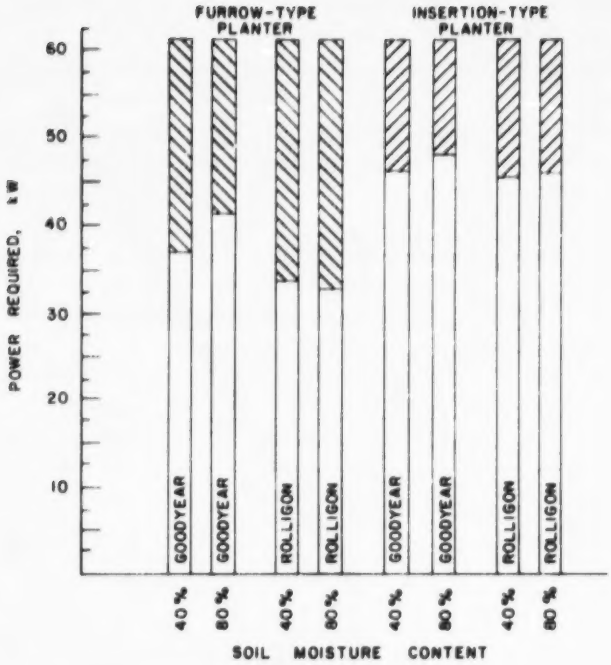

Figure 27. Comparison between power requirements for furrow and insertion-type planters, in Prescott soil at 40 and 80% moisture content. Blank areas denote power required, the hatched ones, the power surplus. Hypothetical Rolligon size: 40 × 50 - 12; Goodyear tire size: 16.9 - 24

However, forest plantations shown in Fig. 28 represent practically a "terra incognita."

Such soil represents an overlay of leaves, roots, and organic matter build up during the 5-year period of forest growth. The original ground and the underlying soil are represented by Prescott type soil, previously investigated. Thus, while the top soil may be likened to turf, the subsoil is different from wet loose organic layer.

Turf Analog

Turf analog may be used, however, if it is assumed that the regular "punching" pressure and mat deformation of turf are nonexistent, and that the original 10-15 cm load-penetration test of bevameter plates preserves its character, beyond the top layer.

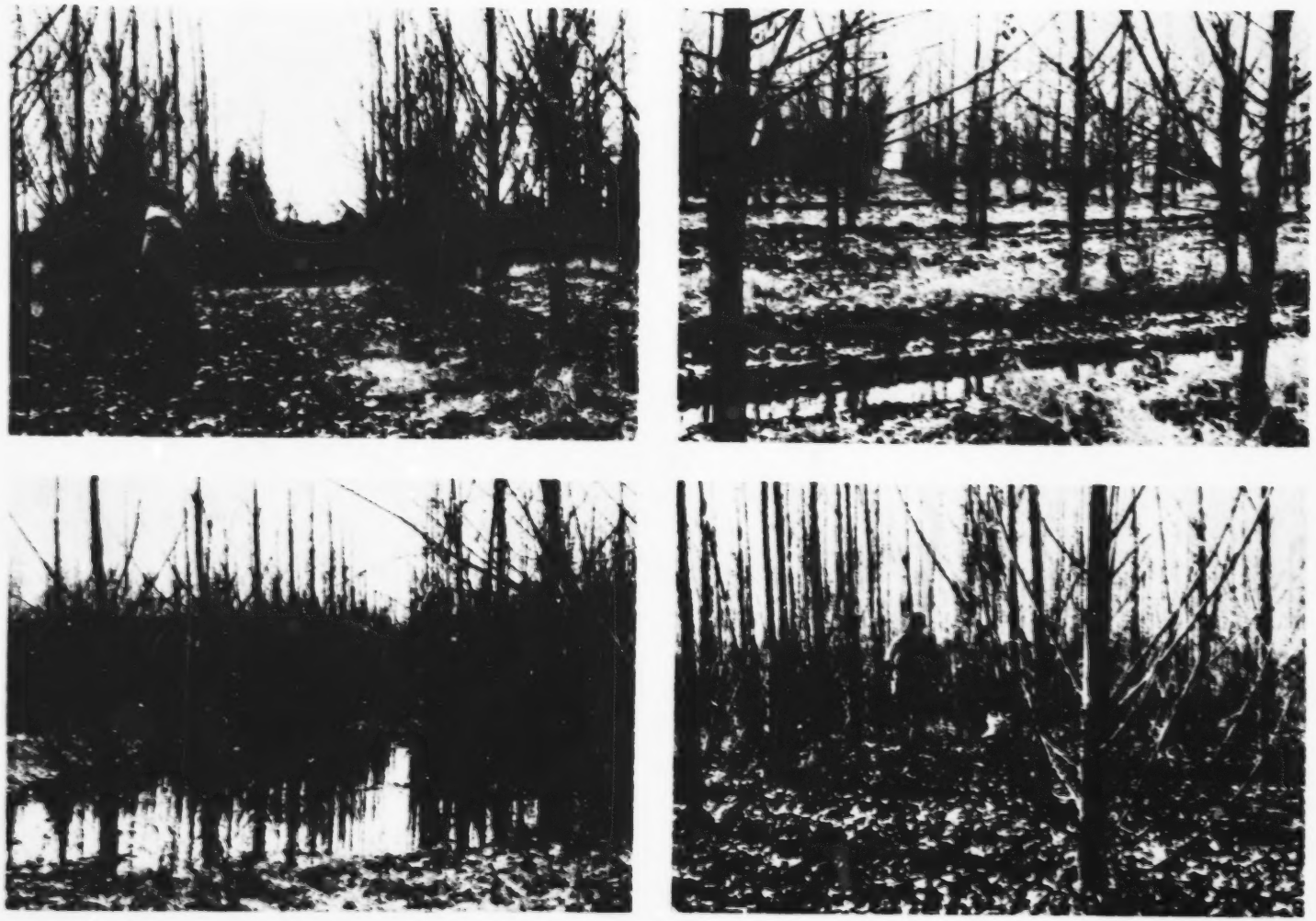

Figure 28. Turf-like terrain in which skidding of forwarding and harvesting take place

Literature survey shows the plausibility of such an assumption. Consequently, bevameter turf tests made in Germany were taken as a starting point (1), and were replotted in the SI System, in Fig. 29, which yields $k_\phi \cong 0$; $k_c = 700$; $n = 1$.

Turf-Soil Characteristics

Trial computations showed that such soil is rather strong because of low moisture content, 20-40% (1). This does not resemble the pictures in Fig. 28. Thus, as an educated guess, the turf-like soil parameters given in Table 18 were assumed.

Table 18. Turf-like soil values (SI units)

Pass	ϕ	γ	k_ϕ	k_c	n	c	K_γ	K_c	K
I*	30	10	50	235	1.0	4.673	15	13	0.05
II*	30	10	50	235	1.0	4.673	15	13	0.05*

*Unchanged.

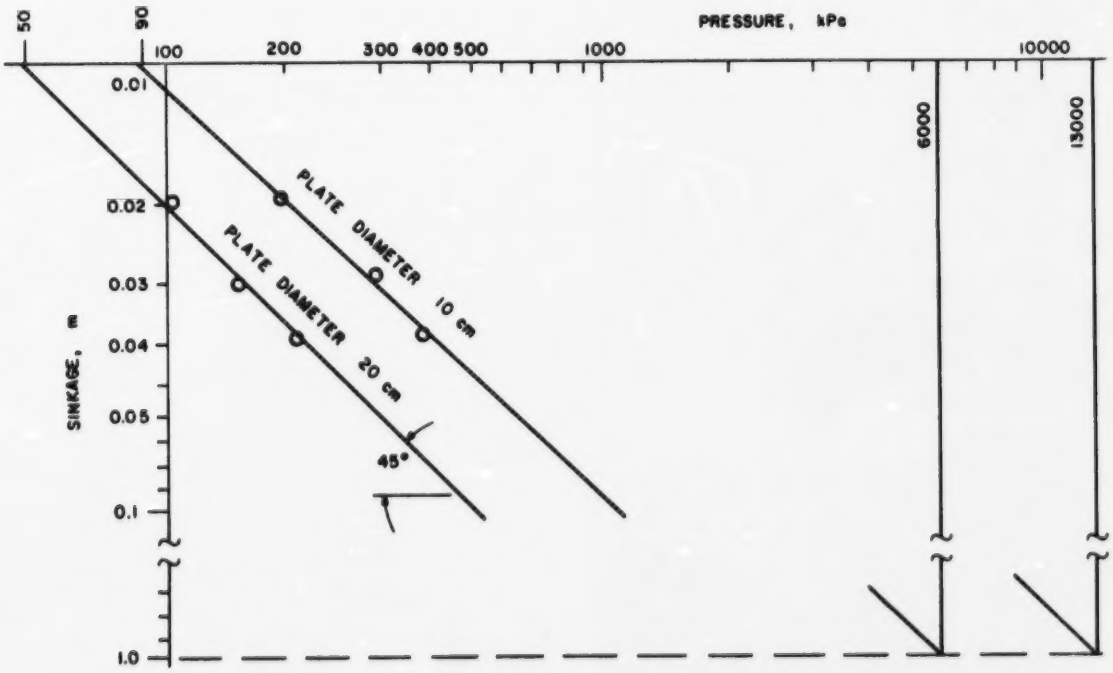

Figure 29. Bevameter log-log plot for turf measured by part of a Söhne-Sonnen (1), reproduced in SI units

These parameters may represent meadow-like terrain with high moisture content of a thick organic mat and of the underlying ground. Properties of such quasi-elastic terrain should not change much with the second pass, and are assumed constant. Obviously, actual field measurements are needed to corroborate the data in Table 18.

A PLANTER IN TURF-LIKE SOIL

Although the turf-like soil is the result of years of forest growth, and as such is not the subject of tree planting, Versatile tractor was recomputed as a planter in order to obtain a direct comparison with similar operations performed in Prescott soil.

Insertion Planter-Tractor Power

This requirement was calculated as previously, with changed soil characteristics and loads. Calculations yielded data given in Table 19 and depicted graphically in Fig. 30.

Furrow Planter-Tractor Power

This requirement in turf-like soils presents a similar picture (Table 20).

The drawbar pull was plotted in Fig. 31.

Table 19. Insertion planter-tractor power

	Hypothetic Rolligon 40 × 50 - 12		16.9 - 24	
	One planter	Two planters	One planter	Two planters
Rolling resistance, tractor-planter (kN)	8.43	10.87	14.47	16.90
Power required (2.4 km/h) (kW)	6.50	8.83	12.20	16.00
Power required, planter mechanism (kW)	22.00	44.00	22.00	44.00
Total power (kW)	28.50	52.83	34.20	60.30
Gross engine power (kW)	62.00	62.00	62.00	62.00

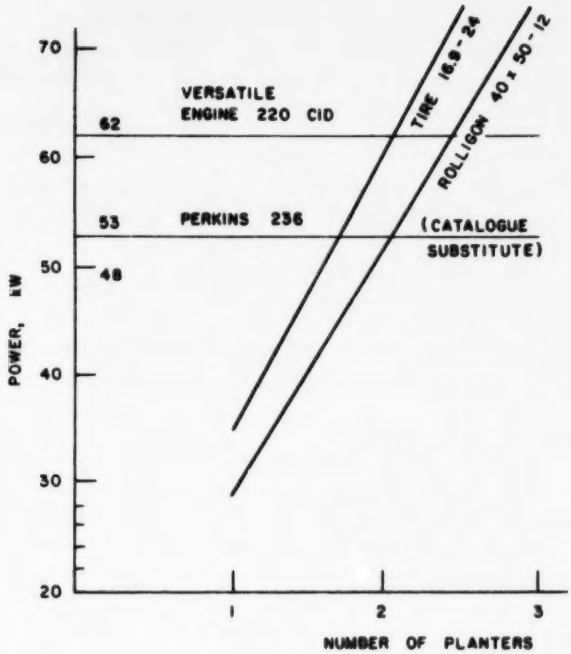

Figure 30. Power required to operate 1, 2 and 3 planters of insertion type in turf-like soils (Fig. 28) with 40 × 50 - 12 Rolligon and 16.9 - 24 tire, vs. engine power

Table 20. Furrow planter-tractor power

	Hypothetic Rolligon 40 × 50 - 12		16.9 - 24	
	One planter	Two planters	One planter	Two planters
Rolling resistance, tractor-planter (kN)	8.4368	10.8666	14.4744	16.9042
Dibble drag (kN)*	6.2	12.4	6.2	12.4
Operating power (kN)	22.0	44.0	22.0	44.0
Total resistance to motion (kN)	36.6368	67.2666	42.6744	73.3042

*No other values available.

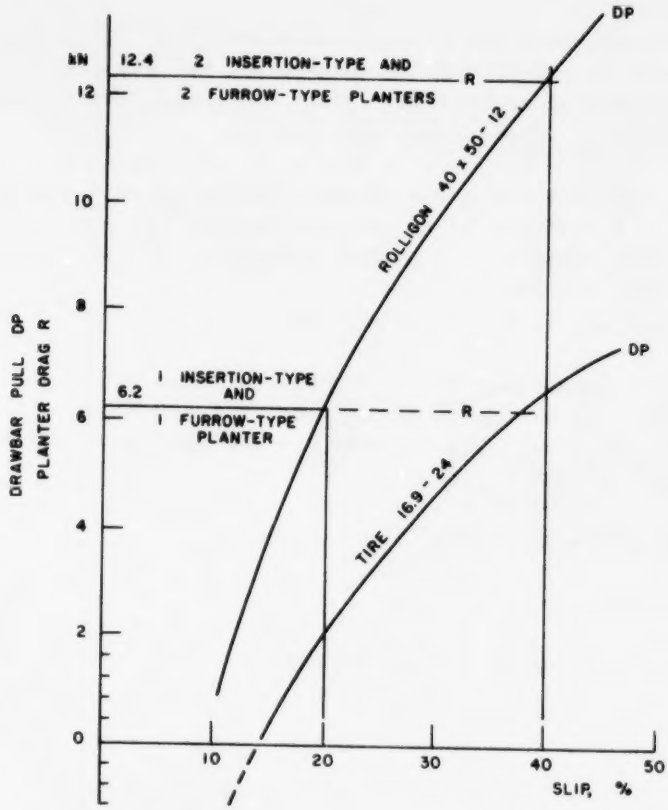

Figure 31. Drawbar pull of the Versatile and furrow-planter drag vs. slip for hypothetical 40 x 50 - 12 and 16.9 - 24 tires in turf-soil (Fig. 28). Though planting is not expected to take place in such soil, the graph serves the general purpose of illustrating performances in very soft "marshy" ground

TREE HARVESTER IN TURF-LIKE SOIL

Harvesting is performed only in turf-like soils, which eliminates from this study the prepared Prescott soils.

The general layout of the harvesting tractor-attachment unit was shown in Fig. 32.

Drawbar Pull and Slip

These curves read out directly from computer tapes were plotted in Fig. 33. Skid resistance of the supporting ski was assumed to be mainly caused by compaction resistance. Thus, following the sinkage-resistance equations, Phase I, Appendix D, and Fig. 32:

$$z_e = 9.83/0.305 \times 0.6\ [(235/0.305) + 50] = 0.064 \text{ m}$$
$$R_c = 0.305[(235/0.305) + 50 \times 0.0644)^2]/2 = 0.5190 \text{ kN}$$
$$R_b = 0.305(0.6667 \times 0.0064 \times 4.637 \times 13 + 0.5 \times 0.0644^2 \times 150)$$
$$= 0.884 \text{ kN}$$

Total ski resistance 1.403 kN

Figure 33 shows that the hypothetical tractor equipped with the Rolligon will slip at approximately 10% if 1.403 load is accepted. Doubling the ski drag will not much affect the outcome. The 16.9 - 24 tire will slip at i = 16%.

Rolling Resistance and Power

From the tapes:

Rolling resistance	16.9 - 24 Tire:	15.48 kN
	40 × 50 - 12 Rolligon:	9.13 kN (hypothetic)

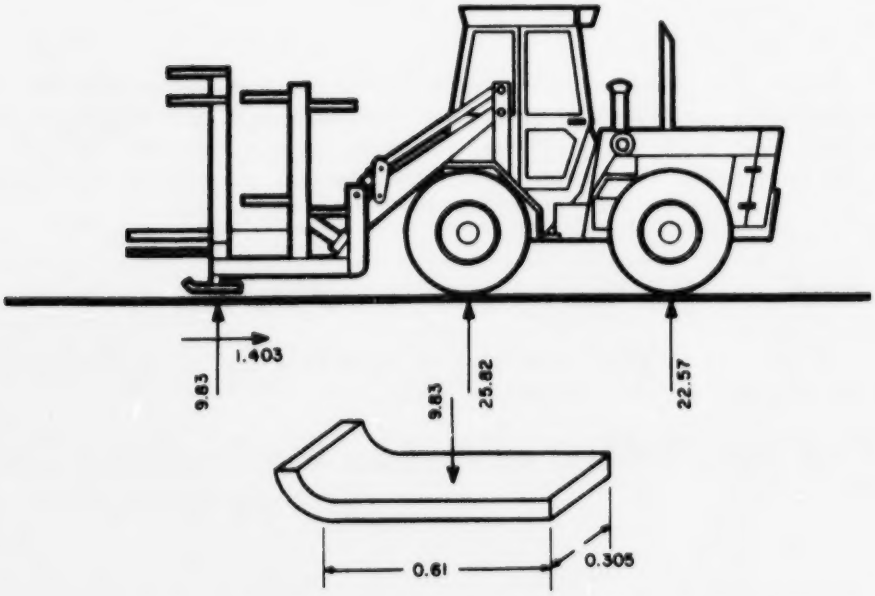

Figure 32. Axle loads and geometry of Versatile 160 test tractor with harvester attachment

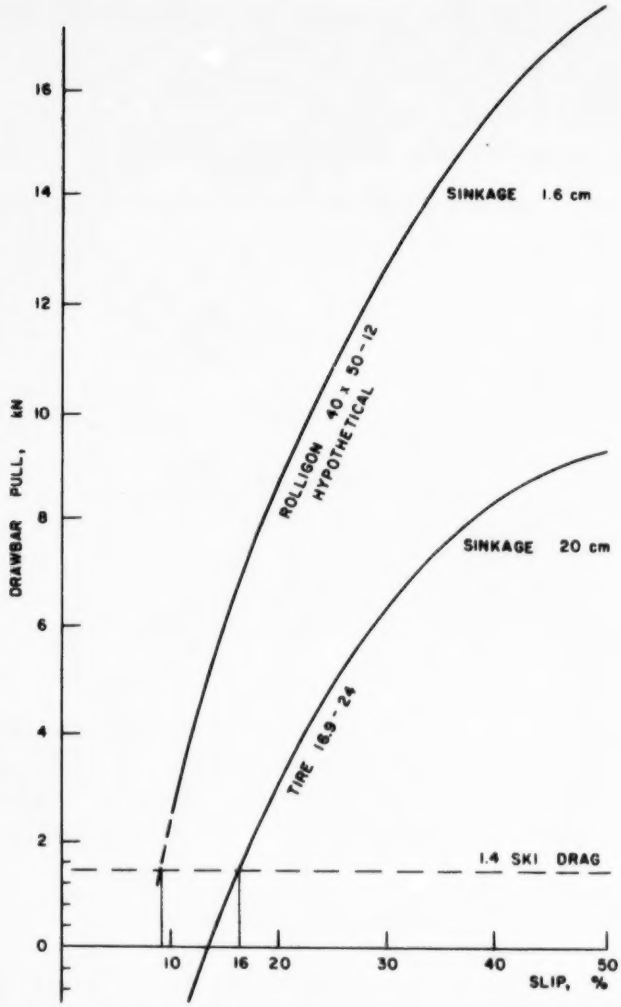

Figure 33. Drawbar pull-slip curves for Versatile 160 used with harvester attachment and two different tires as specified on the graph. Sinkage also indicated

Consequently, the power required to operate each unit at various speeds is as shown in Fig. 34, where slips 10% and 16% were assumed (Fig. 33). Power required to operate the harvester attachment is 15.4 kW.

Figure 34 shows that the Versatile's power available for locomotion, 62 - 15.4 = 46.6 is sufficient to operate the equipment when harvesting with speed 5 km/h, even when using the 16.9 - 24 tires.

Again, the matching of the tractor and harvester attachment subsystem could be performed before the analysis of the complete system.

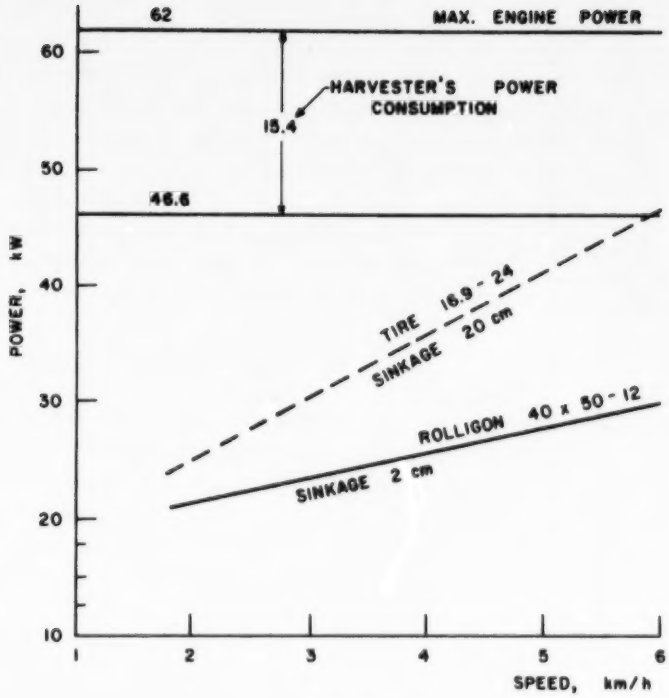

Figure 34. Power required to operate the Versatile 160 tractor as a harvester with tires specified on the graph. Harvester attachment consumes 15.4 kW of engine power

FORWARDING AND SKIDDING

Only turf-like soils were assumed for evaluation of forwarding and skidding by the Holder A60 tractor (see Table 18). General outline of loads and geometry of the tractor were shown in Fig. 14. Figure 35 displays the load-geometry scheme with forwarding and skidding attachments.

Tires and Attachments

Two types of tires were used in performance evaluation: hypothetic Rolligon, 40 × 50 - 12 and Dunlop, 14.5 - 75/20 tire. The attachments were used alternatively. Engine power was 36.5 kW.

Computation of Pull-Slip, Thrust and Power

This followed the usual pattern. Computer tapes yielded drawbar pull

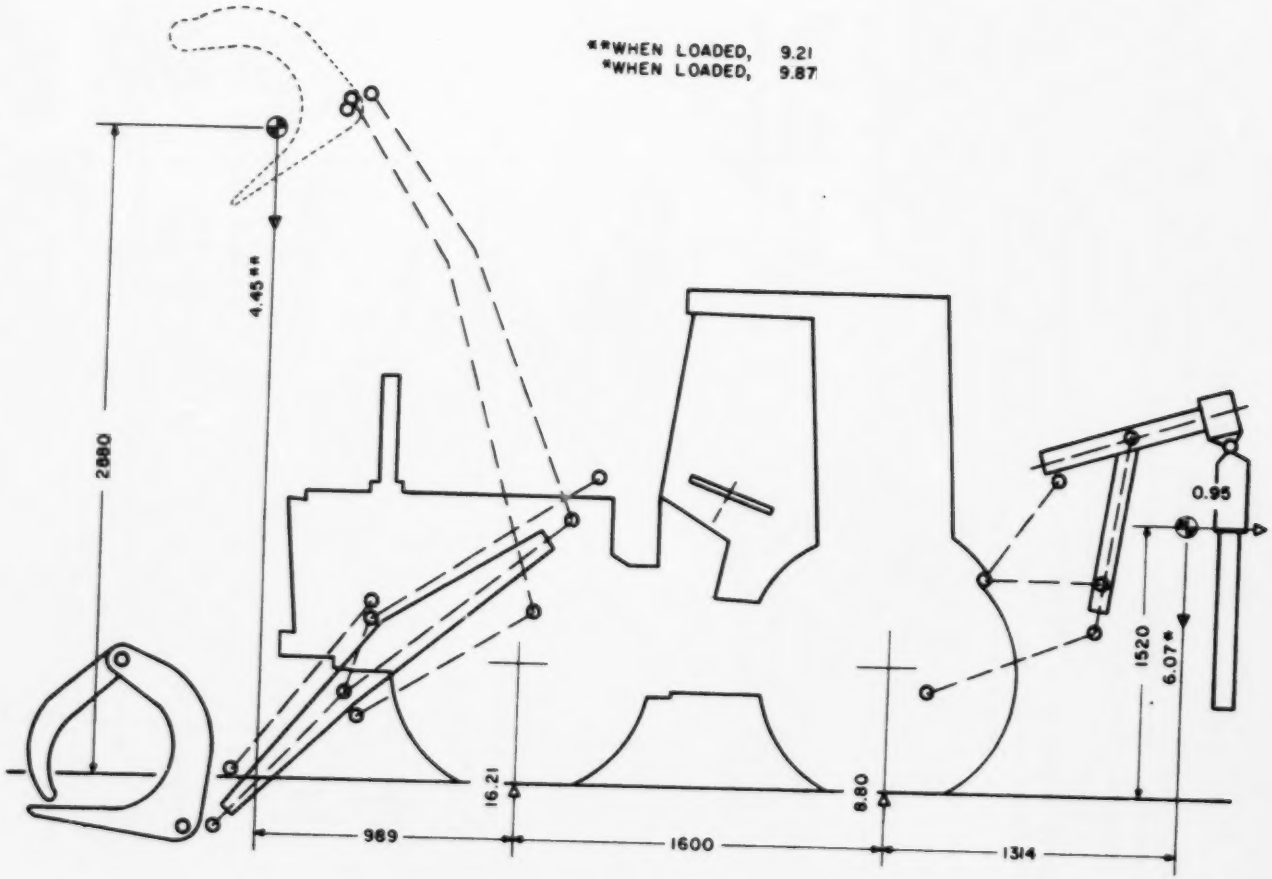

Figure 35. Geometry and load distribution of Holder A60 with forwarding and skidding attachments

and soil thrust plotted in Fig. 36. As expected, Rolligon would perform better than the Dunlop tire.

Soil thrust generated by the Holder with Rolligon and Dunlop tires also was plotted. It differs for each case so little that one line could have been assumed.

Figure 37 shows soil thrust and the motion resistance of the four considered cases. Note the slips at which each particular operation takes place (Table 21). Numbers in parentheses denote the motion resistance. These figures yield the power HP required at a given speed v in the form shown in Table 22. This was based again on the assumption that transmission efficiency $\eta = 0.85$, and the slip was indicated in Table 21. Substituting speeds $v = 1, 2, 3, \ldots, 10$ km/h, graph Fig. 38 was obtained.

It shows that the skidder with Dunlop tires can operate with speeds up to 7 km/h. The forwarder, with the same tires, may make up to 9.2 km/h. The same tractor with the Rolligon may reach 15 km/h in both operations.

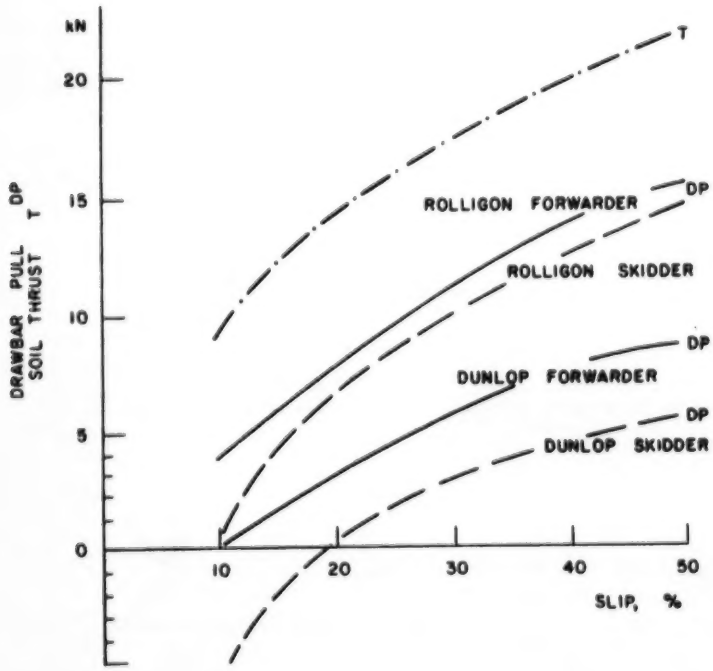

Figure 36. Drawbar pull and soil thrust vs. slip for Dunlop and hypothetic Rolligon tires of Holder A 60 used as forwarder and skidder. Turf-like soil

Table 21. Slip at thrust-motion resistance equilibrium

Tire	Skidder	Forwarder
Rolligon*	10.5 (7.47)	10 (6.8)
Dunlop	22 (14.34)	16% (11.72 kN)

*Hypothetic.

Table 24. Power equations for skidding and forwarding with two types of tires

Tire	Skidder	Forwarder
Rolligon	2.3468v	2.1244v
Dunlop	5.1693v	3.9230v

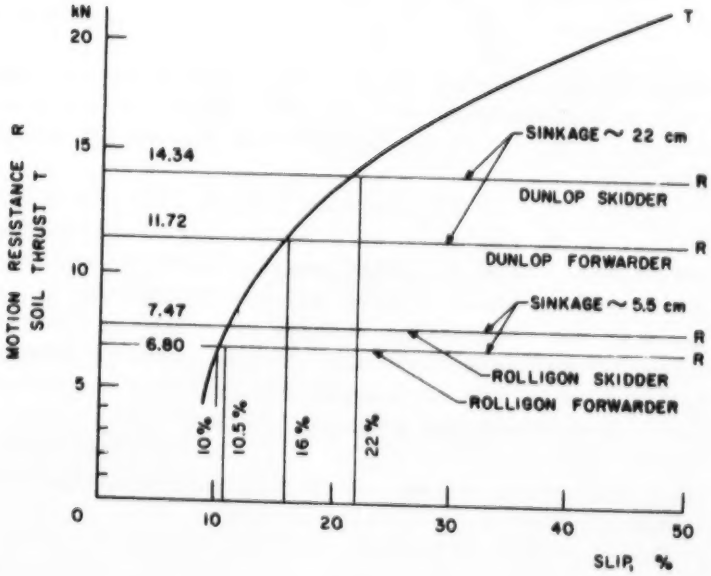

Figure 37. Motion resistance and soil thrust vs. slip, of Holder A 60 with Dunlop and Rolligon tires in forwarding and skidding operations. Turf-like soil

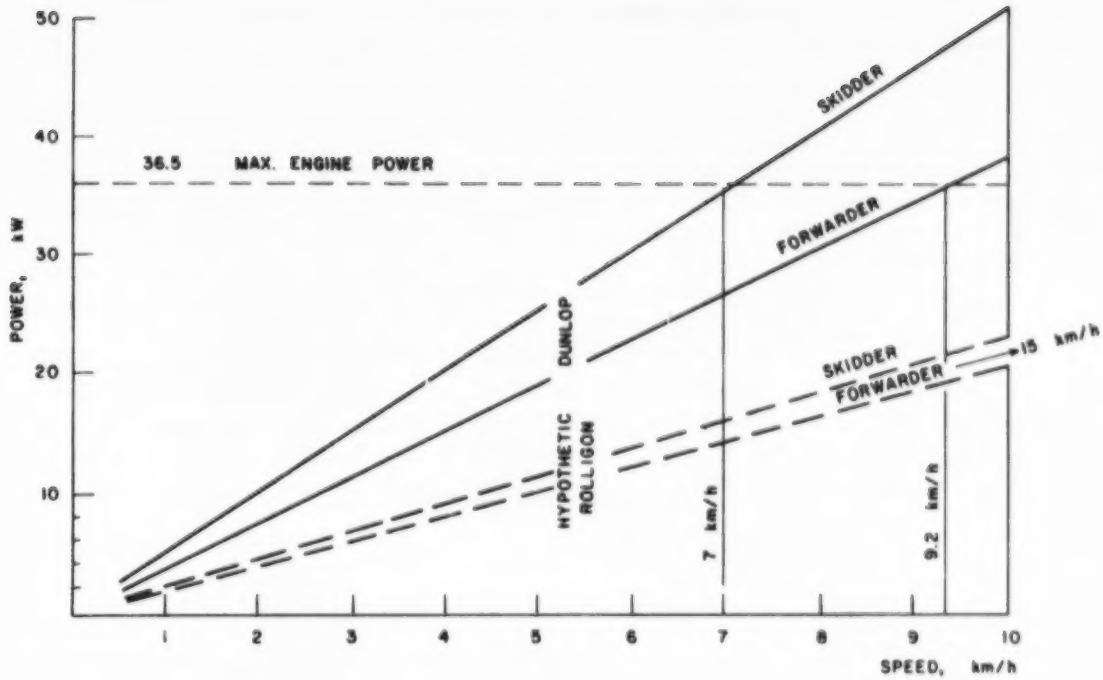

Figure 38. Power required to operate Holder A 60 as a skidder and forwarder at various speeds. Turf-like soil

Conclusions

Conclusions as to the merit of a particular tractor-tire combination may be drawn directly from pertinent graphs discussed before. However, the decision is related to other factors not considered here. It may be noted, for example, that the theoretical sinkage of Dunlop tires is approximately 22 cm, whereas the Rolligon tires sink to the depth of approximately 5.5 cm. Unfortunately, the manufacturer will not consider providing a special axle to accomodate the Rolligon.

The study suggests the need for a different tire concept, and possibly different running gear.

The use of forwarding attachment is not necessarily in economic consonant with the use of skidding attachment. Perhaps a radical departure from conventional tractor-attachments design could remedy the incompatibility of performing two different functions by the same tractor.

This may become the subject of the analysis of the tractor-attachments subsystem, for forwarding and skidding purposes.

GENERAL CONCLUSIONS

This study has hopefully illustrated a great variety of parametric analyses of vehicle traction performance, and the nature of mechanical terrain damage.

The analyses based on bevameter techniques have been effective and verifiable in unique solutions of the following problems:

- drawbar pull-slip
- traction efficiency
- slope climbing
- power consumption
- fuel consumption
- designation of optimum operational soil moisture content
- total vehicle performance: second pass of rear wheels
- optimum tire selection
- optimum axle load distribution
- ground surface shear
- rut making

The solutions based on unified value system and on equations compatible with applied mechanics offer an opportunity for comparative evaluation of terrain-vehicle systems parameters which include

- width-length of tire ground contact area
- tire deflection
- tire internal structure: p_c-test
- tire inflation pressure
- tire load
- ground pressure
- vehicle geometry and load distribution
- tractor-trailer geometry and load distribution
- engine power, torque
- transmission characteristics
- vehicle vs. soil values relationship in sinkage, shear, slip
- moisture content of soil vs. bevameter values in operation time optimization

Parametric analyses thus construed enable one to optimize any parameter, usually

- design concept: geometry and forces, size, form and power
- loads of the system
- geometry of subsystems
- power, fuel consumption
- environmental damage
- cost and effectiveness

REFERENCES

1. W. Söhne and F.J. Sonnen. Messungen von Rollwiderstand und Zugkraft von luftbereiften Ackerschleppern.... Proc. 1st Int. Conf. on Terrain-Vehicle Systems. Torino-St. Vincent. Edizioni Minerva Tecnica, Torino. 1961.

2. J.Y. Wong. Evaluation Study of Soil Strength Measurements. Division of Energy, National Research Council of Canada, Ottawa, Canada, December 1983.

3. M.G. Bekker. Introduction to Terrain-Vehicle Systems. The University of Michigan Press, Ann Arbor, Mich. 1969.